Intraspezifische Variabilität alkenspaltender Enzymaktivitäten in monokaryotischen und dikaryotischen Stämmen von *Pleurotus sapidus*

Von der Naturwissenschaftlichen Fakultät der

Gottfried Wilhelm Leibniz Universität Hannover

zur Erlangung des Grades

Doktorin der Naturwissenschaften (Dr. rer. nat.)

genehmigte Dissertation

von

Nina-Katharina Krahe, M. Sc.

2021

Referent: Prof. Dr. rer. nat. Dr.-Ing. habil. Ralf G. Berger

Korreferent: Prof. Dr. rer. nat. habil. Claus-Peter Witte

Korreferent: Prof. Dr. rer. nat. habil. Dirk Hoffmeister

Tag der Promotion: 09.12.2021

Danksagung

An erster Stelle möchte ich meinem Doktorvater Prof. Dr. Dr. Ralf G. Berger besonders danken, der es mir ermöglichte meine Promotion zu einem sehr spannenden Thema am Institut für Lebensmittelchemie (LCI) unter hervorragenden Arbeitsbedingungen durchzuführen. Ferner bedanke ich mich für die sehr gute wissenschaftliche Betreuung, die stete Diskussionsbereitschaft, das entgegengebrachte Vertrauen und den gewährten Freiraum bei der Durchführung der experimentellen Arbeiten.

Herrn Prof. Dr. Claus-Peter Witte (Institut für Pflanzenernährung, Leibniz Universität Hannover) und Herrn Prof. Dr. Dirk Hoffmeister (HKI Jena) möchte ich für die freundliche Übernahme des Korreferats und Herrn Prof. Dr. Jakob Franke (Institut für Botanik, Leibniz Universität Hannover) für die Bereitschaft, den Vorsitz meiner Disputation zu übernehmen, danken.

Herrn PD Dr. Ulrich Krings und im Besonderen Frau Dr. Franziska Ersoy danke ich für ihre stets offene Tür, ihre Hilfsbereitschaft, Anregungen und wertvollen Tipps, die entscheidend zum erfolgreichen Gelingen dieser Arbeit beigetragen haben. Vielen Dank!

Dr. Diana Linke, Dr. Annabel Nieter und Dr. Kathrin Schulz danke ich herzlich für die anfängliche Betreuung meiner Arbeit.

Dank gilt ebenfalls dem BMBF Cluster *Bioeconomy International* 2015 (031B0307A) für die finanzielle Unterstützung des Projekts „*Monokaryotic strains of* Pleurotus sapidus *to obtain natural products with biological activity using side-streams of the* Citrus *processing industries* (MOPSACI)“, in dessen Rahmen die vorliegende Arbeit entstanden ist.

Ein besonderer Dank gilt allen Kolleginnen und Kollegen, die mich während meiner Zeit am LCI begleitet haben, für die hervorragende Arbeitsatmosphäre sowie gute und hilfsbereite Zusammenarbeit. Die gemeinsam verbrachte Zeit hat mir viel Freude bereitet.

Nicht zuletzt möchte ich mich von ganzem Herzen bei meinen Eltern Heike und Heinz-Friedrich Krahe und im Besonderen meinem Freund Lars Klepzig für die bedingungslose und liebevolle Unterstützung bedanken. Ohne ihr Vertrauen und Verständnis sowie ihren moralischen und emotionalen Beistand über die letzten Jahre wäre diese Arbeit nicht möglich gewesen.

Zusammenfassung

Viele kleine Aldehyde und Ketone sind Aromastoffe mit hohem Wert für die Aromenindustrie. Diese können beispielsweise über die Spaltung analoger Alkene gebildet werden. Biotechnologische Ansätze sind von hohem industriellem Interesse, da sie zur Bildung natürlicher Aromastoffe führen, welche vom Verbraucher besonders im Lebensmittelbereich deutlich bevorzugt werden.

Ein alkenspaltendes Enzym aus *Pleurotus sapidus* (PsaPOX), das das Arylalken *trans*-Anethol zu dem Aromastoff *p*-Anisaldehyd transformiert, wurde als *Dye-decolorizing* Peroxidase (DyP) identifiziert. Die DyP wurde heterolog produziert und biochemisch charakterisiert. PsaPOX enfärbte *β*-Carotin und Annatto. Biotransformationsexperimente verifizierten weiterhin die alkenspaltende Aktivität von PsaPOX gegenüber *trans*-Anethol, welche in Gegenwart von Mn^{2+} erhöht wurde, sowie gegenüber (*E*)-Methylisoeugenol und *α*-Methylstyren, die als Vorläufer von Veratrumaldehyd und Acetophenon dienten. PsaPOX ist die erste beschriebene DyP, für die eine alkenspaltende Aktivität gegenüber Arylalkenen nachgewiesen werden konnte.

Für die Optimierung der Aktivität von PsaPOX wurde eine Tochtergeneration von 100 monokaryotischen *P. sapidus*-Stämmen erzeugt, die sich bezüglich der Wachstumsrate, Peroxidase- und alkenspaltenden Aktivität unterschieden. Die intraspezifische Variabilität der Enzymaktivitäten war stabil, wobei zehn Stämme höhere Aktivitäten als der parentale Dikaryot aufwiesen. Die intraspezifische Variabilität konnte auf die Existenz von drei Enzymvarianten zurückgeführt werden, die sich in ihrer spezifischen Aktivität und Stabilität unterschieden. Weiterhin resultierte die stark erhöhte Enzymaktivität eines der Monokaryoten aus einer erhöhten Expression des entsprechenden *PsaPOX*-Gens.

Die Lipoxygenase $LOX_{Psa}1$ wurde als weiteres alkenspaltendes Enzym von *P. sapidus* identifiziert. Dieses spaltete das Pfefferalkaloid Piperin in Gegenwart von mehrfach ungesättigten Fettsäuren co-oxidativ zu den Vanille-Aromen Piperonal und 3,4-Methylendioxyzimtaldehyd. Durch die Anpassung der Reaktionsparameter wurden die Ausbeuten mit dem rekombinanten Enzym optimiert. Die zuvor generierten monokaryotischen *P. sapidus*-Stämme zeigten auch für die Piperinkonversion eine intraspezifische Diversität.

Schlagworte: Alkenspaltung; Biotransformation; Dikaryot; *Dye-decolorizing* Peroxidase; Genexpression; Genmutation; Intraspezifische Variabilität; Lipoxygenase; Monokaryot; *Pleurotus sapidus*.

Abstract

Many small aldehydes and ketones are aroma compounds that are valuable for the flavor and fragrance industry. These can be formed by the cleavage of analogous alkenes. Biotechnological approaches are of high interest as they yield natural aroma compounds, which are preferred by the consumers especially in the food area.

An alkene cleaving enzyme from *Pleurotus sapidus* (PsaPOX), which transforms the aryl alkene *trans*-anethole to the aroma compound *p*-anisaldehyde, was identified as dye-decolorizing peroxidase (DyP). The DyP was produced heterologously and biochemically characterized. PsaPOX bleached *β*-carotene and annatto. Furthermore, biotransformation experiments verified the alkene cleaving activity of PsaPOX towards *trans*-anethole, which was increased in the presence of Mn^{2+}, and also towards (*E*)-methyl isoeugenol and *α*-methylstyrene, which yielded veratraldehyde and acetophenone, respectively. PsaPOX is the first described DyP with an alkene cleaving activity towards aryl alkenes.

To optimize the activity of PsaPOX, a daughter-generation of 100 monokaryotic *P. sapidus* strains was generated. These strains differed in growth rate, peroxidase and alkene cleaving activity. The intraspecific variability of the enzyme activities was stable, with ten strains showing higher activities than the parental dikaryon. Sequence analysis and heterologous expression identified the intraspecific variability as result of the existence of three enzyme variants, which differed regarding their specific activities and stabilities. Furthermore, the strongly increased activity of one of the monokaryotic strains resulted from the higher expression of the corresponding *PsaPOX* gene.

The lipoxygenase $LOX_{Psa}1$ was identified as additional alkene cleaving enzyme from *P. sapidus*. It cleaved the pepper alkaloid piperine co-oxidatively to the vanilla-like aroma compounds piperonal and 3,4-methylenedioxycinnamaldehyde. The product concentrations were optimized for the biotransformation with the recombinant enzyme. The monokaryotic *P. sapidus* strains, which were generated before, showed an intraspecific diversity also for the piperine conversion.

Keywords: Alkene cleavage; Biotransformation; Dikaryon; *Dye-decolorizing* peroxidase; Gene expression; Gene mutation; Intraspecific variability; Lipoxygenase; Monokaryon; *Pleurotus sapidus*.

Inhaltsverzeichnis

Abkürzungsverzeichnis

AauDyP	DyP aus *Auricularia auricula-judae*
ABTS	(2,2-Azino-di-(3-ethylbenzthiazolin-6-sulfonsäure)
AgaDyP	DyP aus *Armillaria gallica*
a-L	α-Linolensäure
AtCCD1	Carotinoidabbauende Oxygenase aus *Arabidopsis thaliana*
Bis-Tris	Bis(2-hydroxyethyl)amino-tris(hydroxymethyl)methan
BLAST	*Basic local alignment search tool* (Algorithmus für die allgemeine und lokale Sequenzvergleichsanalyse)
BMBF	Bundesministerium für Bildung und Forschung
BMMY	*Buffered methanol medium + yeast extract* (Gepuffertes Minimalmedium mit Methanol und Hefeextrakt)
BSA	*Bovine serum albumin* (Rinderserumalbumin)
CBS	*Centraalbureau voor Schimmelcultures*, Westerdijk *Fungal Biodiversity Institute*
cDNA	*Complementary* (komplementäre) DNA
CHAPS	3-[(3-Cholamidopropyl)dimethylammonio]-1-propanesulfonat
CIS	*Cold injection system* (Kaltaufgabesystem)
CtrDyP	DyP aus *Coriolopsis trogii*
Da	Dalton (atomare Masseneinheit)
DK	Dikaryot
DNA	*Deoxyribonucleic acid* (Desoxyribonukleinsäure)
DSMZ	Deutsche Sammlung von Mikroorganismen und Zellkulturen
DTT	Dithiothreitol
DyP	*Dye-decolorizing peroxidase* (Farbstoff entfärbende Peroxidase)
DyP2B	DyP aus *Pseudomonas fluorescens*
EC	*Enzyme commission number* (Enzymklassifizierungsnummer)

EDTA	*Ethylendiaminetetraacetic acid* (Ethylendiamintetraessigsäure)
EndoH	Endoglycosidase H
ESI	Elektrospray-Ionisation
ESI-MS/MS	Elektrospray-Ionisation-Tandem-Massenspektrometrie
FID	Flammenionisationsdetektor
FPLC	*Fast protein liquid chromatography* (Proteinflüssigchromatographie)
Ftr-DyP	DyP aus *Funalia trogii*
fw	*Forward primer* (Primer in Vorwärtsrichtung)
GC	Gaschromatographie
gDNA	Genomische DNA
GluDyP	DyP aus *Ganoderma lucidum*
GMC	Glucose-Methanol-Cholin
gpd3	Glycerinaldehyd-3-phosphatdehydrogenase
GRAS	*General recognized as safe* (allgemein als sicher anerkannt)
HPLC	*High performance liquid chromatography* (Hochleistungsflüssigkeitschromatographie)
HRP	*Horse radish peroxidase* (Meerrettichperoxidase)
IEF	Isoelektrische Fokussierung
IEX	*Ion exchange chromatography* (Ionenaustauschchromatographie)
IS	Interner Standard
k_{cat}	Wechselzahl
K_m	Michaelis-(Menten-)konstante
LA	Linolsäure
LMMF	*Low molecular mass fraction* (niedermolekulare Fraktion)
LOX	Lipoxygenase
$LOX_{Psa}1$	LOX aus *Pleurotus sapidus*

LRET	*Long range electron transfer* (Langdistanz-Elektronentransfer)
LSD-I	Lignostilben-*α*,*β*-dioxygenase I
MDCA	*3,4-Methylenedioxycinnamaldehyde* (3,4-Methylendioxyzimtaldehyd)
MK	Monokaryot
MM	Minimalmedium
MnLOX	Mangan-Lipoxygenase
MS	Massenspektrometrie
MWCO	*Molecular weight cut off* (Moleküllmassengrenze)
n.d.	Nicht detektiert
NCBI	*National center for biotechnology information* (Nationales Zenter für bioinformatische Informationen)
Ni-IMAC	*Nickel-immobilized metal affinity chromatography* (Nickel-immobilisierte Metallaffinitätschromatographie)
Ni-NTA	*Nickel-nitrilotriacetic acid* (Nickel-Nitrilotriessigsäure)
ODP	*Olfactory detection port* (Olfaktometer)
p.a.	*Pro analysi* (analysenrein)
PAGE	Polyacrylamid-Gelelektrophorese
PCR	*Polymerase chain reaction* (Polymerasekettenreaktion)
PDB	*Protein data bank* (Proteindatenbank)
PDMS	Polydimethylsiloxan
PES	Polyethersulfon
phos	Purinphosphorylase
pI	Isoelektrischer Punkt
PLAT	Polycystin-1, Lipoxygenase, und Alpha-Toxin
Pleos-DyP4, (PosDyP)	DyP aus *P. ostreatus* PC15
PsaPOX	DyP aus *P. sapidus*

PsaPOX_DK	Parentale PsaPOX-Variante
PsaPOX_high	PsaPOX-Variante mit höherer (*higher*) Aktivität als PsaPOX_DK
PsaPOX_low	PsaPOX-Variante mit niedrigerer (*lower*) Aktivität als PsaPOX_DK
PUFA	*Poly-unsaturated fatty acid* (mehrfachungesättigte Fettsäure)
QTOF	*Quadrupole time of flight* (Quadropol-Flugzeitmassenspektrometer)
RB5	*Reactive black* 5 (Reaktiv Schwarz 5)
RBB19	*Reactive blue* 19 (Reaktiv Blau 19)
rev	*Reverse primer* (Primer in Rückwärtsrichtung)
RNA	(*Ribonucleic acid*) Ribonukleinsäure
rpm	*Rounds per minute* (Umdrehungen pro Minute)
RT	Raumtemperatur
RT-qPCR	Quantitative reverse Transkriptase-PCR
SDS	*Sodium dodecyl sulfate* (Natriumdodecylsulfat)
SNL	*Standard nutrient liquid* (Standardnährflüssigkeit)
TDS	Thermodesorptionssystem
TRIS-HCl	Tris(hydroxymethyl)aminomethan-Hydrochlorid
*Tv*DyP1	DyP1 aus *Trametes versicolor*
TveDyP	DyP aus *Trametes versicolor*
U	Unit (µmol/min)
UV	Ultraviolett
v/v	*Volume per volume* (Volumen pro Volumen)
Vis	*Visible (light)* (sichtbares Licht)
VvoDyP	DyP aus *Volvariella volvacea*
w/v	*Weight per volume* (Gewicht pro Volumen)
YEPD	*Yeast extract peptone dextrose* (Hefeextrakt-Peton-Dextrose-Lösung)

Aminosäuren werden nach dem internationalen Ein- bzw. Dreibuchstabencode abgekürzt.

Abbildungsverzeichnis

Tabellenverzeichnis

1 Einordnung der Forschungsthemen und wichtigsten Erkenntnisse aus den Publikationen im Kontext der wissenschaftlichen Literatur

1.1 Basidiomycota

Die Basidiomycota (Ständerpilze) bilden zusammen mit den Ascomycota (Schlauchpilzen) das Unterreich der Dikarya im Reich der Fungi und gehören damit zu den „höheren“ Pilzen [1,2]. Sie umfassen etwa 30.000 Arten und damit ca. 30 % aller bisher beschriebenen Pilze [1]. Die meisten der Basidiomycota werden in die drei Unterabteilungen *Agaricomycotina*, *Pucciniomycotina* und *Ustilaginomycotina* eingeteilt [2]. Zu den beiden letzteren gehören die pflanzenpathogenen Rost- und Brandpilze. Die *Agaricomycotina* (ca. 70 % aller Basidiomycota [2]) beinhalten dagegen verschiedene saprophytische Pilze, die sich von abgestorbenen organischen Materialien ernähren, parasitäre Arten, sowie einige mykorrhizabildende Mutualisten, die in Symbiose mit pflanzlichen Organismen leben [2,3]. Auch die meisten Speisepilze wie der Champignon (*Agaricus bisporus*), der Shitake (*Lentinula edodes*) und der Steinpilz (*Boletus edulis*) gehören den *Agaricomycotina* an. Dies gilt ebenfalls für die Vertreter der Gattung *Pleurotus* (Seitlinge), Holzdestruenten (meist Laub-, selten Nadelhölzer), die weltweit in terrestrischen Ökosysteme auftreten und zu den meist kultivierten Speisepilzen zählen [4–6]. Insgesamt sind elf Arten bekannt [5] – u. a. *Pleurotus sapidus*, der im Rahmen dieser Arbeit genutzt wurde.

Basidiomycota sind heterotrophe Organismen und somit auf die Aufnahme von Nährstoffen aus ihrer Umwelt angewiesen [7]. Hierzu scheiden sie Enzyme aus, die komplexe Substrate in kleinere Moleküle spalten, sodass diese anschließend aufgenommen und verstoffwechselt werden können. Eine effiziente Nährstoffaufnahme wird dabei durch die Erschließung der Nahrungsquelle durch filamentöse Hyphen (vielzellige Pilzfäden) und der damit einhergehenden Bildung eines ausgedehnten und verzweigten Pilzgeflechts, dem sogenannten Myzel, erzielt [1,7]. Die Ausdehnung des Myzels über das Längenwachstum der Hyphen kann der Erschließung neuer Habitate und Nahrungsquellen dienen [7]. Alternativ können sich Basidiomycota über Sporulation (siehe Kapitel 1.1.1) verbreiten.

Unter geeigneten Umweltbedingungen (Lichtexposition, Luftfeuchtigkeit, Temperatur, etc.) können sich aus dem vegetativen Myzel der meisten Basidiomycota Fruchtköper (Basidiokarpien) entwickeln [7]. Diese bestehen aus verzweigten, mehr oder weniger verwachsenen Hyphen, dem Plektenchym (Scheingewebe), und dienen der geschlechtlichen Fortpflanzung [1]. Hierzu werden in der Fruchtschicht (Hymenium) die Basidien (lat.

„kleines Fußgestell“, namensgebend für die Basidiomycota) angelegt, die die Meiosporen (Basidiosporen) bilden (vgl. Kapitel 1.1.1). Aufgrund der äußeren Form ihrer Fruchtkörper können Blätterpilze/Lamellenpilze (z. B. *Pleurotus sapidus*), Röhrenpilze und Bauchpilze unterschieden werden [1]. Bei Blätterpilzen befindet sich das Hymenium auf Lamellen (Hutunterseite), bei Röhrenpilzen auf der Innenseite von Röhren (Hutunterseite) und bei Bauchpilzen im Inneren des Fruchtkörpers (Abbildung 1.1). Daraus resultiert, dass zur Freisetzung der Sporen von Bauchpilzen das Hymenium schon während der Sporenreifung zerfallen muss, sodass eine staubartige Masse (Gleba) aus Sporen und Fasern zurückbleibt, die nach Zerfall des Fruchtkörpers durch Wind oder Insekten verbreitet werden kann. Die Sporen der Lamellen- und Röhrenpilze werden dagegen durch Erhöhung des Turgors (Zellinnendruck) in den Basidien freigesetzt [1].

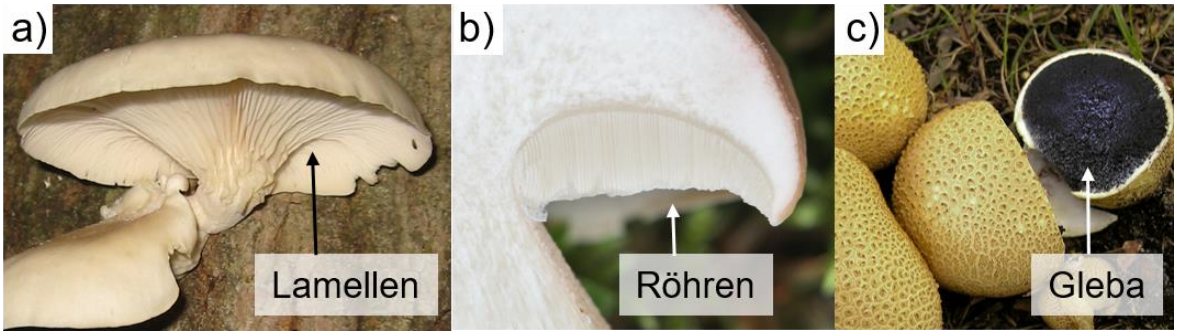

Abbildung 1.1. Fruchtkörper eines **a**) Lamellen-, **b**) Röhren- und **c**) Bauchpilzes. a) *Pleurotus ostreatus* (verändert nach Sherman [8]), b) *Boletus edulis* (verändert nach Kohl [9]) und c) *Scleroderma citrinum* (verändert nach Baker [10]).

1.1.1 Lebenszyklus der Basidiomycota

Basidiomycota durchlaufen innerhalb ihres Lebenszyklus verschiedene Phasen und Entwicklungsstadien [7,11] (Abbildung 1.2). Der Zyklus startet dabei mit der Reifung einer Basidiospore zu einem monokaryotischen Myzel (Monokaryon), das sich aus haploiden Hyphenzellen (ein Zellkern pro Zelle, einfacher Chromosomensatz, 1*n*) bildet. In der Regel ist das monokaryotische Myzel nicht in der Lage, Fruchtkörper auszubilden [12,13], jedoch sind Ausnahmen (z. B. für *Agrocybe aegerita*) bekannt [14,15].

Wenn zwei monokaryotische Hyphenzellen aufeinander treffen, können die Cytoplasmata der Zellen verschmelzen (Plasmogamie) und so eine dikaryotische Zelle ausbilden (Abbildung 1.2) [11]. Hierbei verschmelzen die beiden elterlichen haploiden Zellkerne jedoch nicht, sondern bleiben getrennt erhalten ($n + n$). Voraussetzung für die Paarung ist in der Regel, dass die elterlichen monokaryotischen Myzelien unterschiedliche Kreuzungstypen

aufweisen, welche durch die Allele des oder der *mating-type locus* oder *loci* bestimmt werden [16,17]. Die entsprechenden Genbereiche kodieren für Transkriptionsfaktoren, Pheromonrezeptoren und Pheromon-bildende Proteine, die u. a. an der Bildung und Teilung der dikaryotischen Zellen beteiligt sind [16–18]. Die meisten Basidiomyceten, wie *P. sapidus* [19], besitzen zwei unabhängige *mating-type loci* und damit ein tetrapolares Kreuzungssystem mit mindestens vier Kreuzungstypen [18]. Es sind aber auch bipolare Systeme mit einem *mating-type locus* bekannt [11,17,18]. Monokaryotische Zellen von *Cryptococcus neoformans* können dagegen unter bestimmten Bedingungen auch mit Zellen des gleichen Kreuzungstyps verschmelzen (unipolares Kreuzungssystem) [17].

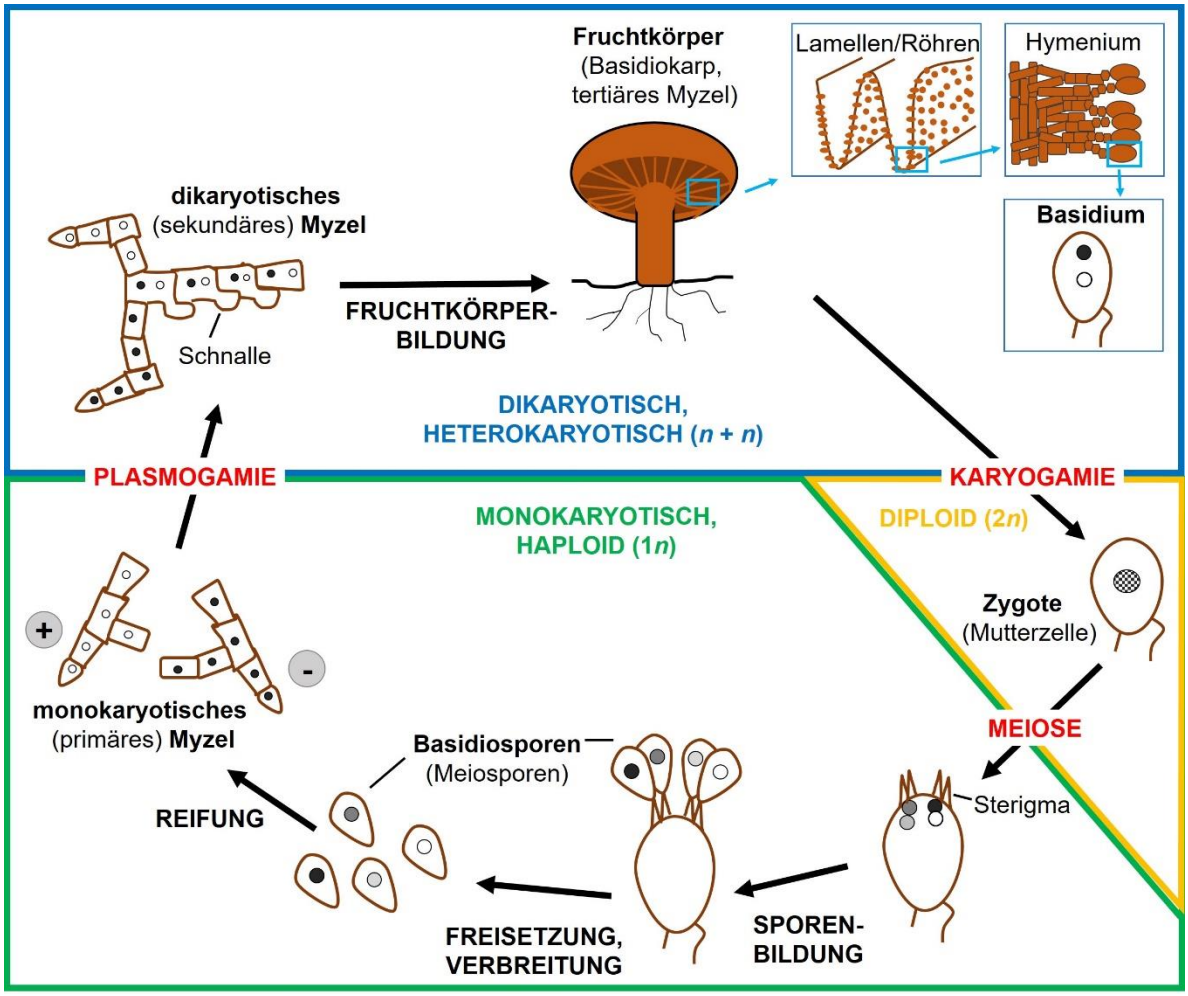

Abbildung 1.2. Schematische Darstellung des Lebenszyklus der Basidiomycota am Beispiel eines Lamellen- oder Röhrenpilzes. *n*: Anzahl der Zellkerne/Chromosomensätze pro Zelle; + und – repräsentieren die unterschiedlichen Kreuzungstypen der monokaryotischen Myzelien. (Frei nach Campbell und Reece [7] und Nieuwenhuis und Aanen [16]).

Die durch die Plasmogamie gebildete dikaryotische Zelle wächst mittels multipler mitotischer Zellteilungen zu einem vegetativen, dikaryotischen Myzel (Dikaryon) heran (Abbildung 1.2) [7]. Hierbei bleibt die Koexistenz der beiden elterlichen Zellkerne erhalten,

indem diese sich parallel teilen. Die gleichmäßige Verteilung der beiden Kerne auf die entstehenden Tochterzellen wird in der Regel durch die Ausbildung sogenannter Schnallen gewährleistet (Abbildung 1.3) [11,15]. Diese sind spezifisch für dikaryotische Zellen und treten im Monokaryon nicht auf, sodass die Enzwicklungsstadien anhand der Schnallen unterschieden werden können [11].

Die dikaryotische Phase kann abhängig von der Pilzart und den vorliegenden Umweltbedingungen Wochen, Monate oder Jahre andauern [2,7] und endet mit der Fruchtköperbildung und einhergehenden Ausbildung der Basidien (vgl. Kapitel 1.1 und Abbildung 1.2) [11]. Im Zuge der geschlechtlichen Fortpflanzung verschmelzen die beiden haploiden Zellkerne im Basidium (Karyogamie), sodass eine Zygote (Mutterzelle) mit diploidem Zellkern (mit zwei Chromosomensätzen) entsteht [7,11]. Anschließend durchläuft der Zellkern die Meiose, welche in die Bildung von vier haploiden Kernen resultiert, die wiederum über die Sporenständer (Sterigma) auf vier Basidiosporen aufgeteilt werden [1,7,11,13]. Nach der Freisetzung der Sporen können diese unter geeigneten Bedingungen zu neuen monokaryotischen Hyphen und Myzelien heranreifen und den Lebenszyklus reinitialisieren.

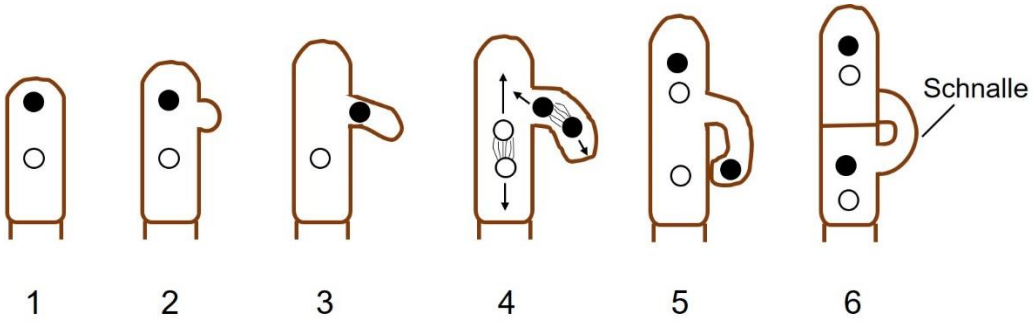

Abbildung 1.3. Wachstum der dikaryotischen Hyphen der Basdiomycota („Schnallenbildung“). Die Endzelle einer dikaryotischen Hyphe (paarkernig mit zwei verschiedengeschlechtlichen Zellkernen; 1) bildet während des Längenwachstums eine seitliche Ausbuchtung (2). Einer der beiden Zellkerne wandert zur Ausbuchtung (3). Anschließend teilen sich die beiden Zellkerne (Mitose; 4). Die Ausbuchtung wächst weiter in Richtung der Basis (unterer Teil) der Endzelle, während zwei verschiedengeschlechtliche Kerne zur Spitze der Zelle wandern (4, 5). Die Spitze der Endzelle wird durch die Bildung von Septen (Zellwände) von der Ausbuchtung und Basis der Mutterzelle abgetrennt, wohingegen an der Kontaktstelle zwischen Basis und Ausbuchtung die Zellwand aufgelöst wird. Der in der Ausbuchtung befindliche Zellkern wandert in die Hyphenzelle. Damit ist der dikaryotische Zustand wieder hergestellt (6). Die mit der Hyphe verwachsene Ausbuchtung wird Schnalle genannt. (Frei nach Lüttge *et al.* [1]).

1.1.2 Intraspezifische Variabilität von Mono- und Dikaryoten

Während der sexuellen Fortpflanzung (vgl. Kapitel 1.1.1) der Basdiomycota kommt es im Rahmen der Meiose zur Rekombination des elterlichen, „dikaryotischen" Erbguts (zufällige Neukombination und Verteilung der elterlichen Chromosomen auf die Basdiosporen und z. T. Austausch von einzelnen DNA-Bereichen zwischen homologen Chromosomen durch *Crossing-over*). Hierdurch unterscheiden sich die aus den Basdiosporen entstehenden Monokaryoten genetisch und auch phänotypisch [11,20]. Die geschlechtliche Fortpflanzung trägt damit zur intraspezifischen (innerhalb einer Art) Variabilität der Basdiomycota bei, die der Anpassung an neue Lebensräume und Umweltbedingungen und damit der Verbreitung der Pilze dienen kann [5,21,22].

Verschiedene Studien wiesen eine Diversität monokaryotischer Basidiomycota untereinander und im Vergleich zum elterlichen Dikaryoten bezüglich ihrer Wachstumsrate, Morphologie sowie ihres Polysaccharid- und Triterpengehalts nach [23–28]. Weiterhin konnte gezeigt werden, dass sich Monokaryoten und Dikaryoten ebenfalls bezüglich ihres Transkriptoms und Sekretoms unterscheiden können [25,29–32]. Orban *et al.* und Freihorst *et al.* detektierten Unterschiede im Volatilom monokaryotischer und dikaryotischer Stämme von *Cyclocybe aegerita* und *Schizophyllum commune*, wobei die Dikaryoten jeweils ein breiteres Spektrum an flüchtigen Verbindungen produzierten als die entsprechenden monokaryotischen Stämme [29,33]. Eine Reihe an Arbeiten beschäftigte sich ebenfalls mit der mono- und dikaryotischen Diversität verschiedener Enzymaktivitäten [20,23,24,28,30,34]. Hierbei lag das Augenmerk hauptsächlich auf den Laccasen und anderen lignolytischen Enzymen wie den Manganperoxidasen. Eine Analyse der intraspezifischen Diversität bezüglich einer *Dye-decolorizing* Peroxidase war vor Beginn der vorliegenden Promotionsarbeit noch nicht durchgeführt worden.

Aufgrund der großen Spannbreite an Laccase- bzw. Lipoxygenaseaktivitäten von mono- und dikaryotischen *P. ostreatus*- bzw. *P. sapidus*-Stämmen vermuteten Eichlerová *et al.*, del Vecchio *et al.* und Omarini *et al.*, dass diese aus einer Heterozygotie der an der Enzymproduktion beteiligten Gene resultiert [24,27,34]. Jedoch führten sie hierzu keine weiteren experimentellen Untersuchungen durch. Nur zwei Studien beschäftigten sich vor der hier dargestellten Promotionsarbeit näher mit der Aufklärung von potentiellen Ursachen für die enzymatischen Unterschiede zwischen Mono- und Dikaryoten [28,30]. Castanera *et al.* wiesen dabei eine erhöhte Genexpression als Ursache für die erhöhte Laccaseaktivität

eines dikaryotischen *P. ostreatus*-Stamms im Vergleich zu seinen elterlichen Monokaryoten nach. [30]. Linke *et al.* stellten dagegen fest, dass die im Vergleich zum parentalen Dikaryot und weiteren Monokaryoten verbesserte carotinoidspaltende Laccaseaktivität eines monokaryotischen *P. ostreatus*-Stamms auf einer erhöhten sekretierten Enzymaktivität beruhte. Die spezifische, biochemische Ursache blieb aber ungeklärt, da experimentelle Analysen den Einfluss einer genetischen Mutation oder einer veränderten Genexpressionsrate des codierenden Gens ausschlossen. Linke *et al.* vermuteten, dass die intraspezifischen Variabilität durch ein multifaktorielles, multiallelisches Expressionssystem oder Unterschiede auf der regulativen Ebene hervorgerufen wurden [28]. Beispielsweise ist posttranskriptionelles Gen-*Silencing* über *small interfering* RNAs oder Transposon-assoziierte DNA-Methylierungen aus Basdiomyceten bekannt [35,36].

Im Rahmen der vorliegenden Arbeit konnte das erste Mal eine genetische Mutation als Ursache für eine intraspezifische enzymatische Variabilität von Mono- und Dikaryoten experimentell nachgewiesen werden.

1.2 Biotechnologie und Biokatalyse

Biotechnologie beschreibt die Anwendung von biologischen Prozessen und Verfahren sowie die Nutzung von lebenden Organismen, Zellen und deren Produkten (z. B. Enzyme) zur Herstellung, Modifizierung und Entwicklung von Produkten oder Bereitstellung von Dienstleistungen [37,38]. Obwohl der Begriff „Biotechnologie“ erst 1919 geprägt wurde, wird sie schon seit vielen Jahrtausenden empirisch genutzt. Beispiele hierfür sind die Herstellung von Bier, Wein, Käse oder Brot, die auf fermentativen Prozessen beruhen [37,39]. Jedoch konnte sich die moderne Biotechnologie erst durch die Entstehung verschiedener wissenschaftlicher Disziplinen, wie u. a. die Mikro-, Molekularbiologie und Biochemie und deren Fortschritte im Laufe des letzten Jahrhunderts entwickeln [39]. Die moderne Biotechnologie ist eine interdisziplinäre und anwendungsbezogene Wissenschaft, die verschiedene Bereiche, Verfahren und Erkenntnisse der Biologie, Medizin, Chemie, Verfahrenstechnik, Ingenieurswissenschaften und Informationstechnologie vereint [40,41].

Neben Anwendungen im medizinischen Bereich (Rote Biotechnologie; z. B. Entwicklung neuer Therapeutika und diagnostischer Verfahren, *Tissue Enginieering* und Stammzelltherapie) und in der Agrar- und Landwirtschaft (Grüne Biotechnologie; z. B. Generierung von resistenten Pflanzen mittels Gentechnik) wird die Biotechnologie auch

industriell genutzt (Weiße oder industrielle Biotechnologie) [37,42]. Beispiele hierfür sind die biotechnologische Produktion diverser Lebensmittelzusatzstoffe, Aromastoffe, Vitamine, Bio-Farbstoffe, -plastik, -kraftstoffe, Pharmazeutika und Chemikalien mittels Biokatalyse [42]. Dabei können zwei grundlegende Produktionswege unterschieden werden: Die *de novo*-Synthese und die Biotransformation [42–44]. Erstere beschreibt die Synthese komplexer Produkte durch Mikroorganismen, die durch die Verstoffwechslung einfacher Startermoleküle, wie z. B. Aminosäuren und Zucker, gebildet werden („Fermentation“) [44]. Als Biotransformation wird dagegen die enzymatische Umwandlung von Vorläufermolekülen zu strukturanalogen Produkten mittels isolierter Enzyme oder Ganzzellsysteme (Mikroorganismen) innerhalb eines oder in seltenen Fällen einiger Reaktionsschritte/s bezeichnet [43,44].

Die Nachfrage nach biotechnologischen Verfahren für die industrielle Produktion und die damit einhergehende Relevanz der industriellen Biotechnologie hat in den letzten Jahren zugenommen [45–47]. Dies resultiert aus dem gewachsenen ökologischen Bewusstsein der Gesellschaft und den politischen und gesellschaftlichen Forderungen nach nachhaltigen und umweltfreundlichen Prozessmethoden [42,48]. Biokatalyse wird als „grüne“, nachhaltige Technologie beschrieben, da sie weniger Abfälle als die traditionelle chemische Synthese produziert und bioabbaubare, in der Regel ungefährliche und aus erneuerbaren Ressourcen gebildete Katalysatoren verwendet [49]. Weiterhin ermöglicht sie die Verwendung von milden Reaktionsbedingungen (verhältnismäßig niedrige Temperaturen, atmosphärischer Druck) und nutzt in der Regel erneuerbare Rohstoffquellen (Biomasse) anstelle von fossilen Rohstoffen als Substrate, wodurch eine verbesserte Öko- und CO_2-Bilanz erzielt wird [42,49]. Ein weiterer Vorteil der Biokatalyse im Vergleich zur chemischen Synthese sind hohe Chemo-, Regio- und Stereoselektivitäten, die eine hohe Reinheit und einfache Isolierung der Biokatalyseprodukte ermöglichen [50,51]. Dies hat z. B. hohe Relevanz für die Produktion von Pharmazeutika.

1.2.1 Nebenströme der Agrar- und Lebensmittelindustrie als Substrat

In der Agrar- und Lebensmittelindustrie fallen jährlich große Mengen verschiedener Nebenströme während der Herstellung und Verarbeitung von Lebensmitteln an [52,53]. Zu diesen zählen u. a. Frucht- (z. B. *Citrus*) und Gemüseschalen (z. B. Kartoffel), Trester (z. B. Trauben oder Apfel), Pulpe (u. a. Kaffee oder Zuckerrübe), Kleie (z. B. Weizen oder Reis) und Ölpresskuchen (z. B. Raps oder Olive) [52,54,55]. In der Regel werden die Nebenströme

als Abfälle entsorgt oder als Dünger oder Viehfutter verwertet. Keine dieser Optionen ist wirtschaftlich interessant oder kann die zunehmende Problematik der „Abfallentsorgung“, die sich aus einer steigenden Nebenstrommenge und dem potentiellen Umweltrisiko bei falscher und unregulierter Entsorgung ergibt, lösen [52].

Eine Alternative bietet die Verwendung der Nebenströme als Nährmedium für die industrielle Biotechnologie, da Nebenströme abhängig von ihrer chemischen Zusammensetzung eine gute Quelle für Polysaccharide, Proteine und Fettsäuren darstellen [53,55]. Weiterhin können die Nebenströme zusätzliche Moleküle enthalten, z. B. sekundäre Pflanzenstoffe, die als Substrat für eine mögliche Biokatalyse dienen. Hieraus ergibt sich, dass die biotechnologische Verwendung der Nebenströme ökonomisch sehr interessant ist, da zum einen die Prozesskosten, die sich zu 38 bis 73 % aus den Nährmedienkosten ergeben, reduziert [56] und zum anderen die Nebenströme zu wertvollen Produkten umgewandelt werden und damit eine Wertsteigerung erfahren [57]. Zusätzlich wird das Konzept der Bioökonomie unterstützt, das eine nachhaltige, biobasierte Kreislaufwirtschaft anstrebt [46].

Verschiedene Produkte wie Aromastoffe, Polymere, Enzyme, Antibiotika oder auch reine Biomasse können auf Nebenstrom-Basis biotechnologisch emers oder submers produziert werden [53,55,58,59]. Ahlborn *et al.* zeigten beispielsweise, dass Apfeltrester gut zur Biomasseproduktion des essbaren Pilzes *P. ostreatus* geeignet ist [58]. Dagegen konnten Nebenströme der Olivenölproduktion für die Bildung von Glucanen durch *Ganoderma ludicum* und *Pleurotus eryngii* genutzt werden [60,61]. Weiterhin ist die Produktion von Pektinasen und Laccasen auf Orangenschalen durch *Pleurotus pulmonarius* bekannt [62]. Orangenschalen wurden ebenfalls, wie auch Weizenkleie, Mandarinen- und Bananenschalen, für die Bildung von Peroxidasen durch verschiedene Basdiomycota genutzt [63–65]. Ein Beispiele für die Aromastoffherstellung ist die Bildung von 3-Phenylpropanal (süß, blumig), 3-Phenyl-1-propanol (Karamel, Zimt), Benzylalkohol (süß, Vanille, Zimt), Zimtaldehyd (Zimt) und Zimtsäuremethylester (fruchtig, erdbeerartig) durch die Kultivierung von *Tyromyces chineus* auf Apfeltrester [66].

1.2.2 Biotechnologisches Potential der Basidiomycota

Obwohl Pilze bereits seit Beginn der Biotechnologie genutzt werden [67,68], rückten Basidiomycota erst in den letzten Jahren zunehmend in den Fokus der biotechnologischen Forschung [69]. Aufgrund ihrer Diversität und ihres weiten Verbreitungsraums weisen

Basidiomycota ein großes Potential für die Entdeckung neuer oder alternativer, industriell interessanter Biokatalysatoren und Naturstoffe auf [70–73]. Dies wird dadurch verstärkt, dass davon ausgegangen wird, dass bisher nur ein Bruchteil aller existierender Arten beschrieben wurde [69,74]. Ein weiterer Vorteil ist, dass sich die Basidiomycota an verschiedene Kohlenstoff- und Stickstoffquellen anpassen und hierdurch auf unterschiedlichen Substraten, wie auch industriellen Nebenströmen, wachsen können [58,59,61,62,66,75]. Weiterhin weisen die Vertreter der essbaren „Pilze" den GRAS-Status („*Generally Recognized As Safe*") auf, was eine Applikation in der Lebensmittelindustrie erleichtert [57].

Verschiedene Arbeiten haben gezeigt, dass Basidiomycota verschiedene Pharmazeutika, Fungizide und Pestizide bilden können [72]. Weiterhin ist die Bildung von verschiedenen für die Industrie interessanten Aromastoffen bekannt. Beispielsweise bildet *Fomitopsis betulina* das nach Ananas riechende Polyketid (5*E*/*Z*,7*E*,9)-Decatrien-2-on [76] und *Nidula niveo-tomentosa* 4-(4-Hydroxyphenyl)-butan-2-on, ein Keton mit Himbeeraroma, das in der Himbeere selbst nur in äußerst geringen Mengen vorkommt [77]. Das lyophilisierte Myzel von *P. sapidus* kann biokatalytisch das Minzaroma Verbenol bzw. das *Citrus*-Aroma Perillen durch die Oxidation der entsprechenden Vorläufermoleküle bilden [78,79].

Basidiomyceten weisen weiterhin ein breites Spektrum an intra- und extrazellulären Enzymen auf. Holzzersetzende Basidiomycota produzieren und sekretieren eine Reihe von spezialisierten Enzymen, um die Lignocellulose (hauptsächlich bestehend aus Lignin, Cellulose und Hemicellulose) pflanzlicher Biomasse abzubauen und als Nährstoffquelle zu nutzen [75]. Hierzu zählen u. a. Lignin-degradierende Oxidoreduktasen, wie Laccasen und Peroxidasen (Lignin-, Mangan-, versatile und *Dye-decolorizing* Peroxidasen) [69,80–82] und verschiedene Hydrolasen, die Cellulose und Hemicellulose spalten [83]. Verschiedene Studien haben gezeigt, dass die genannten Enzyme nicht nur von ökologischer Relevanz sind, sondern auch biotechnologisches Potential besitzen [73,81,84]. So können Laccasen in der Papierproduktion zur Bleichung von Zellstoff verwendet werden, da sie das enthaltene Lignin, das zu einer unerwünschten bräunlichen Färbung führt, abbauen [85]. Lanfermann *et al.* stellten die Eignung zweier Isoenzyme einer Manganperoxidase aus *Ganoderma applantum*, die *β*-Carotin spalten, zur Applikation als Bleichmittel in Waschmitteln fest [86]. Eine Chlorogensäureminderung zur Herstellung von bekömmlicheren Kaffeegetränken durch die Behandlung mit einer Ferulasäureesterase aus *Rhizoctonia solani* wurde von Siebert *et al* beschrieben [87,88]. Auch andere basidiomycetische Enzyme wie Peptidasen aus *P. pulmonarius* und *Piptoporus soloniensis* sowie eine Lipase aus *P. ostreatus* wiesen

biotechnologisches Potential auf (z. B. Applikation in der Waschmittel-, Lebensmittel- oder Textilindustrie) [89–91].

Nachfolgend sollen die für diese Arbeit relevanten Enzymklassen näher betrachtet werden.

1.2.2.1 Dye-decolorizing Peroxidasen

Dye-decolorizing Peroxidasen (DyPs) (EC: 1.11.1.19) gehören zu den Oxidoreduktasen und bilden eine relativ neue Superfamilie der Häm-Peroxidasen, die aufgrund ihrer Fähigkeit verschiedene Farbstoffe abzubauen benannt wurde [82,92,93]. Der erste Vertreter wurde 1999 aus dem Basidiomyceten *Bjerkandara adusta* (zunächst fälschlicherweise als *Geotrichum candidum* identifiziert) isoliert [82,93–95]. Typischerweise degradieren DyPs xenobiotische Anthrachinonfarbstoffe, welche kaum von anderen Peroxidasen oxidiert werden können [92]. Weiterhin wurde der Abbau von Azo- und natürlichen Farbstoffen wie *β*-Carotin oder Annatto beobachtet [93,96–98]. Aber auch typische Peroxidase-Substrate wie ABTS (2,2‘-Azino-di(3-ethylbenzthiazolin-6-sulphonsäure)) und verschiedene phenolische Substanzen können durch DyPs oxidiert werden [98,99]. Die natürliche Funktion der DyPs ist noch nicht abschließend geklärt. Es wird aber vermutet, dass sie unterschiedliche physiologische Funktionen besitzen, da DyPs für eine Vielzahl an Organismen beschrieben wurden [82]. Dazu zählen überwiegend Bakterien, aber auch eine Reihe an Basidiomycota [99,100]. Es wird vermutet, dass basidiomycetische DyPs beispielsweise dem Schutz vor antifungalen Anthrachinonen dienen könnten [82,101]. DyPs scheinen aber auch am Abbau von Lignin beteiligt zu sein [82].

Struktur- und Sequenzanalysen zeigten, dass sich die DyPs stark von den klassischen Häm-Peroxidasen unterscheiden, sodass 2007 die neue Familie der *Dye-decolorizing* Peroxidasen klassifiziert wurde [102]. Diese unterteilt sich in die Subklassen A–D [99,100]. Vertreter der Klassen B und C sind vorwiegend intrazelluläre, bakterielle Enzyme, wohingegen Klasse A DyPs beinhaltet, die ein Signal für einen Tat-abhängigen Transport aufweisen und damit in der Regel sekretiert werden. Bei Enzymen der Klasse D handelt es sich hauptsächlich um pilzliche DyPs [100]. Yoshida und Sugano schlugen 2015 ein weiteres Klassifizierungsmodel vor, das anders als zuvor (Klassifizierung anhand der Primärstruktur der Enzyme) auf dem Vergleich der tertiären Struktur der DyPs beruht [103]. Hierdurch werden die DyPs in drei Klassen eingeteilt: I (*Intermediate*, entspricht Subklasse A), P (*Primitive*, entspricht Klasse B) und V (*adVanced*, vereinigt Subklasse C und D). Es zeigt sich, dass die dreidimensionale Struktur der DyPs im Allgemeinen sehr konserviert ist, auch wenn sich die Subklassen

bezüglich ihrer Sequenzidentität stark unterscheiden [100,103]. Die Strukturen der Klassen I und V bauen dabei auf der Struktur der Klasse P auf. Typischer Weise besitzen DyPs eine molekulare Masse zwischen 50 und 60 kDa, wobei bakterielle Enzyme auch kleiner sein können [100]. Weiterhin treten DyPs sowohl als Monomere (meist basidiomycetische DyPs) als auch als Oligomere (Dimere bis Hexamere, meist bakterielle DyPs) auf [95,100].

Die Grundstruktur der DyPs besteht aus zwei Domänen mit Ferredoxin-ähnlicher Struktur, die wiederum aus α-Helices und vier antiparallelen β-Faltblättern gebildet werden [95,99]. Damit unterscheiden sich DyPs strukturell von den klassischen Häm-Peroxidasen, die hauptsächlich aus α-Helices bestehen [104,105]. Zwischen den beiden Domänen der DyPs befindet sich die Häm- bzw. Wasserstoffperoxid-Bindedomäne (aktives Zentrum) mit einem nicht-kovalent gebundenen Häm als Cofaktor sowie dem konservierten, DyP-typischen GXXDG-Motiv [95,99,100]. Weiterhin beinhaltet diese einen Arginin- und einen katalytischen Asparaginsäurerest (Bestandteil des GXXDG-Motivs) oberhalb der Häm-Ebene (distal) sowie ein Histidin unterhalb der Häm-Ebene (proximal, dient als fünfter Ligand für das Häm-Eisen [106]) (Abbildung 1.4) [95]. Damit ist die Häm-Bindedomäne der DyPs zwar ähnlich aufgebaut wie die der klassischen Häm-Peroxidasen, jedoch weisen letztere Histidin anstelle von Asparaginsäure als katalytische Aminosäure auf [95,102,107]. Dies erklärt, wieso DyPs in der Regel ein niedrigeres pH-Optimum als klassische Peroxidasen besitzen [82,102].

Der katalytische Zyklus der DyPs startet mit Eintritt eines Wasserstoffperoxidmoleküls in die Häm-Bindedomäne (Abbildung 1.4). Dort katalysiert der deprotonierte Asparaginsäurerest (Aspartat) die Bindung des Wasserstoffperoxids und des Häm-Eisens sowie die Umlagerung eines Protons des Wasserstoffperoxids mittels eines Schwingmechanismus [106,108]. Hierdurch kommt es zur heterolytischen Spaltung des Wasserstoffperoxids, die in der Bildung von Wasser und der gleichzeitigen Oxidation des Häm-Cofaktors zu Verbindung I (radikalisch-kationische Oxoferryl-Spezies) resultiert [106]. Der distale Argininrest unterstützt durch die Koordination des Wasserstoffperoxids dessen heterolytische Spaltung und stabilisiert ebenfalls die entstehende Verbindung I [106]. Durch die Oxidation von zwei Substratmolekülen wird Verbindung I reduziert, sodass der Ruhezustand des Enzyms wiederhergestellt wird. Dieser Prozess erfolgt vermutlich analog zum Mechanismus der klassischen Häm-Peroxidasen in zwei Schritten (Ein-Elektronen-Übertragung) mit Verbindung II als Intermediat [107]. Jedoch konnte Verbindung II, im Gegensatz zu Verbindung I, nicht für alle DyPs nachgewiesen werden [82,109]. Shrestha *et*

al. stellten die Vermutung auf, dass Verbindung I durch die gleichzeitige Übertragung von zwei Elektronen während der Substratoxidation ohne Übergangszustand direkt in den Ruhezustand des Häms überführt werden kann (Abbildung 1.5) [110]. Dem widerspricht jedoch die Tatsache, dass die Deaktivierung von DyPs in Gegenwart eines Wasserstoffperoxidüberschusses (*suicide inhibition*) beobachtet wurde [111,112]. Das Phänomen ist auch von klassischen Peroxidasen bekannt und resultiert aus der Bildung von Verbindung III (Fe^{III}–O_2) durch die Reaktion von Verbindung II mit Wasserstoffperoxid [113,114].

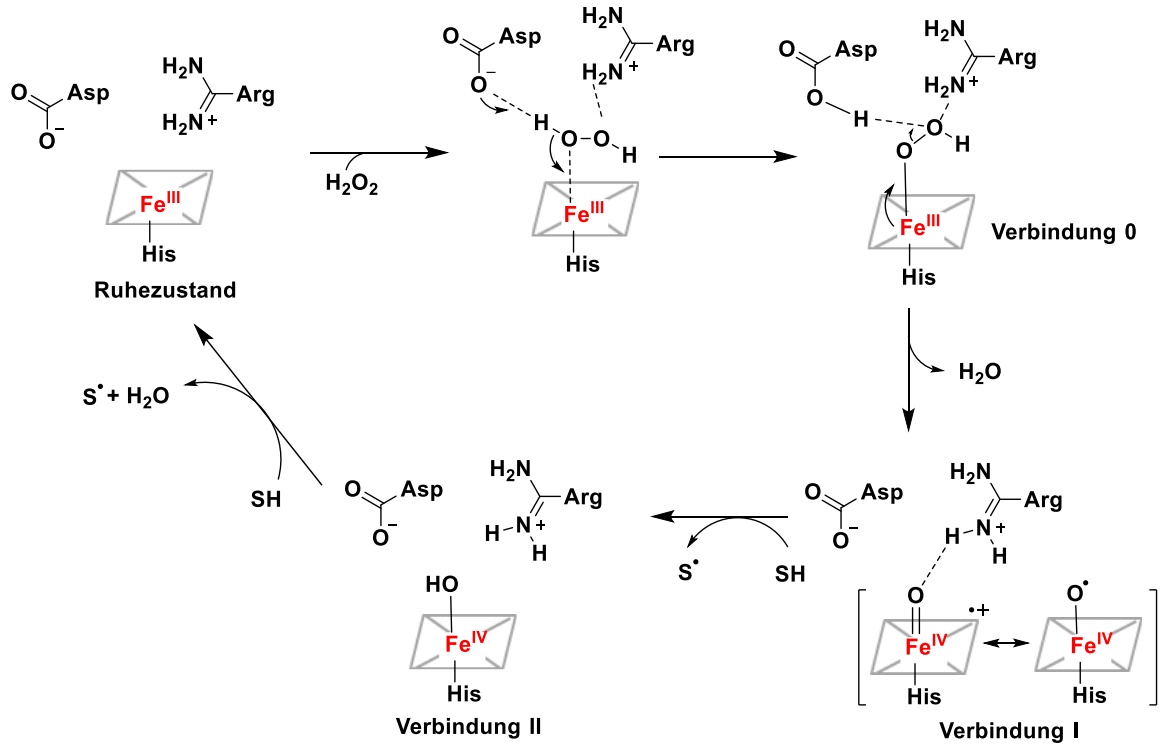

Abbildung 1.4. Katalytischer Mechanismus der *Dye-decolorizing* Peroxidasen. Schematisch dargestellt ist das aktive Zentrum mit dem Häm-Cofaktor (in grau, Häm-Eisen in rot) sowie den wichtigsten Aminosäureresten (Asparaginsäure/Aspartat: katalytische Aminosäure, Arginin: unterstützt bei der heterokatalytischen Wasserstoffperoxidspaltung und stabilisiert Verbindung I, Histidin: fünfter Ligand des Häm-Eisens). S: Substrat. (Frei nach Hofrichter *et. al* [92] und Pfanzagl *et al.* [115]).

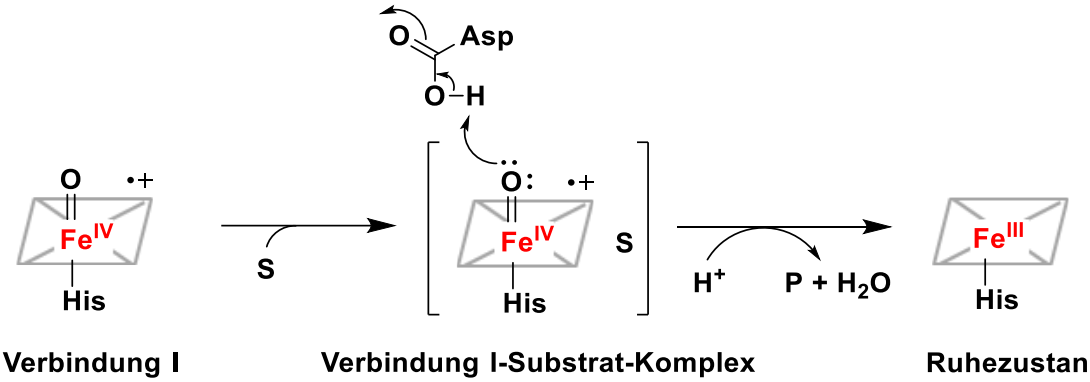

Abbildung 1.5. Schematische Darstellung der Zwei-Elektronen-Oxidation eines Substratmoleküls durch Verbindung I. Dargestellt ist der Häm-Cofaktor (in grau, Häm-Eisen in rot). S: Substrat, P: Produkt. (Frei nach Shrestha *et. al* [110] und Sugano und Yoshida [82]).

Bemerkenswerterweise können DyPs auch Substrate (z. B. Lignin oder *Reactive Blue* 19) oxidieren, die zu groß für die Häm-Bindetasche sind und damit nicht direkt mit dem Häm-Cofaktor interagieren können [82,116]. Dies scheint aus einem Langdistanz-Elektronentransfer (*long-range electron transfer*, LRET) von einer Oxidationsstelle auf der Enzymoberfläche zum Häm zu resultieren wie Linde *et al.* für eine DyP aus *Auricularia auricula-judae* zeigten [106,116]. Ein Tryptophan-Rest an Position 377 (Trp-377) wurde als wahrscheinlichste Oxidations-Stelle identifiziert [106,116] und eine Elektronenübertragung von dort über Pro-310/Arg-309, Arg-306 und His-304 zum Häm und eine gleichzeitige antiparallele Übertragung eines Radikals auf das Substrat vermutet [116]. Sequenzvergleiche mit anderen basidiomycetischen DyPs zeigten, dass auch diese einen homologen Tryptophanrest zu Trp-377 besitzen [95,116].

Fernandez-Fueyo *et al*. wiesen neben einer Oxidationsstelle für große Substratmoleküle eine weitere Oxidationsstelle für Mn^{2+}-Ionen auf der Oberfläche für eine DyP aus *P. ostreatus* nach, die aus vier aziden Resten (drei Aspatat- und ein Glutamatrest) gebildet wird. Ausgehend vom Glutamat-Rest findet von dort ein LRET über einen essentiellen Tyrosinrest zum Häm-Cofaktor statt [117]. Mn^{2+}-Oxidation wurde auch für einige andere basidomycetische wie auch bakterielle DyPs beobachtet [118–122].

Mögliche industrielle Applikationen für DyPs sind die Aufbereitung von Farbstoff-kontaminierten Abwässern oder der Einsatz in der Papierindustrie zur Zellstoffbleichung [100,123]. Weiterhin kann eine DyP aus *Marasmius scorodonius* (MsP1 bzw. MaxiBright™), für die Entfärbung von Molke durch den Abbau von Carotinoiden in der Käseherstellung verwendet werden [124]. Auch ein Einsatz in der Aromenindustrie ist denkbar, wie die Spaltung von verschiedenen Carotinoiden durch MsP1 zeigte, die in der Bildung verschiedener Aromastoffe wie *β*-Ionon oder *β*-Cyclocitral resultiert [125].

1.2.2.2 Lipoxygenasen

Lipoxygenasen (LOX) (EC: 1.13.11.12) sind Nicht-Häm-Eisenhaltige Dioxygenasen und gehören zu den Oxidoreduktasen. Sie katalysieren die regio- und stereoselektive Insertion von molekularem Sauerstoff in mehrfach ungesättigte Fettsäuren (*polyunsatturated fatty acids*, PUFAs) wie Linol-, Arachidon- oder Linolensäure, die mindestens ein 1*Z*,4*Z*-Pentadiensystem aufweisen. Hierdurch entstehen Fettsäurehydroperoxide mit einer konjugierten *E,Z*-Dienstruktur [126–128]. LOX treten ubiquitär in Pflanzen und Tieren auf und wurden auch in anderen Organismen wie Pilzen nachgewiesen [126,128–130]. Für die Basidiomycota sind bisher nur wenige isolierte Enzyme bekannt. Diese stammen aus einigen *Pleurotus*-Arten und *Agrocybe aegerita* [131–134]. Die Klassifizierung der LOX erfolgt anhand der Spezifität für die Position der Sauerstoffinsertion (Kohlenstoffnummer) [129]. Typische Substrate pflanzlicher LOX sind Linolsäure und *α*-Linolensäure (9- und 13-LOX), wohingegen tierischen LOX bervorzugt Arachidonsäure oxidieren (5-, 8-, 12- und 15-LOX) [129,135]. Die durch die LOX gebildeten Hydroperoxide haben verschiedene biologische Funktionen und können beispielsweise als Oxidantien oder als Vorläufer für Signalmoleküle (z. B. Jasmonate (Pflanzen) und Leukotriene (Tiere)) dienen, die an der Regulation verschiedener physiologischer Prozesse (z. B. Wundheilung oder Entzündungsreaktionen) beteiligt sind [128,130]. Es wird vermutet, dass pilzliche Oxilipine u. a. am programmierten Zelltod, *quroum sensing* und der Mycotoxinbildung einiger Pilzarten wie *Aspergillus ochraceus* beteiligt sind [136].

Obwohl sich LOX bezüglich ihrer Größe (z. B. Pflanzen: 90–110 kDa [135], Tiere: 75–80 kDa [137]), Substratspezifität und auch Aminosäuresequenz unterscheiden, sind sie sich strukturell sehr ähnlich [126,127,129]. LOX sind monomere Proteine, die in der Regel aus zwei Domänen bestehen: der kleineren N-terminalen PLAT (Polycystin-1, Lipoxygenase, und Alpha-Toxin)-Domäne, die eine *β*-Fassstrukur bildet, sowie der größeren katalytischen und helikalen C-terminalen Domäne [127,129]. Es wird vermutet, dass die PLAT-Domäne an der Membranbindung der LOX beteiligt ist und Einfluss auf die Enzymaktivität und -stabilität hat. Dennoch scheint sie nicht essentiell zu sein, da einige LOX ohne PLAT-Domäne existieren [129]. Die C-terminale Domäne beinhaltet das aktive Zentrum mit dem katalytischen Nicht-Häm-Eisen [127,129]. Letzteres ist in einigen ascomycetischen LOX, die als Mangan-Lipoxygenasen (MnLOX) bezeichnet werden, durch Mangan ersetzt [129]. Der Aufbau ihres aktiven Zentrums sowie ihr katalytischer Mechanismus entsprechen aber

prinzipiell dem der herkömmlichen Eisen-Liopxygenasen [129,138]. Das katalytische Zentralatom der LOX wird von fünf Aminosäuren-Liganden sowie einem Hydoxidion bzw. Wassermolekül koordiniert (Abbildung 1.6), sodass sich eine oktaedrische Koordinationssphäre ausbildet [127]. Bei den konservierten Aminosäureliganden handelt es sich um die Seitengruppen dreier Histidine und eines Asparagins sowie um die Carboxylgruppe eines C-terminalen Isoleucins. In tierischen LOX ist das Asparagin durch ein weiteres Histidin ersetzt und MnLOX weisen häufig ein Valin anstelle des Isoleucins auf [129,130].

Von der Proteinoberfläche ausgehend hin zum aktiven Zentrum erstreckt sich eine hydrophobe Substratbindetasche durch die PUFAs zum aktiven Zentrum gelangen [139]. Eindringtiefe und Substratorientierung (Carboxyl- oder Methylende zuerst) beeinflussen dabei die Regiospezifität der LOX-Reaktion [130,140]. Weiterhin entscheidet die sogenannte „*Coffa site*“ (eine Aminosäure im aktiven Zentrum; Alanin oder Glycin) über die Stereospezifität [137]. Der für die Reaktion benötigte Sauerstoff gelangt vermutlich über spezielle Kanäle in das aktive Zentrum [140].

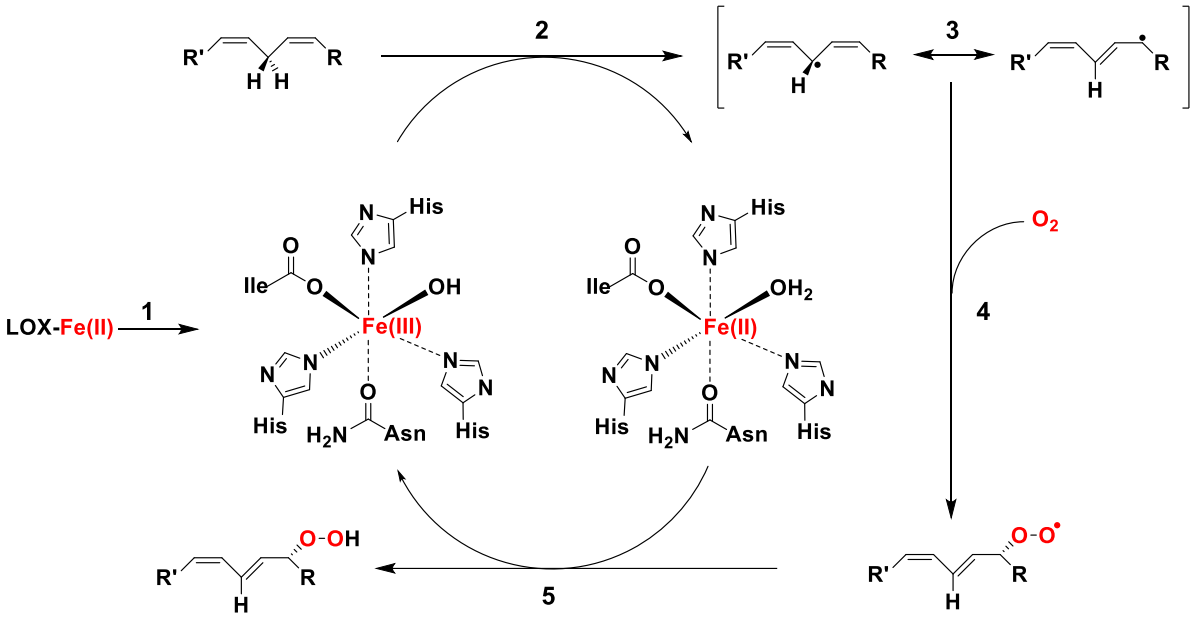

Abbildung 1.6. Katalytischer Mechanismus der Lipoxygenasen. 1) Aktivierung, 2) Wasserstoffabstraktion, 3) Radikalumlagerung, 4) Insertion von molekularem Sauerstoff, 5) Peroxyradikalreduktion. Fe(III): aktiver Zustand der LOX, Fe(II): inaktiver Zustand. Eisen ist in MnLOX durch Mangan ersetzt. Asparagin kann durch Histidin (tierische LOX) und Isoleucin durch Valin (MnLOX) ersetzt sein. (frei nach Hayward *et. al* [127]).

Der radikalische Mechanismus der LOX-katalysierten Oxygenierung von PUFAs verläuft in fünf Schritten (Abbildung 1.6): Der erste Schritt beschreibt die Aktivierung des inaktiven Enzyms (Fe(II)), welche die Initialisierung der Reaktionszyklus bewirkt. Hierbei wird Fe(II)

durch bereits vorhandene Fettsäurehydroperoxide zu Fe(III) oxidiert (Abbildung 1.6, 1) [127,128]. Der folgende Schritt ist geschwindigkeitsbestimmend für die Gesamtreaktion und beschreibt die Abstraktion eines Protons der PUFA aus bisallylischer Position durch den Hydroxid-Liganden des Eisenkomplexes. Das hierbei frei werdende Elektron wird auf Fe(III) übertragen, wodurch dieses zu Fe(II) reduziert wird (Abbildung 1.6, 2) [127,141]. Das entstandene Pentadienylradikal wird Mesomerie-stabilisiert und unter Ausbildung eines konjugierten *Z,E*-Diensystems um zwei Positionen in Richtung des Carboxyl- oder Methylendes der PUFA verschoben (Abbildung 1.6, 3) [126,127]. Anschließend erfolgt die antarafaciale Insertion (von der gegenüberliegenden Seite im Vergleich zur Wasserstoffabstraktion) von molekularem Sauerstoff, die in der Bildung eines Peroxiradikals resultiert (Abbildung 1.6, 4) [129,139]. Im letzten Schritt wird das Peroxiradikal unter Rückgewinnung des aktiven Enzyms (Fe(III)) zunächst zum korrespondierenden Anion reduziert, welches anschließend durch ein Proton des Wasser-Liganden des Eisens zum Fettsäurehydroperoxid protoniert wird (Abbildung 1.6, 5) [129,141].

Neben der Dioxygenierung von PUFAs können LOX auch die oxidative Entfärbung von verschiedenen Pflanzenfarbstoffen, wie *β*-Carotin, Canthaxanthin und Chlorophyll *a* katalysieren [142–144]. Jedoch ist hierfür die Gegenwart von PUFAs erforderlich, wodurch die Pigmententfärbung auf einen co-oxidativen Prozess zurückgeführt wurde [126,144]. Auch andere LOX-katalysierte Co-Oxidationen wurden beobachtet. So wiesen Gorden und Barimalaa den Abbau von fettlösliche Vitaminen (Vitamin A, D_2, D_3 und E) mit einer LOX aus der Sojabohne nach, wohingegen Waldmann und Schreier die Epoxidierung von ungesättigte Verbindungen wie *β*-Ionon und 4-Hydroxy-*β*-ionon zeigten [145,146]. Auch die Co-Oxidation von anderen Substraten wie Guaiacol, Benzidin oder Triphenylfarbstoffen ist bekannt [147,148]. Weiterhin wird vermutet, dass co-oxidative Prozesse an der Verbesserung der Rheologie von Brotteigen in Gegenwart von LOX beteiligt sind [127]. Arens *et. al.* stellten die Vermutung auf, dass die LOX-katalysierten Co-Oxidationsreaktionen durch Radikale des LOX-Reaktionszyklus verursacht werden, da die LOX-gebildeten Hydroperoxide alleine nicht zum Abbau von *β*-Carotin führten [149]. Diese Hypothese konnte durch verschiedene Inhibitionsstudien, die LOX-Co-Oxidationen in Gegenwart von Antioxidantien (Radikalfänger) wie Tocopherol und verschiedene Flavonoide untersuchten, bestätigt werden [147,150]. Jedoch ist der genaue Mechanismus der LOX-katalysierten Co-Oxidation bisher noch ungeklärt. Es wird aber vermutet, dass verschiedene Vertreter des

katalytischen LOX-Mechanismus wie LOX-Fe(II)-PUFA• und LOX-Fe(II)-PUFA-OO• mit ungesättigten Substraten interagieren können [126].

LOX werden bereits industriell für die Entfärbung und Verbesserung der rheologischen Eigenschaften von Teigen in der Backindustrie während der Herstellung von Weizenbrot verwendet [127]. Weiterhin zeigen sie Potential für die Aromastoffproduktion, da sie beispielsweise an der Bildung von C6- und C9-Aldehyden und Alkoholen mit frischem grünem Geruch beteiligt sind oder auch das blumig riechende *β*-Ionon aus *β*-Carotin mittels Co-Oxidation bilden können [129,151]. Zusätzlich wird das wertvolle Grapefruit-Aroma Nootkaton durch Transformation von (+)-Valencen mit einer Lipoxygenase aus *P. sapidus* ($LOX_{Psa}1$) gebildet [133,152–154]. Im Verlauf der vorliegenden Arbeit wurde festgestellt, dass dieses Enzym ebenfalls für die Biotransformation von Piperonal zu den Vanille-Aromen Piperonal und 3,4-Methylendioxyzimtaldehyd durch *P. sapidus* verantwortlich ist (Vgl. Kapitel 10).

1.2.3 Optimierung von Biokatalysatoren und Produktionsstämmen

Die Wirtschaftlichkeit eines Bioprozesses ist von großer Bedeutung für die industrielle Implementierung. Wesentliche Faktoren sind dabei die Produkt-Zeit-Ausbeute sowie die Gesamtkosten des Prozesses, welche durch die Effektivität der Biokatalyse bzw. des/der verwendeten Biokatalysators/en (isoliertes Enzym oder als Bestandteil des mikrobiellen Produktionsstammes) mitbestimmt werden [155]. Eine ausreichende Enzymkonzentration, Enzymaktivität, -stabilität, Substrataffinität und -spezifität sind also von hoher Wichtigkeit. Häufig ist hierfür die Optimierung des gewählten Produktionsstamms bzw. des/der Enzyms/e erforderlich [155,156]. Mögliche gentechnische Ansatzpunkte und Verfahren sind aus der Literatur bekannt [155,157–159].

Zur Erhöhung der Enzymproduktion können zusätzliche Kopien des kodierenden Gens in den Produktionsstamm eingebracht oder die Überexpression dieses Gens induziert werden. Letzteres kann beispielsweise durch Veränderungen im zugehörigen Promotorbereich erreicht werden [155,159]. Eine Verbesserung der spezifischen Enzymaktivität, Enzymstabilität, -affinität und -spezifität ist dagegen durch die Veränderung der Aminosäuresequenz über die Mutation des korrespondierenden Gens möglich. Hierbei können zwei Ansätze unterschieden werden: die zufällige Mutagenese (*Directed Evolution*), die unspezifische Verfahren wie *error-prone* PCR oder DNA *shuffling* verwendet, und das *Rational Protein Design*, das die gezielte Änderung bestimmter Proteinbereiche (z. B. mittels

site-directed Mutagenese) nutzt und Kenntnisse über die Art und Funktion der Aminosäuresequenz des Zielproteins erfordert [157,158]. Teilweise bietet sich auch eine heterologe Enzymproduktion in einem anderen Organismus (z. B. *Escherichia coli* oder *Komagataella phaffii* [160,161]) an, um die Raum-Zeit-Ausbeuten der Enzymproduktion und, damit eingehend, der Biokatalyse zu verbessern [162].

Gentechnische Arbeiten, wie auch die Herstellung und Verwendung gentechnisch veränderter Organismen, sind gesetzlich streng reguliert [163,164]. Weiterhin werden Gentechnik und gentechnisch erzeugte Produkte allgemein von der europäischen Bevölkerung, im Besonderen im Lebensmittelbereich, abgelehnt [50,165]. Daher sind alternative Methoden zur Optimierung von Biokatalysatoren und Produktionsstämmen für die industrielle Biokatalyse von Interesse. Eine Option bietet die sexuell erzeugte genetische und biochemische intraspezifische Variabilität monokaryotischer Basidiomycota (vgl. Kapitel 1.1.2). So haben verschiedene Studien gezeigt, dass monokaryotische Tochterstämme ihren parentalen dikaryotischen Elternstamm nicht nur anhand ihrer Wachstumsgeschwindigkeit, sondern auch bezüglich der Enzymaktivität übertreffen können [20,24,27,28]. Linke *et al.* zeigten, dass die erhöhte *β*-Carotinabbauende Laccaseaktivität eines Monokaryons von *P. ostreatus* langzeitstabil war [28]. Die Bildung einer monokaryotischen Tochtergeneration kann damit der Identifikation neuer, natürlicher Stämme mit optimiertem Biokatalysepotential dienen und folglich eine Alternative zu gentechnischen Optimierungsverfahren bieten. Einige Studien konnten weiterhin zeigen, dass die Kreuzung monokaryotischer Stämme ebenfalls in der Bildung eines optimierten neuen dikaryotischen Stammes resultieren kann [24,27,30,34]. Die Kreuzung zweier monokaryotische *P. ostreatus*-Stämme, die eine höhere bzw. stark erhöhte Carotinabbauende Aktivität im Vergleich zum dikaryotischen Elternstamm besaßen, führte hingegen zur Bildung eines Dikaryoten mit nur ähnlicher Aktivität wie die des elterlichen Ursprungsstamm [28]. Eine vorherige Aussage über den Erfolg der Kreuzung lässt sich also anhand der Aktivitätsleistung der elterlichen Monokaryoten nicht treffen.

1.3 Aromastoffe

Ursache für die Geruchswahrnehmung ist die Interaktion von flüchtigen, mehr oder minder hydrophoben, geruchsaktiven Molekülen (Molekulare Masse <300-350 g/mol), die als Geruchs- oder Aromastoffe bezeichnet werden, mit den Rezeptoren der Riechsinneszellen in der Nase [166,167]. Dabei können die Aromastoffe orthonasal (direkt durch die Nase) oder

retronasal (über die Mund-Rachen-Nasen-Verbindung, z. B. beim Kauen von Lebensmitteln) aufgenommen werden [168]. Neben ihrer eigentlichen Geruchsfunktion spielen Aromastoffe damit auch eine wichtige Rolle bei der Bildung eines Geschmackeindruckes, der sich durch das Zusammenspiel von Geschmacks- (salzig, sauer, bitter, süß, umami), Textur- und Geruchseigenschaften zusammensetzt [168,169]. Die Aromastoffe können in verschiedene chemischen Klassen (u. a. Alkohole, Aldehyde, Ketone, Säuren, Ester, Phenole, Terpene) eingeteilt werden [167], wobei die Art der funktionellen Gruppen einen geringeren Einfluss auf den Geruch einer Substanz hat als die geometrische Struktur [169]. Hierbei spielt auch die Stereokonformation eine Rolle, wie z. B. der unterschiedliche Geruchseindruck von (*R*)-(-)- (Pfefferminze) und (*S*)-(+)-Carvon (Kümmel) (Abbildung 1.7) zeigt [170].

Industrielle Anwendung finden Aromastoffe in der Lebensmittel-, Kosmetik-, chemischen und pharmazeutischen Industrie in einer Vielzahl von Produkten [43]. Dabei ist die Nachfrage nach Aromastoffen steigend wie die Zunahme des weltweiten Umsatzes der Aromenindustrie um etwa 4 bis 5 % jährlich zeigt [43]. In 2019 wurde allein ein Umsatz von fast 35 Mrd. US$ erzielt [171]. Um die hohe Nachfrage bedienen zu können, werden Aromastoffe zum größten Teil mittels chemischer Prozesse hergestellt [51]. Auf diese Weise können zwar hohe Produktmengen erzielt werden, jedoch weist die Chemosynthese diverse Nachteile auf. Zu diesen zählen: Harsche Reaktionsbedingungen, wie hohe Temperaturen und Drücke, die zu hohen Energiekosten führen, geringe Regio- und Stereospezifitäten, die in unerwünschten Nebenprodukten resultieren und eine aufwendige Produktabtrennung erfordern, sowie die Verwendung von toxischen oder umweltunfreundlichen Chemikalien und Lösungsmitteln [43,56,172]. Weiterhin bietet die Chemosynthese nicht die Möglichkeit Aromastoffe zu bilden, die mit der Bezeichnung „natürlich“ klassifiziert werden dürfen. Dies resultiert aus der gesetzlichen Definition natürlicher Aromastoffe. In der europäischen Rechtsprechung (Verordnung (EG) Nr. 1334/2008, Artikel 3 (2)) werden natürliche Aromastoffe als Aromastoffe definiert, die „[...] durch geeignete physikalische, enzymatische oder mikrobiologische Verfahren aus pflanzlichen, tierischen oder mikrobiologischen Ausgangsstoffen gewonnen […]“ werden und „[…] natürlich vorkommen und in der Natur nachgewiesen wurden“ [173]. Die Definition der US-Regulierung ist analog [50].

Da heutzutage Verbraucher natürliche, „*clean-label*“-Produkte favorisieren und synthetische Produkte ablehnen, im Besonderen im Lebensmittelbereich, ist die industrielle Nachfrage nach Aromastoffen natürlichen Ursprungs groß [45,50]. Weiterhin ist der Marktwert

natürlicher Aromastoffe im Vergleich zu den entsprechenden synthetischen Verbindungen um ein Vielfaches höher (ca. 10–100-fach) [43]. Eine Möglichkeit zur Gewinnung von natürlichen Aromastoffen besteht in der Extraktion aus natürlichen Quellen. Hierbei handelt es sich zwar um eine einfache Methode, jedoch sind die natürlichen Ressourcen meist durch ihre geographische Verbreitung, Klimaeinflüsse und Saisonalität beschränkt [51]. Weiterhin treten die zu isolierenden Aromastoffe in der Regel nur in geringen Konzentrationen in der natürlichen Quelle auf, sodass hohe Produktionskosten anfallen und die globale Nachfrage nach natürlichen Aromastoffen mittels Extraktion allein nicht gestillt werden kann [51,56].

Eine vielversprechende Alternative bietet die Produktion natürlicher Aromastoffe mittels biotechnologischer Verfahren. Diese zeichnen sich durch die bereits in Kapitel 1.2 beschrieben Vorteile aus. Hohe Chemo-, Regio- und Stereoselektivitäten der Biokatalysatoren resultieren in einer geringen Nebenproduktbildung und damit einer einfacheren und kostengünstigeren Produktabtrennung [174]. Zusätzlich ermöglicht die biotechnologische Produktion eine kontinuierliche, von äußeren Faktoren (z. B. Klima und Saisonalität) unabhängige Produktion durch kontrollierbare und anpassungsfähige Prozessparameter [56]. Bereits heute werden mehr als 100 kommerzielle Aromastoffe (z. B. Vanillin, (+)-Nootkaton und Menthol [41]) biotechnologisch erzeugt [50]. Dabei findet die Herstellung sowohl durch *de novo*-Synthese als auch Biotransformation mittels Ganzzellsystemen und isolierten Enzymen statt [43].

1.4 Biotechnologische Alkenspaltung zur Produktion geruchsaktiver Aldehyde und Ketone

Viele in der Natur vorkommende Aldehyde und Ketone wirken als Aromastoffe und sind von hohem Interesse für die Aromenindustrie [167]. Zu diesen zählen u. a. Vertreter der aliphatischen, terpenoiden und aromatischen Carbonylverbindungen (Abbildung 1.7). Vanillin, *p*-Anisaldehyd, Veratrumaldehyd und Piperonal, die wie generell alle Vertreter der „phenolischen“ Aldehyde einen angenehmen Geruch aufweisen, sind nicht nur wichtige Aromastoffe für den Einsatz in Lebensmitteln, Kosmetika und Parfums, sondern werden auch als Intermediate verschiedener industrieller Prozesse wie der Herstellung von Pharmazeutika verwendet [167]. Vanillin ist wohl der weltweit meinst genutzte Aromastoff und damit von besonderer Wichtigkeit für die Aromenindustrie [175]. Aber auch Piperonal, welches aufgrund seines süßlich, blumigen, vanilleartigen Geruchs Bestandteil vieler floraler Parfums

ist und zur Aromatisierung von diversen Lebensmitteln wie Milchprodukten, Süßwaren und Getränken genutzt wird, weist eine hohe Wertigkeit auf [176,177].

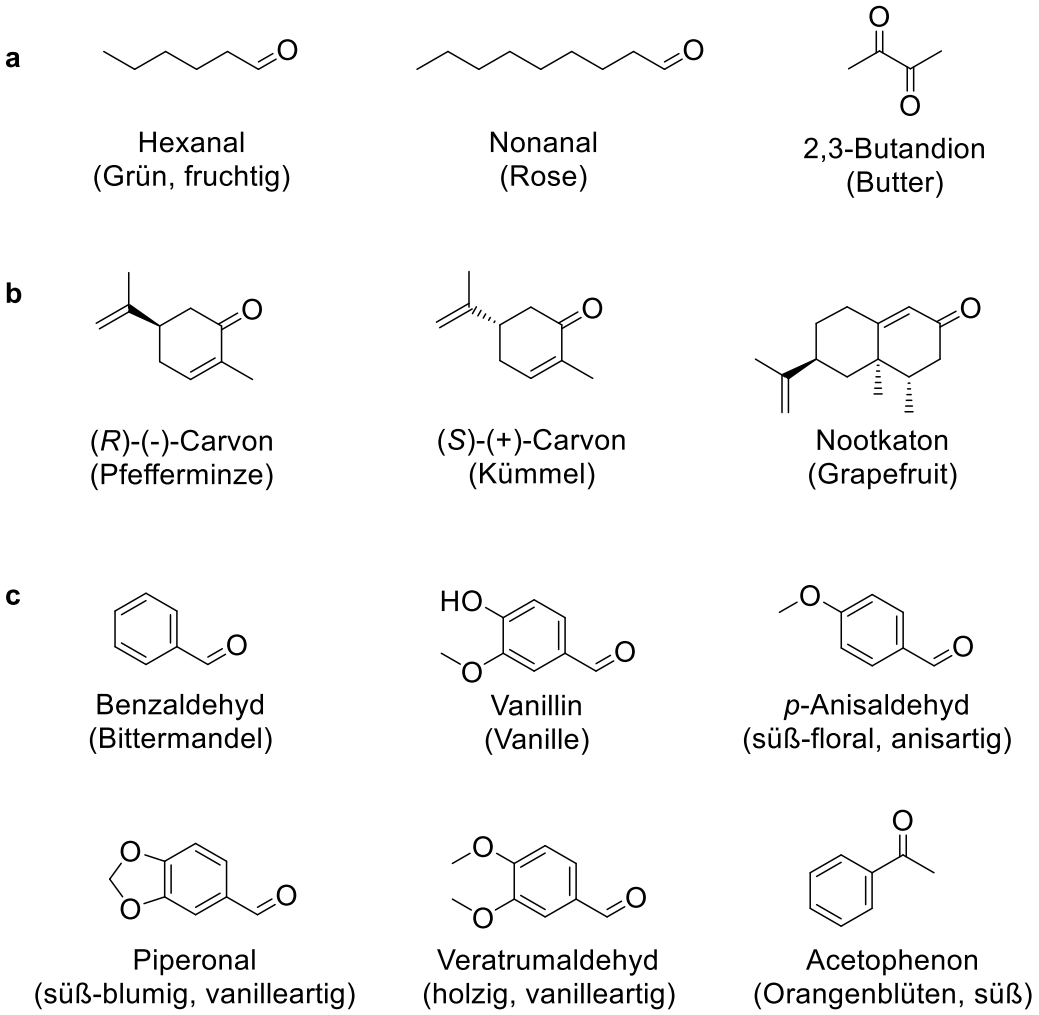

Abbildung 1.7. Beispiele geruchsaktiver Aldehyde mit Anwendung in der Aromenindustrie. **a**) Aliphatische, **b**) terpenoide und **c**) aromatische Verbindungen. Die zugehörigen Geruchseindrücke [167] sind unter der jeweiligen Verbindung in Klammern angegeben.

Eine Möglichkeit zur Synthese von Aldehyden und Ketonen stellt die oxidative Spaltung der π- und σ-Bindung von strukturanalogen Alkenen dar. Verschiedene chemische und biokatalytische Ansätze zur Alkenspaltung sind bekannt [178,179]. Die chemischen Methoden weisen jedoch eine Reihe an Nachteilen auf, wie u. a. die Bildung von explosiven Intermediaten sowie die Verwendung von umweltschädlichen und/oder toxischen Oxidationsmitteln und Katalysatoren [172]. Weiterhin bieten chemische Verfahren, wie bereits beschrieben (Kapitel 1.3), keine Möglichkeit zur Herstellung von natürlichen Aromastoffen. Daher soll folgend nur näher auf die biokatalytische Alkenspaltung eingegangen werden.

Verschiedene Enzyme mit alkenspaltender Aktivität wurden in der Literatur beschrieben. Bei diesen handelt es sich um Häm-Eisen-, nicht-Häm-Eisen- und nicht-Eisen-metallabhängige Proteine, meist Peroxidasen und Oxygenasen, die sich anhand ihrer Struktur, ihres katalytischen Mechanismus und ihrer Substrate unterscheiden [178,179]. Zwei Häm-abhängige Dioxygenasen, Tryptophan- und Indolamin-2,3-dioxygenase, katalysieren beispielsweise die oxidative Spaltung der Doppelbindung des Pyrolrings des Tryptophans [180], wohingegen die Dioxygenase RoxA aus *Xanthomonas* sp., natürliches und synthetisches Gummi durch die regiospezifische Spaltung der *cis*-1,4-Isopreneinheiten abbauen kann [181]. Die Alkenspaltung von verschiedenen Catecholen durch nicht-Häm-Eisen-abhängige Catechol-Dioxygenasen [182] sowie die radikalische Spaltung von konjugierten Dienestern durch eine Chloroperoxidase aus *Caldariomyces fumago* als Nebenreaktion unter aeroben Bedingungen [179,183] sind ebenfalls bekannt.

Weitere alkenspaltende Enzyme sind die stilbenspaltenden Oxygenasen, die *trans*-Stilben (Diphenylethen)-Derivate zu ihren korrespondierenden phenolischen Aldehyden durch die Spaltung der zentralen Doppelbindung umsetzen [179,184]. Die Isoenzyme einer Lignostilben-*α*-*β*-dioxygenase aus *Sphingomonas paucimobilis* katalysieren beispielsweise die Biotransformation von 4,4‘-Dihydroxy-3,3‘-dimethoxystilben zu Vanillin (Abbildung 1.8) [185]. Weiterhin ist die Alkenspaltung von PUFAs durch die Zusammenarbeit von LOX und Fettsäurehydroperoxid-Lyasen bekannt [179]. Hierzu wird zunächst eine Doppelbindung der PUFA durch die LOX oxygeniert (vgl. Kapitel 1.2.2.2) und anschließend das entstandene Fettsäurehydroperoxid durch die Lyase gespalten. Solche gekoppelte Reaktionen sind für die Entstehung „grüner“ Blattduftstoffe wie Hexanal oder *trans*-2-Hexenal verantwortlich [129,186].

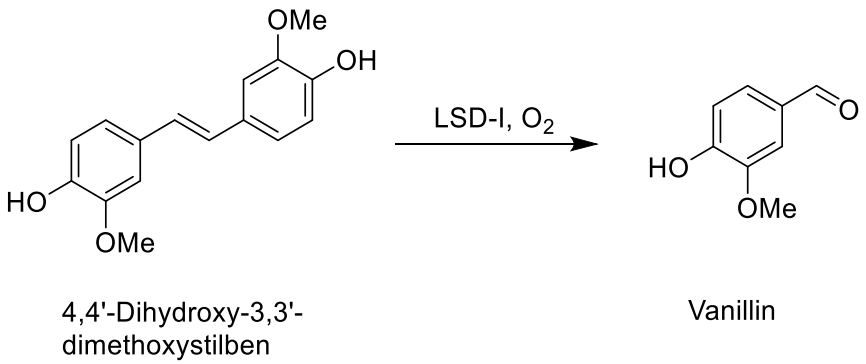

Abbildung 1.8. Spaltung von 4,4‘-Dihydroxy-3,3‘-dimethoxystilben zu Vanillin durch die Lignostilben-*α*-*β*-dioxygenase I (LSD-I) aus *Sphingomonas paucimobilis*.

Wie bereits in Kapitel 1.2.2.1 und 1.2.2.2 angedeutet, kann die Carotinoidspaltung der Aromastoffbildung dienen und beispielsweise durch DyPs bzw. co-oxidativ durch LOX erfolgen [125,129,151,187,188]. Eine weitere Enzymklasse, die die Alkenspaltung der Carotinoide katalysiert, sind die sogenannten carotinoidspaltenden Oxygenasen. Diese sind Nicht-Häm-Eisen-Enzyme, die sich durch eine sehr hohe Regiospezifität auszeichnen und ihre Substrate entweder zentral (mittig, z. B. C-15=C15‘) oder dezentral spalten können [179,187,188]. AtCCD1 aus *Arabidopsis thaliana* spaltet beispielsweise verschiedene Carotinoide an der 9,10- bzw. 9‘,10‘-Doppelbindung [189]. Die Alkenspaltung von *β*-Apo-8‘-Carotinal resultiert dabei in der Bildung des Aromastoffs *β*-Ionon (Abbildung 1.9) [190].

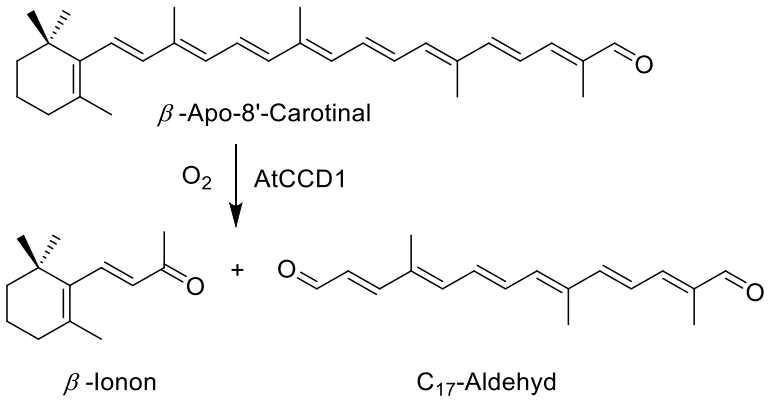

Abbildung 1.9. Alkenspaltung von *β*-Apo-8‘-Carotinal zu *β*-Ionon durch AtCCD1.

Zusätzlich zu den bisher beschriebenen Proteinen sind weitere Enzyme bekannt, die die oxidative Spaltung der benzylischen Doppelbindung von verschiedenen Arylalkenen (Vinylaromaten/Styrenderivate) katalysieren (Abbildung 1.10). Die Alkenspaltung resultiert dabei in der Bildung der strukturanalogen aromatischen Aldehyde oder Ketone, bei denen es sich häufig um Aromastoffe handelt (vgl. Abbildung 1.7) [167,177,191,192]. Eine Isoeugenol- und *trans*-Anetholoxygenase, die Isoeugenol bzw. *trans*-Anethol zu Vanillin bzw. *p*-Anisaldehyd umwandeln, sind aus *Pseudomonas putida* bekannt [177,193,194]. Die *trans*-Anetholoxygenase kann neben dem namensgebenden Substrat auch Isoeugenol und Isosafrol (Vorläufer für Piperonal) umsetzen [177,194]. Die Spaltung von *trans*-Anethol sowie Isosafrol wurde ebenfalls für eine Mn^{3+}-abhängige Peptidase aus dem Basdiomyceten *Trametes hirsuta* nachgewiesen [191]. Ein weiteres Mangan-abhängiges, alkenspaltendes Enzym wird in *Thermotoga maritima* gebildet, welches eine Cupin-Struktur aufweist und z. B. 4-Chloro-*α*-Methylstyrol zu 4-Chloroacetophenon spaltet [195]. Auch verschiedene Peroxidasen sind bekannt, die die Spaltung von Arylalkenen katalysieren. Zu diesen gehören eine Peroxidase aus *Coprinus cinereus* und eine menschliche Myeloperoxidase, für die die Spaltung verschiedener Styrenderivate als Nebenreaktion zur Epoxidierung der Substrate

beobachtet wurde [196]. Die Meerrettichperoxidase weist dagegen eine hohe Chemoselektivität (92 %) für die Biotransformation von *trans*-Anethol zu *p*-Anisaldehyd (90 % Umsatz) auf. [192]. Die Biotransformation von *O*-Ethylisoeugenol wurde weiterhin für eine Ligninperoxidase beobachtet [178].

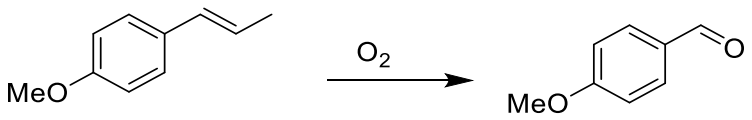

Abbildung 1.10. Oxidative Alkenspaltung eines Arylalkens zum korrespondierenden aromatischen Aldehyd am Beispiel des *trans*-Anethols.

Im Rahmen der vorliegenden Arbeit wurden die erste DyP und eine LOX identifiziert, die eine Alkenspaltung von Arylalkenen katalysierten.

2 Problemstellung und Zielsetzung der Arbeit

Die Nachfrage und Popularität natürlicher Aromastoffe, zu denen auch viele flüchtige Aldehyde und Ketone zählen, nimmt stetig zu. Eine Möglichkeit zur Aldehyd- bzw. Ketonbildung und damit zur Aromastoffsynthese stellt die Alkenspaltung dar. Diese kann prinzipiell mittels verschiedener chemischer Verfahren erfolgen, welche jedoch eine Reihe an Nachteilen aufweisen, wie die Verwendung und Bildung von gesundheits- und umweltgefährdenden Chemikalien sowie geringe Ausbeuten und Selektivitäten. Ein weiterer bedeutender Nachteil ist, dass die Chemosynthese nicht zur Herstellung als „natürlich" klassifizierter Aromastoffe geeignet ist. Die Biotechnologie bzw. Biokatalyse bietet eine Alternative, die die genannten Hindernisse überwinden kann und die zunehmende Forderung der Gesellschaft nach natürlichen Produkten sowie umweltverträglichen und nachhaltigen Produktionsverfahren erfüllt. Basidiomycota bieten hierfür eine bisher relativ unausgeschöpfte Quelle von biotechnologisch interessanten Enzymen. Weiterhin können sie auf einer Reihe von agroindustriellen Nebenströmen wachsen, was dem Wunsch nach einer nachhaltigen Bioökonomie entgegen kommt. Daher fokussierte sich die vorliegende Promotionsarbeit auf basidiomycetische alkenspaltende Enzymaktivitäten.

Vorarbeiten zeigten, dass *P. sapidus trans*-Anethol zu dem Aromastoff *p*-Anisaldehyd spaltet. Weiterhin wurde die Konversion des Pfefferinhaltsstoffs Piperin zu dem für die Industrie sehr wertvollen Vanille-Aroma Piperonal beobachtet [197]. Ziel der vorliegenden Arbeit war die Identifikation der verantwortlichen alkenspaltenden Enzyme sowie die Optimierung der Biokatalyse. Hierfür sollten die Enzyme gereinigt und identifiziert werden. Für eine biochemische Charakterisierung sowie die Verifizierung der Biotransformation sollte eine heterologe Expression erfolgen. Weiterhin sollte das Substratspektrum und das Potential der Enzyme für eine industrielle Applikation analysiert werden.

Eine Optimierung der *trans*-Anethol- und Piperin-spaltenden Aktivität sollte ohne die Verwendung gentechnischer Methoden durch die Generierung monokaryotischer Tochterstämme des dikaryotischen *P. sapidus*-Stamm erzielt werden. Es wurde erwartet, dass sich die Stämme bezüglich ihrer genetischen und biochemischen Eigenschaften unterscheiden, da diese aus einem sexuellen Fortpflanzungsprozess resultieren. Ziel war es, einen oder mehrere Stämme mit im Vergleich zum dikaryotischen Elternstamm überdurchschnittlichem Biotransformationspotential zu identifizieren. Ferner sollten die Ursachen für die erwartete intraspezifische Variabilität der *P. sapidus*-Stämme ermittelt werden, da sich bisher nur wenige Studien mit der Aufklärung von Gründen für die

enzymatische Diversität von monokaryotischen Stämmen beschäftigten. Hierfür sollten die Gen- und Aminosäuresequenzen sowie die Genexpression von Stämmen mit unterschiedlichem Biotransformationspotential analysiert werden.

Voranalysen sollten zeigen, ob agroindustrielle Nebenströme der *Citrus*-Industrie (Zitronen- und Orangenschalen) als Nährsubstrat für die Biomasseproduktion von *P. sapidus* allgemein und zur Produktion der alkenspaltenden Enzyme geeignet sind. Hierzu sollte der Einfluss der Nebenströme auf die Wachstumsrate sowie die Enzymaktivität analysiert werden.

3 Vorwort zu den Vorarbeiten zum Thema „Influence of *Citrus* Side-Streams on Growth Rate and Alkene Cleavage Activity of *Pleurotus sapidus*“

Wie in Kapitel 1.2.1 geschildert, entstehen bei der Herstellung und Verarbeitung von Lebensmitteln in der Agrar- und Lebensmittelindustrie große Mengen an Nebenströmen. Diese sind für die weiße Biotechnologie als kostengünstige Nährmedien für die biokatalytische Herstellung von wertvollen Produkten wie Aromastoffen oder Enzymen von Interesse.

Im Rahmen der Promotionsarbeit sollte in Vorarbeiten analysiert werden, ob sich *Citrus*-Nebenströme (Zitronen- und Orangenschalen) als Nährsubstrate für die Kultivierung von *P. sapidus* allgemein und zur Produktion der alkenspaltenden Enzyme des Pilzes eignen (vgl. Kapitel 2). Für letzteres wurden exemplarisch Biotransformationsexperimente mit *trans*-Anethol durchgeführt. Aus vorherige Studien war bekannt, dass andere *Pleurotus*-Arten auf oder in Orangen- und Mandarinenschalen-haltigen Nährmedien wachsen können [62,198,199]. Beispielsweise wurde die Produktion verschiedener hydrolytischer und oxidativer Enzyme, hauptsächlich Pektinasen und Laccasen, durch die Kultivierung von *Pleurotus pulmonarius* auf Orangenschalen beschrieben [62].

Der Vergleich der Wachstumsrate verschiedener *P. sapidus*-Stämme für die Kultivierung auf Agarplatten mit den *Citrus*-Nebenströmen sowie einem komplexen Standardnährmedium zeigte, dass sowohl Zitronen- als auch Orangenschalen einen wachstumsfördernden Effekt auf *P. sapidus* hatten. Dahingegen führte die submerse Kultivierung der *P. sapidus*-Stämme in den *Citrus*-Schalen-haltigen Medien zu einer verringerten alkenspaltenden Aktivität. Orangen- und Zitronenschalen waren damit zwar prinzipiell als Nährsubstrat für die Kultivierung von *P. sapidus* geeignet, jedoch nicht für die Fragestellung der vorliegenden Promotionsarbeit, die sich auf alkenspaltende Aktivtäten aus *P. sapidus* fokussierte. Die Kultivierung des Basidiomyceten erfolgte daher im Verlauf der weiteren Arbeit in dem komplexen Standardnährmedium.

4 Preliminary work: Influence of *Citrus* Side-Streams on Growth Rate and Alkene Cleavage Activity of *Pleurotus sapidus*

4.1 Introduction

Annually, around 124.2 million tons of *Citrus*, such as orange, lemon, and mandarin, are produced, of which approximately 33% are processed for juice production [200,201]. About half of the fresh fruit mass remains after juice pressing including peels, seeds, cell walls, and core. These side-streams cause a growing problem for the *Citrus* industry as their accumulation is a source of environmental contamination [52,202]. The utilization of *Citrus* side-streams as additive for animal feed or as a resource of pectin production is known, but not commercially attractive. A more valuable option is the use of the low-cost side-streams as cultivation media for biotechnological processes to produce valuable products, such as aroma compounds or enzymes [53,57,203]. Production of the flavor compounds isoamyl acetate ("banana") and phenylethyl acetate ("rose-like, honey, fruity") was observed for cultivation of the wine yeast Vitilevure MT^{TM} (*Saccharomyces cerevisiae*) on orange peels [203], while *Antrodia cinnamomea* generated triterpernoids on grapefruit peels [204]. In addition, several studies described the production of enzymes, such as pectinases, cellulases, laccases, and peroxidases using *Citrus* peels as growth substrate [62,64,199,205–207]. Cultivation of *Pleurotus pulmonarius* on orange peels was used for the production of pectinases and laccases [62], while cellulase, xylanase, laccase, and manganese peroxidase formation during submerged fermentation of mandarin peels was shown for *Pleurotus dryinus* [199].

The purpose of the presented work was to analyze, if lemon and orange peel side-streams were suitable growth substrates for the cultivation of *Pleurotus sapidus*, especially for the production of alkene cleaving activities. For this, the influence of the side-streams on the growth rate and alkene cleaving activity of *P. sapidus* was investigated.

4.2 Results and Discussion

To determine the influence of the *Citrus* peels on the growth rate of *P. sapidus*, different strains (the parental dikaryon and five monokaryons) were cultivated on agar plates with a rich medium (standard nutrient liquid (SNL) for cultivation of basidiomycota [96]; used as control) and minimal media (MM) supplemented with lemon or orange peels. Before this, the most beneficial peel concentration was exemplarily investigated with the lemon side-

stream (Figure 4.1). A concentration of 5% (w/v) showed the best results considering the growth rate and optically evaluated mycelial density and was used for the following cultivation of all strains. For the comparability of the results, the same concentration was also used for the cultivation with the orange peels.

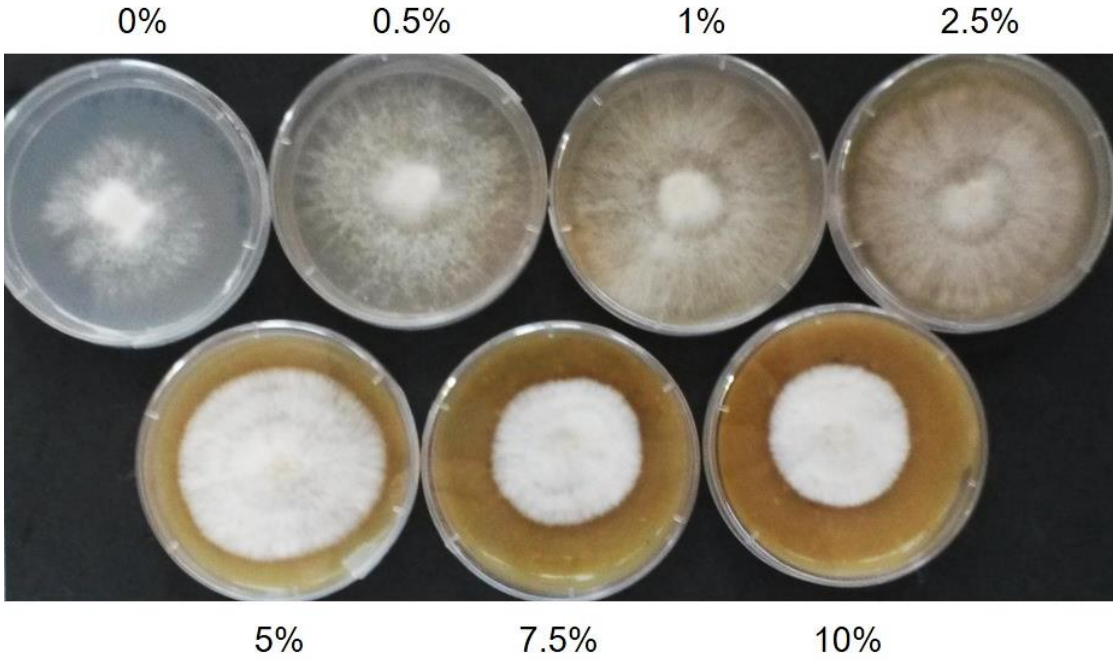

Figure 4.1. Dikaryotic *P. sapidus* strain grown on agar plates with MM supplemented with 0–10% (w/v) lemon peel. The peel concentrations are shown above or below the agar plates.

The growth rates of the *P. sapidus* strains were increased for the cultivation on both *Citrus* peel supplemented media in comparison to the cultivation on SNL (lemon peel: up to twofold, orange peel: up to 3-fold) (Figure 4.2a). Thus, the *Citrus* peels were identified as promising substrates for the cultivation and biomass generation of *P. sapidus*. Nicolini *et al.* also observed good growth of *P. ostreatus*, a near relative of *P. sapidus*, on orange peels in a previous study [198].

To evaluate if the *Citrus* peel-based media were also beneficial for the production of alkene cleaving enzymes, a submerged cultivation of the *P. sapidus* strains was performed in SNL and MM supplemented with 5% (w/v) lemon or orange peel. Afterwards, the lyophilized mycelium of the fungi was used for the biotransformation of *trans*-anethole to *p*-anisaldehyde to analyze the alkene cleavage activity of the strains (Figure 4.2b). The *p*-anisaldehyde concentrations of all strains were lower for the cultivation in the *Citrus* peel-based media than for the cultivation in SNL (lemon peel: around two- to five-fold lower, orange peel: three- to sixteen-fold lower). Thus, lemon and orange peels were not appropriate stimuli for the production of alkene cleaving enzymes in *P. sapidus*, even though a good growth of the

P. sapidus strains in the peel containing media was observed. Influence of the medium composition on enzyme activities in general is known from basidiomycota [63,64].

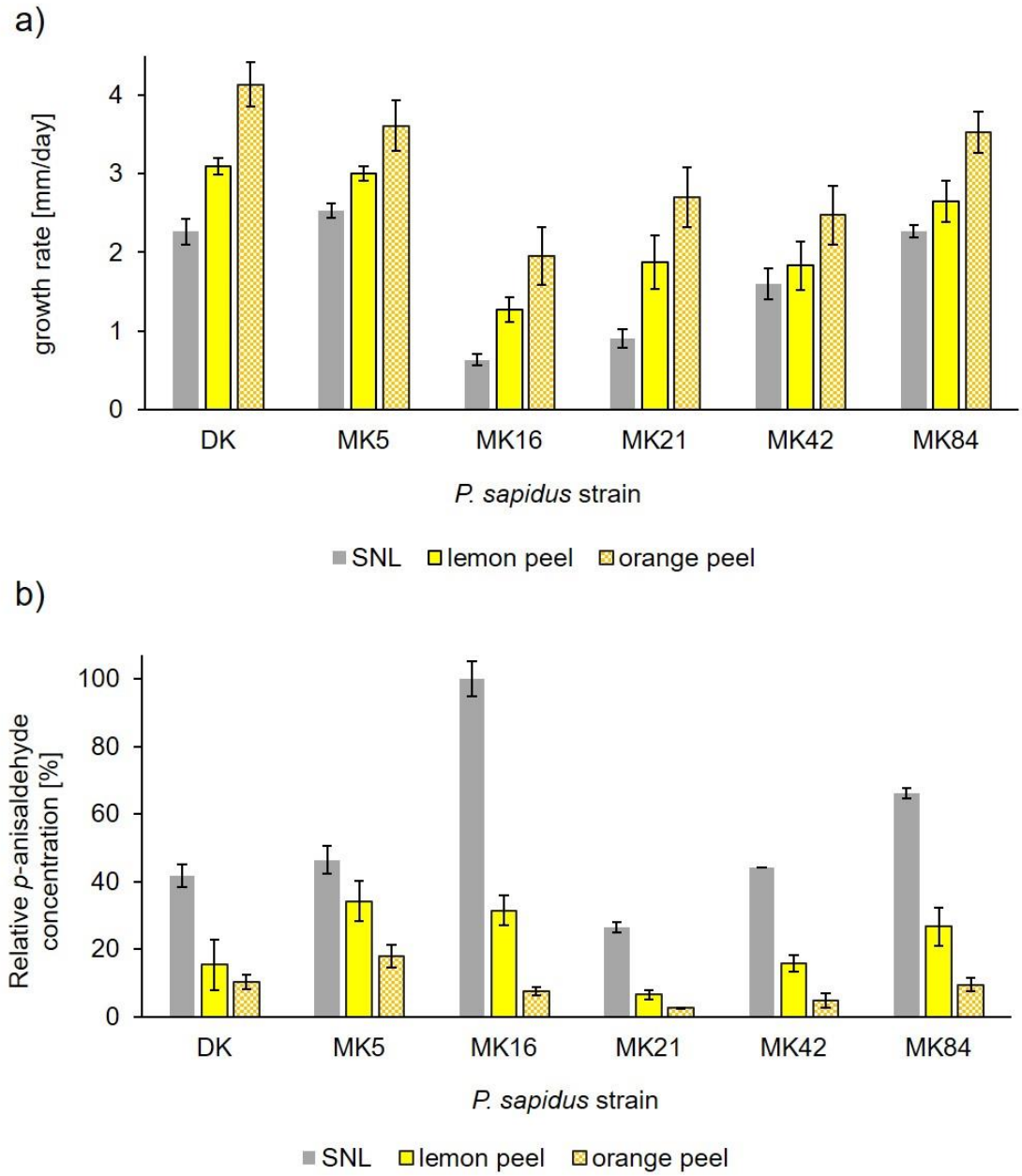

Figure 4.2. Influence of different cultivation media on the growth rate and alkene cleavage activity of *P. sapidus*. **a**) Radial growth rate on agar plates. **b**) Enzymatically generated concentration of *p*-anisaldehyde after cleavage of *trans*-anethole using 30 mg/mL finely ground lyophilized *P. sapidus* mycelium (16 h, RT, 200 rpm). Concentrations were calculated relative to the highest *p*-anisaldehyde concentration. Lemon peel: MM supplemented with 5% lemon peel (w/v), orange peel: MM supplemented with 5% orange peel, DK: dikaryon, MK: monokaryon.

4.3 Materials and Methods

4.3.1 Materials

Chemicals were obtained from Sigma-Aldrich (Seelze, Germany), Carl Roth (Karlsruhe, Germany), or Merck (Darmstadt, Germany) in *p.a.* quality. Lemon peels were received from Döhler (Darmstadt, Germany) and orange peels from ECA Agroindustria SA (Concordia, Entre Ríos, Argentina). The *Citrus* peels were lyophilized as described elsewhere [78] and finely ground.

4.3.2 *P. sapidus* Strains

P. sapidus (Deutsche Sammlung von Mikroorganismen und Zellkulturen GmbH, DSMZ, strain no. 2866 and five monokaryotic daughter strains [208]) was pre-grown on 1.5% (w/v) agar plates with SNL medium and maintained at 4 °C until use [96].

4.3.3 Analysis of the Growth Rate on Agar Plates

To determine the optimal *Citrus* peel concentration for the cultivation of *P. sapidus*, 1.5% (w/v) agar plates with MM (same composition as SNL but without asparagine and with reduced glucose (3 g/L) and yeast extract concentrations (0.3 g/L)) supplemented with 0–10% lemon peel were prepared. The peels were added to the MM after autoclaving directly before plate casting. Afterwards, the dikaryotic *P. sapidus* strain was cultivated on the agar plates for six days. For this, 5 mm^2 of actively growing mycelium of the strain were transferred to the agar plates. The growth was analyzed by measurement of the radial growth rate (increase of the colony) and the optical mycelial density.

After the pre-test, all *P. sapidus* strains were cultivated on agar plates containing MM supplemented with 5% (w/v) lemon or orange peel or on SNL agar plates for six days. Radial growth was measured every two days as mm/day.

All experiments were performed in duplicates.

4.3.4 Submerged Cultivation

For pre-cultivation, 1 cm^2 of grown agar was transferred to 100 mL SNL medium and treated with an Ultraturrax homogenizer (ART Prozess- & Labortechnik, Müllheim, Germany). The pre-cultures were incubated for 5 days at 150 rpm and 24 °C. Afterwards, 6.5 g wet biomass

was washed twice with sterile water and used to inoculate 250 mL SNL or MM supplemented with 5% (w/v) lemon or orange peel. The main culture was incubated at 150 rpm and 24 °C. After six days, the mycelium was washed above a sieve filter with water to remove remaining *Citrus* peel particles. Afterwards, the mycelium was separated from the supernatant by centrifugation (5000× g, 4 °C, 15 min) and lyophilized as described elsewhere [78]. The lyophilisates were finely ground. The cultivations were performed in duplicates.

4.3.5 Biotransformation

Biotransformation of 1 µL (6.7 mM) *trans*-anethole was carried out with 30 mg *P. sapidus* lyophilisate (see Section 4.3.4), buffered in sodium acetate (100 mM, pH 3.5) in the presence of 1 mM $MnSO_4$ in a total volume of 1 mL for 16 h at RT and 200 rpm according to Krahe *et al.* [209]. Controls (chemical blank: without lyophilisate; biological blank: with heat inactivated mycelium (2 h at 95 °C)) were performed accordingly. All experiments were performed in duplicates. Sample preparation, analysis by gas chromatography, as well as quantification of the conversion product *p*-anisaldehyde was performed as described elsewhere [209]. To calculate the enzymatically generated product concentration, the product concentrations in the blanks were subtracted from the concentrations yielded with the active mycelium.

5 Vorwort zur Publikation „A DyP-Type Peroxidase of *Pleurotus sapidus* with Alkene Cleaving Activity"

Wie in Kapitel 1.4 beschrieben, handelt es sich bei vielen Aromastoffen um Aldehyde oder Ketone, welche mittels Alkenspaltung hergestellt werden können. Da die Nutzung von biotechnologischen Verfahren eine Reihe von Vorteilen bietet (vgl. Kapitel 1.2, 1.3 und 1.4), ist die Identifizierung neuer alkenspaltender Enzyme für die Aromaherstellung von hohem Interesse.

In Rahmen einer Vorarbeit wurde eine alkenspaltende Aktivität aus *P. sapidus* nachgewiesen, die für die Umwandlung von *trans*-Anethol zu dem süß-floralen, anisartigen Aromastoff *p*-Anisaldehyd verantwortlich ist [197]. Teil der nachfolgend dargestellten Publikation war die Identifizierung des verantwortlichen Enzyms. Weiterhin sollte das als DyP identifizierte Protein heterolog in *K. phaffi* produziert werden, um eine biochemische Charakterisierung und Verifizierung der alkenspaltenden Aktivität zu ermöglichen. Interessanterweise wies die DyP keine Aktivität gegenüber dem Anthrachinonfarbstoff *Reactive Blue* 19, einem typischen DyP-Substrat (vgl. Kapitel 1.2.2.1), auf. Im Gegensatz dazu konnte die DyP Mn^{2+} zu Mn^{3+} oxidieren und Carotinoide entfärben. Beide Reaktionen wurden bereits für andere DyPs beschrieben [96–98]. Das Enzym katalysierte die Biotransformation von *trans*-Anethol, wobei die Zugabe von Mn^{2+} zu einer Aktivitätssteigerung führte. Zusätzlich wurde die Biotransformation weiterer Arylalkene, die ebenfalls in der Bildung industriell relevanter Aromastoffe resultierte, beobachtet. Damit zeigte sich das Potential der DyP für eine industrielle Applikation zur Aromastoffproduktion. Ferner ist sie die erste beschriebene DyP, die eine alkenspaltende Aktivität gegenüber Arylalkenen aufweist. Die nachfolgende Publikation dient damit der Erweiterung des bisher bekannten Substratspektrums von DyPs, die eine noch relativ neue Enzymfamilie bilden (vgl. Kapitel 1.2.2.1).

An der Arbeit beteiligt waren Herr Prof. Berger und Frau Dr. Ersoy. Herr Prof. Berger war in seiner Funktion als Arbeitsgruppenleiter für die Projektidee sowie die Akquise der erforderlichen Drittmittel verantwortlich. Ferner übernahm Herr Prof. Berger zusammen mit Frau Dr. Ersoy die wissenschaftliche Betreuung der Arbeit.

Die nachfolgende Arbeit wurde in der *peer-reviewed* Zeitschrift *Molecules* (MDPI) veröffentlicht (https://doi.org/10.3390/molecules25071536) [209].

6

molecules

MDPI

Article

A DyP-Type Peroxidase of *Pleurotus sapidus* with Alkene Cleaving Activity

Nina-Katharina Krahe *, Ralf G. Berger and Franziska Ersoy

Institut für Lebensmittelchemie, Gottfried Wilhelm Leibniz Universität Hannover, Callinstraße 5, 30167 Hannover, Germany; rg.berger@lci.uni-hannover.de (R.G.B.); franziska.ersoy@lci.uni-hannover.de (F.E.)

* Correspondence: nina.krahe@lci.uni-hannover.de; Tel.: +49-511-762-17257

6.1 Abstract

Alkene cleavage is a possibility to generate aldehydes with olfactory properties for the fragrance and flavor industry. A dye-decolorizing peroxidase (DyP) of the basidiomycete *Pleurotus sapidus* (PsaPOX) cleaved the aryl alkene *trans*-anethole. The PsaPOX was semi-purified from the mycelium *via* FPLC, and the corresponding gene was identified. The amino acid sequence as well as the predicted tertiary structure showed typical characteristics of DyPs as well as a non-canonical Mn^{2+}-oxidation site on its surface. The gene was expressed in *Komagataella phaffii* GS115 yielding activities up to 142 U/L using 2,2′-azino-bis(3-ethylbenzthiazoline-6-sulphonic acid) as substrate. PsaPOX exhibited optima at pH 3.5 and 40 °C and showed highest peroxidase activity in the presence of 100 µM H_2O_2 and 25 mM Mn^{2+}. PsaPOX lacked the typical activity of DyPs towards anthraquinone dyes, but oxidized Mn^{2+} to Mn^{3+}. In addition, bleaching of *β*-carotene and annatto was observed. Biotransformation experiments verified the alkene cleavage activity towards the aryl alkenes (*E*)-methyl isoeugenol, *α*-methylstyrene, and *trans*-anethole, which was increased almost twofold in the presence of Mn^{2+}. The resultant aldehydes are olfactants used in the fragrance and flavor industry. PsaPOX is the first described DyP with alkene cleavage activity towards aryl alkenes and showed potential as biocatalyst for flavor production.

Keywords:

alkene cleavage; aryl alkenes; basidiomycota; biocatalysis; carotene degradation; dye-decolorizing peroxidase (DyP); manganese; *Komagataella phaffii*; *Pleurotus sapidus*

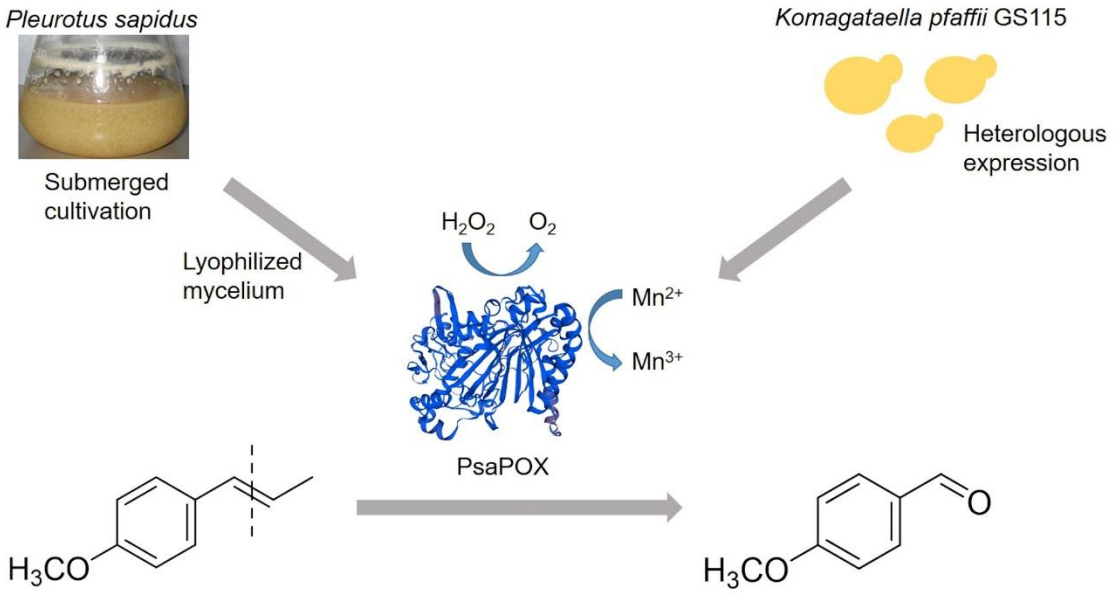

Figure 6.1. Graphical abstract.

6.2 Introduction

Many small aromatic aldehydes and ketones are volatiles with olfactory properties and therefore of high interest to the fragrance and flavor industry [167]. One method to generate aldehydes and ketones is the oxidative cleavage of alkenes. Chemical options are ozonolysis, dihydroxylation followed by oxidative glycol cleavage, or metal-based methods [172,178,210]. However, all of these methods have disadvantages, such as the generation of explosive intermediates, the use of environmentally unfriendly and/or toxic oxidants and metal catalysts, or low yield and low chemoselectivity [172]. An alternative is the application of enzymes due to their high chemo-, regio-, and stereospecificity as well as the possibility to use mild reaction conditions [178]. Another advantage is the generation of "natural" flavors according to effective legislation in Europe and the US. This becomes more and more important considering the rising popularity of natural products [211]. Different proteins of different enzyme classes, which are heme, non-heme iron, or non-iron metal dependent and have different protein structures as well as different reaction mechanism are known to catalyze alkene cleavage reactions [178]. Specifically, an isoeugnol and *trans*-anethole oxygenase from *Pseudomonas putida* and two manganese dependent enzymes from *Thermotoga maritima* (manganese-dependent Cupin TM1459) and *Trametes hirsuta* (Mn^{3+}-dependent proteinase A homologue) oxidatively cleaved the benzylic double bond of different aryl alkenes, such as isoeugenol and *trans*-anethole to form the respective aldehydes [191,193–195]. In addition, alkene cleavage activity towards aryl alkenes was also detected for several peroxidases. Cleavage of different styrene derivatives was described for *Coprinus cinereus* peroxidase and a human myeloperoxidase as minor side reaction [196], while horseradish peroxidase (HRP) showed a chemoselectivity of 92% for the conversion of *trans*-anethole (90%) to *p*-anisaldehyde [192]. Furthermore, transformations of *o*-ethylisoeugenol and *trans*-anethole to the corresponding benzaldehyde derivatives by lignin peroxidases were described [178,192]. However, to our best knowledge no alkene cleavage activity of a dye-decolorizing peroxidase (DyP) is known.

DyP-type peroxidases (EC: 1.11.1.19) are a new superfamily of heme peroxidases that oxidize various dyes, in particular xenobiotic anthraquinone dyes, which are hardly oxidized by other peroxidases [92]. Furthermore, typical peroxidase substrates, such as ABTS (2,2'-azino-bis(3-ethylbenzthiazoline-6-sulphonic acid) and phenolic compounds are also substrates for DyPs [98,99]. However, amino acid sequences, protein structures, and catalytic residues differ highly between DyPs and other classes of heme peroxidases [95]. Typical

structural characteristics of DyPs are the ferredoxin-like fold, which is formed by two domains containing α-helices and four-stranded antiparallel *β*-sheets, and a GXXGD motif [95,99]. The active site (heme pocket) including a catalytic aspartic acid and arginine over the heme plane (distal) and proximal histidine is structurally similar to other heme peroxidases, even though other peroxidases contain histidine instead of aspartic acid [106]. The proximal histidine in the heme pocket functions as the fifth ligand of the heme iron, while the distal aspartic acid and arginine are involved in the activation of the enzyme [95,99]. The deprotonated aspartic acid (or aspartate) mediates the rearrangement of a proton from hydrogen peroxide after it enters the heme pocket in the resting state. This results in the heterolytic cleavage of hydrogen peroxide to water and oxidation of the heme to the radicalic-cationic oxoferryl species Compound I by two-fold single electron transfer [106]. Even though the distal arginine is not directly involved in the rearrangement of hydrogen peroxide, it is essential for the coordination of hydrogen peroxide to the heme iron and the stabilization of Compound I [106]. During the following reaction cycle, Compound I is reduced by oxidation of two substrate molecules to the state during enzyme resting state in two sequential steps with Compound II as intermediate. However, the existence of Compound II has not been confirmed universally for all DyP-type peroxidases [109]. In the presence of excessive hydrogen peroxide suicide inhibition was observed for different DyPs [111,112]. This is also well known for classical peroxidases as a result of an inactive oxidative state (Compound III) and results from reaction of hydrogen peroxide with Compound II [113,114].

The objective of the present study was to identify new enzymes of basidiomycetes with alkene cleavage activity towards aryl alkenes. A screening was performed using *trans*-anethole as model alkene. A new DyP-type peroxidase from *P. sapidus* was semi-purified and the coding gene was identified. Heterologous expression resulted in the production of soluble protein and allowed the biochemical characterization of the DyP. The enzyme was able to oxidize Mn^{2+}, but did not catalyze the degradation of anthraquinone dyes, which is typical for other DyPs. Biotransformation experiments verified the cleavage activity towards different alkenes. This is the first study describing a DyP with alkene cleavage activity towards aryl alkenes.

6.3 Results and Discussion

6.3.1 Purification and Identification of the Alkene Cleavage Activity

Within a screening of 17 basidiomycetes for alkene cleavage activity using the substrate *trans*-anethole (Supporting Table 6.1, Section 6.7) *P. sapidus* turned out to be a promising candidate for the production of the desired activity. The lyophilized mycelium as well as the culture supernatant was examined for the ability to cleave *trans*-anethole after submerged cultivation. The culture supernatant showed no activity, whereas the incubation in the presence of the mycelium resulted in formation of 5.36 mM *p*-anisaldehyde (molar yield of 79.03%; Figure 6.2).

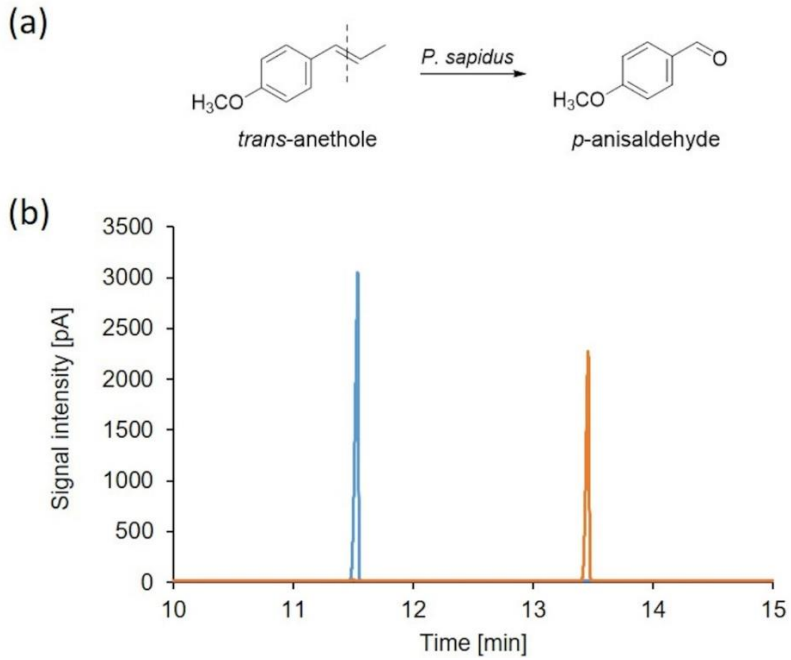

Figure 6.2. Bioconversion of *trans*-anethole by *P. sapidus*. (**a**) Alkene cleavage of *trans*-anethole resulted in the formation of *p*-anisaldehyde. (**b**) GC-FID chromatogram of an *n*-hexane extract of the conversion of the blank sample (blue) and after incubation with lyophilized mycelium of *P. sapidus* (orange). Retention times: *trans*-anethole (11.53 min) and *p*-anisaldehyde (13.45 min).

For the identification of the enzyme catalyzing the *trans*-anethole cleavage, it was semi-purified from the rehydrated mycelium by hydrophobic interaction and anion exchange chromatography (IEX). During the purification, a high activity loss occurred, which resulted in low product concentrations after conversion (Supporting Table 6.2, Section 6.7). This was most likely a result of protein loss, enzyme degradation or denaturation as described for other enzymes [118,212,213]. Another possibility is the loss of cofactors or –substrates, such as metal ions or peroxides during the purification steps [191]. Addition of Mn^{2+} led to a 15-fold increase in *p*-anisaldehyde concentration, which was further increased by addition of

hydrogen peroxide, indicating a cosubstrate dependency (Supporting Table 6.2, Section 6.7). Chemical conversion by Mn^{2+} alone was excluded, while product formation was observed with hydrogen peroxide (18 µM), but with a yield around 30-fold lower than the one for the enzymatic reaction (Supporting Table 6.2, Section 6.7). Thus, the improved bioconversion in the presence of Mn^{2+} and hydrogen peroxide was verified to be the result of an increased enzyme activity.

A class of fungal enzymes that requires hydrogen peroxide and some of which need Mn^{2+} for catalysis are peroxidases [92,214,215]. The anion exchange fractions, which showed alkene cleavage activity, also exhibited peroxidase activity, thus verifying the presence of a peroxidase. For visualization of the activity, a semi-native PAGE was performed and stained with ABTS in the presence of hydrogen peroxide (Figure 6.3). Two peroxidases running at 45 and 52 kDa were detected. The respective protein bands stained with Coomassie Brilliant Blue were excised for electrospray ionization tandem mass spectrometry. Due to the low protein concentration of the 52 kDa band, no meaningful peptides were found (Figure 6.3, lane 1). This paper presents the data obtained for the protein running at 45 kDa (Figure 6.3, arrow).

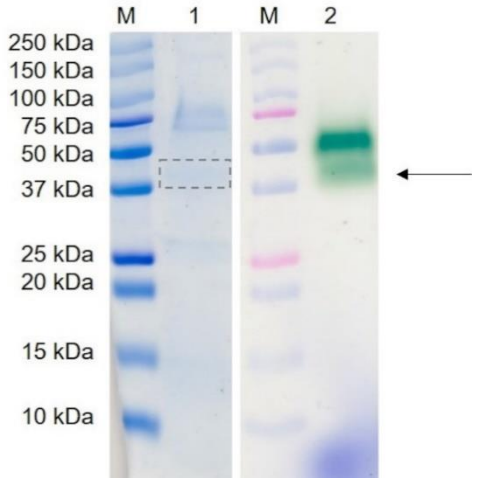

Figure 6.3. Semi-native PAGE of the active fraction after purification of the alkene cleavage enzyme from *P. sapidus* by IEX. 1: gel stained with Coomassie Brilliant Blue; 2: gel stained with ABTS in the presence of hydrogen peroxide, M: pre-stained molecular mass marker. An arrow and a box marks the protein that was successfully identified by sequencing.

Three tryptic peptides (EGSELLGAR, DGSFLTFR, and SGAPIEITPLKDDPK) were identified by ESI-MS/MS. Homology searches against the public database NCBI using the mascot search engine (Matrix Science, London, UK) identified a DyP-type peroxidase of *P. ostreatus* PC15 (*Pleos*-DyP4 [216]; GenBank accession no. KDQ22873.1), a close relative of *P. sapidus*, as the best hit.

6.3.2 Amplification and Expression of *PsaPOX*

Specific primers successfully amplified the 1512 bp coding region of the gene from *P. sapidus*. The translated amino acid sequence of 504 aa contained the peptide fragments that were obtained by ESI-MS/MS and showed highest identity (94%) to the sequence of *Pleos*-DyP4 (Figure 6.4), which has not been investigated for its alkene cleavage activity against *trans*-anethole or other substrates before [117,216]. In our hands, *P. ostreatus* showed a weaker *trans*-anethole cleavage activity, too (Supporting Table 6.1, Section 6.7). Identity of the *P. sapidus* peroxidase (PsaPOX) to other DyPs and proteins was lower than 60%. A sequence alignment with other DyPs (Figure 6.4) confirmed that PsaPOX exhibited the typical GXXGD motif and all important residues known for the catalytic activity of DyPs, such as the proximal histidine (His-334) (fifth ligand of heme iron) and distal Asp-196 and Arg-360 involved in the activation of the enzyme (formation of compound I) by H_2O_2 cleavage [95,99]. Furthermore, Trp-405 was identified as a homolog to the surface exposed Trp-377 of AauDyP of *Auricularia auricula-judae*, which serves as an oxidation site for bulky substrates such as Reactive blue 19 (RBB19) using a long-range electron transfer [116]. Comparison of the PsaPOX and *Pleos*-DyP4 sequence indicated that PsaPOX exhibited a non-canonical Mn^{2+}-oxidation site on its surface (Asp-215, Glu-345, Asp-352 and Asp-354; Trp-339 participates in the electron transport from the oxidation site to the heme) like *Pleos*-DyP4 [117] and can oxidize Mn^{2+} to Mn^{3+}, which is known for a few fungal DyPs only [118–120,216].

A structural homology model of PsaPOX (Supporting Figure 6.1, Section 6.7), which was generated using the X-ray crystal structure of *Pleos*-DyP4 (PDB-ID 6fsk) on the SWISS-MODEL server, possessed typical characteristics of the DyP-type peroxidase family (N- and C-terminal ferredoxin-like domain, each formed by four-stranded antiparallel β-sheets and several α-helices) [95] and supported the classification of PsaPOX as DyP. Furthermore, the analysis of the amino acid sequence using PeroxiBase [217] related the *P. sapidus* peroxidase (PsaPOX) to the class “DyP-type peroxidase D”. As known from literature, DyPs differ significantly in amino acid sequence, tertiary structure, and catalytic residues from other representatives of the heme peroxidases, such as HRP, human myeloperoxidase, lignin peroxidase, or *Coprinus cinereus* peroxidase [92,95,100], all of which are able to cleave *trans*-anethole or structurally related alkenes [192,196]. So far no DyP is known to catalyze the mentioned reaction.

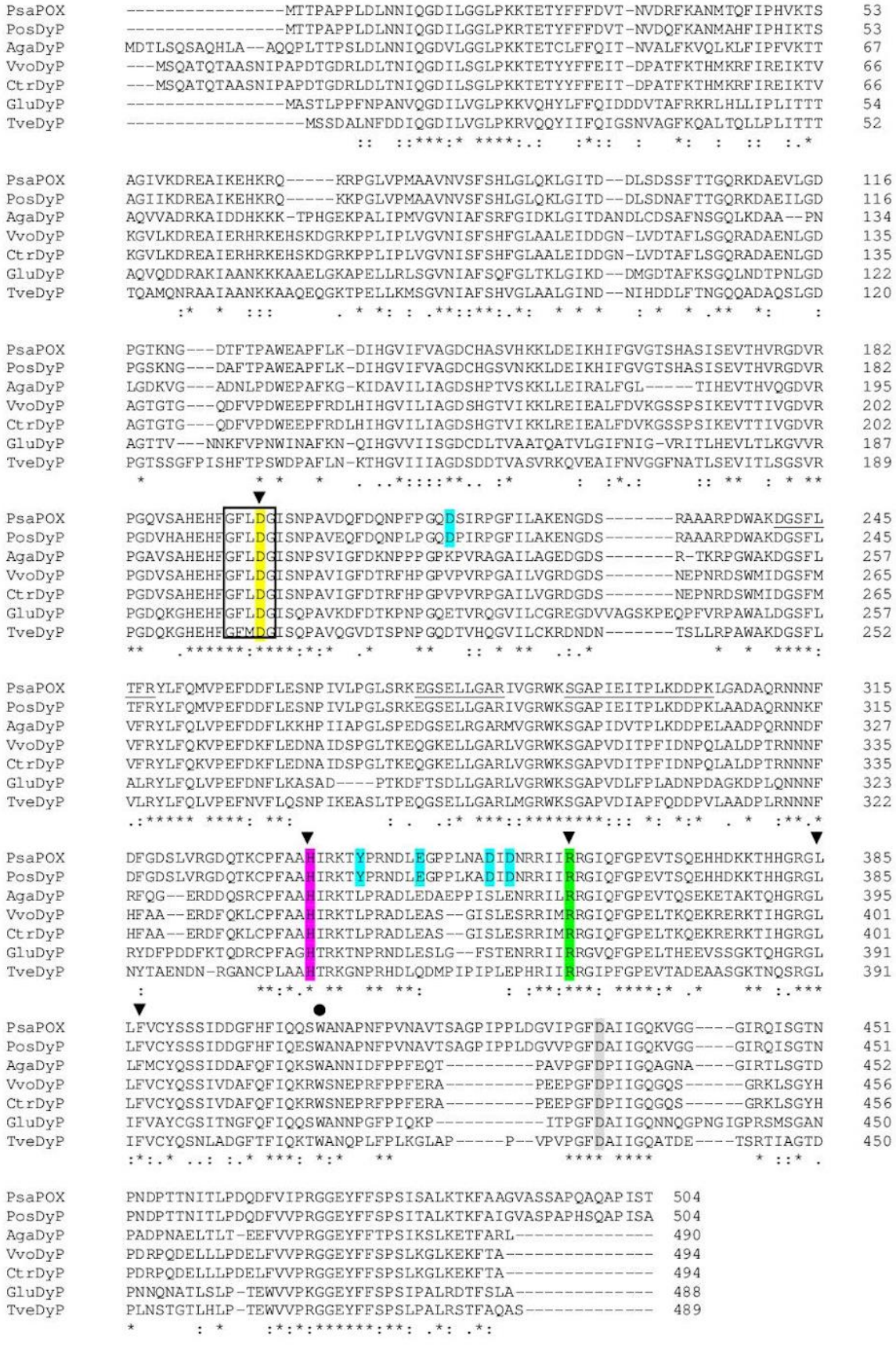
PsaPOX ----------MTTPAPPLDLNNIQGDILGGLPKKTETYFFFDVT-NVDRFKANMTQFIPHVKTS 53
PosDyP ----------MTTPAPPLDLNNIQGDILGGLPKRTETYFFFDVT-NVDQFKANMAHFIPHIKTS 53
AgaDyP MDTLSQSAQHLA--AQQPLTTPSLDLNNIQGDVLGGLPKKTETCLFFQIT-NVALFKVQLKLFIPFVKTT 67
VvoDyP ---MSQATQTAASNIPAPDTGDRLDLTNIQGDILSGLPKKTETYYFFEIT-DPATFKTHMKRFIREIKTV 66
CtrDyP ---MSQATQTAASNIPAPDTGDRLDLTNIQGDILSGLPKKTETYYFFEIT-DPATFKTHMKRFIREIKTV 66
GluDyP ----------MASTLPPFNPANVQGDILVGLPKKVQHYLFFQIDDDVTAFRKRLHLLIPLITTT 54
TveDyP ----------MSSDALNFDDIQGDILVGLPKRVQQYIIFQIGSNVAGFKQALTQLLPLITTT 52
PsaPOX AGIVKDREAIKEHKRQ-----KRPGLVPMAAVNVSFSHLGLQKLGITD--DLSDSSFTTGQRKDAEVLGD 116
PosDyP AGIIKDREAIKEHKRQ-----KKPGLVPMAAVNVSFSHLGLQKLGITD--DLSDNAFTTGQRKDAEILGD 116
AgaDyP AQVVADRKAIDDHKKK-TPHGEKPALIPMVGVNIAFSRFGIDKLGITDANDLCDSAFNSGQLKDAA--PN 134
VvoDyP KGVLKDREAIERHRKEHSKDGRKPPLIPLVGVNISFSHFGLAALEIDDGN-LVDTAFLSGQRADAENLGD 135
CtrDyP KGVLKDREAIERHRKEHSKDGRKPPLIPLVGVNISFSHFGLAALEIDDGN-LVDTAFLSGQRADAENLGD 135
GluDyP AQVQDDRAKIAANKKKAAELGKAPELLRLSGVNIAFSQFGLTKLGIKD--DMGDTAFKSGQLNDTPNLGD 122
TveDyP TQAMQNRAAIAANKKAAQEQGKTPELLKMSGVNIAFSHVGLAALGIND--NIHDDLFTNGQQADAQSLGD 120
PsaPOX PGTKNG---DTFTPAWEAPFLK-DIHGVIFVAGDCHASVHKKLDEIKHIFGVGTSHASISEVTHVRGDVR 182
PosDyP PGSKNG---DAFTPAWEAPFLK-DIHGVIFVAGDCHGSVNKKLDEIKHIFGVGTSHASISEVTHVRGDVR 182
AgaDyP LGDKVG---ADNLPDWEPAFKG-KIDAVILIAGDSHPTVSKKLLEIRALFGL-----TIHEVTHVQGDVR 195
VvoDyP AGTGTG---QDFVPDWEEPFRDLHIHGVILIAGDSHGTVIKKLREIEALFDVKGSSPSIKEVTTIVGDVR 202
CtrDyP AGTGTG---QDFVPDWEEPFRDLHIHGVILIAGDSHGTVIKKLREIEALFDVKGSSPSIKEVTTIVGDVR 202
GluDyP AGTTV---NNKFVPNWINAFKN-QIHGVVIISGDCDLTVAATQATVLGIFNIG-VRITLHEVLTLKGVVR 187
TveDyP PGTSSGFPISHFTPSWDPAFLN-KTHGVIIIAGDSDDTVASVRKQVEAIFNVGGFNATLSEVITLSGSVR 189
PsaPOX PGQVSAHEHFGFLDGISNPAVDQFDQNPFPGQDSIRPGFILAKENGDS-------RAAARPDWAKDGSFL 245
PosDyP PGDVHAHEHFGFLDGISNPAVEQFDQNPLPGQDPIRPGFILAKENGDS-------RAAARPDWAKDGSFL 245
AgaDyP PGAVSAHEHFGFLDGISNPSVIGFDKNPPPGPKPVRAGAILAGEDGDS-------R-TKRPGWAKDGSFL 257
VvoDyP PGDVSAHEHFGFLDGISNPAVIGFDTRFHPGPVPVRPGAILVGRDGDS-------NEPNRDSWMIDGSFM 265
CtrDyP PGDVSAHEHFGFLDGISNPAVIGFDTRFHPGPVPVRPGAILVGRDGDS-------NEPNRDSWMIDGSFM 265
GluDyP PGDQKGHEHFGFLDGISQPAVKDFDTKPNPGQETVRQGVILCGREGDVVAGSKPEQPFVRPAWALDGSFL 257
TveDyP PGDQKGHEHFGFMDGISQPAVQGVDTSPNPGQDTVHQGVILCKRDNDN-------TSLLRPAWAKDGSFL 252
PsaPOX TFRYLFQMVPEFDDFLESNPIVLPGLSRKEGSELLGARIVGRWKSGAPIEITPLKDDPKLGADAQRNNNF 315
PosDyP TFRYLFQMVPEFDDFLESNPIVLPGLSRKEGSELLGARIVGRWKSGAPIEITPLKDDPKLAADAQRNNKF 315
AgaDyP VFRYLFQLVPEFDDFLKKHPIIAPGLSPEDGSELRGARMVGRWKSGAPIDVTPLKDDPELAADPQRNNDF 327
VvoDyP VFRYLFQKVPEFDKFLEDNAIDSPGLTKEQGKELLGARLVGRWKSGAPVDITPFIDNPQLALDPTRNNNF 335
CtrDyP VFRYLFQKVPEFDKFLEDNAIDSPGLTKEQGKELLGARLVGRWKSGAPVDITPFIDNPQLALDPTRNNNF 335
GluDyP ALRYLFQLVPEFDNFLKASAD----PTKDFTSDLLGARLVGRWKSGAPVDLFPLADNPDAGKDPLQNNNF 323
TveDyP VLRYLFQLVPEFNVFLQSNPIKEASLTPEQGSELLGARLMGRWKSGAPVDIAPFQDDPVLAADPLRNNNF 322
PsaPOX DFGDSLVRGDQTKCPFAAHIRKTYPRNDLEGPPLNADIDNRRIIRRGIQFGPEVTSQEHHDKKTHHGRGL 385
PosDyP DFGDSLVRGDQTKCPFAAHIRKTYPRNDLEGPPLKADIDNRRIIRRGIQFGPEVTSQEHHDKKTHHGRGL 385
AgaDyP RFQG--ERDDQSRCPFAAHIRKTLPRADLEDAEPPISLENRRILRRGIQFGPEVTQSEKETAKTQHGRGL 395
VvoDyP HFAA--ERDFQKLCPFAAHIRKTLPRADLEAS--GISLESRRIMRRGIQFGPELTKQEKRERKTIHGRGL 401
CtrDyP HFAA--ERDFQKLCPFAAHIRKTLPRADLEAS--GISLESRRIMRRGIQFGPELTKQEKRERKTIHGRGL 401
GluDyP RYDFPDDFKTQDRCPFAGHTRKTNPRNDLESLG--FSTENRRIIRRGVQFGPELTHEEVSSGKTQHGRGL 391
TveDyP NYTAENDN-RGANCPLAAHTRKGNPRHDLQDMPIPIPLEPHRIIRRGIPFGPEVTADEAASGKTNQSRGL 391
PsaPOX LFVCYSSSIDDGFHFIQQSWANAPNFPVNAVTSAGPIPPLDGVIPGFDAIIGQKVGG----GIRQISGTN 451
PosDyP LFVCYSSSIDDGFHFIQESWANAPNFPVNAVTSAGPIPPLDGVVPGFDAIIGQKVGG----GIRQISGTN 451
AgaDyP LFMCYQSSIDDAFQFIQKSWANNIDFPPFEQT---------PAVPGFDPIIGQAGNA----GIRTLSGTD 452
VvoDyP LFVCYQSSIVDAFQFIQKRWSNEPRFPPFERA---------PEEPGFDPIIGQGQS------GRKLSGYH 456
CtrDyP LFVCYQSSIVDAFQFIQKRWSNEPRFPPFERA---------PEEPGFDPIIGQGQS------GRKLSGYH 456
GluDyP IFVAYCGSITNGFQFIQQSWANNPGFPIQKP----------ITPGFDAIIGQNNQGPNGIGPRSMSGAN 450
TveDyP IFVCYQSNLADGFTFIQKTWANQPLFPLKGLAP-----P--VPVPGFDAIIGQATDE----TSRTIAGTD 450
PsaPOX PNDPTTNITLPDQDFVIPRGGEYFFSPSISALKTKFAAGVASSAPQAQAPIST 504
PosDyP PNDPTTNITLPDQDFVVPRGGEYFFSPSITALKTKFAIGVASPAPHSQAPISA 504
AgaDyP PADPNAELTLT-EEFVVPRGGEYFFTPSIKSLKETFARL---------- 490
VvoDyP PDRPQDELLLPDELFVVPRGGEYFFSPSLKGLKEKFTA---------- 494
CtrDyP PDRPQDELLLPDELFVVPRGGEYFFSPSLKGLKEKFTA---------- 494
GluDyP PNNQNATLSLP-TEWVVPKGGEYFFSPSIPALRDTFSLA---------- 488
TveDyP PLNSTGTLHLP-TEWVVPRGGEYFFSPSLPALRSTFAQAS---------- 489

◀ **Figure 6.4.** Alignment of alkene cleaving peroxidase from *P. sapidus* (PsaPOX) with the *Pleos*-DyP4 of *P. ostreatus* (PosDyP; KDQ22873.1) and other characterized DyPs. AgaDyP: *Armillaria gallica* (PBK80505.1), VvoDyP: *Volvariella volvacea* (AKU04643.1), CtrDyP: *Coriolopsis trogii* (AUW34346.1), GluDyP: *Ganoderma lucidum* (ADN05763.1), and TveDyP: *Trametes versicolor* (XP_008039377.1). Inverted triangles show amino acids important for heme binding (histidine (magenta) functions as ligand for heme and the four other amino acid residues form a hydrogen peroxide binding pocket). Aspartic acid, which forms a hydrogen bond with histidine to stabilize compound I (oxidized heme after transfer of two electrons to H_2O_2) is shown in grey. The black box indicates the GXXDG motif containing the catalytic aspartic acid residue (yellow), which cleaves H_2O_2 heterolytically with the help of the neighboring arginine (green) to form compound I, and the circle presents an exposed tryptophan potentially involved in an LRET (long range electron transfer). Important amino acids for Mn^{2+}-oxidation are highlighted in cyan; asterisks indicate conserved residues, colons equivalent residues and dots partial residue conservation. Peptides identified by protein sequencing are underlined. Alignment was performed with Clustal Omega (European Bioinformatics Institute, Hinxton, UK).

6.3.3 Production and Purification of the Recombinant PsaPOX

The *PsaPOX* gene was amplified and cloned into the *K. phaffii* expression vector pPIC9. The initial expression of the gene yielded average peroxidase activities of 65 U/L after 72 h of cultivation. The best performing colonies produced activities up to 142 U/L, indicating a multiple insertion of the expression construct [218]. Similar results were obtained for the heterologous production of a DyP from *Funalia trogii* in *K. phaffii* previously [118]. Further experiments were performed using the clone with the highest peroxidase activity for maximum protein production.

The recombinant peroxidase was purified by Ni-NTA affinity. Using SDS-PAGE, a molecular mass of around 61 kDa was determined (Figure 6.5a), which is slightly higher than the calculated molecular mass of 54.9 kDa (ExPASy). In addition, the native recombinant enzyme was detected at 52 kDa after semi-native PAGE, while the native wild-type enzyme showed a band at 45 kDa (Figure 6.3 and 6.5b). Deglycosylation by endoglycosidase H (EndoH) showed that the higher molecular mass was attributed to post-translational modifications by *K. phaffii*, as has been described for other proteins [219,220]. The wild-type peroxidase, on the contrary, was not glycosylated (see Figure 6.3 and 6.5b). That is uncommon for DyPs, which usually exhibit a carbohydrate content of 9 to 30% [92]. The molecular mass of the monomeric PsaPOX was similar to other DyP-type peroxidases [92].

Analysis of the purified recombinant peroxidase by isoelectric focusing indicated an isoelectric point around pH 6.7 (Figure 6.5c), which differs slightly from the calculated value of 6.28 (ExPASy), but was similar to the isoelectric point of another DyP-type peroxidase

from *P. sapidus* [112]. Most other proteins belonging to the DyP-type peroxidase family showed lower values (pI 3.5-4.3, [92]).

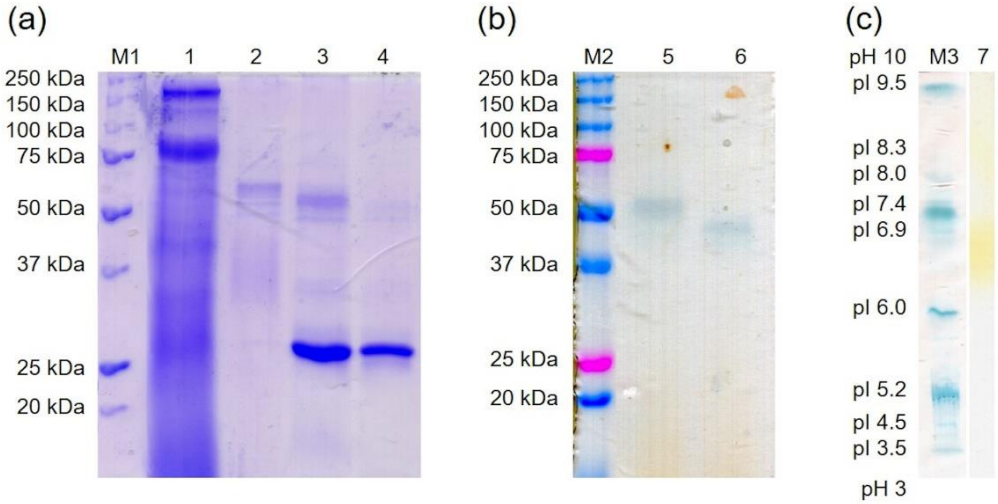

Figure 6.5. Purification of the recombinant PsaPOX by Ni-IMAC. (**a**) SDS-PAGE stained with Coomassie Brilliant Blue. 1: flow through, 2: elution fraction, 3: elution fraction incubated with EndoH, 4: EndoH, M1: molecular mass marker. (**b**) Semi-native PAGE stained with ABTS in the presence of hydrogen peroxide. 5: elution fraction, 6: elution fraction incubated with EndoH, M2: pre-stained molecular mass marker. (**c**) Isoelectric focusing gel. 7: elution fraction stained with phenylendiamine in the presence of urea peroxide. M3: standard protein marker for isoelectric focusing stained with Coomassie Brilliant Blue.

6.3.4 Biochemical Characterization of PsaPOX

The influence of pH and temperature on PsaPOX activity and stability was determined using ABTS in the presence of hydrogen peroxide as substrate (Figure 6.6). The enzyme showed a pH optimum of 3.5 while more than 50% of activity was conserved between pH 3 and 5 (Figure 6.6a). At lower or higher pH values of ≤ 25% of activity remained, most likely due to conformational changes of the enzyme. The results were consistent with the findings for other fungal DyPs, which had pH optima in the range between pH 2 and 5 [98,112,216]. PsaPOX showed the highest pH stability with a residual peroxidase activity of ≥ 90% between pH 2.0 and 5.5 after 1 h of incubation (Figure 6.6c). At pH values higher than six, near the isoelectric point, the stability decreased drastically, probably due to a reduced solubility and changes of the protein structure, which may have resulted in protein aggregation.

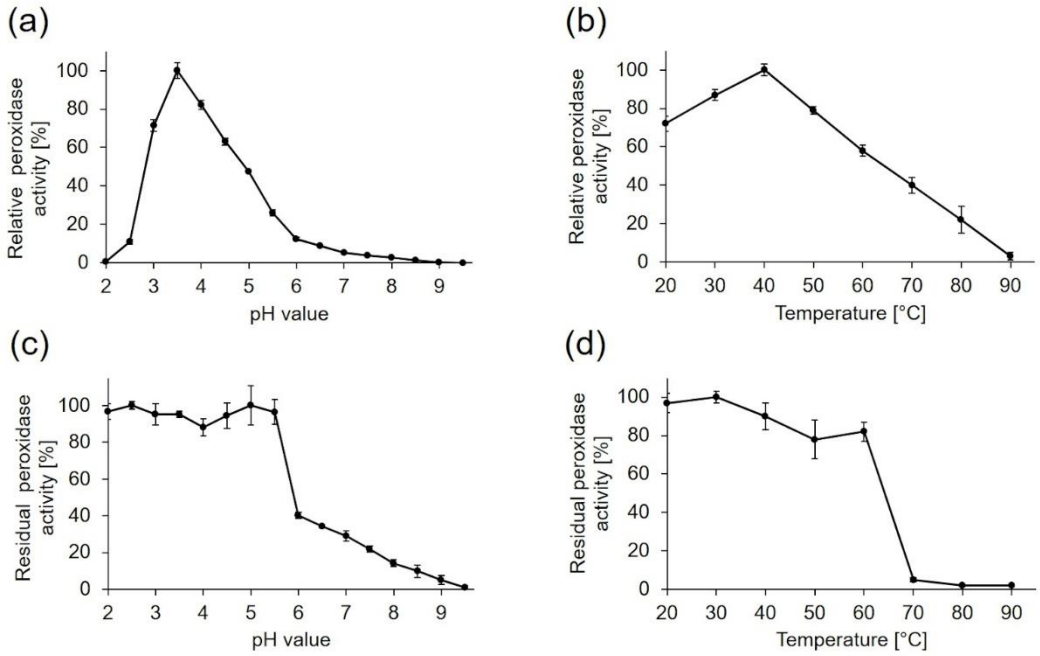

Figure 6.6. Influence of pH and temperature on activity and stability of PsaPOX. The pH optimum (**a**) was determined to be 3.5 and the temperature optimum (**b**) 40 °C. Relative peroxidase activity [%] was defined as the percentage of activity detected with respect to the highest activity in each experiment. pH stability (**c**) was determined after incubation of PsaPOX in Britton Robinson buffer ranging from pH 2.0 to 9.5 for 1 h at RT and temperature stability (**d**) after incubation at 20 to 90 °C and pH 3.5 for 1 h. Residual activities were determined at pH 3.5 and 40 °C. Values are the average of triplicate experiments with standard deviations shown as error bars.

Peroxidase activity of PsaPOX increased with rising temperature, reaching its maximum at 40 °C (Figure 6.6b), which was similar to the optimum (30–40 °C) of a recombinant DyP from *P. ostreatus* [98], but higher than the optimum (RT) of another DyP-type peroxidase of *P. sapidus* produced heterologously in *Escherichia coli* [221]. With further temperature increase, the peroxidase activity of PsaPOX decreased continuously. The temperature stability of PsaPOX was determined after an incubation for 1 h at different temperatures (Figure 6.6d). The enzyme was relatively stable at temperatures from 20 to 60 °C with a residual activity ≥80%. At higher temperatures, a high loss of activity was observed due to protein denaturation, resulting in residual activities <5%. The temperature stability of PsaPOX was higher than the stabilities of DyPs from *Bjerkandara adusta* and *Auricularia auricular-judae*, which were produced heterologously in *E. coli* (residual activity ≥80% and <5% after 1 h at 20–50 °C and 60 °C, respectively [98]), and of a DyP from *P. sapidus* produced in *Trichoderma reesei* (residual activity ≥80% and <65% after 5 min at 15-45 °C and 50 °C, respectively [112]).

As mentioned above, the addition of hydrogen peroxide as well as Mn^{2+} led to an increase of the product concentration for the biotransformation of *trans*-anethole using the lyophilized mycelium of *P. sapidus* containing the wild-type PsaPOX (Supporting Table 6.2, Section 6.7). For this reason, the hydrogen peroxide and Mn^{2+} dependencies were examined for the recombinant enzyme using ABTS as substrate at optimal pH and temperature (Figure 6.7). As expected, no peroxidase activity was detectable without hydrogen peroxide. The activity rose with increasing peroxide concentration and reached its optimum in the presence of 100 µM H_2O_2 (Figure 6.7a). An increase of the hydrogen peroxide concentration led to a continuous activity decrease. Suicide inhibition in the presence of excess hydrogen peroxide is well known for classical peroxidases as a result of the formation of an inactive oxidative state (Compound III) by reaction of H_2O_2 and Compound II [113,114], even if the existence of Compound II has not been confirmed for DyP-type peroxidases universally [109]. However, inhibition of other DyPs in the presence of higher hydrogen peroxide concentrations has been reported [111,112].

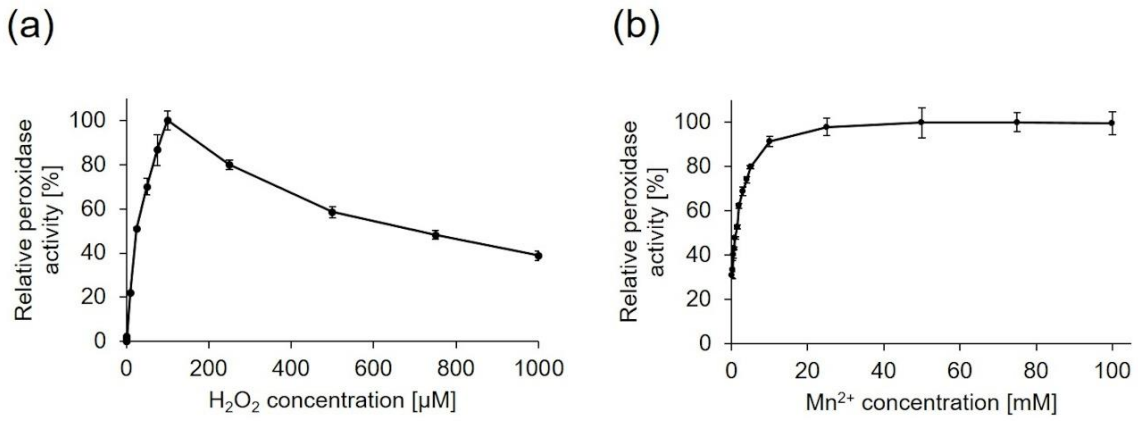

Figure 6.7. Effect of hydrogen peroxide (**a**) and Mn^{2+} concentration (**b**) on the activity of PsaPOX. Relative peroxidase activity [%] was defined as the percentage of activity detected with respect to the highest activity obtained in each experiment. Values are the average of triplicate experiments with standard deviations shown as error bars.

Investigation of the Mn^{2+} dependency (Figure 6.7b) showed that PsaPOX activity rose with increasing Mn^{2+} concentration, but was not completely dependent on the addition of Mn^{2+}. 30% of peroxidase activity were detected without addition of Mn^{2+}. PsaPOX reached the maximal activity in the presence of 25 mM Mn^{2+}. Evaluation of Mn^{3+} formation by Mn^{2+} oxidation revealed a manganese peroxidase activity of 0.4 U compared to 1 U of peroxidase activity using ABTS as substrate. This result fits the prediction of a Mn^{2+} oxidation site. Only a few fungal DyPs are known to catalyze the oxidation of Mn^{2+} [118–120,216]. Calculation

of kinetic constants (Table 6.1) showed that the catalytic efficiency of PsaPOX towards Mn^{2+} was similar to the one of *Pleos*-DyP1 from *P. ostreatus* and Ftr-DyP from *Funalia trogii* [118,216]. However, the catalytic efficiency of *Pleos*-DyP4 was higher [216].

Table 6.1. Michaelis constants (K_m), catalytic constants (k_{cat}), and catalytic efficiencies (k_{cat}/K_m) for PsaPOX using ABTS, Mn^{2+}, Reactive blue 19 (RB19), and Reactive black 5 (RB5) as substrate. Values are the average of triplicate experiments with indication of standard deviations.

Substrate	K_m (µM)	k_{cat} (s^{-1})	k_{cat}/K_m (s^{-1} mM^{-1})
ABTS	37 ± 4	6.8 ± 0.2	184 ± 5
Mn^{2+}	1025 ± 79	7.2 ± 0.1	7 ± 0.1
RB19	n. d.	-	-
RB5	n. d.	-	-

n. d.: no activity was detected.

Kinetic parameters were also calculated for the oxidation of ABTS at optimal conditions (Table 6.1). The affinity of PsaPOX to ABTS (37 µM) was similar to a DyP from *Irpex lacteus* (28 µM), but higher in comparison to the FtrDyP from *F. trogii* (182 µM) and the *Pleos*-DyP2 from *P. ostreatus* (787 µM) [111,118,216]. In contrast, the catalytic efficiency of PsaPOX (184 s^{-1} mM^{-1}) was lower than the efficiency of the DyP from *Irpex lacteus* (8000 s^{-1} mM^{-1}) and *Pleos*-DyP4 (352 s^{-1} mM^{-1}), but higher than the efficiency of the FtrDyP (54 s^{-1} mM^{-1}).

It is known that DyP-type peroxidases typically oxidize anthraquinones and other dyes. Exemplary, decolorization of Reactive blue 19 (anthraquinone dye) and Reactive black 5 (recalcitrant azo dye) by recombinant PsaPOX (1 U/L) was tested. Unexpectedly, PsaPOX showed activity for neither of the substrates (Table 6.1), although the protein sequence and tertiary structure as well as the presence of typical catalytic residues and the GXXDG motif identified the enzyme as a DyP-type peroxidase. However, *Pleos*-DyP1 from *P. ostreatus* and *Tv*DyP1 from *Trametes versicolor* also did not oxidize the high redox-potential Reactive black 5, although they degraded Reactive blue 19 [119,216]. A missing activity against Reactive blue 19 or another anthraquinone has not been described for a fungal or class D type DyP before, but one bacterial DyP of *Pseudomonas fluorescens* (DyP2B, DyP typ class B) is known not to oxidize the anthraquinone dye Reactive blue 4 [121].

6.3.5 Alkene Cleavage Activity of PsaPOX

To prove the ability of PsaPOX to convert *trans*-anethole to *p*-anisaldehyde, biotransformation experiments were performed at optimal conditions using 1 U/mL peroxidase activity. Substrate cleavage was detected in the presence of hydrogen peroxide (Supporting Table 6.3, Section 6.7), whereas no activity was observed in its absence as expected from the peroxidase activity measurement with ABTS (Figure 6.7a). Due to the fact that the semi-purified wild-type DyP showed an alkene cleavage activity without addition of hydrogen peroxide (see Supporting Table 6.2, Section 6.7) a low amount of H_2O_2 must have been present in the analyzed IEX fraction. This was verified by incubation of the fraction with *o*-dianisidine and HRP in the presence of *trans*-anethole. Oxidation of *o*-dianisidine by HRP, which requires H_2O_2 as cosubstrate, and formation of a red-brown reaction product occurred (Supporting Figure 6.2, Section 6.7). Further, analysis of the IEF fraction regarding a hydrogen peroxide producing enzyme revealed a hypothetical protein from *P. ostreatus* (KDQ29984.1). It belongs to the glucose-methanol-choline (GMC) oxidoreductase family as evident from the best hit for the protein band at 75 kDa (Figure 6.3, lane 1) according to protein sequencing (identified tryptic peptides: AADLIK, AIAVEFVR, ELGGVVDTELR, AQYDAWAELNR, VADASIIPIPVSAHTSSTVYMIGER, DLASGDPHGVGVSPESIDV TNYTR, VLGGSTTINAMLFPR, EVVVSAGTIGTPK) and homology search against the public database NCBI (Supporting Figure 6.3, Section 6.7). The protein contained seven of the eight tryptic peptides identified for the 75 kDa band. The last one was found with an amino acid exchange (Arg instead of Lys), which is most likely a result of the different fungal strains the proteins originate from. The protein from *P. ostreatus* showed >92% identity to another hypothetical GMC oxidoreductase from *P. ostreatus* and ≥55% identity to a glucose oxidase from *Moniliophthora roreri* and other fungal alcohol oxidases (Supporting Figure 6.3, Section 6.7), which belong to the GMC oxidoreductase family and are known for the production of hydrogen peroxide during substrate oxidation. Thus, the oxidase (75 kDa band) most likely produced the detected hydrogen peroxide, which was subsequently used as cosubstrate by the wild-type PsaPOX. Due to the fact that the formation of *p*-anisaldehyde by the oxidase under production of H_2O_2 seemed highly unlikely and as no further oxidation products of *trans*-anethole were detected, *trans*-anethole was excluded as substrate. Instead, the buffer component Bis-Tris, which contains several alcohol groups, or carbohydrate functionalities of other proteins in the IEX fraction were assumed to be used as substrate by the oxidase.

As described for the wild-type DyP the *p*-anisaldehyde concentration increased for the biotransformation with the recombinant enzyme in the presence of 25 mM Mn^{2+} (Supporting Table 6.3, Section 6.7). However, product formation in general was low. The residual peroxidase activity was determined during the biotransformation of *trans*-anethole (Supporting Figure 6.4, Section 6.7). After 16 h, 62% of the activity remained, thus inactivation of the enzyme was not responsible for the relatively low product yields.

PsaPOX (1 U/mL) was further examined for alkene cleavage activity regarding other substrates in the presence of hydrogen peroxide and Mn^{2+}. The aryl alkenes (*E*)-methyl isoeugenol as well as *α*-methylstyrene, which are derivatives of *trans*-anethole, were converted to the expected products (veratraldehyde and acetophenone), while piperine was not cleaved (Figure 6.8a). However, the resulting product concentration was fivefold lower for the biotransformation of (*E*)-methyl isoeugenol and more than tenfold lower for the conversion of *α*-methylstyrene than for *trans*-anethole. Different substrate specificities were also observed for the alkene cleavage by other peroxidases, such as HRP, *Coprinus cinereus* peroxidase, and a human myeloperoxidase [192,196], but a conversion of aryl alkenes using a DyP-type peroxidase has not been described before.

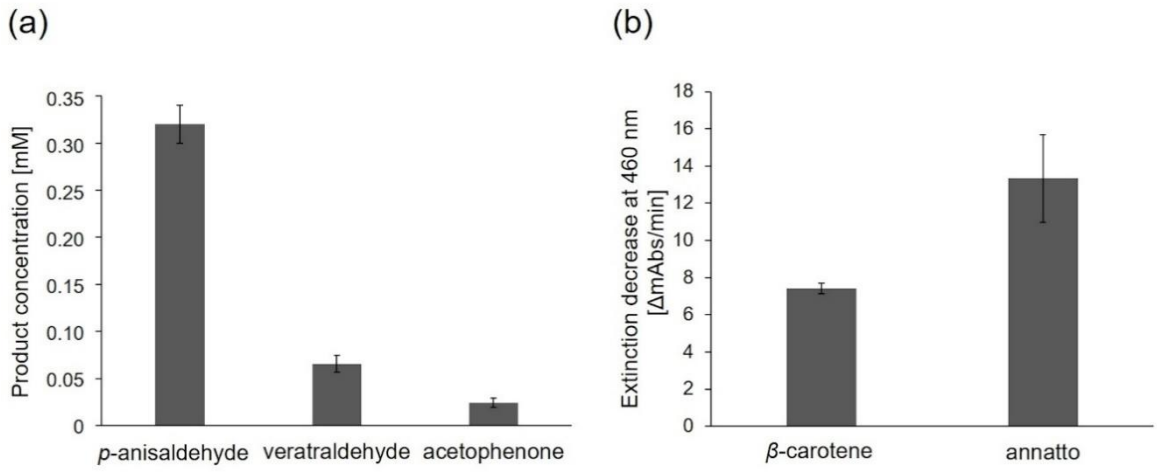

Figure 6.8. Alkene cleavage activity of PsaPOX on different substrates in the presence of 100 µM H_2O_2 and 25 mM $MnSO_4$ at pH 3.5. (**a**) Product concentration after conversion of *trans*-anethole (6.7 mM) to *p*-anisaldehyde, (*E*)-methyl isoeugenol (6.7 mM) to veratraldehyde, and *α*-methylstyrene (6.7 mM) to acetophenone by PsaPOX (1 U/mL) at RT. The presented product concentrations are the differences between the values determined for the reaction with the active and heat inactivated enzyme (blank) (the original values are shown in Supporting Table 6.4, Section 6.7). (**b**) Decolorization of 7% (v/v) *β*-carotene and 7% (v/v) annatto by PsaPOX (1 U/L) at 40 °C. Cleavage of carotenoids was shown as extinction decrease per min. Values are the average of triplicate experiments with standard deviations shown as error bars.

In addition to the described substrates, PsaPOX (1 U/L) also showed an alkene cleavage activity towards the natural dyes *β*-carotene and annatto (mixture of the xanthophylls bixin and norbixin), which was detected by substrate bleaching (Figure 6.8b). The activity for annatto was higher than for *β*-carotene. Cleavage of *β*-carotene and annatto is also known for other fungal DyPs [96,97,112,222]. For example, cleavage of *β*-carotene by a DyP from *Lepista irina* resulted in formation of the volatiles *β*-ionone, *β*-cyclocitral, dihydroactinidiolide, and 2-hydroy-2,6,6-trimethylcyclohexanone [222].

6.4 Materials and Methods

6.4.1 Chemicals and Materials

Chemicals were obtained from Sigma-Aldrich (Seelze, Germany), Carl-Roth (Karlsruhe, Germany), or Merck (Darmstadt, Germany) in *p. a.* quality. Enzymes were from Thermo Fisher Scientific (Braunschweig, Germany), if not stated otherwise. PCR primers were obtained from Eurofins MWG Operon (Ebersberg, Germany).

6.4.2 Cultivation of *P. sapidus*

P. sapidus (Deutsche Sammlung von Mikroorganismen und Zellkulturen GmbH, DSMZ, strain no. 2866) was pre-grown on 1.5% (*w/v*) agar plates with standard nutrient liquid (SNL) medium and maintained at 4 °C until use [96]. For pre-cultivation, 1 cm^2 of grown agar was transferred to 100 mL SNL medium and homogenized using an Ultraturrax homogenizer (ART Prozess- & Labortechnik, Müllheim, Germany). The pre-cultures were incubated for 5 days at 150 rpm and 24 °C. Afterwards, 6.5 g of pre-grown mycelium was used to inoculate 250 mL SNL. The main culture was incubated at 150 rpm and 24 °C. After six days, the mycelium was separated from the culture supernatant by centrifugation (5000 ×*g*, 4 °C, 15 min) and lyophilized as described elsewhere [78].

6.4.3 Purification Strategy

Ten g of lyophilized mycelium were re-suspended in 400 mL buffer A (50 mM Bis-Tris, pH 6.0, 1 M $(NH_4)_2SO_4$) and extracted for 1 h at 4 °C in horizontal position in an orbital shaker. Insoluble components were removed by centrifugation (5000 ×*g*, 4 °C, 15 min) followed by filtration (PES filter, 0.45 µm, Merck). Subsequently, 80 mL filtered supernatant were applied on a Phenyl Sepharose fast flow column (20 mL, GE Healthcare Bio-Sciences

AB, Uppsala, Sweden) pre-equilibrated with buffer A. After the column was washed with buffer A, the active enzyme was eluted with a linear gradient (130 mL, 100–0% buffer A) with 100% distilled water at a constant flow rate of 2 mL/min. Active fractions were pooled, desalted and concentrated by ultrafiltration (3 kDa cut off, polyethersulfone (PES), Sartorius, Göttingen, Germany). Concentrate (20 mL) was diluted two times with 20 mM sodium acetate pH 4.0 (buffer B) and loaded onto three linked HiTrap SP Sepharose columns (1 mL, GE Healthcare Bio-Sciences AB) pre-equilibrated with buffer B. Proteins were eluted with a stepwise ionic strength gradient (0, 20, 100% buffer C: 20 mM sodium acetate pH 4.0, 1 M NaCl) with 100% buffer C at a constant flow rate of 1 mL/min.

6.4.4 Gel Electrophoresis

SDS-PAGE analysis was performed as described elsewhere [28]. Semi-native PAGE was performed under non-denaturing conditions using 12% gels. For this, samples were prepared with a native loading buffer (without DTT and without 2% (w/v; 6.9 mM) SDS) and gel electrophoresis was performed at 10 mA per gel and 4 °C. Gels were stained with 0.5 mM ABTS (dissolved in 100 mM sodium acetate buffer pH 3.5 or 4.5) in the presence of 100 µM hydrogen peroxide for detection of peroxidases. For deglycosylation, samples were treated with 1 µL (500 U) endoglycosidase H (EndoH, New England BioLabs, Ipswich, MA, USA) in 20 µL for 2 h at 37 °C before gel electrophoresis.

6.4.5 Isoelectric Focussing

Analytical isoelectric focusing polyacrylamide gel electrophoresis was performed on a HPE™ BlueHorizon™ system (Serva Electrophoresis GmbH, Heidelberg, Germany) using Servalyt™ Precotes™ Precast Gels (Serva Electrophoresis GmbH) with an immobilized pH gradient of pH 3 to 10. To determine the isoelectric points of the enzymes, marker proteins (IEF-Marker 3-10, Serva Electrophoresis GmbH) were used. Gels were stained with Coomassie Brilliant Blue, or for specific visualization of peroxidases, with 1% (w/v; 9.2 mM) phenylendiamine and 1% (w/v; 10.6 mM) urea peroxide (dissolved in 100 mM sodium acetate buffer pH 3.5) at RT until a yellow band was observed.

6.4.6 Peptide Mass Fingerprinting

Protein bands were excised from SDS gels, dried, and tryptically hydrolysed. The resulting peptides were extracted and purified according to standard protocols and the amino acid sequence was analyzed with electrospray ionization-tandem mass spectrometry (ESI-MS/MS) using a maXis quadrupole time of flight (QTOF) mass spectrometer (Bruker, Bremen, Germany) as described previously [28,223]. The obtained partial sequences of PsaPOX and of the oxidase were used for a similarity search against public databases (NCBI BlastP).

6.4.7 cDNA Synthesis and Gene Amplification

Isolation of total RNA from mycelium of *P. sapidus* at culture day six and cDNA synthesis were performed as described previously [98] using the primer 5′-AAGCAGTGGTATCAACGCAGAGTACGCTTTTTTTTTTTTTTTTT-3′ for reverse transcription. Specific primers for gene amplification were deduced from the ORF-start (P1: 5′-ATGACTACACCTGCACCACCCCTCGACCTC-3′) and -stop (P2: 5′-TCAAGCAGAGATTGGAGCTTGGGTSWGAGGA-3′) region of the homologous peroxidase of *Pleurotus ostreatus* PC15 (GenBank accession no. KDQ22873.1). PCRs were performed with Phusion High-Fidelity DNA Polymerase and the Master Cycler gradient (Eppendorf, Hamburg, Germany) as described elsewhere [224]. The cycler program was as follows: denaturation for 2 min at 98 °C, 35 cycles at 98 °C for 1 min, 62 °C for 30 s and 72 °C for 90 s, and a final elongation at 72 °C for 10 min. Analysis of PCR products, ligation, transformation in *Escherichia coli*, colony PCR, and sequencing were performed as described by Behrens *et al.* [98]. Translation of DNA sequences was performed using SnapGene® (GSL Biotech LLC, Chicago, IL, USA). Sequence homology was examined using BLAST [225]. Alignments were produced by ClustalOmega [226].

6.4.8 Heterologous Expression of PsaPOX in *Komagataella phaffii*

The gene of PsaPOX was amplified with a C-terminal 6x His tag using the primers PsaPOX_fw 5′-AAAAAGAATTCatgactacacctgcaccacccctcgacctcaacaa-3′ and PsaPOX_rev 5′-atatatGCGGCCGCtcaGTGGTGATGGTGATGATGgtagagatcggagcctgggcctg-3′ (underlined are the EcoRI and NotI restriction sites, respectively; lower cases represent parts of the coding *PsaPOX*). In addition, it was inserted in frame with the *Saccharomyces cerevisiae* α-factor secretion signal sequence into the *K. phaffii* pPIC9 expression vector

(Invitrogen, Karlsruhe, Germany). The resulting expression construct pPIC-PsaPOX-His was transformed into *E. coli* TOP10 for vector propagation, isolated (NucleoSpin, Macherey-Nagel, Düren, Germany), linearized with PmeI, and used for transformation of *K. phaffii* GS115 according to a standard protocol [227]. The linearized empty vector was transformed in the same way and served as negative control. Forty-eight transformants were tested for peroxidase activity after selection according to their ability to grow on histidine-deficient agar plates in 96-well plates for 120 h, as described elsewhere [228]. Gene expression was induced by daily addition of 1% (v/v) methanol.

6.4.9 His-Tag Purification of Recombinant PsaPOX

For purification of the His-tag labelled recombinant enzyme from *K. phaffii* culture supernatant, Ni-NTA affinity chromatography was used according to Nieter *et al.* [229].

6.4.10 Biotransformation

Transformation of *trans*-anethole was carried out in 4 mL gas tight glass vials in horizontal position at a shaking rate of 200 rpm for 16 h at RT in the absence of light. Reaction mixtures contained 30 mg *P. sapidus* lyophilisate or 100 µL liquid sample buffered in Bis-Tris (50 mM, pH 6) with or without addition of 1 mM manganese sulfate in a total volume of 1 mL and 1 µL (6.7 mM) *trans*-anethole. Blanks (chemical: without lyophilisate or liquid sample; biological: with heat inactivated mycelium (1 h at 95 °C)) were performed the same way. All experiments were performed as duplicates. After incubation, *trans*-anethole and its conversion product *p*-anisaldehyde were extracted with 1 mL hexane containing 100 mg/L (1 mM) cyclohexanol as internal standard (IS). The organic phase was dried with anhydrous sodium sulfate and subsequently analyzed by gas chromatography (GC). GC measurements were performed with an Agilent 7890 instrument equipped with a DB-WAX UI column (30 m × 0.32 mm, 0.25 µm, Agilent, Santa Clara, CA, USA), a split/splitless injector port (1:5) and a flame ionization detection (FID) system. Hydrogen was used as carrier gas at a constant flow rate of 2.1 mL per minute. One µL sample was injected *via* an autosampler and measured using the following method: 40 °C (3 min), a temperature increase of 10 °C per minute until 230 °C and a final hold time of 10 min. The *trans*-anethole and *p*-anisaldehyde were semi-quantified referring to the area of the internal standard. Biotransformation products were identified using standards and comparison of retention indices with literature.

6.4.11 Enzyme Activities

Total peroxidase activity was determined photometrically (EON^{TM} High Performance Microplate Spectrophotometer, BioTek Instruments GmbH, Bad Friedrichshall, Germany) by monitoring the oxidation of ABTS in the presence of hydrogen peroxide at 420 nm ($\varepsilon_{420} = 3.6 \times 10^4\ M^{-1}\ cm^{-1}$) and 30 °C for 10 min. For this, the samples were mixed with sodium acetate buffer (100 mM, pH 4.0 or pH 3.5), 0.1 mM hydrogen peroxide, and 0.5 mM ABTS in a total volume of 300 µL. One unit of enzyme activity was defined as 1 µmol substrate oxidized per minute under the experimental conditions.

To determine manganese peroxidase activity, samples were mixed with manganese sulfate (1 mM), malonate buffer (100 mM, pH 3.5), and hydrogen peroxide (0.1 mM) in a total volume of 300 µL. Mn^{3+} formation was monitored photometrically at 270 nm ($\varepsilon_{270} = 1.16 \times 10^4\ M^{-1}\ cm^{-1}$) and 30 °C for 30 min. One unit of enzyme activity was defined as 1 µmol Mn^{3+} per minute released by manganese peroxidases at the given conditions.

Decolorization of Reactive blue 19 (RB19, 150 µM) and Reactive black 5 (RB5, 80 µM) by PsaPOX (1 U/L; 0.25 mg/L) was tested. The respective anthraquinone dye and the enzyme was incubated in the presence of 100 µM hydrogen peroxide, 25 mM manganese sulfate, and 100 mM sodium acetate buffer pH 3.5 in a total volume of 300 µL at 40 °C for 20 min. Decolorization was monitored photometrically at 595 nm (RB19; $\varepsilon_{595} = 1.0 \times 10^4\ M^{-1}\ cm^{-1}$) or 598 nm (RB5; $\varepsilon_{598} = 3.0 \times 10^4\ M^{-1}\ cm^{-1}$). One unit of enzyme activity was defined as 1 µmol dye degraded per minute at the given conditions.
All enzyme assays were performed as triplicates. Blanks were carried out with water instead of enzyme and by omission of hydrogen peroxide.

6.4.12 Biochemical Characterization of PsaPOX

Effects of pH and temperature on peroxidase activity of PsaPOX (0.25 mg/L) were analyzed with ABTS as substrate as described above (see Section 6.4.11). Relative activities were normalized to the highest activity and residual activities to the initial activity prior incubation. The pH optimum was determined using Britton-Robinson buffer [230] in a range of pH 2.0–9.5 instead of sodium acetate buffer. For determination of the temperature optimum the activity assay was performed at different temperatures (20–90 °C) at pH 3.5, whilst for analysis of the temperature stability the enzyme was incubated for 1 h at 20–90 °C prior enzyme activity measurement at pH 3.5 and 40 °C. For the analysis of pH-stability PsaPOX

was incubated in Britton-Robinson buffer from pH 2.0 to 9.5 for 1 h at RT before the peroxidase activity was examined at pH 3.5 and 40 °C.

Hydrogen peroxide as well as Mn^{2+} dependency of PsaPOX were determined for PsaPOX by evaluation of peroxidase activity as described above (Section 6.4.11) with changing hydrogen peroxide and manganese sulfate concentrations (H_2O_2: 0–1 mM H_2O_2, without addition of $MnSO_4$; Mn^{2+}: 100 µM H_2O_2, 0–100 mM $MnSO_4$) at optimal pH and thermal conditions. Kinetic constants of PsaPOX were calculated for Mn^{2+} and ABTS (0–300 µM ABTS in the presence of 100 µM H_2O_2 and 25 mM $MnSO_4$) by SigmaPlot 12.5 (Systat Software Inc., Chicago, IL, USA) with nonlinear regression. Protein concentrations were determined according to Lowry *et al.* [231] using bovine serum albumin as standard.

6.4.13 Alkene Cleavage Activity of PsaPOX

The purified recombinant PsaPOX was used for transformation of *trans*-anethole as mentioned above (Section 6.4.10) to confirm alkene cleavage activity. For this, 1 U/mL (0.25 mg/mL) of enzyme was used for biotransformation. Biotransformation was performed with 100 mM sodium acetate buffer pH 3.5 in the presence of 100 µM hydrogen peroxide and 25 mM manganese sulfate at RT for 16 h. Biotransformation of the alkenes methyl isoeugenol (6.7 mM), *α*-methylstyrene (6.7 mM), and piperine (0.7 mM) was tested accordingly. Blanks were performed without enzyme (chemical blank) or with heat inactivated enzyme (1 h at 95 °C, biological blank). The determined product concentrations for the blanks were subtracted from the concentrations yielded for the reaction with the active enzyme to calculate the enzymatically generated product concentration. For carotene degradation, a *β*-carotene emulsion was prepared according to Linke *et al.* [28]. 7% (v/v) of *β*-carotene emulsion or annatto (Chr. Hansen, Nienburg, Germany, Prod. No. 240569), 100 µM hydrogen peroxide, 25 mM manganese sulfate, 100 mM sodium acetate pH 3.5, and 1 U/L (0.25 mg/L) PsaPOX in a total volume of 300 µL was incubated at 40 °C for 20 min. Alkene cleavage of both substrates was measured photometrically as extinction decrease at 455 nm.

6.4.14 Detection of Hydrogen Peroxide

For the detection of H_2O_2, 75 µL IEX fraction, 50 mM Bis-Tris pH 6.0, 6.7 mM *trans*-anethole, 10 U/mL HRP (Sigma Aldrich), and 0.5 mM *o*-dianisidine in a total volume of 300 µL were incubated at RT for 1 h. In the presence of hydrogen peroxide, formation of a red-brown reaction product occurred. Blanks were performed with 50 mM Bis-Tris pH 6.0 instead of IEX fraction.

6.4.15 Sequence Accession Numbers

The nucleotide sequence of the *PsaPOX* gene has been deposited in the GenBank database under accession number MT043310.

6.5 Conclusions

A DyP-type peroxidase of *P. sapidus* with alkene cleavage activity as well as the corresponding gene were identified and the gene was heterologously expressed in *Komagataella phaffii*. The PsaPOX possessed typical sequence motifs, structural topology, and catalytic residues as described for DyPs, even though the decolorization of the anthraquinone Reactive blue 19, a common reaction for DyPs, was not observed. A non-canonical Mn^{2+}-oxidation site on the protein surface was detected, which allows PsaPOX to oxidize Mn^{2+}. After biochemical characterization, the alkene cleavage activity of PsaPOX towards different aryl alkenes was confirmed by biotransformation. PsaPOX is the first described DyP-type peroxidase with such an activity. In addition, bleaching of *β*-carotene and annatto was determined. The results for the alkene cleavage underline the potential of the PsaPOX as biocatalyst for the generation of aromatic aldehydes with olfactory properties, such as *p*-anisaldehyde, veratraldehyde, or acetophenone, which are used in the fragrance and flavor industry [167]. Improvement of the conversions and product yields may be accomplished by protein engineering, as has been shown for the alkene cleaving manganese-dependent Cupin TM1459 from *Thermotoga maritima* [232]. Another application beyond aroma production could be carotene bleaching of whey or wheat dough.

6.6 Author Contributions, Funding, Acknowlagements, and Conflict of Interest

Author Contributions: Conceptualization, N.K.K. and R.G.B.; methodology, N.K.K.; validation, N.K.K., R.G.B. and F.E.; formal analysis, N.K.K.; investigation, N.K.K; writing—original draft preparation, N.K.K.; writing—review and editing, R.G.B. and F.E.; visualization, N.K.K.; supervision, F.E.; project administration, R.G.B.; funding acquisition, R.G.B. All authors have read and agreed to the published version of the manuscript.

Funding: This research was funded the BMBF cluster Bioeconomy International 2015, grant number 031B0307A. The APC was funded by the Open Access fund of the Gottfried Wilhelm Leibniz Universität Hannover.

Acknowledgments: B. Fuchs and A. Nieter are thanked for detecting the cleavage reaction and the peroxidase activity during the screenings.

Conflicts of Interest: The authors declare no conflict of interest.

6.7 Supplementary Materials

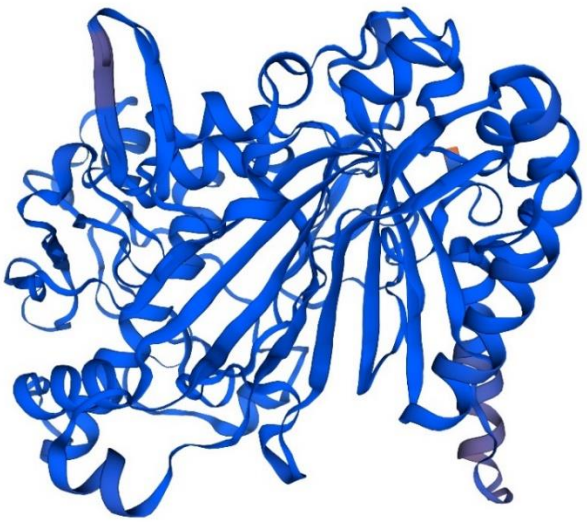

Supporting Figure 6.1. Structural homology model of PsaPOX. The model was generated with the SWISS-MODEL server using the X-ray crystal structure of *Pleos*-DyP4 (PDB-ID 6fsk).

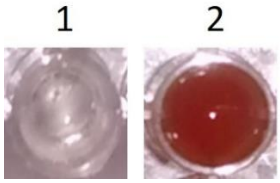

Supporting Figure 6.2. Optical detection of hydrogen peroxide in the IEX fraction with *o*-dianisidine and HRP in the presence of *trans*-anethole after 1 h of incubation at pH 6.0 and RT. 1: blank (buffer instead of IEX fraction); 2: IEX fraction. *o*-Dianisidine was oxidized to a red brown colorant by HRP in the presence of hydrogen peroxide.

```
KDQ29984.1      mlhqsypyltshlawlpltsasafvywrgidlplifpsrlsrhnlragrrmihdtnrgvqgpdwr     65
KDQ29972.1      ----------------------------------------------------mhlflr--lliacv     12
ESK85927.1      ------------------------------------------------------------mfsiyp      6
KLO09144.1      ---------------------------------------------------------mk-ail---s      6
THU81532.1      -------------------------------------------------mt---vk-flvaacv     11

KDQ29984.1      --glrssiatsstydyviigggtaglavanrlsedplvsiavieagpnaehlrevfipglf---g     125
KDQ29972.1      --glrssiatssaydyviigggtaglavasrlsedpsvsivvieagpnaehlpevfipglf---g      72
ESK85927.1      avivlsllhsafsydyvvigggtagltvasrlaeddsvqvavieaganaehrpdvfipgmlgqig      71
KLO09144.1      ylfvlqlalrsvafdyvivgggtagltvasrlsedpsvtvavieagpnaenlpevfvpgli---g      68
THU81532.1      aalapvanvlassydyiiigggtggltvasrlaedksnqvlvleagpnaeglqevfvpgli---g      73
                          : ::**:::****.**:**.**:**    : *:*** ***   :**:**::   *

KDQ29984.1      sgqalttlnwaykttpqpmlnnrslvvnagrvlggsttinamlfpragraqydawaelnrdaswg     190
KDQ29972.1      sgqafttlnwaynttpqpmlnnrslvvnagrvlggsttinamlfpragraqydawaelnrdaswg     137
ESK85927.1      vgtkppelnwayktvpqthlngrvltvnagralggstvinamifprakkeqydawgilnndtswt     136
KLO09144.1      tgqsfttlnwayrtvpqvnlnsrnltvnagkalggstiinsmifpraekeqydvwgalnndsswt     133
THU81532.1      tgqsfttlnwayrtapqenlnnrtltvnagkalggstiinsmifpraekaqydawgtlnndsswt     138
                 *     *****.*.**  **.* *.****:.***** **:*:**** : ***.*. **.*:**

KDQ29984.1      wdallpffrrservtppdafqvnagsvtyvpevhgsa-sdgrvkvgypniffeqstlwrqaavav     254
KDQ29972.1      wdallpffrrservtppdafqvneggityvpevhgsa-sdgrvkvgypniffeqstlwrqaavav     201
ESK85927.1      weallpffkrsesftvpndfqasn-garydpqfhgfd---gslkvgfpnyffpqemlwqntsigl     197
KLO09144.1      wdallpffknseiftppnafqsas-gvrfdpsvhgfs---grvhvgfpnfffeqsqlwvktsegl     194
THU81532.1      wdallpffkkseiftppnefqrdn-gatfvrdvhgfnesegrvkvgfpnfffpqstlwrqtsmgl     202
                *:******:.** .* *: **    .  :  ..**     * ::**:** ** *. ** ::: .:

KDQ29984.1      gfpgerdlasgdphgvgvspesidvtnytrcsaacayytpfasrpnfnvitnatvtrivwdtpsp     319
KDQ29972.1      gfpgerdlasgdphgvgvspesidvtnytrcsaacayytpfasrpnfnvitnatvtrvvwdtpss     266
ESK85927.1      gfpaatdlsngephavgpspfsidainqtrcsaacafytpfadrpnftiitnanvtriiwsesen     262
KLO09144.1      gfpaspdlangdphavgvapdslnaanntrcsaacayftpfaerpnftvflnatvsriiwdsnst     259
THU81532.1      gfpaspdlangsphavgvapdsldaanntrcsaacayftpfaeqpnftvltnvtvtriiwtasaq     267
                ***.  **:.*.**.** :* *::. * ********::****.:***.:: *..*:*::*

KDQ29984.1      gshsnegqrnlraiavefvragsnr-tesvtvrrevvvsagtigtprvfelsgignssiiraagv     383
KDQ29972.1      gshsdksqrnlraiavefvragsnr-tesvtvrrevvvsagtigtpklfelsgignssiiraagv     330
ESK85927.1      n-------sslaatgveyvtnnetm---tlevtgevilsagtigspkilelsgignstilraagv     317
KLO09144.1      an-----agstkaiaveyiasngttlqa--sverevivsagtigspkvlelsgvgnatiltaagv     317
THU81532.1      nd------stltasgveyidslnqtsrailsrkgevivsagtigspkilelsgvgnstilqaagi     326
                         .  * .**::              **::******:*:::****:**::*: ***:

KDQ29984.1      npvlelpsvgenlag-----------------------------------------lltsfpgslgl     409
KDQ29972.1      npvlelpsvgenlagef---------------------------------------clltsfpgslgl     358
ESK85927.1      eplldlptvgenla-------------------------------------------gmyaavsktlgi     342
KLO09144.1      qpqvnlstvgenladhvhnwvnsftsfnltkdl-lnnatflaeqlelwnktrtgllsaaprslgi     381
THU81532.1      spaldlptvgenladhvhswanaftnisltkdalllntdfaqqqldlwfknrtglysaaprslgi     391
                .* ::* :******                                          : ::   :**:

KDQ29984.1      pgplnifndtrilptllqeakanlshfahlfangnallekgiraqheivlrsyaddvalplens-     473
KDQ29972.1      pgplnifnntgilptllqeakanlthfahlfangnallekgiraqheivlrsyaddvalplensl     424
ESK85927.1      tapldvvsqsq-ldtlltqaesnlshyasqfsngnpdlargieaqhrlafslyqenqqlcveln-     406
KLO09144.1      aapsnvfnqsq-ltalvtqsranltataisfsngnadlakgiaaqldhalslyaedkelplemn-     444
THU81532.1      aapsdvfeese-fnrllnqseeslsrfasefsngnpqlakgiesqyrialslyrqnenlplemn-     454
                 .* ::..::  :  *: ::. .*:  *  *:***  * :** :*   .:  * ::  * :* .

KDQ29984.1      ------lfpgyaga--aadrpqrnyttimnvlyaplsrgrthitssdirtapvvdpayymhplda     530
KDQ29972.1      caallsyfpgyaga--aadrpqrnyttimnvlyaplsrgrthitssdirtapvvdpayymhplda     487
ESK85927.1      ------ldagyvgptplesrplrnfttvstilyaplargrshisssdpftvplvdpaywahpmdv     465
KLO09144.1      ------lepgysgptplavrpnrtfttintvlyaplsrgrthitssspsvppavdpnyyahpmdi     503
THU81532.1      ------lepgysgptafadrparnytainsvlysplsrgrthissssplaapvvdpaywahpldv     513
                       ** *      ** *.:*:: .:**:**:***:**:**.  . * *** *: **:*

KDQ29984.1      athaaginlarktlitppmdsiylgefepgkdvtspqdissvlraaivssdnhvtgtmammpkel     595
KDQ29972.1      athaaginlarrtlitppmdsiylgefepgkdvtspqdissvlraaivssdnhvtgtmammpqel     552
ESK85927.1      aihvggiqlakkmlrsppldsiydgefepgve--sdkeienwlrgn-vtsdnhvtgtlsmlprel     527
KLO09144.1      aahiggirlarrmltspplgdsflgefepgaekvsdaqigswlran-atsdnhetgtaammprel     567
THU81532.1      aiqvagiklarkmlqssplsstyegefepgtdketdaeieewlrgv-vasdnhevgslamlpkdm     577
                * : .**.**:: * : *:.. : ****** :  :  :* . **.  .:**** .*: :*:*:::

KDQ29984.1      ggvvdtelrvygignvrvadasiipipvsahtsstvymigeraadlikhsrspl-----------     649
KDQ29972.1      ggvvdtelrvygienvrvadasiipipvsahtvgplrllithladlqpvvdclhdwraresilwv     622
ESK85927.1      ggvvdtqlkvygtmnvrvvdasvipfpvsahtsstvymigeraadiirksrgn-----------     580
KLO09144.1      ggvvdtnlkvygtanvrvvdasiipfpisahisstvyaigekvrqsd-----------------     614
THU81532.1      ggvvdtellvygtsnvrvvdasvipfpisahlsssvymigeraadiikrn---------------     627
                ******:* ***  ****.***:**:*:***  . :  :  :  :

KDQ29984.1      ---------------------------                                         649
KDQ29972.1      lllaafltrvlrlqisssivdihcnhl                                         644
ESK85927.1      ---------------------------                                         580
KLO09144.1      ---------------------------                                         614
THU81532.1      ---------------------------                                         627
```

◀**Supporting Figure 6.3.** Alignment of the hypothetical protein (KDQ29984.1) from *P. ostreatus*, which was revealed as the best hit for the 75 kDa band of the IEX fraction by a homology search against the public database NCBI, and other members of the GMC oxidoreductase family. KDQ29972.1: hypothetical protein from *P. ostreatus*; ESK85927.1: glucose oxidase from *Moniliophthora roreri*; KLO09144.1: alcohol oxidase from *Schizopora paradoxa*; THU81532.1: alcohol oxidase from *Dendrothele bispora*. Asterisks indicate conserved residues, colons equivalent residues and dots partial residue conservation. Peptides identified by protein sequencing are underlined. Alignment was performed with Clustal Omega (European Bioinformatics Institute, Hinxton, UK).

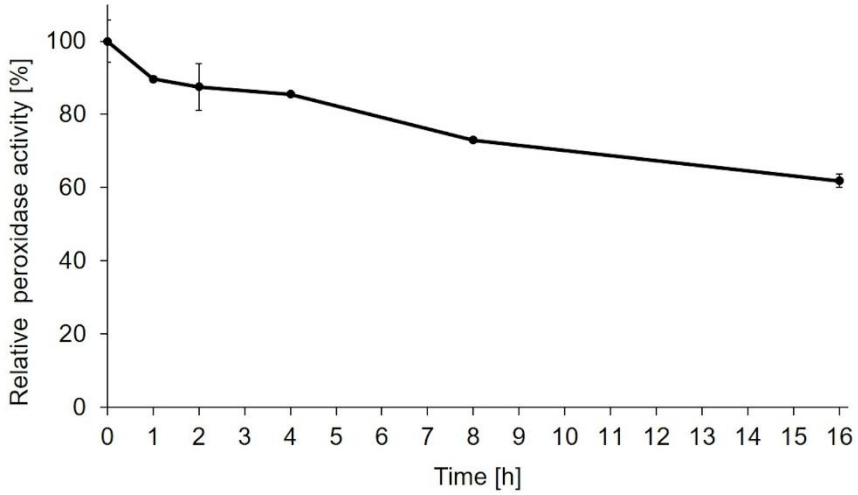

Supporting Figure 6.4. Stability of PsaPOX during biotransformation of *trans*-anethole over 16 h. The reaction was performed in the presence of 100 µM H_2O_2 and 25 mM $MnSO_4$ in 100 mM sodium acetate buffer pH 3.5 at RT. Relative peroxidase activity [%] was defined as the percentage of activity detected with respect to the starting activity. Values are the average of triplicate experiments with standard deviations shown as error bars.

Supporting Table 6.1. *p*-Anisaldehyde concentration after biotransformation of *trans*-anethole with different basidiomycetes.

strain	***p*-anisaldehyde concentration [mM]**	**origin**
Pleurotus sapidus	5.36	DSMZ, strain no. 2866
Pleurotus eryngii	4.07	CBS, strain no. 613.91
Pleurotus ostreatus	3.74	DSMZ, strain no. 1020
Pleurotus ostreatus var. *florida*	2.00	Laboratory collection
Pleurotus sajor-caju	1.14	DSMZ, strain no. 5339
Pleurotus pulmonarius	1.04	DSMZ, strain no. 5331
Trametes versicolor[*]	0.96	Laboratory collection
Trametes suaveolens	0.62	DSMZ, strain no. 5237
Pleurotus lampas	0.79	CBS, strain no. 323.49
Lentinus lepideus	0.29	CBS, strain no. 450.79
Wolfiporia cocos	0.18	CBS, strain no. 279.55
Gloeophyllum odoratum	0.18	CBS, strain no. 444.61
Piptoporus soleniensis	0.17	CBS, strain no. 492.76
Schizophyllum commune	0.10	DSMZ, strain no. 1024
Gloephyllum trabeum	0.00	DSMZ, strain no. 3087
Phanerochaete chrysosporium	0.00	DSMZ, strain no. 1547

[*] Two variants of the strain were tested for the bioconversion. The results for the strain with higher *p*-anisaldehyde concentrations are presented.

DSMZ: Deutsche Sammlung von Mikroorganismen und Zellkulturen GmbH, CBS: Westerdijk Fungal Biodiversity Institute

Supporting Table 6.2. *p*-Anisaldehyde concentration after biotransformation of *trans*-anethole with the active IEX fraction in the presence or absence of Mn^{2+} and/or hydrogen peroxide for 16 h at RT. The shown *p*-anisaldehyde concentrations are the average of duplicate experiments with indication of standard deviations.

$MnSO_4$ concentration [mM]	**H_2O_2 concentration [µM]**	***p*-anisaldehyde concentration [µM]**
0	0	30 ± 1
1	0	450 ± 17
1	50	600 ± 12

Supporting Table 6.3. *p*-Anisaldehyde concentration after bioconversion of *trans*-anethole by recombinant PsaPOX with and without addition of hydrogen peroxide and Mn^{2+} for 16 h at RT. The shown *p*-anisaldehyde concentrations are the average of duplicate experiments with indication of standard deviations.

$MnSO_4$ concentration [mM]	**H_2O_2 concentration [µM]**	***p*-anisaldehyde concentration [µM]**
0	0	0 ± 0
0	100	189 ± 6
25	100	320 ± 20

Supporting Table 6.4. *p*-Anisaldehyde concentration after biotransformation of *trans*-anethole, (*E*)-methyl isoeugenol, and *α*-methylstyrene by recombinant PsaPOX (1 U/mL) in the presence of 100 µM H_2O_2 and 25 mM $MnSO_4$ for 16 h at pH 3.5 and RT. The shown values are the average of duplicate experiments with indication of standard deviations.

Substrate	**Product**	**Product concentration active enzyme [µM]**	**Product concentration inactivated enzyme (control) [µM]**
trans-anethole	*p*-anisaldehyde	342 ± 20	22 ± 7
(*E*)-methyl isoeugenol	veratraldehyde	114 ± 12	48 ± 9
α-methylstyrene	acetophenone	24 ± 7	0 ± 0

7 Vorwort zur Publikation „Monokaryotic *Pleurotus sapidus* Strains with Intraspecific Variability of an Alkene Cleaving DyP-type Peroxidase as Result of Gene Mutation and Differential Gene Expression"

Wie in Kapitel 6 dargestellt, besitzt *P. sapidus* eine alkenspaltende DyP (PsaPOX) mit Aktivität gegenüber verschiedenen Arylalkenen. Für eine spätere industrielle Anwendung zur Aromastoffproduktion sollte die entsprechende Enzymaktivität verbessert werden. Da gentechnische Verfahren von der europäischen Bevölkerung abgelehnt werden [50,165], wurde eine gentechnikfreie Methode verwendet – die Generierung einer Tochterpopulation von monokaryotischen *P. sapidus*-Stämmen mit natürlicher genetischer und biochemischer intraspezifischer Variabilität durch die sexuelle Reproduktion des Dikaryoten (vgl. Kapitel 1.1.2 und 1.2.3). Dieses Verfahren konnte bereits erfolgreich für die Optimierung anderer Enzymaktivitäten genutzt werden [24,27,28]. Im Rahmen der nachfolgenden Publikation wurden zehn monokaryotische Stämme erhalten, die den elterlichen Dikaryoten in ihrer PsaPOX-Aktivität übertrafen. Ein Stamm (MK16) zeigte dabei eine stark erhöhte Aktivität und damit Potential für eine industrielle Applikation als Produzent für PsaPOX. Langzeitstudien wiesen die Stabilität der verbesserten Aktivität dieses Stammes nach, was im Hinblick auf eine spätere industrielle Nutzung wichtig ist.

Ein weiteres Ziel der Arbeit war die Identifizierung der zugrunde liegenden Ursachen der beobachteten intraspezifischen Diversität der *P. sapidus-Stämme*. Dies war besonders von Interesse, da sich bisher nur wenige Studien mit der Aufklärung enzymatischer Unterschiede von monokaryotischen Basidiomyceten (untereinander und im Vergleich zum Dikaryot) beschäftigten [28,30]. Die Diversität der alkenspaltenden Peroxidaseaktivität konnte auf die Existenz von drei PsaPOX-Varianten zurückgeführt werden. Zusätzlich resultierte die stark erhöhte Enzymaktivität von MK16 aus einer höheren Expressionsrate der entsprechenden Genvariante.

Herr Dr. Witt unterstützte bei der Durchführung und Auswertung der Expressionsanalyse. Die in der Arbeit verwendeten monokaryotischen Pilzstämme wurden von Frau Dr. Omarini erzeugt. Weiterhin war Frau Dr. Omarini zusammen mit Herrn Prof. Berger und Herrn Prof. Zorn für die Projektidee und die Akquise der verwendeten Drittmittel verantwortlich. Herr Prof. Berger war ferner für die Betreuung des Forschungsprojekts zuständig. Frau Dr. Ersoy übernahm die Betreuung der wissenschaftlichen Arbeit.

Die nachfolgende Publikation wurde in dem *peer-reviewed* Journal *International Journal of Molecular Sciences* (MDPI) veröffentlicht (https://doi.org/10.3390/ijms22031363) [208].

8

International Journal of *Molecular Sciences*

MDPI

Article

Monokaryotic *Pleurotus sapidus* Strains with Intraspecific Variability of an Alkene Cleaving DyP-Type Peroxidase Activity as a Result of Gene Mutation and Differential Gene Expression

Nina-Katharina Krahe [1,*], Ralf G. Berger [1], Martin Witt [2], Holger Zorn [3], Alejandra B. Omarini [3,4] and Franziska Ersoy [1]

1 Institut für Lebensmittelchemie, Gottfried Wilhelm Leibniz Universität Hannover, Callinstr. 5, 30167 Hannover, Germany; rg.berger@lci.uni-hannover.de (R.G.B.); franziska.ersoy@lci.uni-hannover.de (F.E.)
2 Institute of Technical Chemistry, Gottfried Wilhelm Leibniz University Hannover, Callinstr. 5, 30167 Hannover, Germany; witt@iftc.uni-hannover.de
3 Institute of Food Chemistry and Food Biotechnology, Justus Liebig University Giessen, Heinrich-Buff-Ring 17, 35392 Giessen, Germany; holger.zorn@uni-giessen.de (H.Z.); Alejandra.B.Omarini@lcb.chemie.uni-giessen.de (A.B.O.)
4 INCITAP Institute of Earth and Environmental Sciences of La Pampa (CONICET-UNLPam) National Scientific and Technical Research Council-National University of La Pampa, Mendoza 109, Santa Rosa CP 6300, La Pampa, Argentina
* Correspondence: nina.krahe@lci.uni-hannover.de; Tel.: +49-511-762-17257

8.1 Abstract

The basidiomycete *Pleurotus sapidus* produced a dye-decolorizing peroxidase (PsaPOX) with alkene cleavage activity, implying potential as a biocatalyst for the fragrance and flavor industry. To increase the activity, a daughter-generation of 101 basidiospore-derived monokaryons (MK) was used. After a pre-selection according to the growth rate, the activity analysis revealed a stable intraspecific variability of the strains regarding peroxidase and alkene cleavage activity of PsaPOX. Ten monokaryons reached activities up to 2.6-fold higher than the dikaryon, with MK16 showing the highest activity. Analysis of the *PsaPOX* gene identified three different enzyme variants. These were co-responsible for the observed differences in activities between strains as verified by heterologous expression in *Komagataella phaffii*. The mutation S371H in enzyme variant PsaPOX_high caused an activity increase alongside a higher protein stability, while the eleven mutations in variant PsaPOX_low resulted in an activity decrease, which was partially based on a shift of the pH optimum from 3.5 to 3.0. Transcriptional analysis revealed the increased expression of *PsaPOX* in MK16 as reason for the higher PsaPOX activity in comparison to other strains producing the same PsaPOX variant. Thus, different expression profiles, as well as enzyme variants, were identified as crucial factors for the intraspecific variability of the PsaPOX activity in the monokaryons.

Keywords:

alkene cleavage; basidiomycota; biocatalysis; dikaryon; dye-decolorizing peroxidase (DyP); gene expression; gene mutation; intraspecific variability; monokaryon; *Pleurotus sapidus*

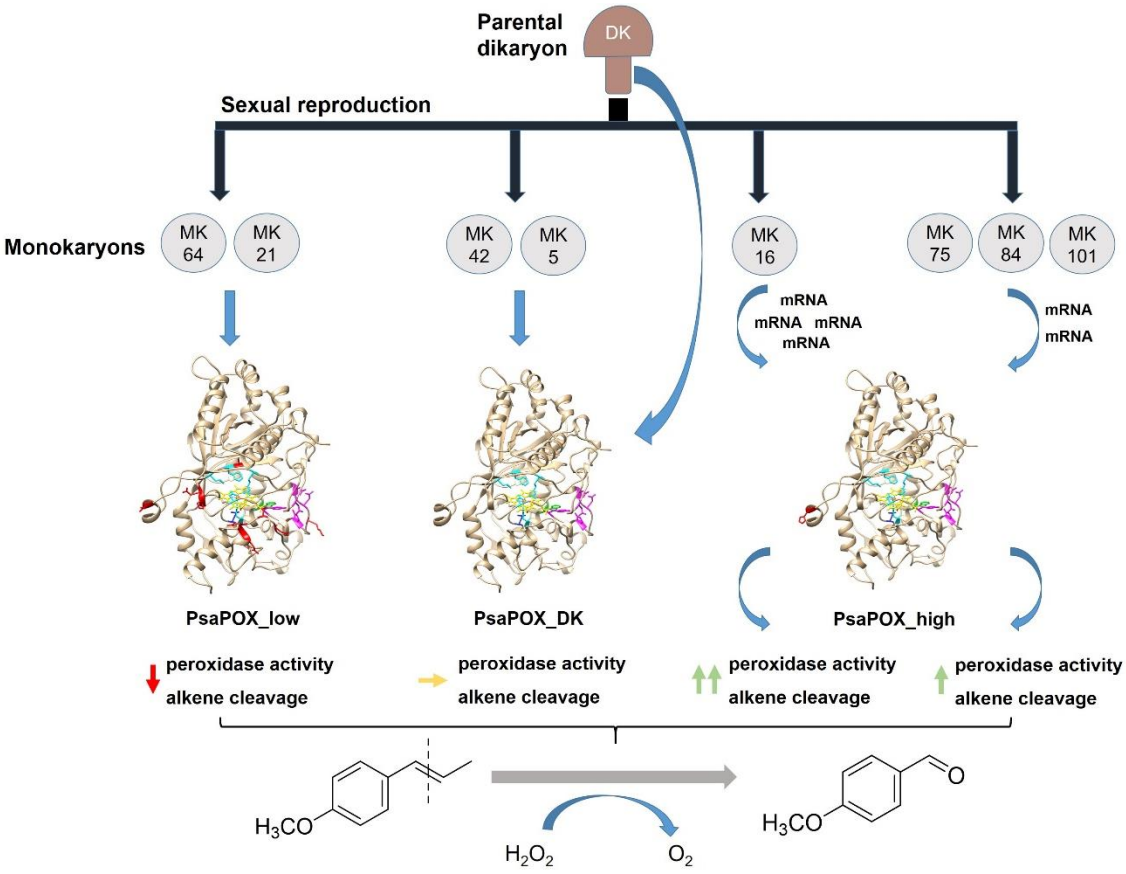

Figure 8.1. Graphical abstract.

8.2 Introduction

Many small aromatic aldehydes and ketones are known for their olfactory properties and are of high interest for the fragrance and flavor industries [167]. Their synthesis *via* chemical oxidative cleavage of the corresponding alkenes is possible [172,178], but a rising demand for natural products and sustainable production processes favors alternative strategies, such as biocatalysis [45,50]. The bottleneck of these bioprocesses is sufficient enzyme activity [155]. To improve their yields, different genetic engineering techniques are available [157], but are refused by the general public and classified as not suitable for "natural and safe processes" (European Directive 2001/18/EC) [34,50]. Thus, alternative strategies are needed.

Basidiomycota, which belong to the higher fungi (*Dikarya*), pass through different life cycle phases [11]. In the dikaryotic mycelium (dikaryon, DK), two independent nuclei coexist throughout vegetative growth. During fructification, basidia are formed, in which karyogamy (fusion of the nuclei) occurs. Meiosis and the generation of four uninucleate basidiospores follow. Hereby, variability of the progenies will result from genetic recombination [11,13]. Germination of the basidiospores causes the formation of monokaryotic mycelia (monokaryon, MK, haploid), which may later fuse to a new dikaryon (plasmogamy), if they are mating-compatible, and, thereby, reinitiate the life cycle [11]. In consequence of the genetic and resulting phenotypic diversity of the basidiospore-derived monokaryons, the basidiomycetous life cycle offers a new option to improve enzyme activities and other traits without the use of genetic engineering.

Several studies demonstrated that monokaryons differ in mycelial growth rate [20,24,27,28,233] and enzyme activities [24,27,28,34,234]. The latter were improved in selected monokaryotic progenies in comparison to the parental dikaryon [27,28]. However, few studies deal with the elucidation of the biochemical reasons for this diversity [28,30]. Castanera *et al.* suggested that a higher laccase activity observed for the dikaryon of *Pleurotus ostreatus* in comparison to its parental monokaryons was due to non-additive transcriptional increase in *lacc6* and *lacc10* [30]. In contrast, Linke *et al.* found a higher carotene degrading activity of a *P. ostreatus* monokaryon as a result of a higher secreted activity of Lacc10 [28]. The specific reasons remained unknown, because mutations and differences in gene expression were experimentally excluded. Heterozygosity in genes was proposed as reason for intraspecific variability, as in studies by Eichlerová and Homolka [24] and del Vecchio *et al.* [34], but never experimentally verified.

While some studies deal with the intraspecific diversity of monokaryons regarding laccase and other lignolytic activities [20,24,28,30,34,234], to the best of our knowledge, no study exists that deals with a dye-decolorizing peroxidase (DyP) activity. DyPs (EC: 1.11.1.19) form a new superfamily of heme peroxidases that differ highly from other classes of heme peroxidases regarding their amino acid sequence, protein structure, and catalytic residues [95]. A GXXGD-motif, which contains the catalytic aspartic acid, as well as a ferrodoxin-like fold, is typical for these enzymes [95,99]. In addition to the distal (above the heme plane) catalytic aspartic acid, which is replaced by a histidine in other heme peroxidases, a distal arginine and a proximal histidine are located in the active site (heme pocket) [95,106]. There, reductive heterolytic cleavage of hydrogen peroxide and substrate oxidation take place [106]. In contrast, oxidation of bulky substrates was proposed to occur at a surface-exposed oxidation site containing a tryptophan residue involving a long-range electron transfer [116]. Furthermore, a surface-exposed Mn^{2+}-oxidation site was detected for two DyPs [209,216]. DyPs are known to oxidize different dyes, especially xenobiotic anthraquinone dyes, as well as classical peroxidase substrates, such as ABTS (2,2'-azino-bis(3-ethylbenzthiazoline-6-sulphonic acid)) and phenolic compounds [92,98,99]. However, only a recently identified DyP (PsaPOX) has been found to cleave aryl alkenes, such as (*E*)-methyl isoeugenole, *α*-methylstyrene, and *trans*-anethole (Figure 8.2) [209]. The resultant aldehydes are odor-active volatiles used in the fragrance and flavor industry [167]; therefore, PsaPOX is a potential biocatalyst for flavor production.

Figure 8.2. Alkene cleavage of *trans*-anethole into *p*-anisaldehyde by the dye-decolorizing peroxidase PsaPOX.

The objective of the present study was to utilize the intraspecific variability of monokaryotic progenies to improve the alkene cleavage activity of *P. sapidus*. A further purpose was the elucidation of the origin of the diversity of enzyme activity. To the best of our knowledge, this is the first report presenting intraspecific diversity concerning a DyP-type peroxidase for monokaryons and their corresponding dikaryon and, in addition, the first study identifying intraspecific differences of monokaryons concerning enzyme activities as result of a gene mutation.

8.3 Results and Discussion

8.3.1 Analysis of Monokaryons

8.3.1.1 Pre-selection of Monokaryons by Analysis of the Radial Growth Rate

To generate new *P. sapidus* strains with an increased alkene cleavage activity, spores were collected from the basidiocarp after fructification of the dikaryotic strain. The colonies derived from the basidiospores were microscopically analyzed to confirm the monokaryotic state through the absence of clamp connections [15]. To assess the physiological diversity of the strains, the growth rate of 101 monokaryotic isolates on standard nutrient liquid (SNL) agar plates was determined as a polygenetic and easy-to-measure trait (Figure 8.3) [20,27,30,233,235]. The measured growth rates ranged from 0.24 ± 0.05 to 2.55 ± 0.08 mm/day, with most strains (66%) exhibiting rates between 1.5 and 2.5 mm/day. According to the growth rate, the *P. sapidus* strains were categorized into slow- (0–1.0 mm/day, 17% of the isolates), moderate- (1.0–2.0 mm/day, 45%), and fast- (2.0–3.0 mm/day, 39%) growing isolates. The dikaryon showed a growth rate of 2.26 ± 0.11 mm/day and was thus classified as fast-growing.

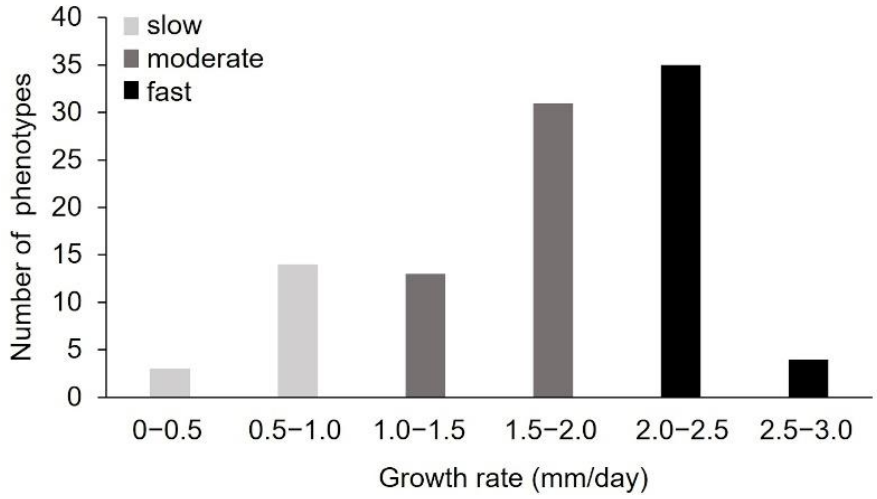

Figure 8.3. Distribution of vegetative growth rate of the *P. sapidus* monokaryons grown on standard nutrient liquid (SNL) agar plates. The strains were categorized as slow-, moderate-, and fast-growing strains according to the growth rate.

The intraspecific variability of the growth rate, which has also been shown for other basidiomycota [20,26–28,233], is an indicator for the biochemical diversity within the *P. sapidus* population and led to the assumption that the strains will also differ in other traits. Thus, five slow- (MK16, MK21, MK23, MK64, MK66), four moderate- (MK34, MK42, MK49, MK101), and five fast-growing (MK5, MK13, MK75, MK84, MK93) representative monokaryons (MK), as well as the parental dikaryon (DK), were selected for further analysis.

8.3.1.2 Profiling of Alkene Cleavage and Peroxidase Activity in Monokaryons

After submerged cultivation, the lyophilized mycelium of the fourteen pre-selected monokaryons and the parental dikaryon was used for the biotransformation of *trans*-anethole to *p*-anisaldehyde to analyze the alkene cleavage activity of the strains (Figure 8.4a). The parental dikaryon produced 2.62 mM *p*-anisaldehyde, which was similar to the product concentrations obtained for MK5 and MK42, while MK21 and MK64 generated an approximately two-fold lower *p*-anisaldehyde concentration. All other monokaryons exhibited higher alkene cleavage activities (1.5–1.7-fold) than the dikaryon, while the activity of MK16 reached a 2.5-fold value. According to their activity, and in comparison, to the results for the dikaryon, the strains were categorized into four groups: (I) low active strains (MK21 and MK64); (II) moderately active strains (DK, MK5, and MK42); (III) highly active strains (MK13, MK23, MK34, MK49, MK75, MK84, MK93, MK101); and (IV) very highly active strains (MK16).

The results evinced that the analyzed *P. sapidus* strains varied not only in the growth rate, but also in the alkene cleavage activity (Figure 8.4b). No correlation between growth and alkene cleavage activity was detected (Figure 8.4b; coefficient of determination $R^2 = 0.12$). This finding was consistent with other studies, which found no correlation between colony appearance or growth and enzyme activity [24,27,28].

The cleavage of *trans*-anethole into *p*-anisaldehyde by the parental *P. sapidus* strain was the result of the activity of the DyP-type peroxidase PsaPOX [209]; therefore, the peroxidase activity of the monokaryons was determined in addition to the alkene cleavage activity. As expected, the peroxidase activity also varied between the strains (Figure 8.4c) and correlated well with the ability to cleave *trans*-anethole (Figure 8.4d, coefficient of determination $R^2 = 0.82$).

Classification of the strains according to their peroxidase activity resulted in the same four activity groups as defined for the alkene cleavage activity (I: ~ two-fold lower than DK; II: similar to DK; III: 1.6–2.0-fold higher than DK; and IV: 2.6-fold higher than DK), which each contained the same strains as described above. Thus, it was shown that the different peroxidase and alkene cleavage activities were most likely evoked by variations of PsaPOX resulting from genetic variations between the fungal strains caused by the sexual reproductive cycle [11,13]. However, the precise reason for the different phenotypes remained to be elucidated. Possible factors included enzyme mutations, different gene expression rates, or

differences on the regulative level, such as posttranscriptional gene silencing, different transposable elements contents, or factors influencing protein stability and degradation [30,36,236–239].

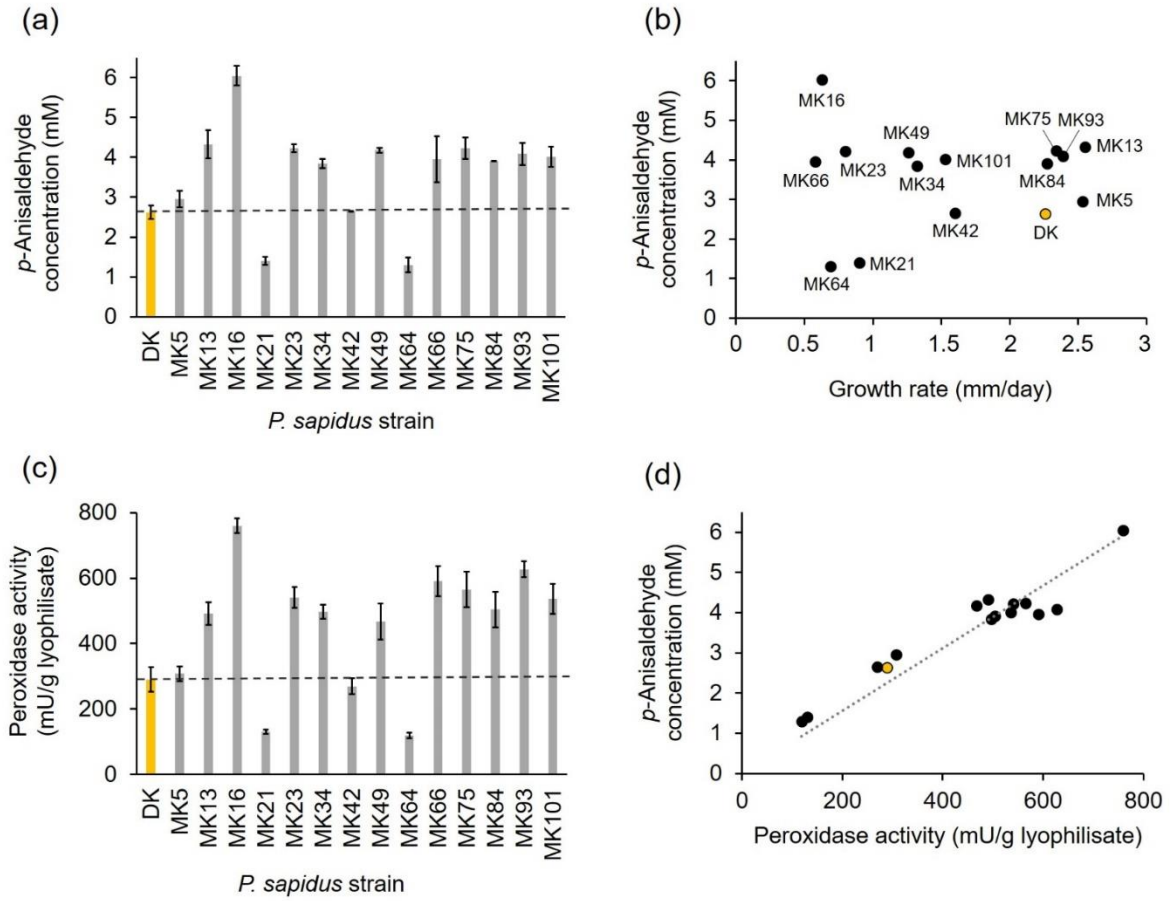

Figure 8.4. Alkene cleavage activity in comparison to peroxidase activity and growth rate of selected monokaryons and the parental dikaryon (yellow bar or circle) of *P. sapidus*. (**a**) Enzymatically generated concentration of *p*-anisaldehyde after conversion of *trans*-anethole (33.5 mM) using 30 mg/mL finely ground lyophilized *P. sapidus* mycelium in the presence of 25 mM $MnSO_4$, 100 µM H_2O_2, and 50 mM sodium acetate buffer pH 3.5 for 16 h at RT and 200 rpm. (**b**) Comparison of alkene cleavage activity for the lyophilized *P. sapidus* mycelium after submerged cultivation and radial growth rate for the cultivation on SNL agar plates. (**c**) Peroxidase activity of the lyophilized mycelium. (**d**) Comparison of alkene cleavage and peroxidase activity of the lyophilized mycelium of the *P. sapidus* strains. *p*-Anisaldehyde concentrations are the average of duplicate experiments, and peroxidase activities the average of triplicate experiments of two independent biological replicates (with standard deviations shown as error bars in (a) and (b)). Growth rates are the average of two independent biological replicates cultivated under the same conditions.

The present study revealed not only intraspecific variability concerning growth, peroxidase, and alkene cleavage activity, but also some improvement of these enzyme activities (alkene cleavage activity: 1.5–2.5-fold; peroxidase activity: 1.6–2.6-fold) for most of the analyzed monokaryons, especially MK16, in comparison to the parental dikaryon (Figure 8.4a,c).

Thus, the opportunity to generate and identify optimized strains by natural reproduction and selection of the resulting progenies was verified. This is consistent with results of previous studies [24,27,28].

8.3.1.3 Phenotypic Stability of Alkene Cleavage Activity in Sequential Cultivations

Phenotypic instability of dikaryons during long-term cultivation resulting in altered properties, such as the growth rate, is known in the literature and is caused by genetic exchanges and recombination between the nuclei of the dikaryon [240]. In contrast, the growth rate of haploid monokaryons of *Schizophyllum commune* [240] and laccase and carotene degrading activity of monokaryotic *P. ostreatus* strains [28] were stable over serial propagation for several months. However, only a few studies concerning the long-term stability [28,240,241], especially regarding the production of enzymes [28] in monokaryons and dikaryons, were published. For this reason, the phenotypic stability regarding alkene cleavage activity was exemplarily examined with *trans*-anethole for the parental dikaryon (activity group II, see Section 8.3.1.2) and three monokaryons (activity group I (MK21), III (MK84), IV (MK16)) over five sequential generations. Sub-cultivation to the fifth generation did not influence the ability to cleave *trans*-anethole within any of the strains (Figure 8.5, variance among the replicate lines was between 4–18%). Thus, the observed variability between the strains was stable. This is the second study that proved the stability of an enzyme activity for basidiomycetous monokaryons and the parental dikaryon during serial propagation over several months [28].

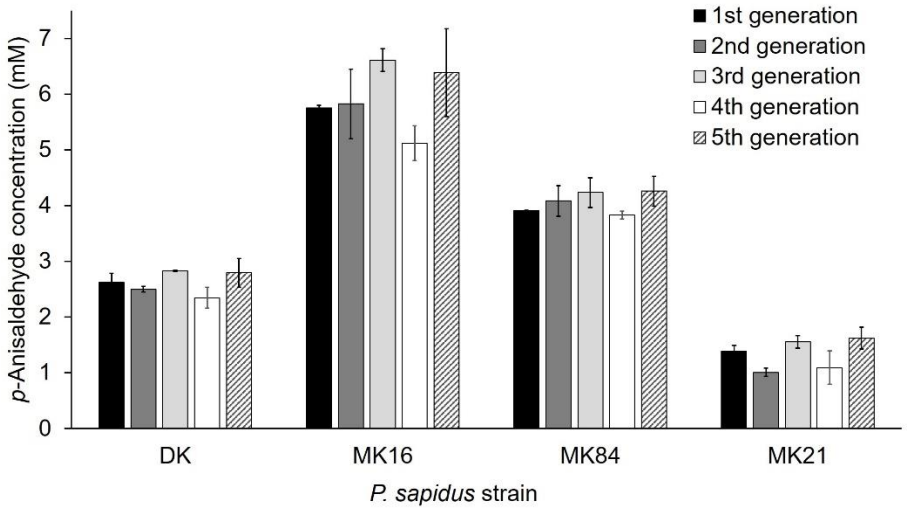

Figure 8.5. Stability of alkene cleavage activity towards *trans*-anethole of selected monokaryons and the parental dikaryon over five serial generations. Values are the average of duplicate experiments of two independent biological replicates with standard deviations shown as error bars.

8.3.1.4 Comparison of PsaPOX from Selected *P. sapidus* Strains

As mentioned above, the observed stable intraspecific variabilities of the analyzed *P. sapidus* strains regarding peroxidase and alkene cleavage activity were attributed to differences concerning PsaPOX. To confirm this, the PsaPOX mRNA sequence of representative monokaryons of each activity group (see Section 8.3.1.2; I: MK21 and MK64; II: MK5 and MK42; III: MK75, MK84, and MK101; IV: MK16) was reverse transcribed, amplified, and sequenced. An alignment (Supporting Figure 8.1, Section 8.7) revealed four different DNA sequences: sequence 1 [209] identified for the dikaryon and MK5, sequence 2 identified for MK42 (differing in 2 bp to sequence 1), sequence 3 identified for MK21 and MK64 (differing in 65 bp to sequence 1), and sequence 4 identified for MK16, MK75, MK84, and MK101 (differing in 4 bp to sequence 1). Even though two different genotypes (gDNA level, corresponding to sequence 1 and 3, plus introns) were detected for the dikaryon (Supporting Figure 8.1, Section 8.7), no sequence in addition to sequence 1 was identified for the dikaryon *via* clone sequencing on the mRNA level. This indicated monoallelic expression, which was previously described for another gene of *P. ostreatus*, a near relative of *P. sapidus* [25]. Sequence 3 originated from the unexpressed gene variant; therefore, sequence 2 and 4 should have represented the consensus sequence of the expressed and unexpressed dikaryotic gene variant if they resulted solely from recombination events during meiosis. The genotype at position 36 in sequence 2 and 4 was in accordance with the genotype of the unexpressed dikaryotic gene sequence (sequence 3), while the main part of sequence 2 and 4 showed a higher identity to sequence 1 (Supporting Figure 8.1, Section 8.7). Thus, the genotype at position 36 is probably the result of meiotic recombination. In contrast, the genotypes at positions 468 (sequence 2 and 4), 1111, and 1112 (sequence 4) must have resulted from random mutations, because they did not correspond to either of the dikaryotic genotypes at the respective positions (see Supporting Figure 8.1, Section 8.7). The high contribution of sequence 4 (present in four of eight tested strains) indicates that the mutations occurred at the early stage of fructification so that the new sequence was distributed over multiple cell divisions before formation of the basidia. Thus, the mutated sequence would have been present in several of the generated spores originating from different basidia, resulting in multiple monokaryons with sequence 4.

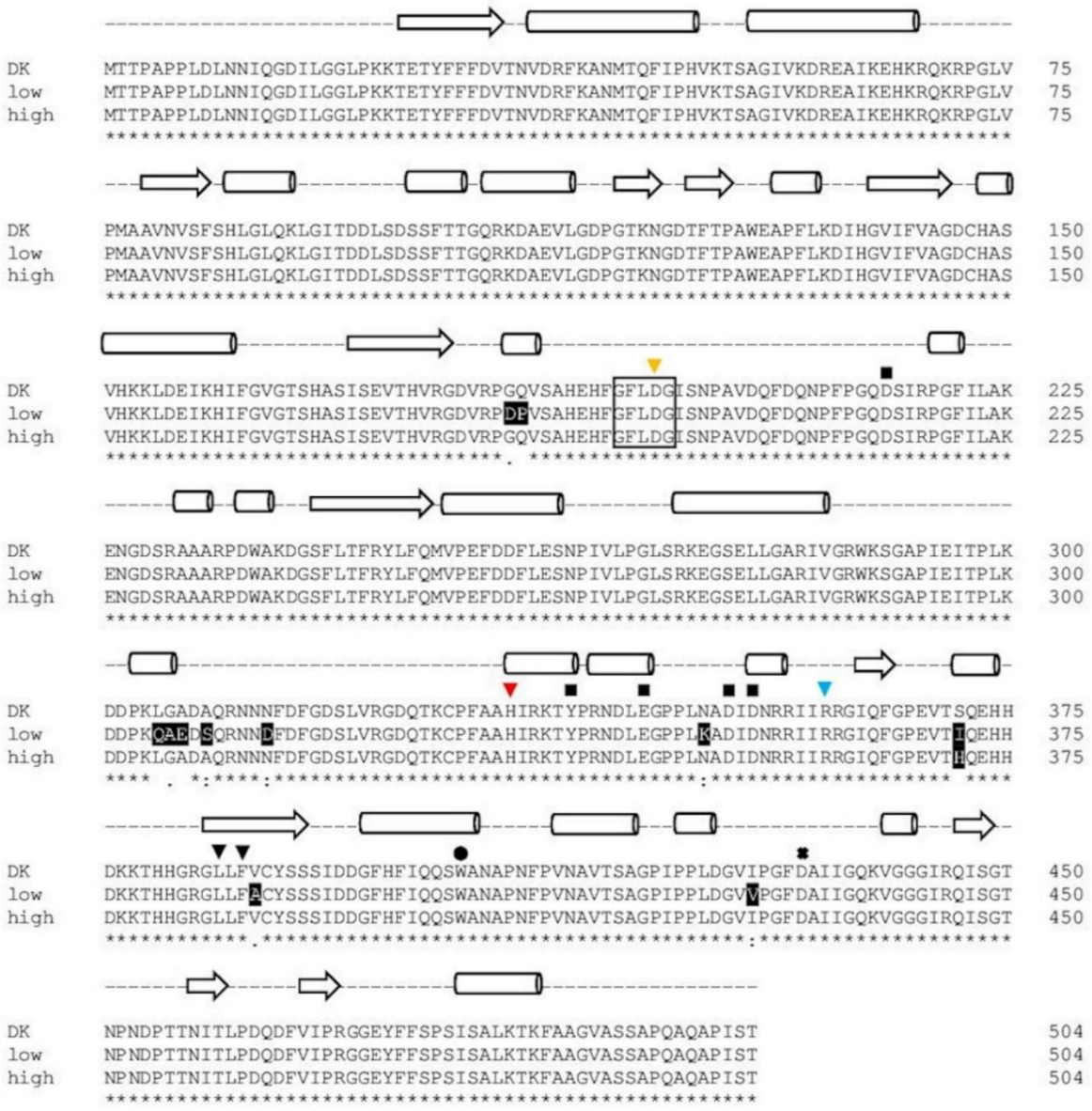

Figure 8.6. Alignment of the amino acid sequence of the PsaPOX variants. DK: PsaPOX_DK; low: PsaPOX_low; high: PsaPOX_high. Inverted triangles show amino acids important for heme binding (H334 (red) functions as ligands for heme and the four other amino acid residues form a hydrogen peroxide binding pocket). Aspartic acid (D433), which forms a hydrogen bond with histidine to stabilize compound I (oxidized heme after transfer of two electrons to H_2O_2), is indicated by a cross. The black box indicates the GXXDG motif containing the catalytic aspartic acid residue (D196, yellow inverted triangle), which cleaves H_2O_2 heterolytically with the help of the neighboring arginine (R360, blue inverted triangle) to form compound I, and the circle presents an exposed tryptophan (W405) potentially involved in a long-range electron transfer. Important amino acids for Mn^{2+}-oxidation (D215, Y339, E345, D352, and D354) are marked by squares. Secondary structure elements are shown above the alignment (arrow: *β*-sheets, barrel: *α*-helices, dashed line: random coil) and were predicted by the SWISS-MODEL server [242] using the X-ray crystal structure of *Pleos*-DyP4 from *P. ostreatus* (PDB-ID 6fsk). Asterisks indicate conserved residues, colons indicate equivalent residues, and dots indicate partial residue conservations. Observed mutations compared to the parental sequence (DK) were highlighted in black with white font. The alignment was performed with Clustal Omega (European Bioinformatics Institute, Hinxton, UK) [226].

While sequence 1 and 2 resulted in identical protein sequences (PsaPOX_DK: parental sequence identified for the dikaryon), the protein resulting from sequence 3 (PsaPOX_low) carried eleven mutations (G184D, Q185P, L305Q, G306A, A307E, A309S, N314D, N350K, S371I, V388A, I429V), while the protein resulting from sequence 4 (PsaPOX_high) carried one amino acid mutation (S371H) (Figure 8.6). None of the observed mutations resulted in the exchange of an amino acid known to be important for DyP activity (see Figure 8.6). However, PsaPOX_low seemed to be correlated with a lower enzyme activity than that exhibited by the dikaryon and PsaPOX_high with a higher activity, as all representative low active strains (MK21 and MK64) contained PsaPOX_low and all highly active strains (MK16, MK75, MK84, MK101) contained PsaPOX_high. This was in line with the finding that MK5 and MK42 contained PsaPOX_DK as well as an activity similar to the dikaryon. Linke *et al*. [28] examined the influence of a sequence mutation as the possible reason for a higher activity of Lacc10 in *P. ostreatus* MK51 in comparison to the dikaryon as well other monokaryons, but did not find any correlation. To the best of our knowledge, no study has yet been able to attribute phenotypic variability of mono- and dikaryons concerning enzyme activity to a specific gene mutation.

8.3.2 Analysis of the Recombinant PsaPOX Variants

8.3.2.1 Activity of the Recombinant PsaPOX Variants

To verify the influence of the detected amino acid sequence exchanges on the PsaPOX activity, the sequences 1, 3, and 4 coding for the three PsaPOX variants (PsaPOX_DK, PsaPOX_low, and PsaPOX_high, respectively, see Section 8.3.1.4) were heterologously expressed in *K. phaffii* as previously described for the parental sequence (sequence 1) [209]. After 72 h of cultivation, the best performing colonies produced maximal peroxidase activities of up to 142 U/L for PsaPOX_DK [209], 138 U/L for PsaPOX_low, and 86 U/L for PsaPOX_high. The recombinant PsaPOX variants were purified by Ni-NTA affinity, which resulted in comparable electrophoretic purities of the enzymes (Supporting Figure 8.2, Section 8.7). Two protein bands were detected, which corresponded to the unmodified peroxidase (lower band, calculated molecular mass using ExPASy [243]: 54.9 kDa) and the *N*-glycosylated enzyme (upper band, result of posttranslational modifications by *K. phaffii*) [209]. The percentage of unmodified (19–21%) and glycosylated (79–81%) enzyme was similar, as shown by an evaluation of the protein band intensities. This was supported by the results of a bioinformatic analysis of the PsaPOX sequences, which identified the same three

putative *N*-glycosylation sites (N42, N81, and N458) for all enzyme variants. Thus, an influence of different glycosylation patterns on the enzyme activity or solubility was excluded.

The purified peroxidase variants were compared, regarding their specific peroxidase and alkene cleavage activity using identical protein concentrations (peroxidase activity: 1 ng/mL; alkene cleavage activity: 0.25 mg/mL) (Figure 8.7a,b). PsaPOX_DK reached a specific peroxidase activity of 1.94 ± 0.02 U/mg, while PsaPOX_low showed a specific activity of 1.23 ± 0.07 U/mg and PsaPOX_high of 2.67 ± 0.10 U/mg (Figure 8.7a). Similar results were obtained for the alkene cleavage activity, which was represented by the produced *p*-anisaldehyde concentration after biotransformation of *trans*-anethole by the PsaPOX variants. In the presence of PsaPOX_DK, 0.28 ± 0.02 mM *p*-anisaldehyde was produced, whereas PsaPOX_low generated 0.16 ± 0.03 mM and PsaPOX_high 0.43 ± 0.02 mM product (Figure 8.7b).

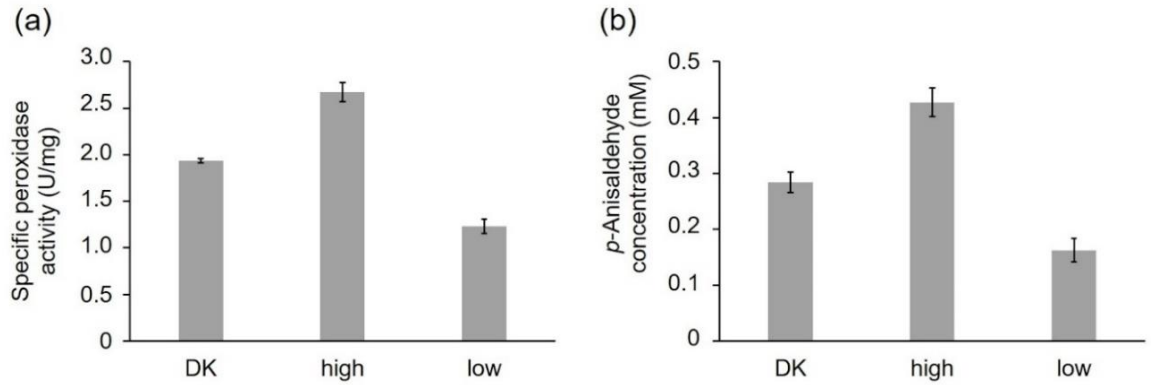

Figure 8.7. Comparison of the PsaPOX variants regarding their peroxidase and alkene cleavage activity. (**a**) Specific peroxidase activity. Values are the average of triplicate measurements using three independent replicates with standard deviations shown as error bars (**b**) *p*-Anisaldehyde concentration after bioconversion of *trans*-anethole (6.7 mM) using 0.25 mg/mL PsaPOX variant in the presence of 25 mM $MnSO_4$, 100 µM H_2O_2, and 50 mM sodium acetate buffer pH 3.5 for 16 h at RT and 200 rpm. Values are the average of duplicate independent experiments with standard deviations shown as error bars. DK: PsaPOX_DK; high: PsaPOX_high; low: PsaPOX_low.

The results verified that the observed point-mutations (see Figure 8.6) in the sequences of PsaPOX_low and PsaPOX_high caused a lower and higher activity, respectively, and was the reason for the higher or lower activity of the (very) highly (activity group III and IV) or low active (activity group I) *P. sapidus* strains (see Section 8.3.1.2). Thus, this is the first experimental proof that a gene mutation resulted in different activities of monokaryons and the parental dikaryon, although an activity change due to amino acid exchanges of a given enzyme in general is well documented [116,244,245].

However, the ratio of activity difference between the recombinant PsaPOX_DK and PsaPOX_low (peroxidase activity: 1.6-fold, alkene cleavage activity: 1.7-fold) or PsaPOX_high (peroxidase activity: 1.4-fold, alkene cleavage activity: 1.5-fold) was slightly less distinctive than for the parental *P. sapidus* dikaryon in comparison to the low (peroxidase activity and alkene cleavage activity: 2-fold) or (very) highly active (peroxidase activity: 1.6–2.6-fold, alkene cleavage activity: 1.5–2.5-fold) strains (Figure 8.4a,c and 8.7a,b). This indicated that further factors, such as different levels of expression (see Section 8.3.3) were involved in the observed phenotypic diversity of the *P. sapidus* strains. MK16 especially (classified as very highly active, activity group IV, see Section 8.3.1.2), reached an at least 1.3- (peroxidase activity) to 1.4-fold (alkene cleavage activity) higher activity than all other analyzed *P. sapidus* strains, although it contained the PsaPOX_high variant like the highly active strains.

8.3.2.2 Structural Analysis of the PsaPOX Variants

To identify the positions of the amino acid mutations and assess a possible impact on the enzyme activity, structural homology models of the PsaPOX variants were generated on the SWISS-MODEL server [242] (Figure 8.8). The template was the X-ray crystal structure of the *Pleos*-DyP4 from *P. ostreatus* (PDB-ID 6fsk; 94% identity). The S371H mutation of PsaPOX_high was surface-exposed, and at least 23 Å away from the conserved amino acids of the active site (*cf.* Figure 8.8a,b). Thus, it seemed highly unlikely that the amino acid exchange directly influenced the catalytic activity, which disagreed with the observed activity improvement for the PsaPOX_high variant. However, some studies reported an activity increase by distant mutations [246–248]. For example, the mutation (I238Y) of a vanillyl alcohol oxidase located at a distance of 33 Å from the flavine–adenine dinucleotide in the active site cavity increased the turnover number for creosol, even though structural changes, which could account for the improvement, were not identified by X-ray crystallography [247]. The structural homology models used in this study cannot serve to analyze structural changes. In addition, conformational differences due to the fact that another protein was used as template cannot be excluded. It is possible that the loop region containing S371H was further orientated towards the entrance of the active site as a consequence of the flexible random coil (Figure 8.8b), so that S371H may affect and improve the accessibility to the catalytic site. Another hypothesis was that S371H influenced the folding or unfolding of the peroxidase, which resulted in a higher percentage of correctly folded proteins or an increase in protein stability (compare with Section 8.3.2.3). The

influence of single-point mutations on the folding and stability of enzymes has been reported before [249].

The eleven amino acid exchanges in PsaPOX_low were mostly positioned at the surface of the enzyme (Figure 8.8c,d). However, one mutation (V388A) was located in the heme cavity at distances of 6, 7, and 10 Å to the conserved residues F387, R360, and D196 of the hydrogen binding pocket, respectively (Figure 8.8c). The exchange of valine to the smaller alanine may have caused a conformational change in the hydrogen binding pocket, which could explain the lower activity of the *P. sapidus* strains containing the PsaPOX_low enzyme. Furthermore, most of the detected mutations (G184D, Q185P, L305Q, G306A, A307E, A309S, N314D, N350K, and S371I) led to a polarity change, which may have resulted in a rearrangement of the three-dimensional protein structure and therefore to a lower protein stability and activity. The change of enzyme activity and stability by conformational changes is known from the literature [244,250,251]. Another hypothesis was that the substrate access to the heme cavity was complicated by several mutations (G184D, Q185P, L305Q, G306A, A307E, and A309S), which mostly increased the steric hindrance near the substrate entrance (Figure 8.8d), as assumed in the case of two other DyP-type peroxidases [244,245]. Furthermore, a negative charge was added by the exchange of glycine to aspartic acid at position 184 (pI of Asp: 2.98 [252]; pK_a of Asp: 3.7 [253]), which probably aggravated the accommodation of the anionic substrate ABTS. Interestingly, position 371, which was mutated in the PsaPOX_high variant (S371H), was also mutated in PsaPOX_low (S371I). This indicated that the position is important for the activity of PsaPOX, despite its remote location in the predicted protein structure model (Figure 8.8b,c). X-ray crystallography will be necessary to ascertain the actual protein folding at this position. Point-mutation studies could be performed to ascertain the influence of position 371 on the enzyme activity as part of a follow-up study.

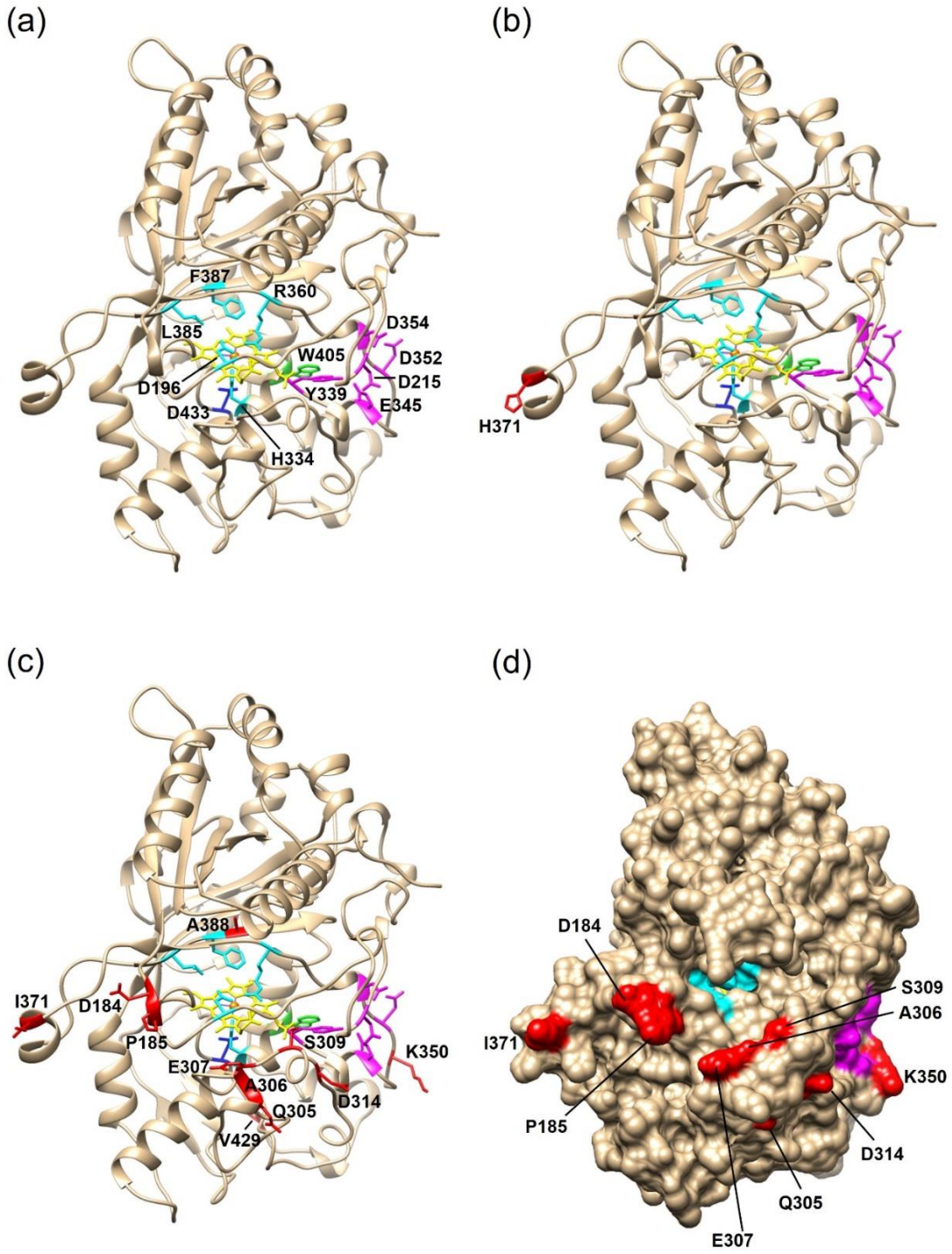

Figure 8.8. Structural homology models of the three PsaPOX variants. The models were generated with the SWISS-MODEL server using the X-ray crystal structure of *Pleos*-DyP4 (PDB-ID 6fsk). (**a**) Overall fold of PsaPOX_DK showing the typical ferredoxin-like fold with the heme cofactor (shown in yellow, the heme iron is highlighted in orange) sandwiched between distal and proximal sides. Conserved amino acids of the active site/hydrogen peroxide pocket (proximal H334, distal D196, R360, L385, and F387) are shown in cyan. D433, which forms a hydrogen bond with H334 to stabilize compound I (oxidized heme after transfer of two electrons to H_2O_2), is presented in blue, and the exposed W405 potentially involved in a long-range electron transfer is shown in green. Important amino acids for Mn^{2+}-oxidation (D215, Y339, E345, D352, and D354) are highlighted in magenta. Overall fold of (**b**) PsaPOX_high, and (**c**) PsaPOX_low. Mutations present in the enzyme variants are shown in red. (**d**) Solvent access surface of PsaPOX_low, showing the heme active site in cyan, the Mn^{2+}-oxidation site in magenta, and the position of the surface-exposed amino acid exchanges in red.

8.3.2.3 Comparative Biochemical Characterization of the PsaPOX Variants

To check if the observed activity variations of the PsaPOX variants were associated with differing biochemical characteristics, the influence of pH and temperature on PsaPOX activity and stability was determined using ABTS in the presence of hydrogen peroxide as a substrate (Figure 8.9). PsaPOX_DK, which has been characterized for its biochemical properties before [209], as well as PsaPOX_high, showed pH optimums of 3.5 (Figure 8.9a). In contrast, the optimum of PsaPOX_low was shifted to the more acidic range at pH 3.0. This shift was probably caused by several mutations in the primary sequence of PsaPOX_low (Figure 8.6 and 8.8c), which led to polarity changes at different sites (G184D, Q185P, L305Q, G306A, A307E, A309S, N314D, N350K, and S371I), including insertion of acidic and basic amino acids (G184D, A307E, N314D, N350K). Thus, it was assumed that PsaPOX_low underwent conformational changes, which resulted in the shift of the pH optimum [244]. A second hypothesis is that the amino acid exchange G184D near the entrance of the active site complicated the accommodation of the anionic substrate ABTS, due to an additional negative charge at pH 3.5 (pI of Asp: 2.98 [252]; pK_a of Asp: 3.7 [253]) [244]. At pH 3.0, this was most likely prevented because the carboxyl side chain of 184D was protonated and the amino acid was uncharged. PsaPOX_low reached only 80% activity at pH 3.5, which was used for all other assays analyzing the specific peroxidase and alkene cleavage activity (Section 8.3.2.1), while PsaPOX_DK exhibited 100% activity (Figure 8.9a). It was concluded that the lower activity of PsaPOX_low in comparison to PsaPOX_DK was partly caused by the shifted pH optimum. However, the measured peroxidase activity (1.23 U/mg, Figure 8.7a) was lower than that calculated for pH 3.5 (1.55 U/mg, equal to 80% of activity of PsaPOX_DK). Further factors seemed to be involved.

All three PsaPOX variants showed a similar pH stability profile, with the highest stability between pH 2.0 and 5.5 (residual peroxidase activity ≥90% after 1 h of incubation) (Figure 8.9c). At pH values higher than 6.0, the stability decreased drastically, which was most likely caused by a reduced solubility and changes of the protein structure, which may have resulted in protein aggregation [209]. At pH 6.0, PsaPOX_high exhibited a residual activity of 52%, which was slightly higher than for PsaPOX_DK (40%) and PsaPOX_low (42%). Thus, S371H may have resulted in a small stability increase, as assumed above (see Section 8.3.2.2).

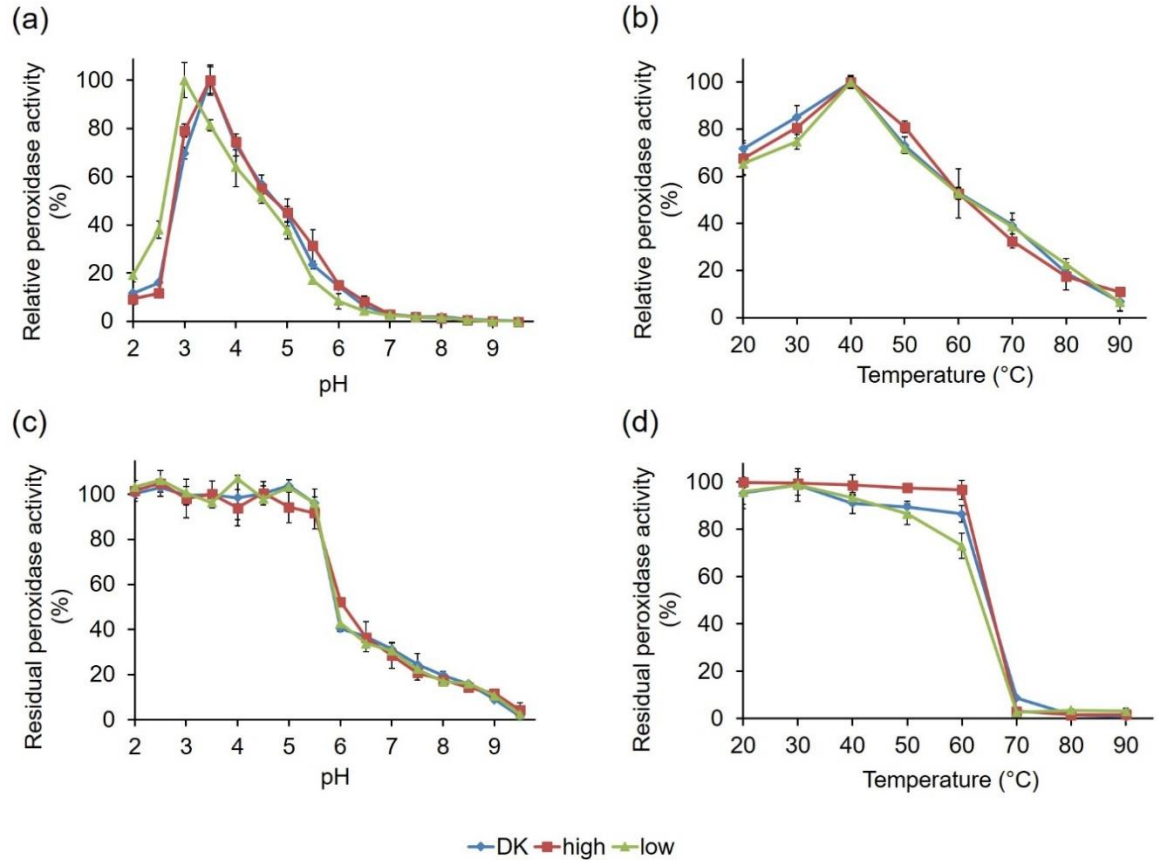

Figure 8.9. Influence of pH and temperature on activity and stability of the PsaPOX variants. (**a**) pH optimum and (**b**) temperature optimum. Relative peroxidase activity was defined as the percentage of activity detected with respect to the highest activity of the corresponding enzyme variant in each experiment. pH stability (**c**) was determined after incubation of PsaPOX in Britton–Robinson buffer, ranging from pH 2.0 to 9.5 for 1 h at RT, and temperature stability (**d**) was determined after incubation at 20–90 °C and pH 3.5 for 1 h. Residual activities were determined at pH 3.5 and 40 °C. Values are the average of triplicate experiments with standard deviations shown as error bars. DK: PsaPOX_DK; high: PsaPOX_high; low: PsaPOX_low.

Determination of the influence of temperature on the peroxidase activity showed that the PsaPOX variants possessed the same optimum (40 °C, Figure 8.9b). Furthermore, they shared a similar temperature–activity profile. On the contrary, differences for the temperature stability, which was determined after an incubation at different temperatures for 1 h, were detected (Figure 8.9d). While >96% peroxidase activity remained in the range between 20 and 60 °C for PsaPOX_high, the residual activity of PsaPOX_DK decreased between 40 and 60 °C from 89 to 84%. PsaPOX_low exhibited similar residual activities as PsaPOX_DK between 20 and 50 °C, but at 60 °C the residual activity (72%) was 12% and 24% lower than for PsaPOX_DK and PsaPOX_high, respectively. At higher temperatures (≥70 °C), a high loss of activity occurred for all PsaPOX variants due to protein aggregation [209], resulting in activities ≤5%. PsaPOX_high exhibited a higher stability, and PsaPOX_low a lower stability, than the parental variant. Thus, S371H (PsaPOX_high) seemed to have a stabilizing

effect on the tertiary structure of PsaPOX, while the amino acid exchanges in the sequence of PsaPOX_low resulted in a destabilization of the protein structure, which caused a higher sensitivity to heat-induced denaturation. Changes of the thermal stability as a result of the mutation of a certain enzyme are well known [250,251].

In addition, the hydrogen peroxide dependency of the three PsaPOX variants was compared (Figure 8.10a). The enzymes shared a similar behavior and reached their activity optimum in the presence of 100 µM, as previously described for PsaPOX_DK [209]. In the presence of higher hydrogen peroxide concentrations, a continuous activity decrease was observed as result of suicide inhibition. This was also observed for other DyPs [111,112] and most likely the result of the formation of an inactive oxidative state of the heme in the enzyme's active site [112–114,209].

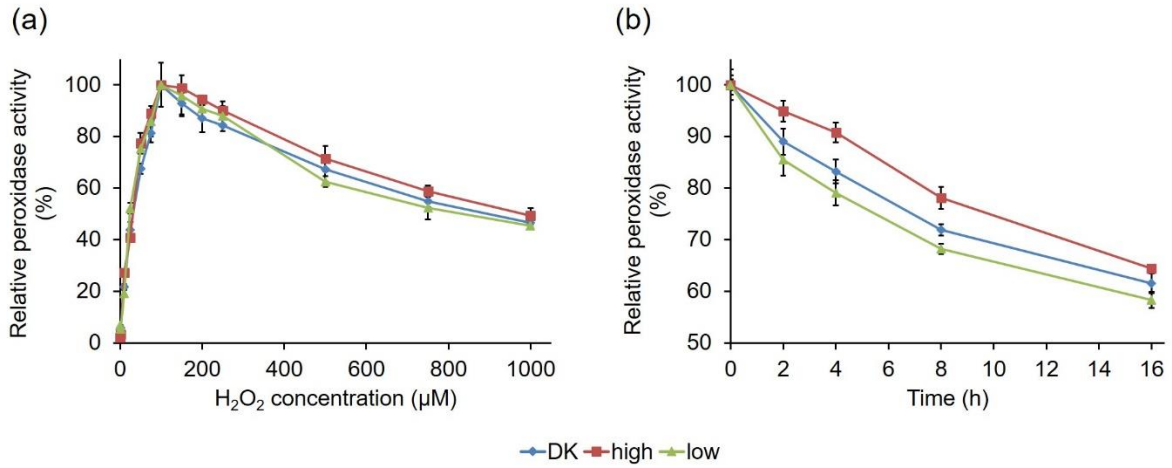

Figure 8.10. Effect of hydrogen peroxide concentration on the activity of the PsaPOX variants (**a**), and relative peroxidase activity of the PsaPOX variants during biotransformation of *trans*-anethole over 16 h (**b**). Relative peroxidase activity was defined as the percentage of activity detected normalized to the highest activity (a) or to the starting activity (b) of the corresponding enzyme variant in each experiment. Values are the average of triplicate experiments with standard deviations shown as error bars. DK: PsaPOX_DK; high: PsaPOX_high; low: PsaPOX_low.

PsaPOX_low and PsaPOX_high showed a changed thermal stability, and the latter also showed a slightly different pH stability in comparison to PsaPOX_DK; therefore, the stability of the PsaPOX variants during the biotransformation of *trans*-anethole over 16 h was determined (Figure 8.10b). In each case, an activity loss occurred during the incubation time, resulting in a remaining activity of 58% (PsaPOX_low) to 64% (PsaPOX_high) after 16 h. However, the activity loss was slower for PsaPOX_high than for PsaPOX_DK and faster for PsaPOX_low.

In conclusion, the peroxidase variants showed different stabilities under biotransformation conditions. The results were in line with the results for the thermal stability —and in the case of PsaPOX_high, also consistent with the findings for the pH stability. Therefore, they supported the deduction that the mutation in PsaPOX_high (S371H) had a stabilizing effect, while the mutations in the sequence of PsaPOX_low destabilized the peroxidase structure, thus influencing the enzyme activity.

To analyze the influence of the amino acid mutations of PsaPOX_low and PsaPOX_high on the Michaelis–Menten constant and catalytic efficiency, the corresponding kinetic parameters were calculated for the oxidation of ABTS at pH 3.5 (Table 8.1).

Table 8.1. Michaelis–Menten constants (K_m), catalytic constants (k_{cat}), and catalytic efficiencies (k_{cat}/K_m) for the PsaPOX variants (1 ng/mL) using 0.5 mM ABTS as a substrate in the presence of 100 µM H_2O_2 and 100 mM sodium acetate buffer, pH 3.5 at 40 °C. Values are the average of triplicate experiments with indication of standard deviations. DK: PsaPOX_DK; high: PsaPOX_high; low: PsaPOX_low.

PsaPOX variant	K_m (µM)	k_{cat} (s^{-1})	k_{cat}/K_m (s^{-1} mM^{-1})
DK	33.0 ± 2.5	6.8 ± 0.1	206 ± 4
high	25.8 ± 1.6	10.5 ± 0.1	408 ± 14
low	31.9 ± 2.3	3.8 ± 0.1	119 ± 2

The three variants showed similar Michaelis–Menten constants (25.8–33.0 µM), which were in the same range as for a DyP from *Irpex lacteus* (28 µM) [111]. Thus, no influence of the mutations on the Michaelis–Menten constant was concluded. However, the turnover numbers (k_{cat}) and, as a consequence, the catalytic efficiencies differed (Table 8.1). As expected from the results for the specific activities (Figure 8.7a), the turnover number and the efficiency of PsaPOX_high (10.5 s^{-1} and 408 s^{-1} mM^{-1}) were higher (~two-fold), while the values for PsaPOX_low (3.8 s^{-1} and 119 s^{-1} mM^{-1}) were lower (~1.7-fold) than for PsaPOX_DK (6.8 s^{-1} and 206 s^{-1} mM^{-1}). The results for PsaPOX_low were attributed to the changed pH optimum as well as the increased steric hindrance due to several mutations near the entrance to the active site (see Section 8.3.2.2), which most likely hampered the substrate access. In contrast, the higher turnover number and catalytic efficiency of PsaPOX_high was attributed to a higher percentage of correctly folded and therefore active protein due to an improved folding process or a reduced unfolding in the presence of the S371H, as assumed above (see Section 8.3.2.2). This would fit to the higher stability of PsaPOX_high. The comparison of the catalytic efficiencies of the PsaPOX variants with other DyP-type enzymes showed that

the S371H mutation resulted not only in an improved catalytic efficiency for PsaPOX_high in comparison to the wild-type enzyme, but also in comparison to the *Pleos*-DyP4 of *P. ostreatus* (352 s^{-1} mM^{-1}) [216]. However, the catalytic efficiency of a DyP from *Irpex lacteus* for ABTS (8000 s^{-1} mM^{-1}) was higher [111].

8.3.3 Expression Profile of the *PsaPOX* Gene from Different *P. sapidus* Strains

The identified mutations of *PsaPOX*, which resulted in three differently active enzyme variants, explained most of the observed intraspecific variability of the peroxidase and alkene cleavage activity, but the residual variances indicated further underlying causes (see Section 8.3.2.1). At least a 1.3–1.4-fold higher peroxidase and alkene cleavage activity was detected for MK16 in comparison to all other *P. sapidus* strains, which cannot have resulted from the observed amino acid exchanges in the PsaPOX sequence. Previous studies have shown differences of the transcriptional profile of mono- and dikaryons [25,29,30,32]. Thus, a transcriptional analysis was performed to monitor the relative expression of the *PsaPOX* gene in the *P. sapidus* strains, whose coding sequence had been evaluated (Figure 8.11a). The strains expressed different gene variants and accordingly produced three differently active enzymes; therefore, the results were examined and categorized in respect to the present PsaPOX variant in each strain.

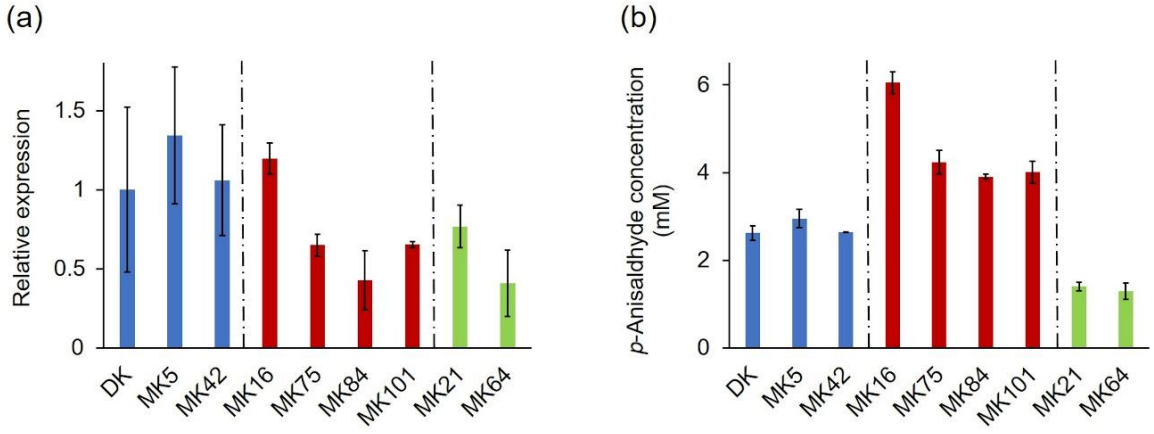

Figure 8.11. Relative expression of the *PsaPOX* gene (**a**) in comparison to the alkene cleavage activity, and (**b**) of selected monokaryons and the dikaryotic *P. sapidus* strain. Expression rates were normalized to the expression of the parental dikaryon. Values are the average of three (expression) or two (alkene cleavage activity) independent biological replicates with standard deviations shown as error bars. *P. sapidus* strains were grouped according to their PsaPOX sequence (blue: PsaPOX_DK; red: PsaPOX_high; green: PsaPOX_low).

MK42 and the parental strain, which produced PsaPOX_DK and showed a similar peroxidase and alkene cleavage activity, also exhibited a similar expression rate (Figure 8.4c and 8.11a,b). In contrast, the expression of MK5, which likewise contained the PsaPOX_DK variant, was slightly increased. This agreed with the slightly higher peroxidase and alkene cleavage activity of MK5 in comparison to the dikaryon, but the differences were smaller for the activities. This indicated the existence of unknown regulative mechanisms, such as posttranslational gene silencing (e.g., small interfering RNA and transposon-associated DNA methylation) or protein degradation [35,36,237].

PsaPOX expression in MK21 and MK64, both containing the PsaPOX_low variant, differed (~ two-fold), even though the enzyme activities of the strains were similar (Figure 8.4c and 8.11a,b). Thus, the regulation of PsaPOX_low production or degradation must have differed in MK21 and MK64.

The expression profiles of MK75, MK84, MK101, and MK16, all of which produced PsaPOX_high, were similar to the pattern of the enzyme activities (Figure 8.4c and 8.11a,b). MK84 exhibited the lowest expression rate and activities; MK75 as well as MK101 demonstrated slightly higher values; while the activities and *PsaPOX* expression of MK16 was noticeable higher (≥1.8-fold). In conclusion, the higher peroxidase and alkene cleavage activity of MK16, which was classified as very highly active (see Section 8.3.1.2), was also the result of a higher expression of the *PsaPOX* gene. However, the difference in expression between MK16 and the other high active strains was more distinctive (≥1.8-fold) than the differences of the peroxidase and alkene cleavage activity (≥1.3-fold). The detected activities of the three strains thus have to be influenced by an additional unknown regulative factor.

So far, only two other studies [28,30] have examined the gene expression of specific genes as the reason for varying enzyme activities of monokaryons and the corresponding dikaryons. Linke *et al*. [28] experimentally excluded the hypothesis, while Castanera *et al*. [30] identified a higher laccase activity of a *P. ostreatus* dikaryon in comparison to its parental monokaryons as result of up-regulation of *lacc6* and *lacc10* expression. Previous studies dealing with the gene expression of mono- and dikaryons focused on the overall differences between these, but not on specific activities [25,29]. Thus, differences in gene expression as a factor involved in intraspecific variability of a DyP-type enzyme were confirmed for the first time.

8.4 Materials and Methods

8.4.1 Chemicals and Materials

Chemicals were obtained from Sigma-Aldrich (Seelze, Germany), Carl Roth (Karlsruhe, Germany), or Merck (Darmstadt, Germany) in p.a. quality. PCR primers were obtained from Eurofins MWG Operon (Ebersberg, Germany).

8.4.2 Fructification of *P. sapidus*, Isolation of Basidiospores, and Screening of Monokaryons

Culture conditions of the dikaryotic strain (*P. sapidus*, Deutsche Sammlung von Mikroorganismen und Zellkulturen, DSMZ, Braunschweig, Germany, strain no. 2866) and the procedure for the production of monosporic colonies as well as their microscopic identification have been published previously [27]. The dikaryotic strain and 101 isolated monokaryotic strains were maintained on 1.5% (w/v) SNL agar [96] and evaluated regarding their radial growth rate in duplicates. For this, 5 mm^2 of actively growing mycelium of each strain were transferred to another SNL agar plate and incubated at 24 °C for ten days. Radial growth (increase of the colony) was measured every two days as mm/day.

8.4.3 Submerged Cultivation of *P. sapidus* Strains

The dikaryon (fast-growing) as well as five slow-, four moderate-, and five fast-growing monokaryotic strains were selected for submerged cultivation (in duplicate). For pre-cultivation, 1 cm^2 of grown agar was transferred to 100 mL SNL medium and treated with an Ultraturrax homogenizer (ART Prozess- & Labortechnik, Müllheim, Germany). The pre-cultures were incubated for 5 days at 150 rpm and 24 °C. Afterwards, 6.5 g (wet biomass) of pre-grown mycelium were used to inoculate 250 mL SNL. The main culture was incubated at 150 rpm and 24 °C. After six days, the mycelium was separated from the culture supernatant by centrifugation (5000× *g*, 4 °C, 15 min) and lyophilized as described elsewhere [78]. Afterwards, the lyophilisates were finely ground.

8.4.4 Phenotype Stability of Different *P. sapidus* Strains

To analyze the phenotype stability of different *P. sapidus* stains regarding the *trans*-anethole cleaving activity, the dikaryotic strain as well as three monokaryons were analyzed over five generations in duplicate. For this, the strains were re-cultivated every month on a fresh SNL

agar plate with the mycelia of the previous month. The mycelium of each generation was subsequently used for submerged cultivation (Section 8.4.3).

8.4.5 cDNA Synthesis and Gene Amplification

Isolation of total RNA from the mycelia of the *P. sapidus* strains at culture day six, cDNA synthesis, and amplification of the *PsaPOX* gene (coding sequence) were performed as described previously for the parental strain [209]. The untreated, as well as the DNase I-treated (Invitrogen, 1 U per µg RNA), RNA was used for cDNA synthesis. gDNA isolation was performed according to Aamir *et al.* [254] using 200 mg of mycelium (culture day six), but without RNase A treatment. The amplification of the *PsaPOX* gDNA sequence was performed as described for the coding sequence using the following cycler program: denaturation for 2 min at 98 °C, 35 cycles at 98 °C for 1 min, 62 °C for 30 s and 72 °C for 2 min, and a final elongation at 72 °C for 10 min. Analysis of PCR products, ligation, transformation in *Escherichia coli*, colony PCR, plasmid isolation, and sequencing were performed as described by Behrens *et al.* [98]. For sequencing of the gDNAs, the respective sequences were re-amplified from the pUC57 constructs after plasmid isolation using the standard primers M13 (5'-GTAAAACGACGGCCAGT-3') and M13r (5'-CAGGAAACAGCTATGAC-3') and Phusion High-Fidelity DNA Polymerase (Thermo Scientific, Wilmington, DE, USA). The thermal cycler program was as follows: denaturation for 2 min at 98 °C, 35 cycles at 98 °C for 1 min, 54 °C for 30 min and 72 °C for 2 min, and a final elongation at 72 °C for 10 min. The PCR products were purified by gel electrophoresis (1.0% agarose gels) and gel elution using the NucleoSpin® Gel and PCR Clean-up Kit (Macherey-Nagel, Düren, Germany). Afterwards the PCR products were used for DNA sequencing (Seqlab, Göttingen, Germany). Translation of DNA sequences was performed using the Software SnapGene® (GSL Biotech LLC, Chicago, USA). Alignments were produced by ClustalOmega [226]. For the prediction of putative *N*-glycosylation sites, the NetNGlyc 1.0 Server [255] was used.

8.4.6 Heterologous Expression of the PsaPOX Variants in *Komagataella phaffii*

The *PsaPOX* gene variants (PsaPOX_high and PsaPOX_low) were amplified with a C-terminal 6x His tag, inserted into the *K. phaffii* pPIC9 expression vector (Invitrogen, Karlsruhe, Germany), and expressed in *K. phaffii* as described for the gene of the dikaryotic strain [209]. The *K. phaffii* transformants were grown in 500 µL YEPD (1% (w/v) yeast

extract, 2% (w/v) peptone, and 2% (w/v) dextrose) in 96-well plates at 28 °C and 320 rpm for 48 h. Afterwards, the pre-cultures were transferred to the main-cultures by a medium change to 500 µL BMMY (1.34% (w/v) yeast nitrogen base, 1% (w/v) yeast extract, 2% (w/v) peptone, 100 mM potassium phosphate (pH 6), 4×10^{-5}% (w/v) biotin, and 1% (w/v) methanol after one washing step with 500 µL sterile water. The main cultures were cultivated for 72 h at RT and 320 rpm. Gene expression was induced by daily addition of 1% (v/v) methanol.

8.4.7 His-Tag Purification of the Recombinant PsaPOX Variants

The His-tagged PsaPOX variants were purified from the *K. phaffii* culture supernatant by Ni-NTA affinity chromatography according to Nieter *et al.* [229]. Afterwards, the eluted fractions were analyzed by SDS-PAGE, as described elsewhere [28]. Protein band intensities were evaluated by ImageJ [256]. Protein concentrations were determined according to Bradford [257] using bovine serum albumin as standard.

8.4.8 Biotransformation

Biotransformation of 5 µL (33.5 mM) *trans*-anethole was carried out with 30 mg *P. sapidus* lyophilisate (see Section 8.4.3), buffered in sodium acetate (50 mM, pH 3.5) in the presence of 25 mM $MnSO_4$ and 100 µM H_2O_2 in a total volume of 1 mL for 16 h at RT and 200 rpm according to Krahe *et al.* [209]. Controls (chemical blank: without lyophilisate; biological blank: with heat inactivated mycelium (2 h at 95 °C)) were performed accordingly. For the bioconversion with the recombinant peroxidase variants, 0.25 mg/mL purified recombinant protein and 1 µL (6.7 mM) *trans*-anethole were used, while all other parameters remained unchanged. Controls were performed without enzyme (chemical blank) or with heat inactivated enzyme (1 h at 95 °C, biological blank). All experiments were performed in duplicates. Sample preparation, analysis by gas chromatography, as well as quantification of the conversion product *p*-anisaldehyde was performed as described elsewhere [209]. To calculate the enzymatically generated product concentration, the product concentrations in the blanks were subtracted from the concentrations yielded with the active enzymes.

8.4.9 Peroxidase Activity

Total peroxidase activity was determined photometrically (EON^{TM} High Performance Microplate Spectrophotometer, BioTek Instruments GmbH, Bad Friedrichshall, Germany) by monitoring the oxidation of ABTS in the presence of hydrogen peroxide at 420 nm ($\varepsilon_{420} = 3.6 \times 10^4\ M^{-1}\ cm^{-1}$) and 40 °C for 10 min. Samples were mixed with sodium acetate buffer (100 mM, pH 3.5), 100 µM H_2O_2 and 0.5 mM ABTS in a total volume of 300 µL. One unit of enzyme activity was defined as 1 µmol substrate oxidized per minute under the experimental conditions. To determine the activity of the lyophilized *P. sapidus* mycelium, the peroxidases were solubilized by pre-incubation of 30 mg lyophilized mycelium in 1 mL sodium acetate buffer (100 mM, pH 3.5) for 2 h at 4 °C and 200 rpm. Afterwards, the samples were centrifuged (5000 ×*g*, 4 °C, 15 min) and the supernatant was used for the ABTS assay. For the calculation of the specific peroxidase activities of the three recombinant PsaPOX variants, identical protein concentrations (1 ng/mL) of the recombinant enzymes were used. All enzyme assays were performed as triplicates. Blanks were performed with water instead of buffer and by omission of hydrogen peroxide.

8.4.10 Comparative Biochemical Characterization of the PsaPOX Variants

Effects of pH, temperature, and hydrogen peroxide concentration on peroxidase activity as well as the kinetic constants for the substrate ABTS were comparatively evaluated for the PsaPOX variants. For this, 1 ng/mL enzyme was used for the ABTS assay (Section 8.4.9). The pH optimum was determined using Britton–Robinson buffer [230] in a range of 2.0 to 9.5 instead of sodium acetate buffer, while for determination of the temperature optimum the peroxidase activity was examined at different temperatures (20–90 °C). For analysis of the pH stability, the enzyme variants were incubated in Britton–Robinson buffer from pH 2.0 to 9.5 for 1 h at RT before the peroxidase activity was examined at pH 3.5 (100 mM sodium acetate buffer). For determination of the temperature stability, the PsaPOX variants were incubated at different temperatures (20–90 °C) for 1 h prior to enzyme activity measurement at 40 °C. The influence of the hydrogen peroxide concentration was examined by evaluation of peroxidase activity with different H_2O_2 concentrations (0–1 mM). Relative activities were normalized to the highest activity and residual activities to the initial activity prior to incubation. Kinetic constants of the enzyme variants for ABTS were calculated after peroxidase measurements with varying ABTS concentration (0–300 µM) by SigmaPlot 12.5 (Systat Software Inc., Chicago, IL, USA) using nonlinear regression.

8.4.11 Quantitative Real-Time PCR

For analysis of *PsaPOX* expression, three independent biological replicates were sampled after submerged cultivation at day six of the main culture (Section 8.4.3). Total RNA was prepared from 300 mg frozen mycelium using the NucleoSpin® RNA Plant Kit (Macherey Nagel). Nucleic acid concentrations were determined using a Nanodrop ND-1000 spectrophotometer (Thermo Scientific). RNA was treated with RNAse-free DNAse I (Invitrogen) using 1 U per µg RNA, and afterwards 1 µg total RNA was reverse-transcribed into cDNA using the FastGene Scriptase II cDNA Kit with oligo-dT primer (in 20 µL, Nippon Genetics Europe, Düren, Germany).

Quantitative real-time PCR (RT-qPCR) was performed in a CFX384 Real-Time PCR detection system (Bio-Rad Laboratories, München, Germany) using GoTaq qPCR Master Mix (Promega, Fitchburg, WI, USA). The primers qRT_*PsaPOX*_for (5'-CGATATCCTCGGaGGATTGCCA-3') and qRT_*PsaPOX*_rev (5'- CGCTTCACGGTCCT TGACTA-3') were chosen from homologous regions of the *PsaPOX* gene variants. Glyceraldehyd-3-phosphate dehydrogenase (*gpd3*; *gpd3*_for 5'-GCCATCAATGACCCGTT CATTG-3' and *gpd3*_rev 5'-CCTTCTCCGCGAAGATGTGG-3') and purine phosphorylase (*phos*; *phos*_for 3'-CATCGCAAATCATCGATCGCACC-3' and *phos*_rev 5'-GCTCTCCAGCCATTGCACCAATT-3'), described to be the best reference genes in *P. sapidus* for the expression analysis of different peroxidase genes [258], were chosen as reference genes. The reaction mix (10 µL final volume) consisted of 5 µL GoTaq qPCR Master Mix, 0.4 µL of both primers (0.2 µM each, final concentration), 2.6 µL nuclease-free water, and 2 µL of a 1:12.5 dilution of the cDNA. The amplification program was as follows: 95 °C for 2 min, 40 cycles at 95 °C for 20 s, 64.8 °C for 30 s and 70 °C for 10 s, and a final elongation at 70 °C for 2 min. Afterwards, a melting curve analysis was performed from 70 to 95 °C with a temperature increase of 0.5 °C/0.1 s to detect potential nonspecific products. Agarose gel electrophoresis was used to check for PCR and primer specificity. Each reaction was performed in triplicate, and non-template controls were included for each primer set. Using a mixture of all sample cDNAs, PCR efficiency for each primer pair was evaluated by the dilution series method (five orders of magnitude, see Supporting Table 8.1, Section 8.7) [259]. The Bio-Rad CFX Maestro Software was used for expression data calculation using the $2^{-\Delta\Delta C_T}$ method [260], for which the relative quantity ΔC_T of the target gene was normalized with respect to the geometric mean of the relative quantities of the reference genes.

8.4.12 Sequence Accession Numbers

The nucleotide sequences of the *PsaPOX* gene variants have been deposited in the GenBank database under accession numbers MT043310 (sequence 1, parental), MT847628 (sequence 3), MT847629 (sequence 4) and MT847630 (sequence 2).

8.5 Conclusions

In this study, basidiospore-derived monokaryons of the basidiomycete *P. sapidus* were used. They showed an intraspecific variability in peroxidase and alkene cleavage activity of the DyP-type peroxidase PsaPOX. The latter was stable over five sub-cultivation cycles. Furthermore, several monokaryons, especially MK16, exhibited higher peroxidase and alkene cleavage activities than the parental dikaryon. Thus, activity improvement was achieved by natural reproduction and selection of the progenies.

Analysis of the *PsaPOX* gene revealed the existence of three PsaPOX variants in the *P. sapidus* strains, which were partly responsible for the intraspecific variability in enzyme activity, as determined by analysis of the recombinant enzymes. This is the first study that verified gene mutation as reason for a differing enzyme activity in mono- and dikaryons. PsaPOX_high contained the S371H mutation, which resulted in a higher activity as well as improved catalytic efficiency, possibly due to a measurable increased stability. However, the molecular basis for the increase in activity of PsaPOX remains to be investigated, due to the peripheral location of the mutation in the predicted protein structure. Thus, X-ray crystallography and molecular modeling to investigate protein dynamics should be performed in follow-up studies. Furthermore, protein folding studies could be useful, because the observed results may be caused by changes in protein folding or unfolding and the resulting increase in ratio of active to inactive protein. In PsaPOX_low, eleven mutations were present that led to a decreased activity as well as a reduced stability. Experiments with the single-point mutants could show which of the amino acid exchanges were crucial for the observed biochemical changes.

Transcriptional analysis of the *P. sapidus* strains identified an up-regulation of the *PsaPOX* gene expression in MK16 in comparison to the other strains containing the PsaPOX_high enzyme variant, as reason of its higher activity. In contrast, the gene expression profiles of the low active strains did not match with the observed results for the peroxidase and alkene

cleavage activities. Thus, it was proposed that the strains differed in further traits, which regulated the detected PsaPOX activity.

The present study gives insights into some factors responsible for the intraspecific variability of PsaPOX activity in the monokaryotic and dikaryotic *P. sapidus* strains, but further research is needed to fully understand the regulatory processes in depth. The study identified one promising overproducing monokaryon (MK16) with potential as production strain for a commercial application of PsaPOX.

8.6 Author Contributions, Funding, Acknowledgements, and Conflicts of Interest

Author Contributions: Conceptualization, N.-K.K., R.G.B., H.Z., and A.B.O.; methodology, N.-K.K., M.W., and A.B.O.; validation, N.-K.K., R.G.B., M.W., H.Z., A.B.O., and F.E.; formal analysis, N.-K.K. and M.W.; investigation; N.-K.K. and A.B.O.; writing—original draft preparation, N.-K.K.; writing—review and editing, R.G.B., M.W., H.Z., A.B.O., and F.E.; visualization, N.-K.K.; supervision, F.E.; project administration, R.G.B.; funding acquisition, R.G.B., H.Z., and A.B.O. All authors have read and agreed to the published version of the manuscript.

Funding: This research was funded by the BMBF cluster Bioeconomy International 2015, grant number 031B0307 A. The APC was funded by the Open Access fund of the Gottfried Wilhelm Leibniz Universität Hannover.

Acknowledgments: We thank the Institute of Technical Chemistry (Leibniz University Hannover) for the measurements of RT-qPCR raw data. A.B.O. was supported as a Georg Forster Research Fellow by the Alexander von Humboldt Foundation.

Conflicts of Interest: The authors declare no conflict of interest. The funders had no role in the design of the study; in the collection, analyses, or interpretation of data; in the writing of the manuscript, or in the decision to publish the results.

8.7 Supplementary Materials

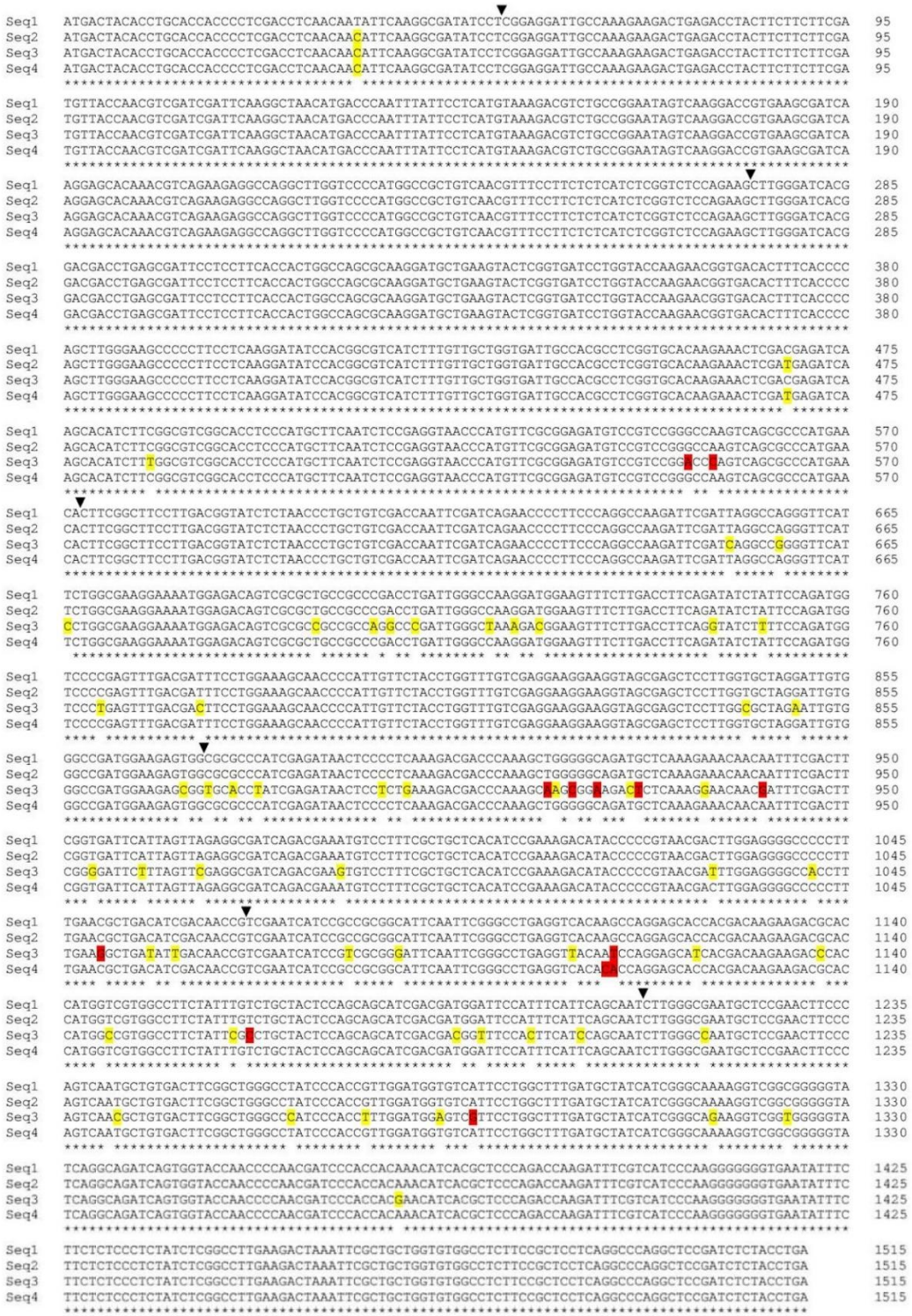

Supporting Figure 8.1. Alignment of *PsaPOX* reverse transcribed mRNA sequences from different monokaryons as well as the parental dikaryon. Seq1: sequence 1 of the dikaryon and MK5; Seq2: sequence 2 of MK42; Seq3: sequence 3 of MK21 and MK64, Seq4: sequence 4 of MK16, MK75, MK84, and MK101. Nucleotide exchanges were highlighted. Mutations resulting in amino acid exchanges are shown in red and exchanges which did not result in amino acid exchanges are presented in yellow. Alignment was performed with Clustal Omega (European Bioinformatics Institute, Hinxton, UK) [38]. Sequence 1 and 3 correspond to the coding regions of the two dikaryotic *PsaPOX* gDNA sequences. Inverted triangles indicate the position of introns.

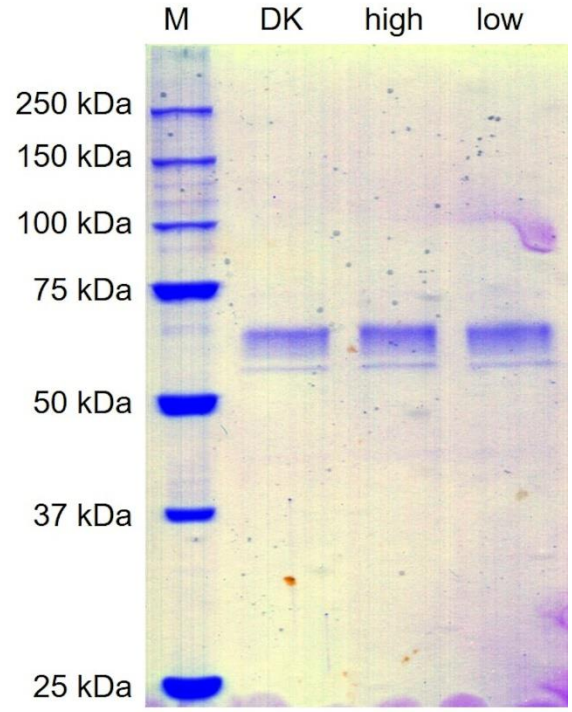

Supporting Figure 8.2. SDS-PAGE analysis of the purified recombinant PsaPOX variants after Ni-IMAC. The gel was stained with Coomassie Brilliant Blue. DK: PsaPOX_DK, high: PsaPOX_high, low: PsaPOX_low, M: molecular mass marker. Two protein bands were detected for the PsaPOX variants belonging to the unmodified (lower band) and glycosylated proteins (upper band).

Supporting Table 8.1. PCR efficiency of the primer pairs used for the RT-qPCR analysis.

target gene	primer pair	PCR efficiency [%]
PsaPOX	qRT_*PsaPOX*_for and qRT_*PsaPOX*_rev	92.8
gpd3	*gpd3*_for and *gpd3*_rev	88.3
phos	*phos*_for and *phos*_rev	95.7

9 Vorwort zur Publikation „Co-Oxidative Transformation of Piperine to Piperonal and 3,4-Methylenedioxycinnamaldehyde by a Lipoxygenase from *Pleurotus sapidus*"

Piperonal ist ein sehr wertvoller Aromastoff mit süß-floralem, vanilleartigem Geruch, der sowohl in Parfüms als auch in diversen Lebensmitteln wie Milchprodukten und Süßwaren (z. B. Eis und Schokolade) Anwendung findet (vgl. Kapitel 1.4). Das Vorkommen des natürlichen Moleküls ist jedoch begrenzt [177], sodass verstärkt nach biotechnologischen Verfahren zur Herstellung von „natürlichem" Piperonal gesucht wird, um das steigende Verlangen nach „natürlichen", „*clean-label*"-Produkten zu erfüllen. Verschiedene Biotransformationsreaktionen zur Gewinnung von Piperonal wurden bereits beschrieben, jedoch führten einige dieser nicht zur Bildung des natürlichen Aromas, da sie nicht-natürliche Substrate nutzten [261,262]. Die anderen Ansätze gingen von Isosafrol aus [177,191,263], welches ein natürliches Substrat ist, aber nur in geringen Mengen in der Natur vorkommt und damit teuer ist [264,265]. Weiterhin ist seine Verwendung streng reguliert, da es als Ausgangsmolekül für die Ecstasysynthese dienen kann [264]. Eine Alternative bietet die Verwendung von Piperin, einem Inhaltsstoff des schwarzen Pfeffers, der für dessen Schärfe verantwortlich ist. Natürliches Piperin ist gut erhältlich, günstiger als Isosafrol und unterliegt nicht dem Grundstoffüberwachunsgsgesetz.

In einer Vorarbeit wurde das Potential von *P. sapidus* zur Piperinspaltung und damit einhergehenden Piperonalbildung beobachtet [197]. Die zuvor beschriebene DyP PsaPOX war hierfür nicht verantworlich (vgl. Kapitel 6). Das Ziel der nachfolgenden Publikation war die Identifizierung des verantwortlichen Enzyms und die Optimierung der Biokonversion unter Verwendung des rekombinanten Enzyms. Hierbei zeigte sich, dass es sich bei dem gesuchten Enzym um die bereits publizierte $LOX_{Psa}1$ [133,152] handelt, welche in Gegenwart von PUFAs Piperin co-oxidativ in Piperonal oder, als konkurrierende Reaktion, in das Vanille-Aroma 3,4-Methylendioxyzimtaldehyd spaltet. Ansatzpunkt für eine weitergehende Optimierung könnte die Verwendung monokaryotischer *P. sapidus*-Stämme sein, da einige Stämme eine erhöhte Biotransformationsleistung bzw. die bevorzugte Bildung von Piperonal gegenüber dem alternativen Spaltprodukt zeigten.

Herr Kahlert führte im Rahmen seiner Bachelorarbeit unter Betreuung von Frau Dr. Fuchs den Hauptteil der Arbeiten mit dem rekombinanten Enzym durch [197]. Herr Prof. Berger war in seiner Rolle als Arbeitsgruppenleiter für die Projektidee, die Akquise der Drittmittel sowie zusammen mit Frau Dr. Ersoy für die wissenschaftliche Betreuung verantwortlich.

Die nachfolgende Publikation wurde in der *peer-reviewed* Zeitschrift *ChemBioChem* (Wiley) veröffentlicht (https://doi.org/10.1002/cbic.202100183) [266].

Zudem wurde zu der Publikation ein Titelbild in *ChemBioChem* veröffentlicht (https://doi.org/10.1002/cbic.202100282) (Abbildung 9.1) [267].

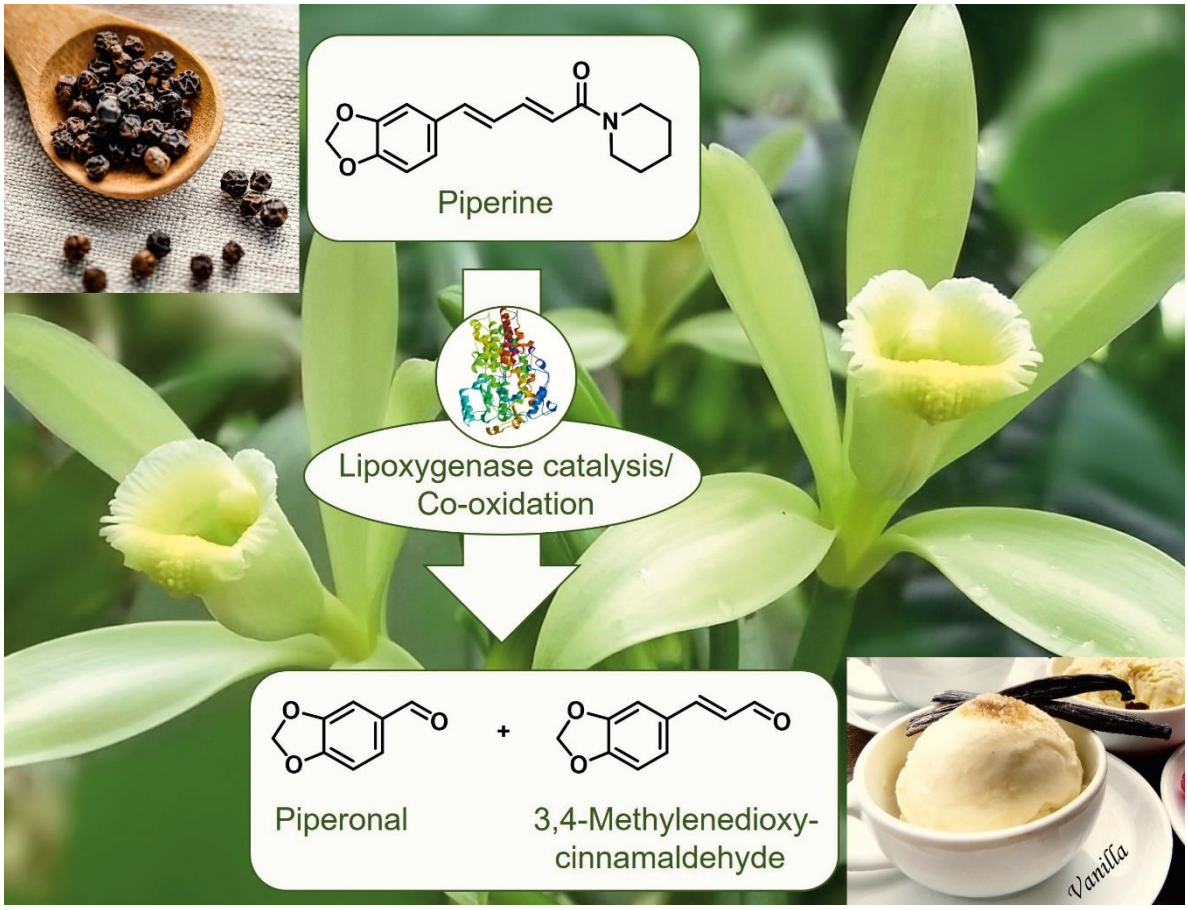

Abbildung 9.1. Titelbild zur Publikation „Co-oxidative Transformation of Piperine to Piperonal and 3,4-Methylenedioxycinnamaldehyde by a Lipoxygenase from *Pleurotus sapidus*” [267].

10

ChemBioChem | Communications
doi.org/10.1002/cbic.202100183
Chemistry Europe
European Chemical Societies Publishing

Co-Oxidative Transformation of Piperine to Piperonal and 3,4-Methylenedioxycinnamaldehyde by a Lipoxygenase from *Pleurotus sapidus*

Nina-Katharina Krahe,*[a] Ralf G. Berger,[a] Lukas Kahlert,[a, b] and Franziska Ersoy[a]

10.1 Abstract

The valuable aroma compound piperonal with its vanilla-like olfactory properties is of high interest for the fragrance and flavor industry. A lipoxygenase ($LOX_{Psa}1$) of the basidiomycete *Pleurotus sapidus* was identified to convert piperine, the abundant pungent principle of black pepper (*Piper nigrum*), to piperonal and a second volatile product, 3,4-methylenedioxycinnamaldehyde, with a vanilla-like odor through an alkene cleavage. The reaction principle was co-oxidation, as proven by its dependence on the presence of linoleic or α-linolenic acid, common substrates of lipoxygenases. Optimization of the reaction conditions (substrate concentrations, reaction temperature and time) led to a 24-fold and 15-fold increase of the piperonal and 3,4-methylenedioxycinnamaldehyde concentration using the recombinant enzyme. Monokaryotic strains showed different concentrations of and ratios between the two reaction products.

Keywords:

Biotransformations, Cleavage Reactions, Co-oxidation, Lipoxygenase, Piperonal

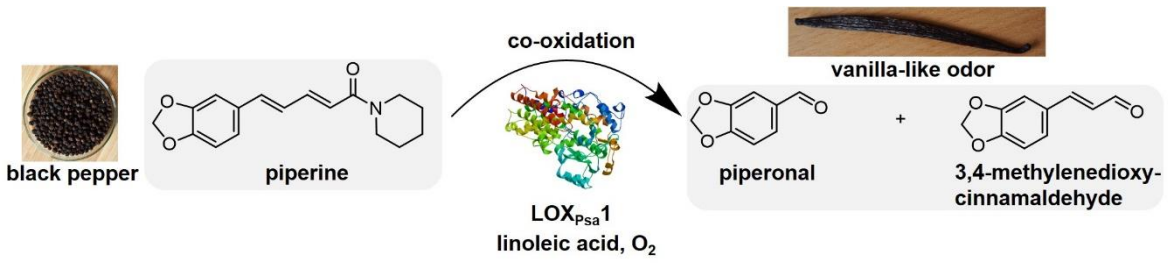

Figure 10.1. Graphical abstract – Biotransformation of piperine to piperonal and 3,4-methylenedioxycinnamaldehyde: A lipoxygenase from *Pleurotus sapidus* ($LOX_{Psa}1$) was identified, which generated the highly valuable, vanilla-like aroma compound piperonal through co-oxidation of piperine, the pungent principle of black pepper, in the presence of polyunsaturated fatty acids. In addition, 3,4-methylenedioxycinnamaldehyde, which also presents a vanilla-like odor, was produced as second product.

10.2 Introduction

Piperonal (3,4-methylenedioxybenzaldehyde or Heliotropin) has a sweet-flowery, vanilla-like odor that is of high interest for the fragrance and flavor industry [177]. It is present in low amounts in different plants, such as violet flower, robinia, meadowsweet, and vanilla. To meet the high demand, it is traditionally produced by chemical synthesis [177]. However, the rising popularity of natural products and sustainable production processes require alternative strategies, such as biocatalysis [50]. Bioconversion of isosafrol, piperonyl alcohol, and piperonylic acid to piperonal has been shown by different enzymes or bacterial and fungal strains [177,191,261,262]. However, some of these use non-natural substrates, thus resulting in non-natural piperonal [50]. Even though isosafrole is a natural starter, it suffers from its limited natural occurrence, high prices, and legislative restrictions as it works as precursor of 3,4-methylenedioxy-N-methylamphtamine (ecstasy) [264,265].

Lipoxygenases (EC: 1.13.11.12; LOX) are non-heme, mostly iron containing dioxygenases and ubiquitously present in eukaryotic organisms. They catalyze the regio- and stereospecific dioxygenation of (*cis*)-polyunsaturated fatty acids (PUFAs) to their corresponding unsaturated fatty acid hydroperoxides by a radical mechanism [126,127]. Co-oxidation of different unsaturated compounds by the enzyme's reactions products first became obvious due to the visually observed bleaching of pigments [142,146]. Investigations using antioxidants confirmed the radical character of the co-oxidation mechanisms [147]. However, the mechanisms behind these effects are not yet fully understood [127].

Herein, we present the bioconversion of piperine, the main alkaloid and pungent aroma principle of black pepper, to natural piperonal and an additional aroma compound, 3,4-methylenedioxycinnamaldehyde, by *Pleurotus sapidus* (Scheme 10.1). A lipoxygenase, which was known to convert (+)-valencene to the grapefruit aroma (+)-nootkatone [152,153], was identified as responsible for the reaction through co-oxidation. To the best of our knowledge, this is the first study using piperine for the biocatalytic generation of natural piperonal and the first report describing cleavage of aryl alkenes by a lipoxygenase activity.

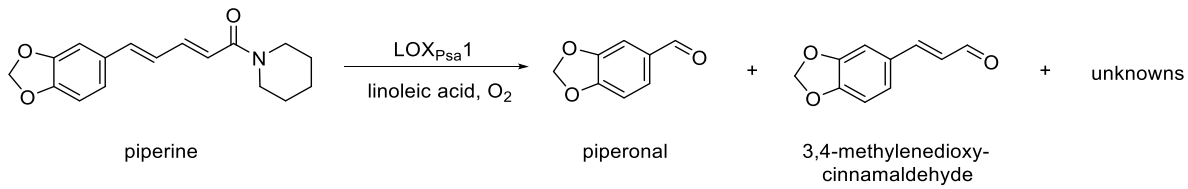

Scheme 10.1. Co-oxidation of piperine to piperonal and 3,4-methylenedioxycinnamaldehyde during linoleic acid oxidation by $LOX_{Psa}1$ from *P. sapidus*.

10.3 Results and Discussion

An alkene cleavage activity of the mycelium of the basidiomycete *P. sapidus* degraded 98% of piperine and generated 44.2 ± 0.1 µM piperonal (6.4% molar yield) (Supporting Figure 10.1 and 10.2, Section 10.6.2). Additionally, 51.8 ± 1.2 µM 3,4-methylenedioxy-cinnamaldehyde ((2*E*)-3-(1,3-benzodioxol-5-yl)-2-propenal; 7.3% molar yield) resulted from the competing cleavage of the second double bond of piperine. Olfactometric analysis of 3,4-methylenedioxycinnamaldehyde revealed a sweet odor, reminding of vanilla, which was in line with speculations of Kollmannsberger *et al.* [268]. Thus, a second potentially interesting aroma compound was generated. Further volatile products were not detected (Supporting Figure 10.1, Section 10.6.2), although the significantly higher degradation of piperine in comparison to the product yield indicated the formation of further by-products. Potentially, consecutive reactions, such as polymerizations, resulted in non-volatile products.

To identify the enzyme catalyzing the biotransformation, semi-purification from the soluble part of the rehydrated mycelium (crude extract) was tested. However, no piperine cleaving activity was found. To improve enzyme stability and solubility, different agents were tested (Supporting Figure 10.3, Section 10.6.2). Dithiothreitol and to a lesser extend glutathione had a significant stabilizing effect on the piperine cleaving activity. Thus, the enzyme was sensitive to sulfhydryl oxidation, which results in disulfide bond formation and most likely in conformational changes of the protein structure, which negatively affected the activity [269].

An activity loss during purification can also result from the loss of cofactors or cosubstrates, as H_2O_2- and/or manganese-dependency is known for other alkene cleaving basidiomycetous enzymes [191,209]. The loss of the LMMF (low molecular mass fraction) decreased the bioconversion (Figure 10.2a), thus confirming its requirement for the piperine cleaving enzyme. Supplementation of H_2O_2 and Mn^{2+} ($MnSO_4$) showed that addition of Mn^{2+} increased the piperonal generation (Figure 10.2b).

Semi-purification of the desired enzyme was performed *via* preparative isoelectric focusing (IEF) after addition of dithiothreitol, thus avoiding washing steps, which would have resulted in a high loss of the LMMF. The biotransformation reaction with the collected fractions was performed in the presence of Mn^{2+} and additional LMMF. Piperine cleavage was observed for fractions collected at pH 4.4 to 5.5 with the highest activity in fraction 9 (pH 4.7) (Figure 10.2c). A white protein precipitate in the active fractions 8 to 10 contained most of the activity (Figure 10.2d). Precipitation at the isoelectric point is well known for proteins [270].

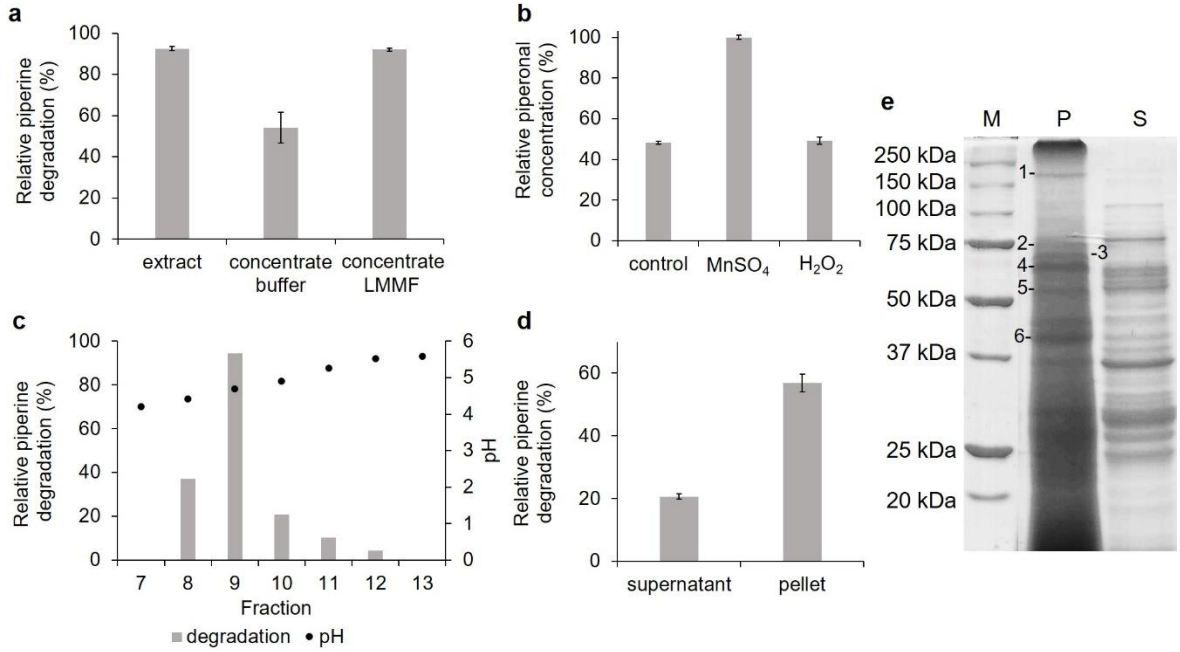

Figure 10.2. Activity analysis and semi-purification of the piperine cleaving enzyme. **a**) Influence of the low molecular mass fraction (LMMF) on the piperine degradation by *P. sapidus*. Extract: crude extract in buffer (25 mM Tris-HCl, pH 8.0). The extract was concentrated by ultrafiltration (3 kDa cut-off) and filled up to the starting volume with buffer or LMMF. **b**) Piperonal concentration after biotransformation in the absence (control) or presence of 1 mM $MnSO_4$ or 100 µM H_2O_2 using the crude extract. Concentrations were calculated relative to the highest piperonal concentration. **c**) Analysis of the preparative IEF fractions. **d**) Piperine degradation by the soluble (supernatant) and insoluble part (pellet) of fraction 8 to 10 of the preparative IEF. The pellet was re-suspended in buffer for analysis (same volume as before centrifugation). **e**) SDS-PAGE of the soluble and insoluble part of fraction 9 after preparative IEF. M: molecular mass marker, P: pellet, S: supernatant. The bands excised for protein sequencing are marked 1 to 9. Piperine degradation (a, c, d) was calculated relative to the starting piperine concentration. All experiments were performed in the presence of 1 mM piperine at pH 4.5 and RT for 16 h.

SDS-PAGE analysis revealed a multitude of protein bands in the insoluble part of fraction 9 (Figure 10.2e). However, further purification would have been challenging due to the LMMF-dependency, a low fraction volume (< 500 µL), and the disability to re-dissolve the precipitated piperine cleaving enzyme completely. Thus, the most dominating protein bands, which were not or less present in the other preparative IEF fractions (data not shown) and the soluble part of fraction 9, were excised and digested using trypsin for electrospray ionization tandem mass spectrometry (Figure 10.2e). Homology searches of the identified peptides using the NCBI database and the mascot search engine (Matrix Science, London, UK) revealed two enzymes potentially responsible for the piperine biotransformation (Supporting Table 10.1, Section 10.6.2): A lipoxygenase ($LOX_{Psa}1$) [152] and a dye-decolorizing peroxidase (DyP; PsaPOX) [208,209]. The latter is known to cleave different aryl alkenes but not piperine [209]. Thus, $LOX_{Psa}1$ was further investigated.

Recombinant $LOX_{Psa}1$ was produced in *E. coli*, purified by Ni-NTA affinity chromatography [153] (Supporting Figure 10.4, Section 10.6.2; specific activity for linoleic acid: 667 nkat/mg, 40 U/mg), and used for biotransformation experiments (Figure 10.3). $LOX_{Psa}1$ (100 nkat/mL, 6 U/mL) converted piperine into piperonal and 3,4-methylenedioxycinnamaldehyde (ratio ~ 0.5:1) in the presence of linoleic acid, a known substrate of $LOX_{Psa}1$ [152]. No activity was observed without linoleic acid (Figure 10.3 and Supporting Figure 10.5, Section 10.6.2). This indicated that piperine was not a direct substrate, but most likely cleaved by co-oxidation during linoleic acid oxidation (Scheme 10.1). Recent work suggested that various members of the catalytic cycle of lipoxygenases might interact with unsaturated substrates in co-oxidation reactions [126]. In the presented case, the initial linoleic acid hydroperoxide radicals may abstract hydrogens from the unsaturated bridge of piperine paving the way for an autoxidative insertion of an oxygen molecule. As a stable dioxene- or hydroperoxo-intermediate was not found, the exact mechanistic route remains obscure. In the mycelium and crude extract, fungal PUFAs most likely initialized the co-oxidation process as substrates, which would well explain the activity loss during the initial purification attempts and the LMMF-dependency (Figure 10.2a). In contrast to the results for the crude extract, addition of Mn^{2+} had no influence on the biotransformation yield of $LOX_{Psa}1$ (Figure 10.2b and 10.3a). A second, Mn^{2+}-dependent enzyme may participate in the piperine conversion. This remains to be elucidated in a follow-up study.

To increase the biotransformation yield, different PUFAs and concentrations were examined as well as the influence of pH, temperature, piperine concentration, and incubation time (Figure 10.3b-e and Supporting Figure 10.6, Section 10.6.2). Biotransformation experiments with linoleic and α-linolenic acid showed that the product concentration increased significantly with rising PUFA concentrations (up to 17.5-fold; exemption: 2.5 mM α-linolenic acid) (Figure 10.3b). The PUFA concentration was the parameter with the highest effect on the biotransformation yield. These findings support the co-oxidative character of the piperine cleavage reaction. Linoleic acid at the highest concentration (2.5 mM) achieved the highest piperonal (25 µM) and 3,4-methylenedixycinnamaldehyde concentrations (53 µM) and was thus used for all subsequent assays.

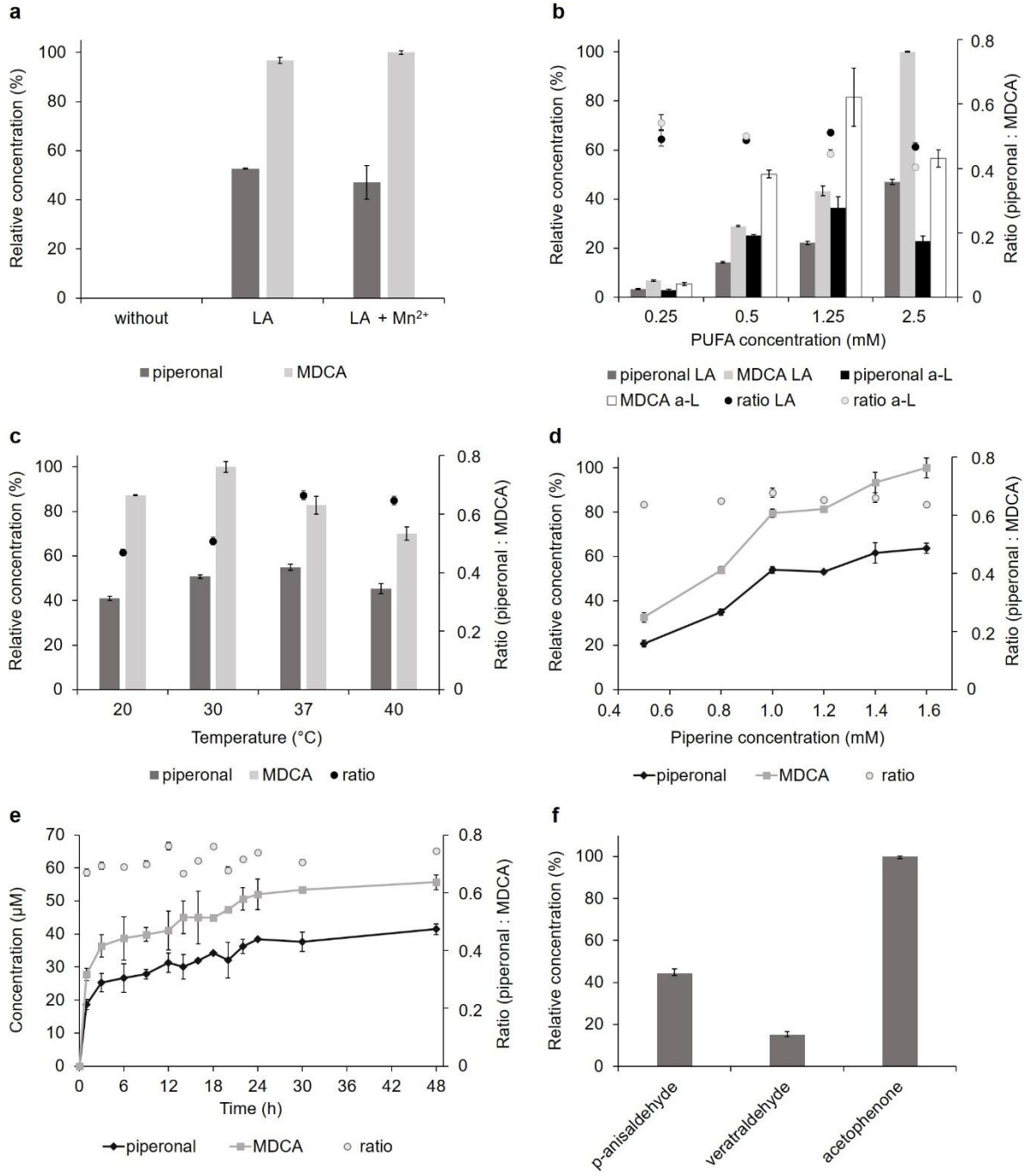

Figure 10.3. Biotransformation of piperine by the recombinant $LOX_{Psa}1$ (100 nkat/mL, 6 U/mL). **a**) Biotransformation of 1 mM piperine in the absence or presence of 0.25 mM linoleic acid (LA) and 1 mM Mn^{2+} (RT). **b**) Influence of the LA and linolenic acid (a-L) concentration (1 mM piperine, RT). **c**) Temperature optimum (2.5 mM LA, 1 mM piperine). **d**) Influence of the piperine concentration (2.5 mM LA, 37 °C). **e**) Reaction kinetic of the piperonal and 3,4-methylenedioxycinnamaldehyde formation (2.5 mM LA, 1.6 mM piperine, 37 °C). **f**) Product concentration after conversion of *trans*-anethole to *p*-anisaldehyde, (*E*)-methyl isoeugenol to veratraldehyde, and α-methylstyrene (all 6.7 mM) to acetophenone (2.5 mM LA, 37 °C). Relative product concentrations were defined as relative to the highest product concentration obtained in each experiment. All experiments were performed at pH 7 for 16 h (exemption: kinetic in e). MDCA: 3,4-methylenedioxycinnamaldehyde.

Analysis of the piperine biotransformation revealed a pH optimum of 7 (Supporting Figure 10.6, Section 10.6.2) and a temperature optimum of 30 °C (overall product concentration, Figure 10.3c). These results agreed with the optima reported for the linoleic acid oxidation by $LOX_{Psa}1$ [152]. However, the product ratio of piperonal to 3,4-methylenedioxy-cinnamaldehyde increased from 0.5 to 0.65 at 37 °C (Figure 10.3c). This most likely resulted from thermodynamic effects [271], which disfavour the cleavage of the second double bond and hence 3,4-methylenedioxycinnamaldehyde formation at higher temperatures. As piperonal is the more valuable cleavage product, 37 °C was considered as optimal for piperonal synthesis and used for the following experiments. Temperature was the only parameter that effected the product-ratio (Figure 10.3b-e and Supporting Figure 10.6, Section 10.6.2).

Additional experiments showed a linear increase in product concentration with rising piperine concentrations (Figure 10.3d, coefficient of determination $R^2 \geq 0.90$). Concentrations higher than 1.6 mM piperine were not investigated due to the lack of solubility. An increase of the incubation time to 48 h resulted in the highest overall piperonal (41 µM) and 3,4-methylenedioxycinnamaldehyde concentrations (56 µM) (Figure 10.3e). Thus, improving the reaction conditions (linoleic acid and piperine concentration, reaction temperature and time) achieved a 24- and 15-fold increase of the piperonal and 3,4-methylenedioxycinnamaldehyde concentrations, respectively.

During the first three hours, over 60% of the maximal product concentration was obtained (Figure 10.3e). The following decrease of the biotransformation rate was most likely the result of a linoleic acid limitation, as it was completely degraded after 16 h (Supporting Figure 10.5, Section 10.6.2). Higher linoleic acid concentrations of a fed-batch regime may be applied. In addition, higher enzyme concentrations may be used, as they led to increased product formation (Supporting Figure 10.7, Section 10.6.2).

$LOX_{Psa}1$ was further examined for bioconversion of other alkenes. The aryl alkenes *trans*-anethole, (*E*)-methyl isoeugenol, and *α*-methylstyrene were converted to the expected olfactants *p*-anisaldehyde, veratraldehyde, and acetophenone, respectively (Figure 10.3f and Supporting Scheme 10.1, Section 10.6.2). The highest product concentration was identified for *α*-methylstyrene followed by *trans*-anethole (about two-fold lower) and (*E*)-methyl isoeugenol (about six-fold lower).

In summary, the biocatalytic generation of piperonal using piperine as substrate was achieved by a co-oxidation reaction catalyzed by $LOX_{Psa}1$ in the presence of linoleic acid. In addition, a second aroma compound, 3,4-methylenedioxycinnamaldehyde, was generated, which also offered a vanilla-like odor. Separation of both aldehydes may be achieved by adsorption to zeolithes as shown, for example, for limonene and carvone [272]. Alternatively, a combined application could be envisaged due to the similar odor attributes. Although the improved reaction conditions increased the product concentrations, further optimization is needed. Besides higher linoleic acid concentrations, monokaryotic daughter-strains of *P. sapidus* are an option, as they showed higher LOX activities [27] and higher product concentrations after piperine transformation (Supporting Figure 10.8, Section 10.6.2). In addition, some of the daughter strains favored the formation of piperonal over 3,4-methylenedioxycinnamaldehyde. As $LOX_{Psa}1$ converted further aryl alkenes to their respective odor-active aldehydes, it showed potential as biocatalyst for aroma production. However, further optimization is needed to improve product concentrations for a potential industrial application.

10.4 Experimental Section

Experimental details are given in the Supporting Information.

10.5 Acknowledgments and Conflicts of Interest

Acknowledgements: This research was funded by the BMBF cluster Bioeconomy International 2015, grant number 031B0307A. We thank B. Fuchs for her preparatory work for this project and C. Theobald and N. Püth for the olfactory analysis of 3,4-methylenedioxycinnamaldehyde. Open access funding enabled and organized by Projekt DEAL.

Conflicts of Interest: The authors declare no conflict of interest.

10.6 Supporting Information

10.6.1 Materials and Methods

10.6.1.1 Chemicals and Materials

Chemicals were obtained from Sigma Aldrich (Seelze, Germany), Carl Roth (Karlsruhe, Germany), or Merck (Darmstadt, Germany) in *p. a.* quality, if not stated otherwise. A piperonal standard was synthesized according to Gallagher *et al.* using aqueous $KMnO_4$ [273].

10.6.1.2 Cultivation of *P. sapidus*

P. sapidus (Deutsche Sammlung von Mikroorganismen und Zellkulturen GmbH, DSMZ, strain no. 2866 and nine monokaryotic daughter strains [208]) was pre-grown on 1.5% (w/v) agar plates with standard nutrient liquid (SNL) medium and maintained at 4 °C until use [96]. For pre-cultivation, 1 cm^2 of grown agar was transferred to 100 mL SNL medium and treated with an Ultraturrax homogenizer (ART Prozess- & Labortechnik, Müllheim, Germany). The pre-cultures were incubated for 5 days at 150 rpm and 24 °C. Afterwards, 6.5 g wet biomass was used to inoculate 250 mL SNL. The main culture was incubated at 150 rpm and 24 °C. After six days, the mycelium was separated from the culture supernatant by centrifugation (5000× g, 4 °C, 15 min) and lyophilized as described elsewhere [78]. Afterwards, the lyophilisates were finely ground.

10.6.1.3 Purification strategy

25 g lyophilized mycelium was re-suspended in 600 mL 25 mM Tris-HCl, pH 8 in the presence of 2 mM dithiothreitol and extracted for 2 h at 4 °C in horizontal position in an orbital shaker (200 rpm). Insoluble components were removed by centrifugation (5000× g, 4 °C, 15 min) followed by filtration (PES filter, 0.45 µm, Merck). Additional 2 mM dithiothreitol was added to the cell free crude extract before the extract was concentrated (ten-times) by cross-flow filtration (10 kDa cut-off, Sartocon® Slice PESU Cassette, Sartorius, Göttingen, Germany). The concentrate was mixed with 2% Servalyt (pH 3–6; Serva, Heidelberg, Germany) and 2 mM dithiothreitol and transferred to the focusing chamber of a Rotofor cell (Bio-Rad, Munich, Germany). The chamber was cooled to 2 °C. Focusing was carried out at constant power of 12 W using 0.5 M ethanoleamine and 0.5 M acetic acid as anode and cathode buffers, respectively. After 4 h, 20 fractions were harvested. Each fraction was analyzed regarding its pH and its capability to convert piperine. SDS-

PAGE analysis and peptide mass fingerprinting was performed as described elsewhere [28,209]. The obtained partial peptide sequences were used for similarity searches against the public databases NCBI using the mascot search engine (Matrix Science, London, UK).

10.6.1.4 Heterologous expression and purification of $LOX_{Psa}1$

The recombinant lipoxygenase ($LOX_{Psa}1$) was produced in *E. coli* BL21 DE3 Star and purified *via* Ni-NTA affinity chromatography as described elsewhere [132,153]. Protein concentrations were determined according to Bradford [257] using bovine serum albumin as standard. Lipoxygenase activities were determined photometrically by monitoring the absorbance change at 234 nm due to the oxidation of 0.25 mM linoleic acid to the respective conjugated hydroperoxydienes at pH 7 and 30 °C following the previously established procedure by Plagemann *et al.* [152].

10.6.1.5 Biotransformation

All experiments were performed as fourfold determination (one duplicate each for GC analysis and HPLC analysis) or in duplicates (only GC analysis). For experiments with *P. sapidus* mycelium or crude extract independent biological replicates were used. The data are shown in the main text and below are the average of the duplicate experiments with standard deviations shown as arrow bars.

For all experiments blanks were performed without *P. sapidus* mycelium or recombinant enzyme (chemical blank) or with heat inactivated mycelium or enzyme (4 h (mycelium) or 1 h (enzyme) at 95 °C, biological blank). The determined product concentrations for the blanks were subtracted from the concentrations yielded for the reaction with the active samples to calculate the enzymatically generated product concentration.

a) *P. sapidus* mycelium

Transformation of piperine was carried out in 4 mL gas tight glass vials in horizontal position at a shaking rate of 200 rpm for 16 h in the absence of light. Reaction mixtures contained 1 mM piperine and 30 mg *P. sapidus* lyophilisate or 250 µL liquid sample (crude extract or preparative IEF fraction) buffered in sodium acetate (50 mM, pH 4.5) with or without addition of 1 mM $MnSO_4$ or 100 µM H_2O_2 in a total volume of 1 mL. For the analysis of the enzyme stability, cell free crude extract (see Section 10.6.1.3) was stored in the presence of a peptidase inhibitor mix (0.5 mM phenylmethylsulfonyl fluoride, 1.5 µM aprotinin, 50 µM bestatin, 10 µM pepstatin A), dithiothreitol (2 and 10 mM), glutathione (2 and 10 mM),

Triton X-100 (0.01 and 0.04% (w/v)), Tween 20 (0.001 and 0.01% (w/v)), 3-[(3-cholamidopropyl)dimethylammonio]-1-propanesulfonate (CHAPS; 0.1 and 0.7% (w/v)), bovine serum albumine (BSA, 1% (w/v)), or glycerol (5% (w/v)) at 4 °C for 0 h to 7 d before biotransformation. For analysis of the influence of the low molecular mass fraction (LMMF) of the crude extract on the biotransformation reaction, the extract was concentrated (10-times) by ultrafiltration (3 kDa cut-off, polyethersulfone (PES), Sartorius) and refilled to the starting volume with Tris-HCl (25 mM, pH 8) or LMMF before bioconversion.

Analysis of the biotransformation products was performed *via* GC after stir bar sorptive extraction (see Section 10.6.1.7a).

b) Recombinant $LOX_{Psa}1$

The purified recombinant lipoxygenase (100 nkat/mL, 6.0 U/mL, 0.15 mg/mL) was used for transformation of piperine as mentioned above to confirm alkene cleavage activity. Conversion of 1 mM piperine was performed in the presence or absence of linoleic or *α*-linolenic acid (0.25–2.5 mM) in sodium phosphate buffer (25 mM, pH 7) at RT for 16 h. In addition, supplementation of 1 mM $MnSO_4$ in the presence of 0.25 mM linoleic acid was tested. The pH optimum was determined using Britton-Robinson buffer [230] in a range of pH 5.0–9.0 in the presence of 2.5 mM linoleic acid at RT, while for analysis of the temperature optimum the bioconversion was performed at different temperatures (20–90 °C) in the presence of 2.5 mM linoleic acid at pH 7 (25 mM sodium phosphate buffer). The influence of the piperine concentration was tested by variation of the concentration (0.5–1.6 mM) in the presence of 2.5 mM linoleic acid at pH 7 and 37 °C. For kinetic studies, the piperine cleavage was performed with 1.6 mM piperine and 25 mM linoleic acid at pH 7 and 37 °C with varying incubation time (0–48 h). Furthermore, varying $LOX_{Psa}1$ concentrations (10-1000 nkat/mL, 0.6–60 U/mL, 0.015–1.5 mg/mL were tested (1.6 mM piperine, 25 mM linoleic acid, pH 7, RT, 16 h).

Analysis of the biotransformation products was performed *via* GC after stir bar sorptive extraction (biotransformation in the presence or absence of linoleic acid or $MnSO_4$, and differing enzyme concentrations; see Section 10.6.1.7a) or after liquid extraction (analysis with different concentrations of linoleic, *α*-linolenic acid, and piperine, pH and temperature optimum, and kinetic studies; see Section 10.6.1.7b).

c) Biotransformation of other aryl alkenes

Biotransformation of the alkenes *trans*-anethole, methyl isoeugenol, and *α*-methylstyrene (6.7 mM each) to *p*-anisaldehyde, veratraldehyde, and acetophenone was tested at pH 7 and RT using 2.5 mM linoleic acid and 100 nkat/mL (6 U/mL) $LOX_{Psa}1$ (16 h of incubation). Analysis of the reaction products was performed *via* GC after liquid extraction (see Section 10.6.1.7c).

10.6.1.6 HPLC analysis for piperine quantification

After biotransformation, the residual piperine concentration was determined by HPLC. For this, 1 mL acetonitrile was added to the biotransformation samples. The samples were mixed, filtered (syringe filter Chromafil® RC-45/25, Macherey-Nagel, Düren, Germany), and analyzed by a LC-10 system (Shimadzu Deutschland GmbH, Duisberg, Germany) equipped with a reversed phase column (Chromolith Performance RP-18e, 100 × 4.6 mm, Merck) and a UV/VIS detector (SPD-10A VP, Shimadzu Deutschland GmbH). The following gradient was used at ambient temperature: initial 90% solvent A (0.1% formic acid in water) and 10% solvent B (acetonitrile), 10–58% solvent B in 6 min, 58–100% solvent B in 2 min (hold for 1 min), 100–10% solvent B in 4 min. Finally, the system was re-equilibrated with 10% solvent B for 2 min. 10 µL sample were injected and the flow rate was 1.5 mL/min. Piperine was detected at 345 nm and its concentration was quantified from the corresponding peak area using external calibration.

10.6.1.7 GC analysis

a) Quantification of piperonal and 3,4-methylenedioxycinnamaldehyde after stir bar sorptive extraction

Detection and quantification of piperonal, 3,4-methylenedioxycinnamaldehyde, and linoleic acid was performed by GC analysis after stir bar sorptive extraction using Twisters (10 × 0.5 mm, Gerstel, Mülheim, Germany) coated with polydimethylsiloxane. 500 µL sample were diluted with 1.5 mL deionized water, containing 2.5 µg/mL (18 µM) 1,2-dimethoxybenzene as internal standard (IS), and extracted for 1 h under vigorous stirring at 290 rpm. Afterwards, the Twister was rinsed with deionized water, dried with a lint free cloth, and analyzed by gas chromatography. The stir bar was measured *via* TDS3 (thermodesorption system)-GC-FID (flame ionization detector) (Agilent 6890N, Agilent Technologies, Santa Clara, CA, USA) equipped with a cold injection system (CIS 4, Gerstel) and FID detector (250 °C, H_2-flow 35 mL/min, air-flow: 300 mL/min, N_2-flow: 25 mL/min).

The initial temperature of the TDS 3 was 20 °C. The sample was heated with 60 °C/min to 300 °C and held for 3 min for splitless desorption. Volatiles were refocused in the CIS 4 at −10 °C on a liner filled with Tenax TA. The CIS was heated to 300 °C with 12 °C/s and held at maximal temperature for 3 min. The sample was injected in the solvent vent mode. As a stationary phase, HP-5 (30 m, 0.32 mm, 0.25 µm, Agilent Technologies) was used. All analyses were performed with a volumetric flow rate of 1.3 mL/min hydrogen using the following temperature program: 40 °C (3 min), a temperature increase of 3 °C per minute until 150 °C, a further temperature increase of 20 °C per minute until 300 °C and a final hold time of 10 min. Piperonal and 3,4-methylenedioxycinnamaldehyde were semi-quantified according to the area of the IS. Biotransformation products were identified using standards and comparison of retention indices with literature. Furthermore, GC mass spectrometry was used for identification (Agilent 6890 N, equipped with a VF-WAX ms column (30 m × 0.25 mm, 0.25 µm, Agilent) and CIS 4; coupled with mass spectrometry (Agilent 5977A) and olfactory detection port (ODP3, Gerstel, 250 °C)). GC–MS analyses were performed with helium as carrier gas, 0.25 µL injection volume and a flow rate of 1.0 mL/min. MS scans were run in a range of m/z 34–500 with a scan rate of 3.1 scans/s. The thermodesorption and GC temperature program was the same as in the GC-FID analyses. Sensory evaluation of 3,4-methylenedioxycinnamaldehyde was performed *via* the ODP3.

b) Quantification of piperonal and 3,4-methylenedioxycinnamaldehyde after liquid extraction

The biotransformation products were extracted by liquid extraction using 1 mL diethylether containing 10 mg/L (0.1 mM) cyclohexanol (IS). The organic phase was dried with anhydrous sodium sulfate and subsequently analyzed by GC with an Agilent 7890 instrument equipped with a HP-5 column (30 m × 0.32 mm, 0.25 µm, Agilent), an on column injection port and FID. Hydrogen was used as carrier gas at a constant flow rate of 2.1 mL/min. One µL sample was injected *via* an autosampler and measured using the following method: 40 °C (3 min), a temperature increase of 5° C per minute until 230 °C, a further temperature increase of 25 °C per minute until 325 °C and a final hold time of 10 min. The biotransformation products were semi-quantified in relation to the area of the IS.

c) Quantification of *p*-anisaldehyde, veratraldehyde, and acetophenone

The conversion products were extracted with 1 mL hexane containing 100 mg/L (1 mM) cyclohexanol (IS). The organic phase was dried with anhydrous sodium sulfate and

subsequently analyzed by gas chromatography (GC). GC measurements were performed with an Agilent 7890 instrument equipped with a DB-WAX UI column (30 m × 0.32 mm, 0.25 µm, Agilent), a split/splitless injector port (1:5) and a FID. Hydrogen was used as carrier gas at a constant flow rate of 2.1 mL/min. One µL sample was injected *via* an autosampler and measured using the following method: 40 °C (3 min), a temperature increase of 10 °C per minute until 230 °C and a final hold time of 10 min. The biotransformation products (*p*-anisaldehyde, veratraldehyde, and acetophenone) were semi-quantified according to the area of the internal standard. Biotransformation products were identified using standards and comparison of retention indices with literature.

10.6.2 Results

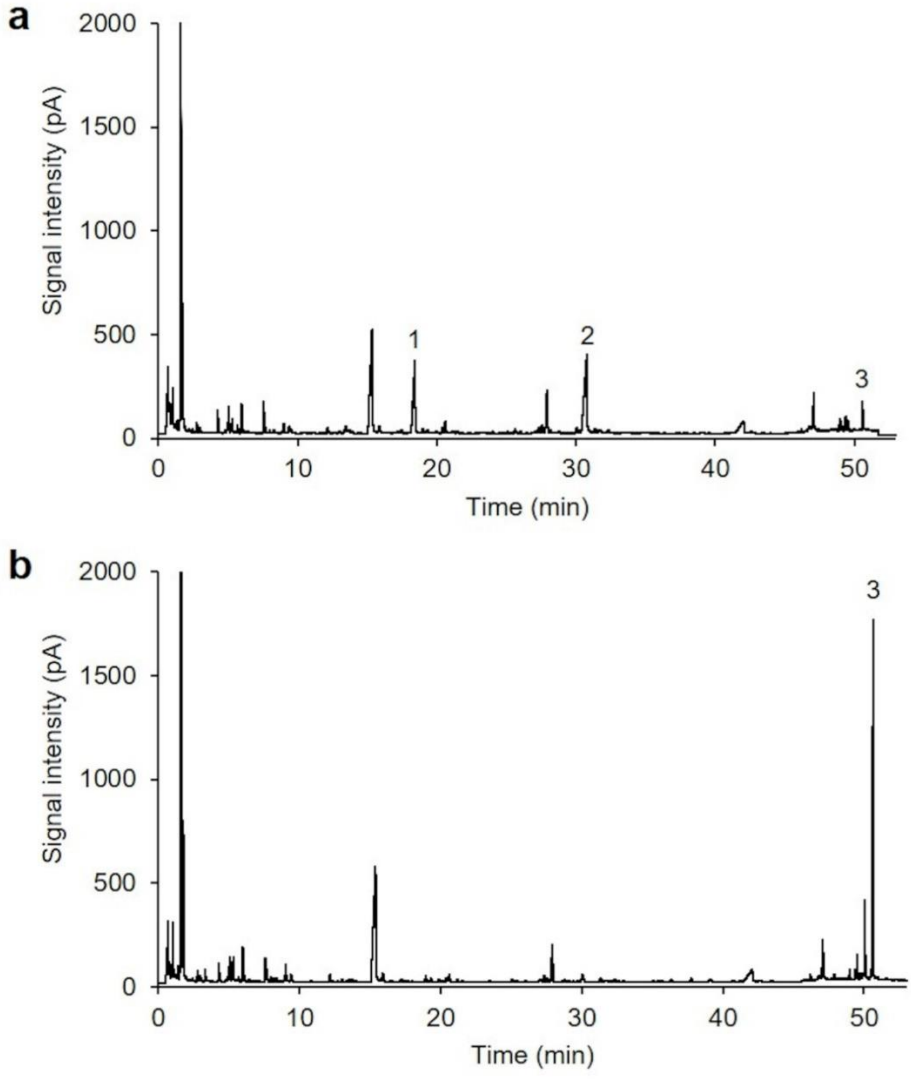

Supporting Figure 10.1. TDS-GC-FID chromatogram of the bioconversion of piperine with lyophilized mycelium of *P. sapidus* after 16 h of incubation. **a**) Active mycelium. **b**) Blank sample with heat inactivated mycelium (4 h, 95 °C). 1: piperonal, 2: 3,4-methylenedioxycinnamaldehyde, 3: piperine.

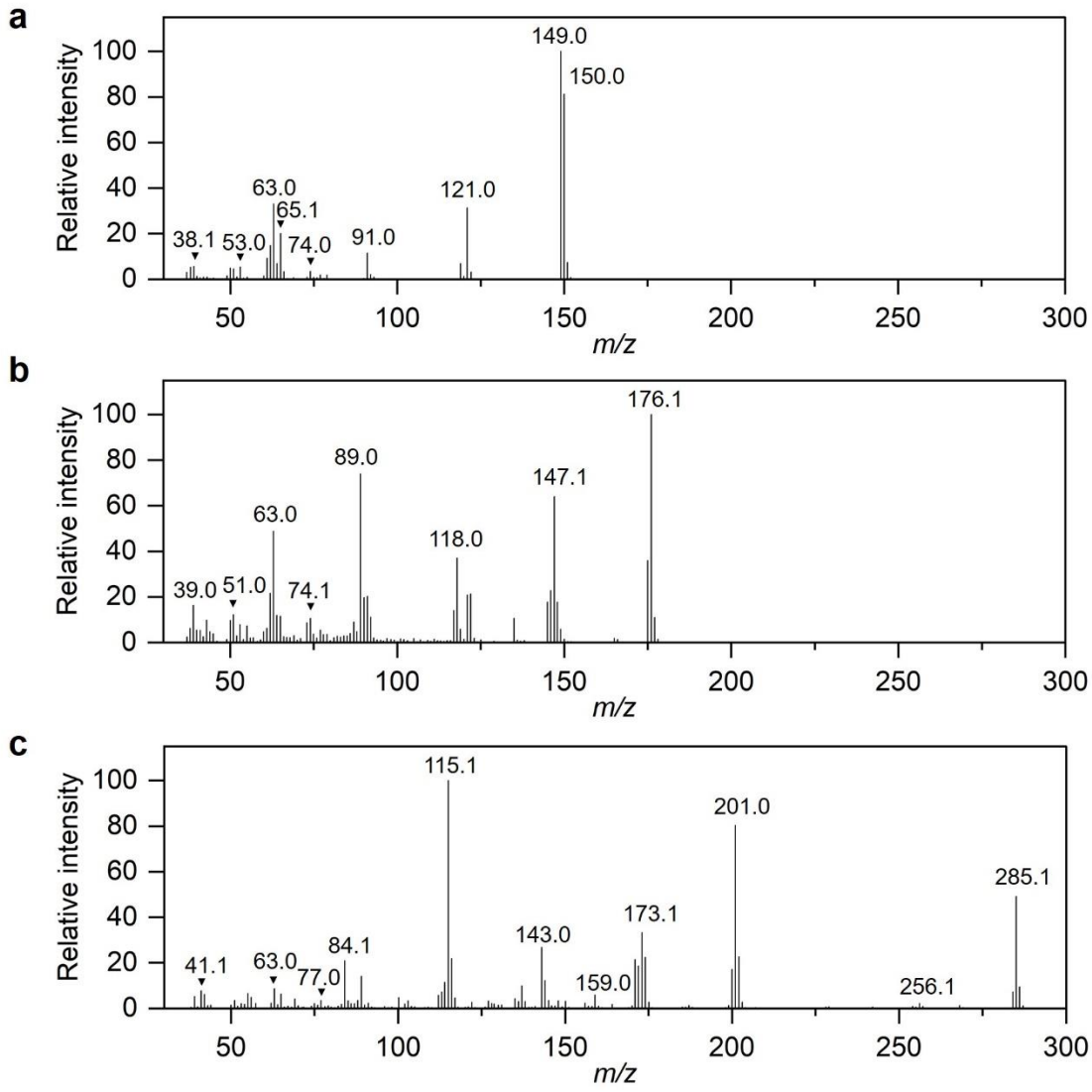

Supporting Figure 10.2. MS spectra resulting from GC-MS analysis that were used for the allocation of the substrate and products to the respective peaks in the TDS-GC-FID chromatogram (Supporting Figure 10.1). **a**) Piperonal, **b**) 3,4-methylenedioxycinnamaldehyde, and **c**) piperine.

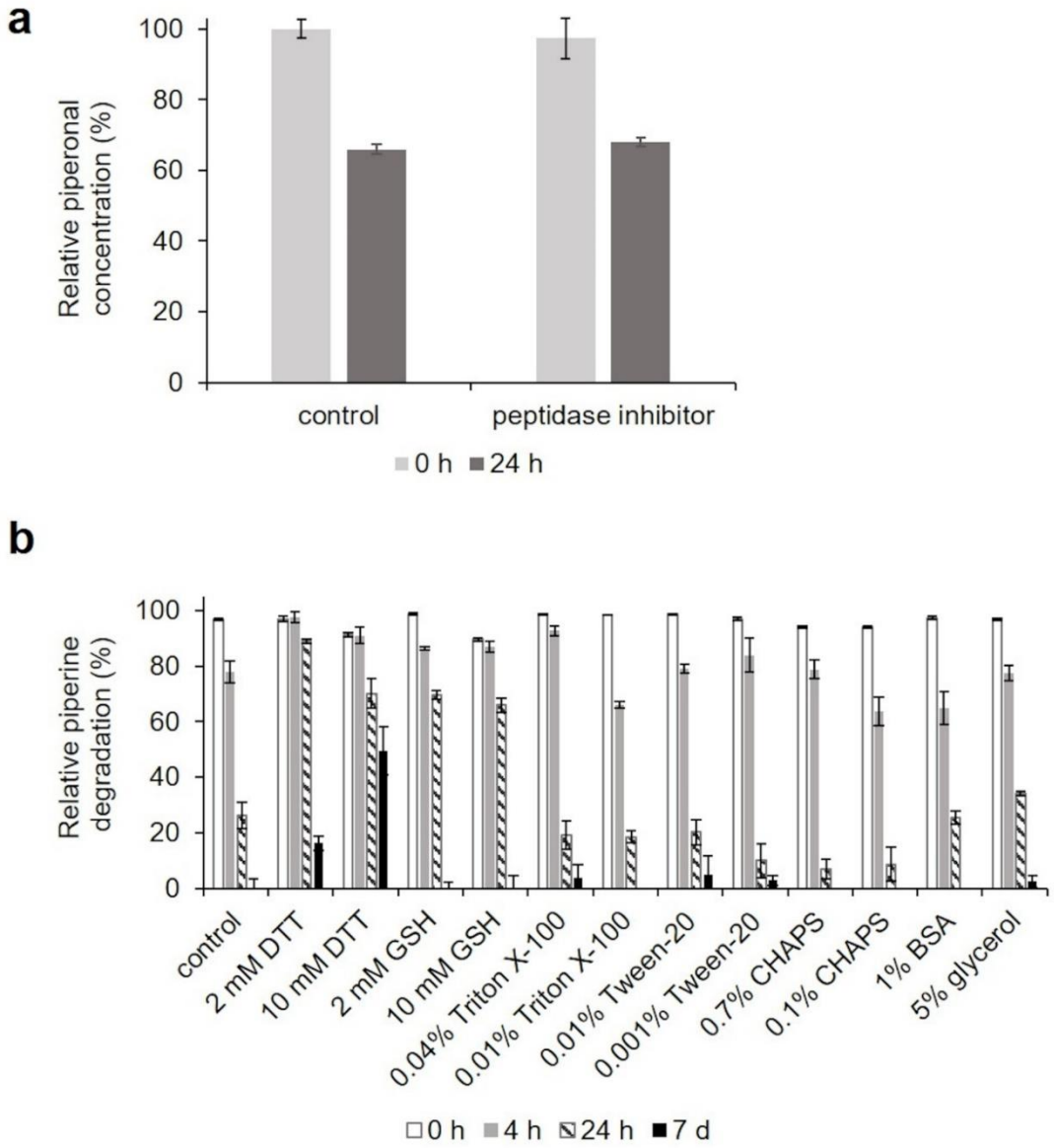

Supporting Figure 10.3. Storage stability of the piperine cleaving enzyme in the soluble fraction after rehydration of the *P. sapidus* mycelium. **a**) Relative piperonal concentration for the biotransformation after storage at 4 °C over 0 and 24 h in the presence or absence of a peptidase inhibitor mix. Concentrations were calculated relative to the value obtained for the control sample after 0 h storage. **b**) Relative piperine degradation for the biotransformation after storage at 4 °C over 0, 4, 24 h, and 7 d in the presence of different stabilizing agents. The degradation was calculated relative to the starting piperine concentration. Control: without addition of stabilizing agent; DTT: dithiothreitol, GSH: glutathione; CHAPS: 3-[(3-cholamidopropyl)dimethylammonio]-1-propanesulfonate; BSA: bovine serum albumine. For the detergents (Triton X-100, Tween-20, and CHAPS) one concentration above and one below the critical micellar concentrations were used.

Supporting Table 10.1. Best hits resulting from the protein sequencing of protein band 1 to 6 from the SDS-PAGE (Figure 10.2e).

Protein band	Protein (GenBank accession no.) and amino acid sequence
1	Glycoside hydrolase (belonging to family 3) of *Pleurotus ostreatus* PC15 (KDQ23735.1) MNGLCVGNIPPVQNWPGLCLEDSPLGVRFGDFSTAFPTAINAAATWNRRLIRLRGLF MGQEHVGKGVNVALGPMMNMGRVANGGRNWEGFGADPFFAGEAAYETILGMQEAGVQ ACAKHFINNEQEHKRTESTSDVDDRTQHEIYAHPFLKSVMAGVASVMCSYNQINGTF ACENDKMLNDVLKREFGFQGYVMSDWQATHSTHSANDGLDMTMPGDITFNSGDSWFG GNLTTSVRDNQTPEARLDDMATRIIAAWYLLKQQRSDFPTPNFDAFRPDNEQTNFHI DVQDDHGDLVREMGAASTVLLKNVRGALPLRKPRSLVLVGSDAGPGVIGPNHFSDQG GVDGVLAMGWGSGTANFTYLVSPYEAISARARKDHTTLSWIFDDFNLARAGNMAIGR SAALVFLNSDSGEGYITVDGNEGDRRNLTAWHGGDNLVTAVAAQNNNTIVVVHSVGP LILEPWIEHPNVTAVVWAGVSGTETGNALVDILYGAWNPSGRLPYTIAKRPEDYPAQ LVLGGGGAENIIPIPYTEGLEIDYRHFDAKNITPRFEFGFGLSYTTFEYSNLKVSKI DSPDHVQSDLERAWAAGKASPHGQGSSTALYLHRPAFRVTFDVKNTGKLFGGDIPQL YVNMPASSGEPPSILKGFTNIELSPNERRTVTINLSRYDLSIWDTAAQGWAKPAGRI AITVGASSRDARLHGRIPL
2, 3*, 4*, 5*, 6*	Lipoxygenase ($LOX_{Psa}1$) of *Pleurotus sapidus* (CCV01581.1) MVHNISLSSRKALHNVHLPYMVQLPKPTGYNVALKNAAEGYDKARRMVAWLYDIADY ESSIPQTFTLQQKTDKYTWELSDNFPPHLAVVPPDQSVSAPSIFSPVRLAQTLLIMS SLWYDDHTDLAPGPEQNTMQKLTQWNQERHKDQGWLIKDMFNAPNIGLRNDWYTDEV FAQQFFTGPNSTTITLASDVWLTAFTSEAKAQGKDKVIALFESAPPNSFYVQDFSDF RRRMGAKPDEELFNDSDGAMRYGCAAVALFYLTAMGKLHPLAIIPDYKGSMAASVTI FNKRTNPLDISVNQANDWPWRYAKTCVLSSDWALHEMIIHLNNTHLVEEAVIVAAQR KLSPSHIVFRLLEPHWVVTLSLNALARSVLIPEVIVPIAGFSAPHIFQFIRESFTNF DWKSLYVPADLESRGFPVDQLNSPKFHNYAYARDINDMWTTLKKFVSSVLQDAQYYP DDASVAGDTQIQAWCDEMRSGMGAGMTNFPESITTVDDLVNMVTMCIHIAAPQHTAV NYLQQYYQTFVPNKPSALFSPLPTSIAQLQKYTESDLMAALPLNAKRQWLLMAQIPY LLSMQVQEDENIVTYAANASTDKDPIIASAGRQLAADLKKLAAVFLVNSAQLDDQNT PYDVLAPEQLANAIVI
4	Alkene cleaving DyP-type peroxidase (PsaPOX) of *Pleurotus sapidus* (QIV15482.1) MTTPAPPLDLNNIQGDILGGLPKKTETYFFFDVTNVDRFKANMTQFIPHVKTSAGIV KDREAIKEHKRQKRPGLVPMAAVNVSFSHLGLQKLGITDDLSDSSFTTGQRKDAEVL GDPGTKNGDTFTPAWEAPFLKDIHGVIFVAGDCHASVHKKLDEIKHIFGVGTSHASI SEVTHVRGDVRPGQVSAHEHFGFLDGISNPAVDQFDQNPFPGQDSIRPGFILAKENG DSRAAARPDWAKDGSFLTFRYLFQMVPEFDDFLESNPIVLPGLSRKEGSELLGARIV GRWKSGAPIEITPLKDDPKLGADAQRNNNFDFGDSLVRGDQTKCPFAAHIRKTYPRN DLEGPPLNADIDNRRIIRRGIQFGPEVTSQEHHDKKTHHGRGLLFVCYSSSIDDGFH FIQQSWANAPNFPVNAVTSAGPIPPLDGVIPGFDAIIGQKVGGGIRQISGTNPNDPT TNITLPDQDFVIPRGGEYFFSPSISALKTKFAAGVASSAPQAQAPIST

Peptides identified by protein sequencing are underlined. * Peptidolytic degradation of $LOX_{Psa}1$ resulted in multiple protein bands as described by Plagemann *et al.* [133].

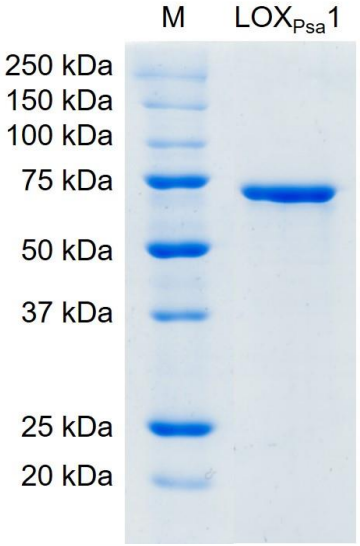

Supporting Figure 10.4. SDS-PAGE analysis of the purified recombinant $LOX_{Psa}1$. M: molecular mass marker, $LOX_{Psa}1$: purified enzyme.

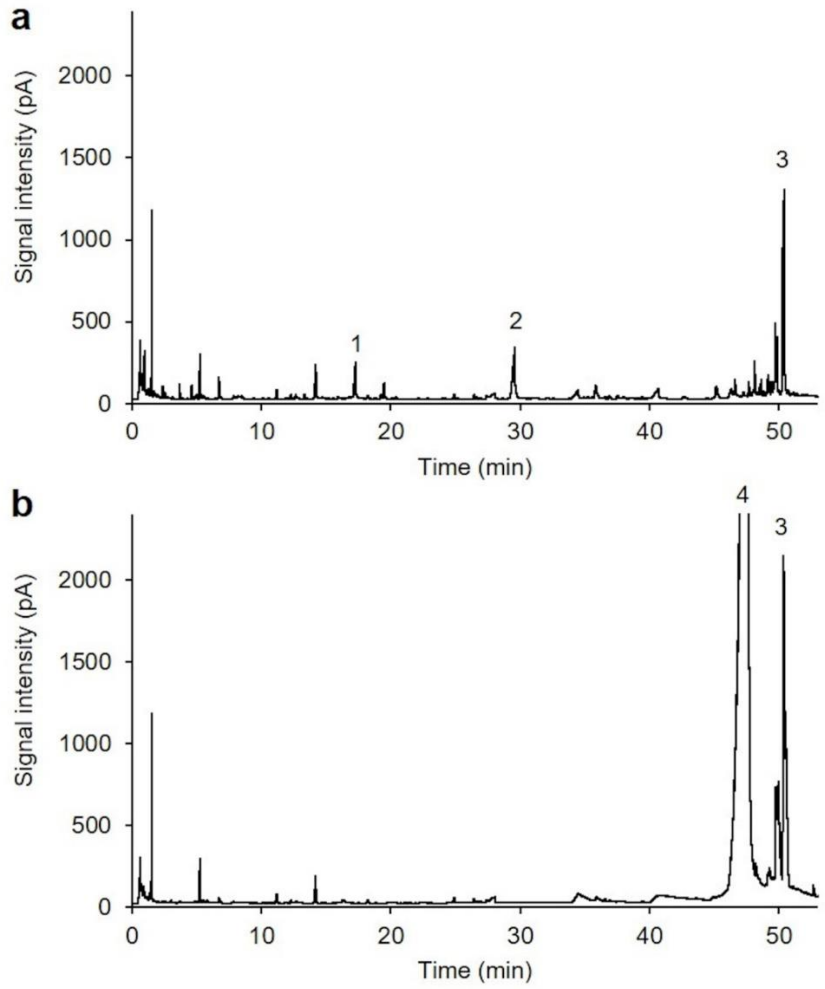

Supporting Figure 10.5. TDS-GC-FID chromatogram of the bioconversion of piperine with $LOX_{Psa}1$ after 16 h of incubation. **a**) Recombinant $LOX_{Psa}1$ (100 nkat/mL, 6 U/mL). **b**) Blank sample with heat inactivated enzyme (1 h, 95 °C). 1: piperonal, 2: 3,4-methylenedioxycinnamaldehyde, 3: piperine, and 4: linoleic acid.

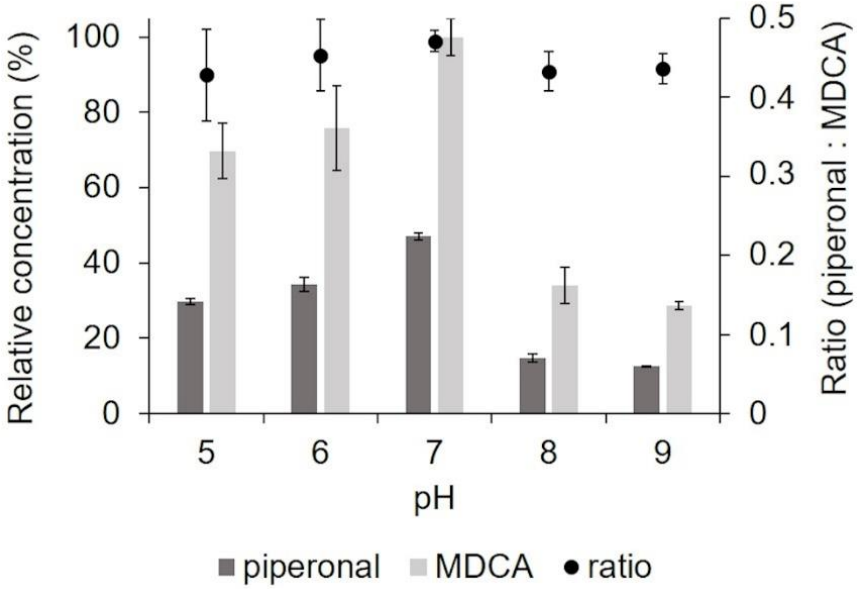

Supporting Figure 10.6. pH optimum of the piperine biotransformation using 100 nkat/mL (6 U/mL) $LOX_{Psa}1$ in the presence of 2.5 mM linoleic acid and 1 mM piperine at RT after 16 h. Concentrations are relative to the highest product concentration. MDCA: 3,4-methylenedioxycinnamaldehyde.

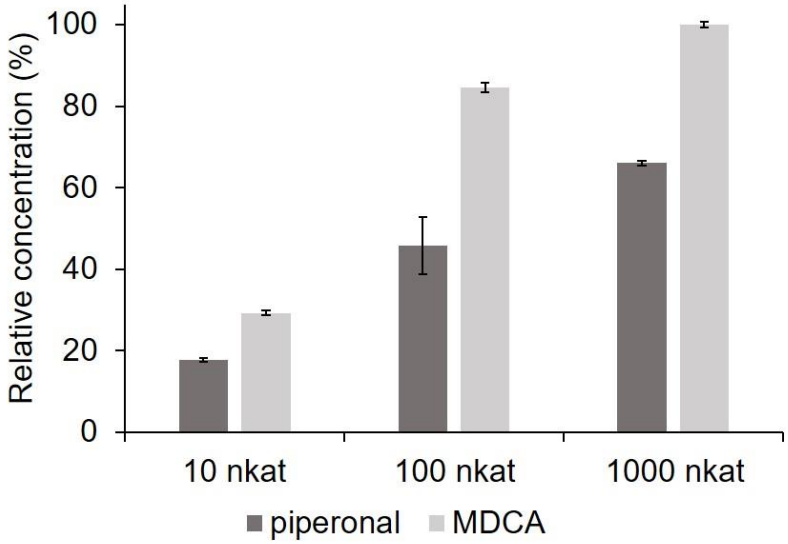

Supporting Figure 10.7. Piperine biotransformation with different $LOX_{Psa}1$ activities in the presence of 2.5 mM linoleic acid and 1 mM piperine at pH 7 and RT after 16 h. Concentrations are relative to the highest product concentration. MDCA: 3,4-methylenedioxycinnamaldehyde.

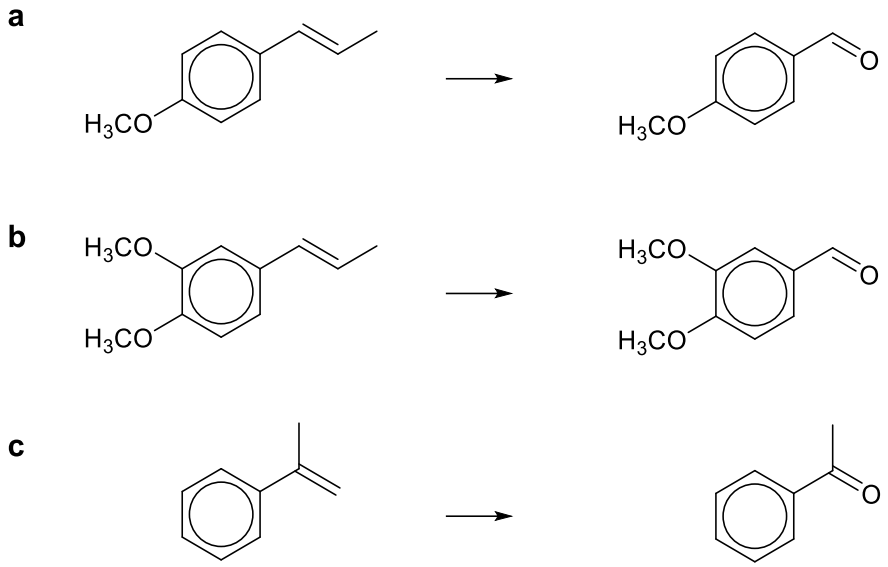

Supporting Scheme 10.1. Bioconversion of **a**) *trans*-anethole to *p*-anisaldehyde, **b**) (*E*)-methyl isoeugenol to veratraldehyde, and **c**) *α*-methylstyrene to acetophenone by $LOX_{Psa}1$.

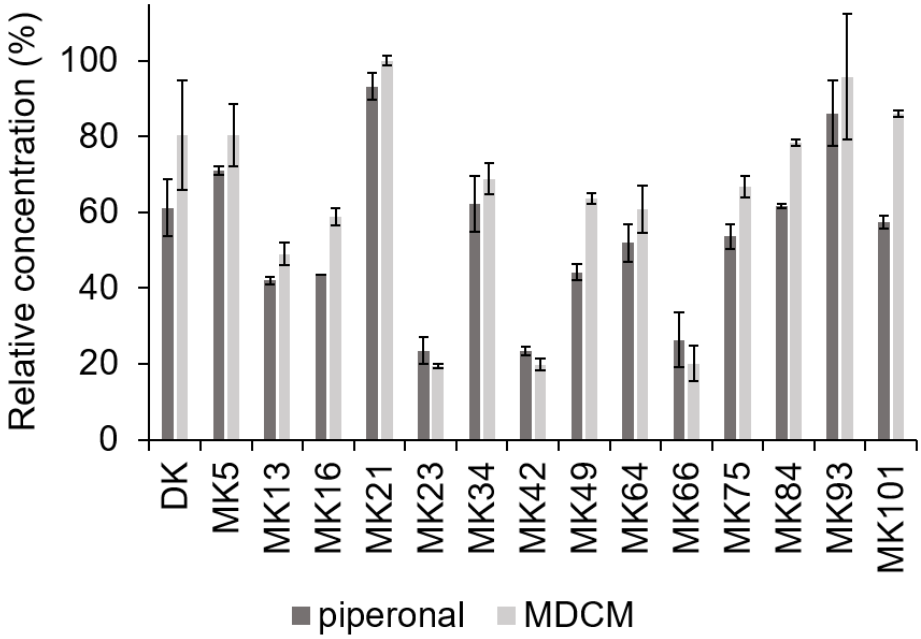

Supporting Figure 10.8. Piperine biotransformation with different *P. sapidus* strains in the presence of 2.5 mM linoleic acid and 1 mM piperine at pH 7 and RT after 16 h. DK: parental strain used in the presented study; MK: monokaryotic daughter strains. Concentrations are relative to the highest product concentration. MDCA: 3,4-methylenedioxycinnamaldehyde.

11 Fazit und Ausblick

In der vorliegenden Arbeit wurden zwei Enzyme aus *P. sapidus* identifiziert, die für die alkenspaltende Aktivität des Basidiomyceten verantwortlich waren: PsaPOX und $LOX_{Psa}1$. PsaPOX katalysierte die Biotransformation von *trans*-Anethol zu *p*-Anisaldehyd sowie die Spaltung von zwei weiteren Arylalkenen ((*E*)-Methylisoeugenol und α-Methylstyrol), jedoch nicht die Umsetzung von Piperin zu den vanilleartigen Aromastoffen Piperonal und 3,4-Methylendioxyzimtaldehyd. Hierfür war $LOX_{Psa}1$ verantwortlich, wobei es sich bei dieser Reaktion um einen co-oxidativen Prozess handelte, der die Anwesenheit von mehrfach ungesättigten Fettsäuren voraussetzte. Neben Piperin konnte $LOX_{Psa}1$ ebenfalls *trans*-Anethol, (*E*)-Methylisoeugenol und α-Methylstyrol zu den ensprechenden geruchsaktiven Aldehyden umsetzen. Damit zeigten sowohl $LOX_{Psa}1$ als auch PsaPOX prinzipiell Potential als Biokatalysatoren für die Aromastoffherstellung. Die zugehörigen Publikationen waren die ersten, die eine Spaltung von Arylalkenen durch eine DyP- bzw. LOX-Aktivität beschrieben.

Für eine potentielle industrielle Applikation der Enzyme wären *Scale-Up*-Studien sinnvoll. Dabei machen die sehr geringen Piperonal und 3,4-Methylendioxyzimtaldehyd-konzentrationen eine Optimierung der Biotransformation mit der LOX erforderlich. Ein vielversprechender Ansatzpunkt wäre die Erhöhung der Linolsäurekonzentration, da diese während der bisherigen Optimierung unter Verwendung des rekombinanten Enzyms den größten Effekt auf die Produktausbeute hatte. Aufgrund der geringen Löslichkeit von Linolsäure und einer möglichen Substratinhibierung der LOX durch hohe Linolsäurekonzentrationen [274], scheint hierbei eine sequentielle Zugabe sinnvoll.

Da sowohl Piperonal als auch 3,4-Methylendioxyzimtaldehyd nach Vanille riechen und gemeinsam während der Biotransformation von Piperin mit $LOX_{Psa}1$ gebildet werden, wäre eine kombinierte Anwendung in möglichen Produkten interessant. Hierfür sollten Studien zur synergistischen Wirkung der Aromastoffe durchgeführt werden. Jedoch ist 3,4-Methylendioxyzimtaldehyd bisher kein zugelassener Aromastoff, sodass dennoch die Trennung der beiden Produkte nötig sein könnte. Hierzu könnten, wie bereits für die Trennung von Limonen und Carvon gezeigt, Zeolithe genutzt werden [272].

Im Rahmen der vorliegenden Arbeit wurde weiterhin gezeigt, dass die natürliche sexuelle Reproduktion des parentalen dikaryotischen *P. sapidus*-Stamms zu einer Tochtergeneration an monokaryotischen Stämmen führte, die eine natürliche intraspezifische Variabilität

bezüglich ihres Biotransformationspotentials gegenüber *trans*-Anethol und Piperin zeigten. Die Diversität wurde dazu genutzt, Stämme mit natürlich optimiertem Biotransformationspotential im Vergleich zum parentalen Dikaryoten zu identifizieren. Damit konnte eine Optimierung der gesuchten Enzymaktivitäten erzielt werden ohne auf die Anwendung von gentechnischen Verfahren angewiesen zu sein. Dies wurde auch für andere Enzymaktivitäten in früheren Studien gezeigt. MK16 zeigte ein sehr hohes Potential für die PsaPOX-Produktion und sollte daher für weitere Applikationsstudien, u. a. für die Testung der Langzeitstabilität unter industriellen Bedingungen, genutzt werden.

Die stabile intraspezifische Variabilität des Dikaryoten und der monokaryotischen *P. sapidus*-Stämme bezüglich der Peroxidase- und alkenspaltenden Aktivität von PsaPOX konnte anteilig auf Mutationen des codierenden Gens und die daraus resultierende Existenz von drei PsaPOX-Varianten mit unterschiedlicher spezifischer Peroxidaseaktivität und Proteinstabilität zurückgeführt werden. Die zugehörige Publikation war damit die erste, die eine Genmutation als Ursache für unterschiedliche Enzymaktivitäten von Dikaryoten und monokaryotischen Stämmen bewies. Unterschiede auf der Genexpressionsebene wurden als weitere Ursache für die intraspezifische Variabilität bezüglich der PsaPOX-Aktivität festgestellt. Dennoch scheinen auch bisher unbekannte regulative Mechanismen an der enzymatischen Diversität der *P. sapidus*-Stämme beteiligt zu sein. Diese sollten im Rahmen nachfolgender Arbeiten identifiziert werden. Weiterhin sollte analysiert werden, welche der elf detektierten Mutationen in PsaPOX_low für die geringere spezifische Aktivität und Stabilität des Enzyms verantwortlich sind. Hierzu sollten Punktmuatationsstudien durchgeführt werden. Auch die Analyse des Einflusses von Position 371 in PsaPOX scheint interessant, da der Austausch von Serin zu Histidin in PsaPOX_high zu einer erhöhten katalytischen Effizienz und spezifischen Aktivität geführt hat, obwohl die Position weit entfernt vom aktiven Zentrum auf der Oberfläche des Enzyms liegt. Es wurde vermutet, dass dies aus der beobachteten erhöhten Proteinstabilität resultiert. Um jedoch die molekularen Ursachen für die beobachteten Ergebnisse zu ermitteln, scheinen Röntgenstrukturanalysen, molekulare Modellierungen der Proteindynamik sowie Faltungsstudien nötig.

In einer Anschlussarbeit könnten ebenfalls die Ursachen für die beobachtete intraspezifische Variabilität der *P. sapidus*-Stämme bzgl. der Piperintransformation untersucht werden.

Literaturverzeichnis

1. Lüttge, U.; Kluge, M.; Thiel, G. *Botanik - Die umfassende Biologie der Pflanzen*; Wiley-Blackwell, 2020; 553–583 ISBN 9783527833252.
2. Taylor, T.N.; Krings, M.; Taylor, E.L. Basidiomycota. In *Fossil Fungi*; Elsevier, 2015; pp. 173–199 ISBN 9780123877314.
3. Hibbett, D.S. A phylogenetic overview of the *Agaricomycotina*. *Mycologia* **2006**, *98*, 917–925.
4. Otieno, O.D.; Onyango, C.; Onguso, J.M.; Matasyoh, L.G.; Wanjala, H.W.; Wamalwa, M.; Harvey, J.J.W. Genetic diversity of Kenyan native oyster mushroom (*Pleurotus*). *Mycologia* **2015**, *107*, 32–38.
5. Urbanelli, S.; Della Rosa, V.; Fanelli, C.; Fabbri, A.A.; Reverberi, M. Genetic diversity and population structure of the Italian fungi belonging to the taxa *Pleurotus eryngii* (DC.:Fr.) Quèl and *P. ferulae* (DC.:Fr.) Quèl. *Heredity (Edinb).* **2003**, *90*, 253–259.
6. Cohen, L. Persky, Y. Hadar, R. Biotechnological applications and potential of wood-degrading mushrooms of the genus *Pleurotus*. *Appl. Microbiol. Biotechnol.* **2002**, *58*, 582–594.
7. Campbell, N.A.; Reece, J.B. *Biologie*; Pearson Studium - Biologie; 8th ed.; Pearson Studium: München [u.a.], 2009; pp. 859–879 ISBN 9781283736411.
8. Sherman, A. An oyster mushroom in the Middlesex Fells Reservation (CC BY 2.5 license) Available online: https://en.wikipedia.org/wiki/Pleurotus#/media/File:Oyster_mushoom_fells.jpg (accessed on Jun 15, 2021).
9. Kohl, B. AD2009Sep13 Boletus edulis 06.jpg (licensing free) Available online: https://upload.wikimedia.org/wikipedia/commons/2/2a/AD2009Sep13_Boletus_edulis_06.jpg (accessed on Jun 15, 2021).
10. Baker, H. 2009-09-03 Scleroderma citrinum Pers 55647 crop.jpg (CC BY-SA 3.0 license) Available online: https://upload.wikimedia.org/wikipedia/commons/8/87/2009-09-03_Scleroderma_citrinum_Pers_55647_crop.jpg (accessed on Jun 15, 2021).
11. Ramírez L, Larraya LM, P.A. Molecular tools for breeding basidimycetes. *Int. J. Microbiol.* **2000**, *3*, 147–152.
12. Casselton, L.A.; Kües, U. Mating-Type Genes in Homobasidiomycetes. In *Growth, Differentiation and Sexuality*; Springer Berlin Heidelberg: Berlin, Heidelberg, 1994; pp. 307–321.
13. Kües, U. Life History and Developmental Processes in the Basidiomycete *Coprinus cinereus*. *Microbiol. Mol. Biol. Rev.* **2000**, *64*, 316–353.
14. Herzog, R.; Solovyeva, I.; Rühl, M.; Thines, M.; Hennicke, F. Dikaryotic fruiting body development in a single dikaryon of *Agrocybe aegerita* and the spectrum of monokaryotic fruiting types in its monokaryotic progeny. *Mycol. Prog.* **2016**, *15*, 947–957.
15. Stahl, U.; Esser, K. Genetics of fruit body production in higher basidiomycetes. *Mol. Gen. Genet. MGG* **1976**, *148*, 183–197.
16. Nieuwenhuis, B.P.S.; Aanen, D.K. Nuclear arms races: Experimental evolution for mating success in the mushroom-forming fungus *Schizophyllum commune*. *PLoS One* **2018**, *13*, e0209671.
17. Kües, U.; James, T.Y.; Heitman, J. 6 Mating Type in Basidiomycetes: Unipolar, Bipolar, and Tetrapolar Patterns of Sexuality. In *Evolution of Fungi and Fungal-Like Organisms*; Springer Berlin Heidelberg: Berlin, Heidelberg, 2011; pp. 97–160.

18. Kronstad, J.W.; Staben, C. Mating type in filamentous fungi. *Annu. Rev. Genet.* 1997, *31*, 245–276.
19. Anderson, N.A.; Furnier, G.R.; Wang, A.S.; Schwandt, J.W. The number and distribution of incompatibility factors in natural populations of *Pleurotus ostreatus* and *Pleurotus sapidus*. *Can. J. Bot.* **1991**, *69*, 2187–2191.
20. L'opez, S.C.; Theelen, B.; Manserra, S.; Issak, T.Y.; Rytioja, J.; Mäkelä, M.R.; de Vries, R.P. Functional diversity in *Dichomitus squalens* monokaryons. *IMA Fungus* **2017**, *8*, 17–25.
21. Heitman, J.; Sun, S.; James, T.Y. Evolution of fungal sexual reproduction. *Mycologia* **2013**, *105*, 1–27.
22. Lee, S.C.; Ni, M.; Li, W.; Shertz, C.; Heitman, J. The Evolution of Sex: a Perspective from the Fungal Kingdom. *Microbiol. Mol. Biol. Rev.* **2010**, *74*, 298–340.
23. Eichlerová, I.; Homolka, L.; Nerud, F.; Zadrazil, F.; Baldrian, P.; Gabriel, J. Screening of *Pleurotus ostreatus* isolates for their ligninolytic properties during cultivation on natural substrates. *Biodegradation* **2000**, *11*, 279–287.
24. Eichlerová, I.; Homolka, L. Preparation and crossing of basidiospore-derived monokaryons - a useful tool for obtaining laccase and other ligninolytic enzyme higher-producing dikaryotic strains of *Pleurotus ostreatus*. *Antonie van Leeuwenhoek, Int. J. Gen. Mol. Microbiol.* **1999**, *75*, 321–327.
25. Liu, T.; Li, H.; Ding, Y.; Qi, Y.; Gao, Y.; Song, A.; Shen, J.; Qiu, L. Genome-wide gene expression patterns in dikaryon of the basidiomycete fungus *Pleurotus ostreatus*. *Brazilian J. Microbiol.* **2017**, *48*, 380–390.
26. Liu, S.-R.; Ke, B.-R.; Zhang, W.-R.; Liu, X.-R.; Wu, X.-P. Breeding of new *Ganoderma lucidum* strains simultaneously rich in polysaccharides and triterpenes by mating basidiospore-derived monokaryons of two commercial cultivars. *Sci. Hortic. (Amsterdam).* **2017**, *216*, 58–65.
27. Omarini, A.B.; Plagemann, I.; Schimanski, S.; Krings, U.; Berger, R.G. Crosses between monokaryons of *Pleurotus sapidus* or *Pleurotus florida* show an improved biotransformation of (+)-valencene to (+)-nootkatone. *Bioresour. Technol.* **2014**, *171*, 113–119.
28. Linke, D.; Omarini, A.B.; Takenberg, M.; Kelle, S.; Berger, R.G. Long-Term Monokaryotic Cultures of *Pleurotus ostreatus* var. *florida* Produce High and Stable Laccase Activity Capable to Degrade *ß*-Carotene. *Appl. Biochem. Biotechnol.* **2019**, *187*, 894–912.
29. Freihorst, D.; Brunsch, M.; Wirth, S.; Krause, K.; Kniemeyer, O.; Linde, J.; Kunert, M.; Boland, W.; Kothe, E. Smelling the difference: Transcriptome, proteome and volatilome changes after mating. *Fungal Genet. Biol.* **2018**, *112*, 2–11.
30. Castanera, R.; Omarini, A.; Santoyo, F.; Pérez, G.; Pisabarro, A.G.; Ramírez, L. Non-Additive Transcriptional Profiles Underlie Dikaryotic Superiority in *Pleurotus ostreatus* Laccase Activity. *PLoS One* **2013**, *8*, e73282.
31. Alfaro, M.; Majcherczyk, A.; Kües, U.; Ramírez, L.; Pisabarro, A.G. Glucose counteracts wood-dependent induction of lignocellulolytic enzyme secretion in monokaryon and dikaryon submerged cultures of the white-rot basidiomycete *Pleurotus ostreatus*. *Sci. Rep.* **2020**, *10*, 12421.
32. Madhavan, S.; Krause, K.; Jung, E.-M.; Kothe, E. Differential regulation of multi-copper oxidases in *Schizophyllum commune* during sexual development. *Mycol. Prog.* **2014**, *13*, 1009.
33. Orban, A.; Hennicke, F.; Rühl, M. Volatilomes of *Cyclocybe aegerita* during different stages of monokaryotic and dikaryotic fruiting. *Biol. Chem.* **2020**, *401*, 995–1004.

34. del Vecchio, C.; Lettera, V.; Pezzella, C.; Piscitelli, A.; Leo, G.; Birolo, L.; Sannia, G. Classical breeding in *Pleurotus ostreatus*: a natural approach for laccase production improvement. *Biocatal. Biotransformation* **2012**, *30*, 78–85.
35. Borgognone, A.; Castanera, R.; Morselli, M.; López-Varas, L.; Rubbi, L.; Pisabarro, A.G.; Pellegrini, M.; Ramírez, L. Transposon-associated epigenetic silencing during *Pleurotus ostreatus* life cycle. *DNA Res.* **2018**, *25*, 451–464.
36. De Jong, J.F.; Deelstra, H.J.; Wösten, H.A.B.; Lugones, L.G. RNA-mediated gene silencing in monokaryons and dikaryons of *Schizophyllum commune*. *Appl. Environ. Microbiol.* **2006**, *72*, 1267–1269.
37. Gupta, V.; Sengupta, M.; Prakash, J.; Tripathy, B.C. An Introduction to Biotechnology. In *Basic and Applied Aspects of Biotechnology*; Springer Singapore: Singapore, 2017; pp. 1–21.
38. Van Beuzekom, B.; Arundel, A. *OECD Biotechnology Statistics - 2006*; 2006;
39. Niar, A.J. *Introduction to Biotechnology and Genetic Engineering*; Infinity Science Press LLC: New Delhi, India, 2008; pp. 3–15 ISBN 978-1-934015-16-2.
40. Hofrichter, M. Die moderne Biotechnologie am Beispiel des Einsatzes von Pilzen. In *Integratives Umweltmanagement*; Gabler: Wiesbaden, 2010; pp. 723–742.
41. Klein, A.; Hilmer, J.-M. *Industrielle Mikrobiologie*; Sahm, H., Antranikian, G., Stahmann, K.-P., Takors, R., Eds.; Springer Berlin Heidelberg: Berlin, Heidelberg, 2013; pp. 1–39, 245–270 ISBN 978-3-8274-3039-7.
42. Soetaert, W.; Vandamme, E. The impact of industrial biotechnology. *Biotechnol. J.* 2006, *1*, 756–769.
43. Ben Akacha, N.; Gargouri, M. Microbial and enzymatic technologies used for the production of natural aroma compounds: Synthesis, recovery modeling, and bioprocesses. *Food Bioprod. Process.* **2015**, *94*, 675–706.
44. Bicas, J.L.; Molina, G.; Cavalcante Barros, F.F.; Pastore, G.M. Chapter 12. Production of Aroma Compounds by White Biotechnology. In *White Biotechnology for Sustainable Chemistry*; Coelho, M.A., Ribeiro, B.D., Eds.; The Royal Society of Chemistry, 2015; pp. 310–332 ISBN 978-1-84973-816-3.
45. Bel-Rhlid, R.; Berger, R.G.; Blank, I. Bio-mediated generation of food flavors – Towards sustainable flavor production inspired by nature. *Trends Food Sci. Technol.* **2018**, *78*, 134–143.
46. Schiller, J.; Aicher, C.; Feresin, E.; Klauer, B.; Hansjürgens, B.; Sauter, A. *Weiße Biotechnologie - Stand und Perspektiven der industriellen Biotechnologie: Umwelt- und Nachhaltigkeitspotenziale*; 2016.
47. Heux, S.; Meynial-Salles, I.; O'Donohue, M.J.; Dumon, C. White biotechnology: State of the art strategies for the development of biocatalysts for biorefining. *Biotechnol. Adv.* **2015**, *33*, 1653–1670.
48. Tang, W.L.; Zhao, H. Industrial biotechnology: Tools and applications. *Biotechnol. J.* 2009, *4*, 1725–1739.
49. Sheldon, R.A.; Woodley, J.M. Role of Biocatalysis in Sustainable Chemistry. *Chem. Rev.* **2018**, *118*, 801–838.
50. Berger, R.G. Biotechnology of flavours—the next generation. *Biotechnol. Lett.* **2009**, *31*, 1651–1659.
51. Pessôa, M.G.; Paulino, B.N.; Molina, G.; Pastore, G.M. Prospective Research and Current Technologies for Bioflavor Production. *Bioprocess. Biomol. Prod.* **2019**, 93–123.
52. Laufenberg, G.; Kunz, B.; Nystroem, M. Transformation of vegetable waste into value added products: *Bioresour. Technol.* **2003**, *87*, 167–198.

53. Rodríguez Couto, S. Exploitation of biological wastes for the production of value-added products under solid-state fermentation conditions. *Biotechnol. J.* **2008**, *3*, 859–870.
54. Martins, S.; Mussatto, S.I.; Martínez-Avila, G.; Montañez-Saenz, J.; Aguilar, C.N.; Teixeira, J.A. Bioactive phenolic compounds: Production and extraction by solid-state fermentation. A review. *Biotechnol. Adv.* **2011**, *29*, 365–373.
55. Šelo, G.; Planinić, M.; Tišma, M.; Tomas, S.; Koceva Komlenić, D.; Bucić-Kojić, A. A Comprehensive Review on Valorization of Agro-Food Industrial Residues by Solid-State Fermentation. *Foods* **2021**, *10*, 927.
56. Felipe, L. de O.; Oliveira, A.M. de; Bicas, J.L. Bioaromas – Perspectives for sustainable development. *Trends Food Sci. Technol.* **2017**, *62*, 141–153.
57. Berger, R.G. Biotechnology as a source of natural volatile flavours. *Curr. Opin. Food Sci.* **2015**, *1*, 38–43.
58. Ahlborn, J.; Stephan, A.; Meckel, T.; Maheshwari, G.; Rühl, M.; Zorn, H. Upcycling of food industry side streams by basidiomycetes for production of a vegan protein source. *Int. J. Recycl. Org. Waste Agric.* **2019**, *8*, 447–455.
59. Sartori, S.B.; Ferreira, L.F.R.; Messias, T.G.; Souza, G.; Pompeu, G.B.; Monteiro, R.T.R. *Pleurotus* biomass production on vinasse and its potential use for aquaculture feed. *Mycology* **2015**, *6*, 28–34.
60. Avni, S.; Ezove, N.; Hanani, H.; Yadid, I.; Karpovsky, M.; Hayby, H.; Gover, O.; Hadar, Y.; Schwartz, B.; Danay, O. Olive mill waste enhances α-glucan content in the edible mushroom *Pleurotus eryngii*. *Int. J. Mol. Sci.* **2017**, *18*, 1564.
61. Zerva, A.; Papaspyridi, L.M.; Christakopoulos, P.; Topakas, E. Valorization of Olive Mill Wastewater for the Production of β-glucans from Selected Basidiomycetes. *Waste and Biomass Valorization* **2017**, *8*, 1721–1731.
62. Inácio, F.D.; Ferreira, R.O.; Araujo, C.A.V. de; Peralta, R.M.; Souza, C.G.M. de Production of Enzymes and Biotransformation of Orange Waste by Oyster Mushroom, *Pleurotus pulmonarius* (Fr.) Quél. *Adv. Microbiol.* **2015**, *05*, 1–8.
63. Steudler, S.; Werner, A.; Walther, T. It Is the Mix that Matters: Substrate-Specific Enzyme Production from Filamentous Fungi and Bacteria Through Solid-State Fermentation. In *Advances in Biochemical Engineering/Biotechnology*; Steudler, S., Werner, A., Cheng, J.J., Eds.; Advances in Biochemical Engineering/Biotechnology; Springer International Publishing: Cham, 2019; Vol. 169, pp. 51–81 ISBN 978-3-030-23674-8.
64. Songulashvili, G.; Elisashvili, V.; Wasser, S.P.; Nevo, E.; Hadar, Y. Basidiomycetes laccase and manganese peroxidase activity in submerged fermentation of food industry wastes. *Enzyme Microb. Technol.* **2007**, *41*, 57–61.
65. Palma, C.; Lloret, L.; Sepúlveda, L.; Contreras, E. Production of versatile peroxidase from *Pleurotus eryngii* by solid-state fermentation using agricultural residues and evaluation of its catalytic properties. *Prep. Biochem. Biotechnol.* **2016**, *46*, 200–207.
66. Bosse, A.K.; Fraatz, M.A.; Zorn, H. Formation of complex natural flavours by biotransformation of apple pomace with basidiomycetes. *Food Chem.* **2013**, *141*, 2952–2959.
67. Meyer, V.; Basenko, E.Y.; Philipp Benz, J.; Braus, G.H.; Caddick, M.X.; Csukai, M.; De Vries, R.P.; Endy, D.; Frisvad, J.C.; Gunde-Cimerman, N.; et al. Growing a circular economy with fungal biotechnology: a white paper. *Fungal Biol Biotechnol* **2020**, *7*, 5.
68. Cairns, T.C.; Nai, C.; Meyer, V. How a fungus shapes biotechnology: 100 years of *Aspergillus niger* research. *Fungal Biol. Biotechnol.* 2018, *5*, 1–14.
69. Schmidt-Dannert, C. Biocatalytic portfolio of Basidiomycota. *Curr. Opin. Chem. Biol.* **2016**, *31*, 40–49.

70. Wang, H.; Guo, S.; Huang, M.; Thorsten, L.H.; Wei, J. Ascomycota has a faster evolutionary rate and higher species diversity than Basidiomycota. *Sci. China Life Sci.* **2010**, *53*, 1163–1169.
71. Tedersoo, L.; Bahram, M.; Põlme, S.; Kõljalg, U.; Yorou, N.S.; Wijesundera, R.; Ruiz, L.V.; Vasco-Palacios, A.M.; Thu, P.Q.; Suija, A.; et al. Global diversity and geography of soil fungi. *Science (80-.).* **2014**, *346*, 1256688.
72. Sandargo, B.; Chepkirui, C.; Cheng, T.; Chaverra-Muñoz, L.; Thongbai, B.; Stadler, M.; Hüttel, S. Biological and chemical diversity go hand in hand: Basidiomycota as source of new pharmaceuticals and agrochemicals. *Biotechnol. Adv.* **2019**, *37*, 107344.
73. Bentil, J.A. Biocatalytic potential of basidiomycetes: Relevance, challenges and research interventions in industrial processes. *Sci. African* **2021**, *11*, e00717.
74. Blackwell, M. The fungi: 1, 2, 3 ... 5.1 million species? *Am. J. Bot.* **2011**, *98*, 426–438.
75. Bouws, H.; Wattenberg, A.; Zorn, H. Fungal secretomes—nature's toolbox for white biotechnology. *Appl. Microbiol. Biotechnol.* **2008**, *80*, 381.
76. Grosse, M.; Wu, S.; Krings, U.; Berger, R.G. Formation of Decatrienones with a Pineapple-like Aroma from 1-^{13}C-Acetate by Cell Cultures of the Birch Polypore, *Fomitopsis betulina*. *J. Agric. Food Chem.* **2020**, *68*, 1678–1683.
77. Böker, A.; Fischer, M.; Berger, R.G. Raspberry ketone from submerged cultured cells of the basidiomycete *Nidula niveo-tomentosa*. *Biotechnol. Prog.* **2001**, *17*, 568–572.
78. Krings, U.; Lehnert, N.; Fraatz, M.A.; Hardebusch, B.; Zorn, H.; Berger, R.G. Autoxidation *versus* Biotransformation of *α*-Pinene to Flavors with *Pleurotus sapidus*: Regioselective Hydroperoxidation of *α*-Pinene and Stereoselective Dehydrogenation of Verbenol. *J. Agric. Food Chem.* **2009**, *57*, 9944–9950.
79. Krügener, S.; Schaper, C.; Krings, U.; Berger, R.G. *Pleurotus species* convert monoterpenes to furanoterpenoids through 1,4-endoperoxides. *Bioresour. Technol.* **2009**, *100*, 2855–2860.
80. Ruiz-Dueñas, F.J.; Martínez, Á.T. Microbial degradation of lignin: How a bulky recalcitrant polymer is efficiently recycled in nature and how we can take advantage of this. *Microb. Biotechnol.* 2009, *2*, 164–177.
81. Mendonça Maciel, M.J.; Castro e Silva, A.; Telles Ribeiro, H.C. Industrial and biotechnological applications of ligninolytic enzymes of the basidiomycota: a review. *Electron. J. Biotechnol.* **2010**, *13*, 0–0.
82. Sugano, Y.; Yoshida, T. DyP-Type Peroxidases: Recent Advances and Perspectives. *Int. J. Mol. Sci.* **2021**, *22*, 5556.
83. Rytioja, J.; Hildén, K.; Yuzon, J.; Hatakka, A.; de Vries, R.P.; Mäkelä, M.R. Plant-Polysaccharide-Degrading Enzymes from Basidiomycetes. *Microbiol. Mol. Biol. Rev.* **2014**, *78*, 614–649.
84. Singh, A.P.; Singh, T. Biotechnological applications of wood-rotting fungi: A review. *Biomass and Bioenergy* 2014, *62*, 198–206.
85. Virk, A.P.; Sharma, P.; Capalash, N. Use of laccase in pulp and paper industry. *Biotechnol. Prog.* **2012**, *28*, 21–32.
86. Lanfermann, I.; Linke, D.; Nimtz, M.; Berger, R.G. Manganese Peroxidases from *Ganoderma applanatum* Degrade *β*-Carotene Under Alkaline Conditions. *Appl. Biochem. Biotechnol.* **2015**, *175*, 3800–3812.
87. Siebert, M.; Berger, R.G.; Nieter, A. Enzymatic mitigation of 5-*O*-chlorogenic acid for an improved digestibility of coffee. *Food Chem.* **2018**, *258*, 124–128.
88. Siebert, M.; Detering, T.; Berger, R.G. An immobilized fungal chlorogenase rapidly degrades chlorogenic acid in a coffee beverage without altering its sensory properties. *LWT* **2019**, *115*, 108426.

89. Leonhardt, R.-H.; Krings, U.; Berger, R.G.; Linke, D. Heterologous production of the stain solving peptidase PPP1 from *Pleurotus pulmonarius*. *Bioprocess Biosyst. Eng.* **2016**, *39*, 845–853.
90. El-Baky, H.A.; Linke, D.; Nimtz, M.; Berger, R.G. PsoP1, a milk-clotting aspartic peptidase from the basidiomycete fungus *Piptoporus soloniensis*. *J. Agric. Food Chem.* **2011**, *59*, 10311–10316.
91. Piscitelli, A.; Tarallo, V.; Guarino, L.; Sannia, G.; Birolo, L.; Pezzella, C. New lipases by mining of *Pleurotus ostreatus* genome. *PLOS One* **2017**, *12*, e0185377.
92. Hofrichter, M.; Ullrich, R.; Pecyna, M.J.; Liers, C.; Lundell, T. New and classic families of secreted fungal heme peroxidases. *Appl. Microbiol. Biotechnol.* **2010**, *87*, 871–897.
93. Kim, S.J.; Shoda, M. Purification and characterization of a novel peroxidase from *Geotrichum candidum* Dec 1 involved in decolorization of dyes. *Appl. Environ. Microbiol.* **1999**, *65*, 1029–1035.
94. Sugano, Y.; Sasaki, K.; Shoda, M. cDNA cloning and genetic analysis of a novel decolorizing enzyme, peroxidase gene dyp from *Geotrichum candidum* Dec 1. *J. Biosci. Bioeng.* **1999**, *87*, 411–417.
95. Linde, D.; Ruiz-Dueñas, F.J.; Fernández-Fueyo, E.; Guallar, V.; Hammel, K.E.; Pogni, R.; Martínez, A.T. Basidiomycete DyPs: Genomic diversity, structural–functional aspects, reaction mechanism and environmental significance. *Arch. Biochem. Biophys.* **2015**, *574*, 66–74.
96. Linke, D.; Leonhardt, R.; Eisele, N.; Petersen, L.M.; Riemer, S.; Nimtz, M.; Berger, R.G. Carotene-degrading activities from *Bjerkandera adusta* possess an application in detergent industries. *Bioprocess Biosyst. Eng.* **2015**, *38*, 1191–1199.
97. Scheibner, M.; Hülsdau, B.; Zelena, K.; Nimtz, M.; de Boer, L.; Berger, R.G.; Zorn, H. Novel peroxidases of *Marasmius scorodonius* degrade *β*-carotene. *Appl. Microbiol. Biotechnol.* **2008**, *77*, 1241–1250.
98. Behrens, C.J.; Zelena, K.; Berger, R.G. Comparative Cold Shock Expression and Characterization of Fungal Dye-Decolorizing Peroxidases. *Appl. Biochem. Biotechnol.* **2016**, *179*, 1404–1417.
99. Sugano, Y. DyP-type peroxidases comprise a novel heme peroxidase family. *Cell. Mol. Life Sci.* **2009**, *66*, 1387–1403.
100. Colpa, D.I.; Fraaije, M.W.; van Bloois, E. DyP-type peroxidases: a promising and versatile class of enzymes. *J. Ind. Microbiol. Biotechnol.* **2014**, *41*, 1–7.
101. Sugawara, K.; Igeta, E.; Amano, Y.; Hyuga, M.; Sugano, Y. Degradation of antifungal anthraquinone compounds is a probable physiological role of DyP secreted by *Bjerkandera adusta*. *AMB Express* **2019**, *9*.
102. Sugano, Y.; Muramatsu, R.; Ichiyanagi, A.; Sato, T.; Shoda, M. DyP, a unique dye-decolorizing peroxidase, represents a novel heme peroxidase family: ASP171 replaces the distal histidine of classical peroxidases. *J. Biol. Chem.* **2007**, *282*, 36652–36658.
103. Yoshida, T.; Sugano, Y. A structural and functional perspective of DyP-type peroxidase family. *Arch. Biochem. Biophys.* **2015**, *574*, 49–55.
104. Zamocky, M.; Jakopitsch, C.; Furtmüller, P.G.; Dunand, C.; Obinger, C. The peroxidase-cyclooxygenase superfamily: Reconstructed evolution of critical enzymes of the innate immune system. *Proteins Struct. Funct. Bioinforma.* **2008**, *72*, 589–605.
105. Veitch, N.C. Horseradish peroxidase: A modern view of a classic enzyme. *Phytochemistry* **2004**, *65*, 249–259.
106. Strittmatter, E.; Liers, C.; Ullrich, R.; Wachter, S.; Hofrichter, M.; Plattner, D.A.; Piontek, K. First Crystal Structure of a Fungal High-redox Potential Dye-decolorizing Peroxidase. *J. Biol. Chem.* **2013**, *288*, 4095–4102.

107. Martínez, A.T. Molecular biology and structure-function of lignin-degrading heme peroxidases. *Enzyme Microb. Technol.* 2002, *30*, 425–444.
108. Yoshida, T.; Tsuge, H.; Konno, H.; Hisabori, T.; Sugano, Y. The catalytic mechanism of dye-decolorizing peroxidase DyP may require the swinging movement of an aspartic acid residue. *FEBS J.* **2011**, *278*, 2387–2394.
109. Rais, D.; Zibek, S. Biotechnological and Biochemical Utilization of Lignin. In *Biorefineries*; Wagemann, K., Tippkötter, N., Eds.; Springer International Publishing: Cham, Switzerland, 2017; pp. 469–518 ISBN 978-3-319-97119-3.
110. Shrestha, R.; Huang, G.; Meekins, D.A.; Geisbrecht, B. V.; Li, P. Mechanistic Insights into Dye-Decolorizing Peroxidase Revealed by Solvent Isotope and Viscosity Effects. *ACS Catal.* **2017**, *7*, 6352–6364.
111. Salvachua, D.; Prieto, A.; Martinez, A.T.; Martinez, M.J. Characterization of a Novel Dye-Decolorizing Peroxidase (DyP)-Type Enzyme from *Irpex lacteus* and Its Application in Enzymatic Hydrolysis of Wheat Straw. *Appl. Environ. Microbiol.* **2013**, *79*, 4316–4324.
112. Lauber, C.; Schwarz, T.; Nguyen, Q.K.; Lorenz, P.; Lochnit, G.; Zorn, H. Identification, heterologous expression and characterization of a dye-decolorizing peroxidase of *Pleurotus sapidus*. *AMB Express* **2017**, *7*, 164.
113. Busse, N.; Wagner, D.; Kraume, M.; Czermak, P. Reaction Kinetics of Versatile Peroxidase for the Degradation of Lignin Compounds. *Am. J. Biochem. Biotechnol.* **2013**, *9*, 365–394.
114. Arnao, M.B.; Acosta, M.; del Rio, J.A.; Varón, R.; García-Cánovas, F. A kinetic study on the suicide inactivation of peroxidase by hydrogen peroxide. *Biochim. Biophys. Acta - Protein Struct. Mol. Enzymol.* **1990**, *1041*, 43–47.
115. Pfanzagl, V.; Nys, K.; Bellei, M.; Michlits, H.; Mlynek, G.; Battistuzzi, G.; Djinovic-Carugo, K.; Van Doorslaer, S.; Furtmüller, P.G.; Hofbauer, S.; et al. Roles of distal aspartate and arginine of B-class dye-decolorizing peroxidase in heterolytic hydrogen peroxide cleavage. *J. Biol. Chem.* **2018**, *293*, 14823–14838.
116. Linde, D.; Pogni, R.; Cañellas, M.; Lucas, F.; Guallar, V.; Baratto, M.C.; Sinicropi, A.; Sáez-Jiménez, V.; Coscolín, C.; Romero, A.; et al. Catalytic surface radical in dye-decolorizing peroxidase: a computational, spectroscopic and site-directed mutagenesis study. *Biochem. J.* **2015**, *466*, 253–262.
117. Fernández-Fueyo, E.; Davó-Siguero, I.; Almendral, D.; Linde, D.; Baratto, M.C.; Pogni, R.; Romero, A.; Guallar, V.; Martínez, A.T. Description of a Non-Canonical Mn(II)-Oxidation Site in Peroxidases. *ACS Catal.* **2018**, *8*, 8386–8395.
118. Kolwek, J.; Behrens, C.; Linke, D.; Krings, U.; Berger, R.G. Cell-free one-pot conversion of (+)-valencene to (+)-nootkatone by a unique dye-decolorizing peroxidase combined with a laccase from *Funalia trogii*. *J. Ind. Microbiol. Biotechnol.* **2018**, *45*, 89–101.
119. Amara, S.; Perrot, T.; Navarro, D.; Deroy, A.; Benkhelfallah, A.; Chalak, A.; Daou, M.; Chevret, D.; Faulds, C.B.; Berrin, J.-G.; et al. Enzyme Activities of Two Recombinant Heme-Containing Peroxidases, Tv DyP1 and Tv VP2, Identified from the Secretome of *Trametes versicolor*. *Appl. Environ. Microbiol.* **2018**, *84*, 1–15.
120. Duan, Z.; Shen, R.; Liu, B.; Yao, M.; Jia, R. Comprehensive investigation of a dye-decolorizing peroxidase and a manganese peroxidase from *Irpex lacteus* F17, a lignin-degrading basidiomycete. *AMB Express* **2018**, *8*, 119.
121. Rahmanpour, R.; Bugg, T.D.H. Characterisation of Dyp-type peroxidases from *Pseudomonas fluorescens* Pf-5: Oxidation of Mn(II) and polymeric lignin by Dyp1B. *Arch. Biochem. Biophys.* **2015**, *574*, 93–98.

122. Santos, A.; Mendes, S.; Brissos, V.; Martins, L.O. New dye-decolorizing peroxidases from *Bacillus subtilis* and *Pseudomonas putida* MET94: Towards biotechnological applications. *Appl. Microbiol. Biotechnol.* **2014**, *98*, 2053–2065.
123. Sahinkaya, M.; Colak, D.N.; Ozer, A.; Canakci, S.; Deniz, I.; Belduz, A.O. Cloning, characterization and paper pulp applications of a newly isolated DyP type peroxidase from *Rhodococcus sp.* T1. *Mol. Biol. Rep.* **2019**, *46*, 569–580.
124. Szweda, R.T.; Schmidt, K.; Zorn, H. Bleaching of colored whey and milk by a multiple-enzyme system. *Eur. Food Res. Technol.* **2013**, *237*, 377–384.
125. Zelena, K.; Hardebusch, B.; Hülsdau, B.; Berger, R.G.; Zorn, H. Generation of norisoprenoid flavors from carotenoids by fungal peroxidases. *J. Agric. Food Chem.* **2009**, *57*, 9951–9955.
126. Chedea, V.S.; Jisaka, M. Lipoxygenase and carotenoids: A co-oxidation story. *African J. Biotechnol.* **2013**, *12*, 2786–2791.
127. Hayward, S.; Cilliers, T.; Swart, P. Lipoxygenases: From Isolation to Application. *Compr. Rev. Food Sci. Food Saf.* **2017**, *16*, 199–211.
128. Oliw, E.H. Plant and fungal lipoxygenases. *Prostaglandins Other Lipid Mediat.* **2002**, *68–69*, 313–323.
129. Stolterfoht, H.; Rinnofner, C.; Winkler, M.; Pichler, H. Recombinant Lipoxygenases and Hydroperoxide Lyases for the Synthesis of Green Leaf Volatiles. *J. Agric. Food Chem.* **2019**, *67*, 13367–13392.
130. Andreou, A.; Feussner, I. Lipoxygenases - Structure and reaction mechanism. *Phytochemistry* 2009, *70*, 1504–1510.
131. Karrer, D.; Rühl, M. A new lipoxygenase from the agaric fungus *Agrocybe aegerita*: Biochemical characterization and kinetic properties. *PLoS One* **2019**, *14*, e0218625.
132. Leonhardt, R.H.; Plagemann, I.; Linke, D.; Zelena, K.; Berger, R.G. Orthologous lipoxygenases of *Pleurotus spp.* - A comparison of substrate specificity and sequence homology. *J. Mol. Catal. B Enzym.* **2013**, *97*, 189–195.
133. Plagemann, I.; Krings, U.; Berger, R.G. Isolation and Characterization of Wild-Type Lipoxygenase $LOX_{Psa}1$ from *Pleurotus sapidus*. *Zeitschrift für Naturforsch. C* **2014**, *69*, 149–154.
134. Kuribayashi, T.; Kaise, H.; Uno, C.; Hara, T.; Hayakawa, T.; Joh, T. Purification and characterization of lipoxygenase from *Pleurotus ostreatus*. *J. Agric. Food Chem.* **2002**, *50*, 1247–1253.
135. Shi, Y.; Mandal, R.; Singh, A.; Pratap Singh, A. Legume lipoxygenase: Strategies for application in food industry. *Legum. Sci.* **2020**, *2*, e44.
136. Brodhun, F.; Feussner, I. Oxylipins in fungi. *FEBS J.* 2011, *278*, 1047–1063.
137. Coffa, G.; Schneider, C.; Brash, A.R. A comprehensive model of positional and stereo control in lipoxygenases. *Biochem. Biophys. Res. Commun.* 2005, *338*, 87–92.
138. Coggins, M.K.; Brines, L.M.; Kovacs, J.A. Synthesis and structural characterization of a series of MnIIIOR complexes, including a water-soluble MnIIIOH that promotes aerobic hydrogen-atom transfer. *Inorg. Chem.* **2013**, *52*, 12383–12393.
139. Ivanov, I.; Heydeck, D.; Hofheinz, K.; Roffeis, J.; O'Donnell, V.B.; Kuhn, H.; Walther, M. Molecular enzymology of lipoxygenases. *Arch. Biochem. Biophys.* **2010**, *503*, 161–174.
140. Newcomer, M.E.; Brash, A.R. The structural basis for specificity in lipoxygenase catalysis. *Protein Sci.* 2015, *24*, 298–309.
141. Rickert, K.W.; Klinman, J.P. Nature of hydrogen transfer in soybean lipoxygenase 1: Separation of primary and secondary isotope effects. *Biochemistry* **1999**, *38*, 12218–12228.

142. Arens, D.; Seilmeier, W.; Weber, F.; Kloos, G.; Grosch, W. Purification and properties of a carotene co-oxidizing lipoxygenase from peas. *BBA - Enzymol.* **1973**, *327*, 295–305.
143. Grosch, Werner; Laskawy, Gudrun; Kaiser, K.-P. Co-Oxydation von ß-Carotin und Canthaxanthin durch gereinigte Lipoxygenasen aus Sojabohnen. *Z. Lebensm. Unters. Forsch.* **1977**, 77–81.
144. Sumner, J.B.; Sumner, R.J. The Coupled Oxidation of Carotene and Fat by Carotene Oxidase. *J. Biol. Chem.* **1940**, *134*, 531–533.
145. Gordon, M.H.; Barimalaa, I.S. Co-oxidation of fat-soluble vitamins by soybean lipoxygenase. *Food Chem.* **1989**, *32*, 31–37.
146. Waldmann, D.; Schreier, P. Stereochemical Studies of Epoxides Formed by Lipoxygenase-Catalyzed Co-oxidation of Retinol, ß-Ionone, and 4-Hydroxy-ß-ionone. *J. Agric. Food Chem.* **1995**, *43*, 626–630.
147. Hu, J.; Huang, Y.; Xiong, M.; Luo, S.; Chen, Y.; Li, Y. The effects of natural flavonoids on lipoxygenase-mediated oxidation of compounds with a benzene ring structure - A new possible mechanism of flavonoid anti-chemical carcinogenesis and other toxicities. *Int. J. Toxicol.* **2006**, *25*, 295–301.
148. Lu, J.; Zhang, C.; Leong, H.Y.; Show, P.L.; Lu, F.; Lu, Z. Overproduction of lipoxygenase from *Pseudomonas aeruginosa* in *Escherichia coli* by auto-induction expression and its application in triphenylmethane dyes degradation. *J. Biosci. Bioeng.* **2020**, *129*, 327–332.
149. Weber, F.; Laskawy, G.; Grosch, W. *Enzymatischer Carotinabbau in Erbsen, Sojabohnen, Weizen und Leinsamen*; 1973; Vol. 152.
150. Takahashi, A.; Shibasaki-Kitakawa, N.; Yonemoto, T. A Rigorous Kinetic Model for *β*-Carotene Oxidation in the Presence of an Antioxidant, *α*-Tocopherol. *JAOCS, J. Am. Oil Chem. Soc.* 2003, *80*, 1241–1247.
151. Waché, Y.; Bosser-De Ratuld, A.; Belin, J.M. Dispersion of *β*-carotene in processes of production of *β*-ionone by cooxidation using enzyme-generated reactive oxygen species. *Process Biochem.* **2006**, *41*, 2337–2341.
152. Plagemann, I.; Zelena, K.; Arendt, P.; Ringel, P.D.; Krings, U.; Berger, R.G. $LOX_{Psa}1$, the first recombinant lipoxygenase from a basidiomycete fungus. *J. Mol. Catal. B Enzym.* **2013**, *87*, 99–104.
153. Zelena, K.; Krings, U.; Berger, R.G. Functional expression of a valencene dioxygenase from *Pleurotus sapidus* in *E. coli*. *Bioresour. Technol.* **2012**, *108*, 231–239.
154. Fraatz, M.A.; Riemer, S.J.L.; Stöber, R.; Kaspera, R.; Nimtz, M.; Berger, R.G.; Zorn, H. A novel oxygenase from *Pleurotus sapidus* transforms valencene to nootkatone. *J. Mol. Catal. B Enzym.* **2009**, *61*, 202–207.
155. Kun, R.S.; Gomes, A.C.S.; Hildén, K.S.; Salazar Cerezo, S.; Mäkelä, M.R.; de Vries, R.P. Developments and opportunities in fungal strain engineering for the production of novel enzymes and enzyme cocktails for plant biomass degradation. *Biotechnol. Adv.* **2019**, *37*, 107361.
156. Madhavan, A.; Sindhu, R.; Binod, P.; Sukumaran, R.K.; Pandey, A. Strategies for design of improved biocatalysts for industrial applications. *Bioresour. Technol.* **2017**, *245*, 1304–1313.
157. Nannemann, D.P.; Birmingham, W.R.; Scism, R.A.; Bachmann, B.O. Assessing directed evolution methods for the generation of biosynthetic enzymes with potential in drug biosynthesis. *Future Med. Chem.* **2011**, *3*, 809–819.
158. Bornscheuer, U.T.; Pohl, M. Improved biocatalysts by directed evolution and rational protein design. *Curr. Opin. Chem. Biol.* 2001, *5*, 137–143.

159. Xiao, H.; Zhong, J.J. Production of Useful Terpenoids by Higher-Fungus Cell Factory and Synthetic Biology Approaches. *Trends Biotechnol.* 2016, *34*, 242–255.
160. Yin, J.; Li, G.; Ren, X.; Herrler, G. Select what you need: A comparative evaluation of the advantages and limitations of frequently used expression systems for foreign genes. *J. Biotechnol.* 2007, *127*, 335–347.
161. Yamada, Y.; Matsuda, M.; Maeda, K.; Mikata, K. The Phylogenetic Relationships of Methanol-assimilating Yeasts Based on the Partial Sequences of 18S and 26S Ribosomal RNAs: The Proposal of *Komagataella* Gen. Nov. (Saccharomycetaceae). *Biosci. Biotechnol. Biochem.* **1995**, *59*, 439–444.
162. Zelena, K.; Eisele, N.; Berger, R.G. *Escherichia coli* as a production host for novel enzymes from basidiomycota. *Biotechnol. Adv.* 2014, *32*, 1382–1395.
163. *Richtlinie 2001/18/EG des Europäischen Parlaments und des Rates vom 12. März 2001 über die absichtliche Freisetzung genetisch veränderter Organismen in die Umwelt und zur Aufhebung der Richtlinie 90/220/EWG des Rates*; EU, 2001; pp. 1–39.
164. *VERORDNUNG (EG) Nr. 1829/2003 des Europäischen Parlaments und des Rates vom 22. September 2003 über genetisch veränderte Lebensmittel und Futtermittel (Text von Bedeutung für den EWR)*; 2003.
165. Clancy, K.A.; Clancy, B. Growing monstrous organisms: the construction of anti-GMO visual rhetoric through digital media. *Crit. Stud. Media Commun.* **2016**, *33*, 279–292.
166. Mücke, W.; Lemmen, C. *Duft und Geruch: Wirkungen und gesundheitliche Bedeutung von Geruchsstoffen*; ecomed Medizin, 2010; ISBN 9783609164366.
167. Fahlbusch, K.-G.; Hammerschmidt, F.-J.; Panten, J.; Pickenhagen, W.; Schatkowski, D.; Bauer, K.; Garbe, D.; Surburg, H. Flavors and Fragrances. In *Ullmann's Encyclopedia of Industrial Chemistry*; Wiley-VCH Verlag GmbH & Co. KGaA: Weinheim, Germany, 2003; pp. 73–140.
168. Belitz, H.-D.; Grosch, W.; Schieberle, P. Aromastoffe. In *Lebensmittelchemie*; Springer Berlin Heidelberg: Berlin, Heidelberg, 2008; pp. 346–411 ISBN 978-3-540-73202-0.
169. Baltes, W.; Matissek, R. *Lebensmittelchemie*; Springer-Lehrbuch; Springer Berlin Heidelberg: Berlin, Heidelberg, 2011; 367–372 ISBN 978-3-642-16538-2.
170. Russell, G.F.; Hills, J.I. Odor Differences between Enantiomeric Isomers. *Science (80-.).* **1971**, *172*, 1043–1044.
171. Ridder, M. Flavor and fragrances market worldwide - Statistics & Facts | Statista Available online: https://www.statista.com/topics/6300/flavor-and-fragrances-market-worldwide/#dossierSummary (accessed on May 11, 2021).
172. Spannring, P.; Bruijnincx, P.C.A.; Weckhuysen, B.M.; Klein Gebbink, R.J.M. Transition metal-catalyzed oxidative double bond cleavage of simple and bio-derived alkenes and unsaturated fatty acids. *Catal. Sci. Technol.* **2014**, *4*, 2182–2209.
173. *Verordnung (EG) Nr. 1334/2008 des Europäischen Parlaments und der Rates vom 16. Dezember 2008 über Aromen und bestimmte Lebensmittelzutaten mit Aromaeigenschaften*; Art. 3 (2) c); 2008.
174. Lin, B.; Tao, Y. Whole-cell biocatalysts by design. *Microb. Cell Fact.* 2017, *16*, 106.
175. Martău, G.A.; Călinoiu, L.F.; Vodnar, D.C. Bio-vanillin: Towards a sustainable industrial production. *Trends Food Sci. Technol.* 2021, *109*, 579–592.
176. Deutscher Verband der Aromenindistrie Fact Sheet: Piperonal Available online: http://aromenverband.de/piperonal/ (accessed on May 12, 2021).
177. Wen, P.; Wu, D.; Zheng, P.; Chen, P.; Liu, S.; Fu, Y. Highly Efficient Biosynthesis of Heliotropin by Engineered *Escherichia coli* Coexpressing *Trans*-Anethole Oxygenase and Formate Dehydrogenase. *J. Agric. Food Chem.* **2019**, *67*, 14121–14128.

178. Rajagopalan, A.; Lara, M.; Kroutil, W. Oxidative Alkene Cleavage by Chemical and Enzymatic Methods. *Adv. Synth. Catal.* **2013**, *355*, 3321–3335.
179. Mutti, F.G. Alkene Cleavage Catalysed by Heme and Nonheme Enzymes: Reaction Mechanisms and Biocatalytic Applications. *Bioinorg. Chem. Appl.* **2012**, *2012*, 1–13.
180. Sono, M.; Roach, M.P.; Coulter, E.D.; Dawson, J.H. Heme-Containing Oxygenases. *Chem. Rev.* **1996**, *96*, 2841–2888.
181. Braaz, R.; Fischer, P.; Jendrossek, D. Novel type of heme-dependent oxygenase catalyzes oxidative cleavage of rubber (poly-cis-1,4-isoprene). *Appl. Environ. Microbiol.* **2004**, *70*, 7388–7395.
182. D. H. Bugg, T.; J. Winfield, C. Enzymatic cleavage of aromatic rings: mechanistic aspects of the catechol dioxygenases and later enzymes of bacterial oxidative cleavage pathways. *Nat. Prod. Rep.* **1998**, *15*, 513.
183. Bougioukou, D.J.; Smonou, I. Chloroperoxidase-catalyzed oxidation of conjugated dienoic esters. *Tetrahedron Lett.* **2002**, *43*, 339–342.
184. McAndrew, R.P.; Sathitsuksanoh, N.; Mbughuni, M.M.; Heins, R.A.; Pereira, J.H.; George, A.; Sale, K.L.; Fox, B.G.; Simmons, B.A.; Adams, P.D. Structure and mechanism of NOV1, a resveratrol-cleaving dioxygenase. *Proc. Natl. Acad. Sci.* **2016**, *113*, 14324–14329.
185. Kamoda, S.; Saburi, Y. Structural and Enzymatical Comparison of Lignostilbene-*α*,*β*-dioxygenase Isozymes, I, II, and III, from *Pseudomonas Paucimobilis* TMY1009. *Biosci. Biotechnol. Biochem.* **1993**, *57*, 931–934.
186. Bourel, G.; Nicaud, J.M.; Nthangeni, B.; Santiago-Gomez, P.; Belin, J.M.; Husson, F. Fatty acid hydroperoxide lyase of green bell pepper: Cloning in *Yarrowia lipolytica* and biogenesis of volatile aldehydes. *Enzyme Microb. Technol.* **2004**, *35*, 293–299.
187. Auldridge, M.E.; McCarty, D.R.; Klee, H.J. Plant carotenoid cleavage oxygenases and their apocarotenoid products. *Curr. Opin. Plant Biol.* **2006**, *9*, 315–321.
188. Kloer, D.P.; Schulz, G.E. Structural and biological aspects of carotenoid cleavage. *Cell. Mol. Life Sci.* **2006**, *63*, 2291–2303.
189. Schwartz, S.H.; Qin, X.; Zeevaart, J.A.D. Characterization of a Novel Carotenoid Cleavage Dioxygenase from Plants. *J. Biol. Chem.* **2001**, *276*, 25208–25211.
190. Schmidt, H.; Kurtzer, R.; Eisenreich, W.; Schwab, W. The carotenase AtCCD1 from *Arabidopsis thaliana* is a dioxygenase. *J. Biol. Chem.* **2006**, *281*, 9845–9851.
191. Rajagopalan, A.; Schober, M.; Emmerstorfer, A.; Hammerer, L.; Migglautsch, A.; Seisser, B.; Glueck, S.M.; Niehaus, F.; Eck, J.; Pichler, H.; et al. Enzymatic Aerobic Alkene Cleavage Catalyzed by a Mn^{3+}-Dependent Proteinase A Homologue. *ChemBioChem* **2013**, *14*, 2427–2430.
192. Mutti, F.G.; Lara, M.; Kroutil, M.; Kroutil, W. Ostensible Enzyme Promiscuity: Alkene Cleavage by Peroxidases. *Chem. - A Eur. J.* **2010**, *16*, 14142–14148.
193. Yamada, M.; Okada, Y.; Yoshida, T.; Nagasawa, T. Purification, characterization and gene cloning of isoeugenol-degrading enzyme from *Pseudomonas putida* IE27. *Arch. Microbiol.* **2007**, *187*, 511–517.
194. Han, D.; Ryu, J.-Y.; Kanaly, R.A.; Hur, H.-G. Isolation of a Gene Responsible for the Oxidation of *trans*-Anethole to *para*-Anisaldehyde by *Pseudomonas putida* JYR-1 and Its Expression in *Escherichia coli*. *Appl. Environ. Microbiol.* **2012**, *78*, 5238–5246.
195. Hajnal, I.; Faber, K.; Schwab, H.; Hall, M.; Steiner, K. Oxidative Alkene Cleavage Catalysed by Manganese-Dependent Cupin TM1459 from *Thermotoga maritima*. *Adv. Synth. Catal.* **2015**, *357*, 3309–3316.

196. Tuynman, A.; Spelberg, J.L.; Kooter, I.M.; Schoemaker, H.E.; Wever, R. Enantioselective Epoxidation and Carbon–Carbon Bond Cleavage Catalyzed by *Coprinus cinereus* Peroxidase and Myeloperoxidase. *J. Biol. Chem.* **2000**, *275*, 3025–3030.
197. Fuchs, B.A.J. Präkursoren, Induktoren, Elicitoren und das Volatilom von Basidiomyceten, Gottfried Wilhelm Leibniz Universität, 2016.
198. Nicolini, L.; Von Hunolstein, C.; Carilli, A. Applied Microbiology Biotechnology Solid state fermentation of orange peel and grape stalks by *Pleurotus ostreatus*, *Ayrocybe aeyerita*, and *Armillariella mellea*. *Appl Microbiol Biotechnol* **1987**, *26*, 95–98.
199. Elisashvili, V.; Penninckx, M.; Kachlishvili, E.; Asatiani, M.; Kvesitadze, G. Use of *Pleurotus dryinus* for lignocellulolytic enzymes production in submerged fermentation of mandarin peels and tree leaves. *Enzyme Microb. Technol.* **2006**, *38*, 998–1004.
200. Food and Agriculture Organization of the United Nations *Citrus Fruit - Fresh and Processed Statistical Bulletin 2016*; Rom, 2017.
201. Lohrasbi, M.; Pourbafrani, M.; Niklasson, C.; Taherzadeh, M.J. Process design and economic analysis of a citrus waste biorefinery with biofuels and limonene as products. *Bioresour. Technol.* **2010**, *101*, 7382–7388.
202. Ledesma-Escobar, C.A.; Luque de Castro, M.D. Towards a comprehensive exploitation of citrus. *Trends Food Sci. Technol.* **2014**, *39*, 63–75.
203. Mantzouridou, F.T.; Paraskevopoulou, A.; Lalou, S. Yeast flavour production by solid state fermentation of orange peel waste. *Biochem. Eng. J.* **2015**, *101*, 1–8.
204. Yang, F.C.; Ma, T.W.; Lee, Y.H. Reuse of citrus peel to enhance the formation of bioactive metabolite-triterpenoid in solid-state fermentation of *A. cinnamomea*. *Biochem. Eng. J.* **2013**, *78*, 59–66.
205. Adeleke, A.J.; Olanbiwoninu, A.; Owoseni, M.C.; Ayodele Odunfa, S. Production of Cellulase and Pectinase from Orange Peels by Fungi. *Nat. Sci.* **2012**, *10*, 107–112.
206. Irshad, M.; Anwar, Z.; Mahmood, Z.; Aqil, T.; Mehmmod, S.; Nawaz, H. Bio-processing of agro-industrial waste orange peel for induced production of pectinase by *Trichoderma viridi*; its purification and characterization. *Turkish J. Biochem.* **2014**, *39*, 9–18.
207. Elisashvili, V.; Kachlishvili, E.; Asatiani, M.D.; Kobakhidze, A.; Rusitashvili, M.; Tsokilauri, A.; Gogebashvili, D. Lignocellulosic Waste Biorefinery for Unlocking the Biotechnological Potential of Basidiomycota. *Int. J. Latest Trends Eng. Technol.* **2019**, 30–34.
208. Krahe, N.-K.; Berger, R.G.; Witt, M.; Zorn, H.; Omarini, A.B.; Ersoy, F. Monokaryotic *Pleurotus sapidus* Strains with Intraspecific Variability of an Alkene Cleaving DyP-Type Peroxidase Activity as a Result of Gene Mutation and Differential Gene Expression. *Int. J. Mol. Sci.* **2021**, *22*, 1363.
209. Krahe, N.-K.; Berger, R.G.; Ersoy, F. A DyP-Type Peroxidase of *Pleurotus sapidus* with Alkene Cleaving Activity. *Molecules* **2020**, *25*, 1536.
210. Criegee, R. Mechanism of Ozonolysis. *Angew. Chemie Int. Ed. English* **1975**, *14*, 745–752.
211. Schrader, J.; Etschmann, M.M.W.; Sell, D.; Hilmer, J.-M.; Rabenhorst, J. Applied biocatalysis for the synthesis of natural flavour compounds – current industrial processes and future prospects. *Biotechnol. Lett.* **2004**, *26*, 463–472.
212. Dako, E.; Bernier, A.-M.; Thomas, A.; K., C. The Problems Associated with Enzyme Purification. In *Chemical Biology*; Ekinci, D., Ed.; InTech: Rijeka, Croatia, 2012; pp. 19–40 ISBN 97-8-953-51-0049-2.

213. Schulz, K.; Nieter, A.; Scheu, A.-K.; Copa-Patiño, J.L.; Thiesing, D.; Popper, L.; Berger, R.G. A type D ferulic acid esterase from *Streptomyces werraensis* affects the volume of wheat dough pastries. *Appl. Microbiol. Biotechnol.* **2018**, *102*, 1269–1279.
214. Hofrichter, M. Review: lignin conversion by manganese peroxidase (MnP). *Enzyme Microb. Technol.* **2002**, *30*, 454–466.
215. Nakayama, T.; Amachi, T. Fungal peroxidase: its structure, function, and application. *J. Mol. Catal. B Enzym.* **1999**, *6*, 185–198.
216. Fernández-Fueyo, E.; Linde, D.; Almendral, D.; López-Lucendo, M.F.; Ruiz-Dueñas, F.J.; Martínez, A.T. Description of the first fungal dye-decolorizing peroxidase oxidizing manganese(II). *Appl. Microbiol. Biotechnol.* **2015**, *99*, 8927–8942.
217. Passardi, F.; Theiler, G.; Zamocky, M.; Cosio, C.; Rouhier, N.; Teixera, F.; Margis-Pinheiro, M.; Ioannidis, V.; Penel, C.; Falquet, L.; et al. PeroxiBase: The peroxidase database. *Phytochemistry* **2007**, *68*, 1605–1611.
218. Romanos, M. Advances in the use of *Pichia pastoris* for high-level gene expression. *Curr. Opin. Biotechnol.* **1995**, *6*, 527–533.
219. Ogawa, S.; Shimizu, T.; Ohki, H.; Araya, T.; Okuno, T.; Miyairi, K. Expression, purification, and analyses of glycosylation and disulfide bonds of *Stereum purpureum* endopolygalacturonase I in *Pichia pastoris*. *Protein Expr. Purif.* **2009**, *65*, 15–22.
220. Behrens, C.J.; Linke, D.; Allister, A.B.; Zelena, K.; Berger, R.G. Variants of PpuLcc, a multi-dye decolorizing laccase from *Pleurotus pulmonarius* expressed in *Pichia pastoris*. *Protein Expr. Purif.* **2017**, *137*, 34–42.
221. Avram, A.; Sengupta, A.; Pfromm, P.H.; Zorn, H.; Lorenz, P.; Schwarz, T.; Nguyen, K.Q.; Czermak, P. Novel DyP from the basidiomycete *Pleurotus sapidus*: substrate screening and kinetics. *Biocatalysis* **2018**, *4*, 1–13.
222. Zorn, H.; Langhoff, S.; Scheibner, M.; Nimtz, M.; Berger, R.G. A Peroxidase from Lepista irina Cleaves β,β-Carotene to Flavor Compounds. *Biol. Chem.* **2003**, *384*, 1049–1056.
223. Schulz, K.; Giesler, L.; Linke, D.; Berger, R.G. A prolyl endopeptidase from *Flammulina velutipes* for the possible degradation of celiac disease provoking toxic peptides in cereal proteins. *Process Biochem.* **2018**, *73*, 47–55.
224. Nieter, A.; Haase-Aschoff, P.; Linke, D.; Nimtz, M.; Berger, R.G. A halotolerant type A feruloyl esterase from *Pleurotus eryngii*. *Fungal Biol.* **2014**, *118*, 348–357.
225. Altschul, S.F.; Gish, W.; Miller, W.; Myers, E.W.; Lipman, D.J. Basic local alignment search tool. *J. Mol. Biol.* **1990**, *215*, 403–410.
226. Sievers, F.; Wilm, A.; Dineen, D.; Gibson, T.J.; Karplus, K.; Li, W.; Lopez, R.; McWilliam, H.; Remmert, M.; Söding, J.; et al. Fast, scalable generation of high-quality protein multiple sequence alignments using Clustal Omega. *Mol. Syst. Biol.* **2011**, *7*, 539.
227. Lin-Cereghino, J.; Wong, W.W.; Xiong, S.; Giang, W.; Luong, L.T.; Vu, J.; Johnson, S.D.; Lin-Cereghino, G.P. Condensed protocol for competent cell preparation and transformation of the methylotrophic yeast *Pichia pastoris*. *Biotechniques* **2005**, *38*, 44–48.
228. Sygmund, C.; Gutmann, A.; Krondorfer, I.; Kujawa, M.; Glieder, A.; Pscheidt, B.; Haltrich, D.; Peterbauer, C.; Kittl, R. Simple and efficient expression of *Agaricus meleagris* pyranose dehydrogenase in *Pichia pastoris*. *Appl. Microbiol. Biotechnol.* **2012**, *94*, 695–704.
229. Nieter, A.; Kelle, S.; Takenberg, M.; Linke, D.; Bunzel, M.; Popper, L.; Berger, R.G. Heterologous production and characterization of a chlorogenic acid esterase from *Ustilago maydis* with a potential use in baking. *Food Chem.* **2016**, *209*, 1–9.
230. Britton, H.T.S.; Robinson, R.A. CXCVIII.—Universal buffer solutions and the dissociation constant of veronal. *J. Chem. Soc.* **1931**, 1456–1462.

231. Lowry, O.H.; Rosebrpugh, N.J.; Randall, R.J. Protein measurement with the Folin phenol reagent. *J. Biol. Chem.* **1951**, *193*, 265–275.
232. Fink, M.; Trunk, S.; Hall, M.; Schwab, H.; Steiner, K. Engineering of TM1459 from *Thermotoga maritima* for increased oxidative alkene cleavage activity. *Front. Microbiol.* **2016**, *7*, 1–9.
233. van der Nest, M.A.; Slippers, B.; Steenkamp, E.T.; De Vos, L.; Van Zyl, K.; Stenlid, J.; Wingfield, M.J.; Wingfield, B.D. Genetic linkage map for *Amylostereum areolatum* reveals an association between vegetative growth and sexual and self-recognition. *Fungal Genet. Biol.* **2009**, *46*, 632–641.
234. Postemsky, P.D.; Bidegain, M.A.; Lluberas, G.; Lopretti, M.I.; Bonifacino, S.; Inés Landache, M.; Zygadlo, J.A.; Fernández-Lahore, M.; Omarini, A.B. Biorefining *via* solid-state fermentation of rice and sunflower by-products employing novel monosporic strains from *Pleurotus sapidus*. *Bioresour. Technol.* **2019**, *289*, 121692.
235. Pringle, A.; Taylor, J.W. The fitness of filamentous fungi. *Trends Microbiol.* **2002**, *10*, 474–481.
236. Meissner, P.N.; Dailey, T.A.; Hift, R.J.; Ziman, M.; Corrigall, A. V.; Roberts, A.G.; Meissner, D.M.; Kirsch, R.E.; Dailey, H.A. A R59W mutation in human protoporphyrinogen oxidase results in decreased enzyme activity and is prevalent in South Africans with variegate porphyria. *Nat. Genet.* **1996**, *13*, 95–97.
237. Maurizi, M.R.; Rasulova, F. Degradation of L-glutamate dehydrogenase from *Escherichia coli*: Allosteric regulation of enzyme stability. *Arch. Biochem. Biophys.* **2002**, *397*, 206–216.
238. Castanera, R.; López-Varas, L.; Borgognone, A.; LaButti, K.; Lapidus, A.; Schmutz, J.; Grimwood, J.; Pérez, G.; Pisabarro, A.G.; Grigoriev, I. V; et al. Transposable Elements versus the Fungal Genome: Impact on Whole-Genome Architecture and Transcriptional Profiles. *PLOS Genet.* **2016**, *12*, e1006108.
239. Castanera, R.; Borgognone, A.; Pisabarro, A.G.; Ramírez, L. Biology, dynamics, and applications of transposable elements in basidiomycete fungi. *Appl. Microbiol. Biotechnol.* **2017**, *101*, 1337–1350.
240. Clark, T.A.; Anderson, J.B. Dikaryons of the basidiomycete fungus *Schizophyllum commune*: Evolution in long-term culture. *Genetics* **2004**, *167*, 1663–1675.
241. Ellingboe, A.H. Breeding for Mushroom Production in *Lentinula Edodes*. In *Genetics and Breeding of Edible Mushrooms*; Chang, S.-T.; Buswell, J. A.; Miles, P.G., Ed.; Routledge: Philadelphia, 2018; pp. 111–123.
242. Waterhouse, A.; Bertoni, M.; Bienert, S.; Studer, G.; Tauriello, G.; Gumienny, R.; Heer, F.T.; de Beer, T.A.P.; Rempfer, C.; Bordoli, L.; et al. SWISS-MODEL: homology modelling of protein structures and complexes. *Nucleic Acids Res.* **2018**, *46*, W296–W303.
243. Artimo, P.; Jonnalagedda, M.; Arnold, K.; Baratin, D.; Csardi, G.; de Castro, E.; Duvaud, S.; Flegel, V.; Fortier, A.; Gasteiger, E.; et al. ExPASy: SIB bioinformatics resource portal. *Nucleic Acids Res.* **2012**, *40*, W597–W603.
244. Brissos, V.; Tavares, D.; Sousa, A.C.; Robalo, M.P.; Martins, L.O. Engineering a Bacterial DyP-Type Peroxidase for Enhanced Oxidation of Lignin-Related Phenolics at Alkaline pH. *ACS Catal.* **2017**, *7*, 3454–3465.
245. Habib, M.H.; Rozeboom, H.J.; Fraaije, M.W. Characterization of a New DyP-Peroxidase from the Alkaliphilic Cellulomonad, *Cellulomonas bogoriensis*. *Molecules* **2019**, *24*, 1208.
246. Whittle, E.; Shanklin, J. Engineering Δ 9 -16:0-Acyl Carrier Protein (ACP) Desaturase Specificity Based on Combinatorial Saturation Mutagenesis and Logical Redesign of the Castor Δ^9-18:0-ACP Desaturase. *J. Biol. Chem.* **2001**, *276*, 21500–21505.

247. van den Heuvel, R.H.H.; van den Berg, W.A.M.; Rovida, S.; van Berkel, W.J.H. Laboratory-evolved Vanillyl-alcohol Oxidase Produces Natural Vanillin. *J. Biol. Chem.* **2004**, *279*, 33492–33500.
248. Morley, K.L.; Kazlauskas, R.J. Improving enzyme properties: When are closer mutations better? *Trends Biotechnol.* **2005**, *23*, 231–237.
249. Bross, P.; Jespersen, C.; Jensen, T.G.; Andresen, B.S.; Kristensen, M.J.; Winter, V.; Nandy, A.; Krautle, F.; Ghisla, S.; Bolund, L.; et al. Effects of two mutations detected in medium chain Acyl-CoA dehydrogenase (MCAD)-deficient patients on folding, oligomer assembly, and stability of MCAD enzyme. *J. Biol. Chem.* **1995**, *270*, 10284–10290.
250. Boer, H.; Koivula, A. The relationship between thermal stability and pH optimum studied with wild-type and mutant *Trichoderma reesei* cellobiohydrolase Cel7A. *Eur. J. Biochem.* **2003**, *270*, 841–848.
251. Garcia-Ruiz, E.; Gonzalez-Perez, D.; Ruiz-Dueñas, F.J.; Martínez, A.T.; Alcalde, M. Directed evolution of a temperature-, peroxide- and alkaline pH-tolerant versatile peroxidase. *Biochem. J.* **2012**, *441*, 487–498.
252. Graf, E. Ullmann's Encyclopedia of Industrial Chemistry; Fifth Compl. Revis. Edit. Vol.'s A 3 and A 4 Ed's W. Gerhartz (executive), Y. St. Yamamoto (Senior Ed.), F. T. Campbell, R. Pfefferkorn und J. F. Rounsaville. VCH Verlagsges. Weinheim 1985, A 3 = 578 S., A 4. *Pharm. Unserer Zeit* **1987**, *16*, 63–63.
253. Sergeant, E.; Dempsey, B. *Ionisation constants of organic acids in aqueous solution, IUPAC chemical data series 2*; Pergamon Press: New York, NY, 1979; ISBN 0080223397.
254. Aamir, S.; Sutar, S.; Singh, S.; Baghela, A. A rapid and efficient method of fungal genomic DNA extraction, suitable for PCR based molecular methods. *Plant Pathol. Quar.* **2015**, *5*, 74–81.
255. NetNGlyc 1.0 Server. Available online: http://www.cbs.dtu.dk/services/NetNGlyc/ (accessed on Nov 14, 2020).
256. Schneider, C.A.; Rasband, W.S.; Eliceiri, K.W. NIH Image to ImageJ: 25 years of image analysis. *Nat. Methods* **2012**, *9*, 671–675.
257. Bradford, M.M. A rapid and sensitive method for the quantitation of microgram quantities of protein utilizing the principle of protein-dye binding. *Anal. Biochem.* **1976**, *72*, 248–254.
258. Galperin, I. Das ligninolytische System von *Pleurotus sapidus*: Transkriptomanalyse und heterologe Expression einer Arylalkoholoxidase, Justus-Liebig-Universität Gießen: Gießen, Germany, 2018.
259. Teste, M.A.; Duquenne, M.; François, J.M.; Parrou, J.L. Validation of reference genes for quantitative expression analysis by real-time RT-PCR in *Saccharomyces cerevisiae*. *BMC Mol. Biol.* **2009**, *10*, 99.
260. Pfaffl, M.W. A new mathematical model for relative quantification in real-time RT-PCR. *Nucleic Acids Res.* **2001**, *29*, 45e – 45.
261. Schwendenwein, D.; Fiume, G.; Weber, H.; Rudroff, F.; Winkler, M. Selective Enzymatic Transformation to Aldehydes in vivo by Fungal Carboxylate Reductase from *Neurospora crassa*. *Adv. Synth. Catal.* **2016**, *358*, 3414–3421.
262. Jankowski, N.; Koschorreck, K.; Urlacher, V.B. High-level expression of aryl-alcohol oxidase 2 from *Pleurotus eryngii* in *Pichia pastoris* for production of fragrances and bioactive precursors. *Appl. Microbiol. Biotechnol.* **2020**, *104*, 9205–9218.
263. Santos, A.S.; Pereira, N.; da Silva, I.M.; Sarquis, M.I.M.; Antunes, O.A.C. Peroxidase catalyzed microbiological oxidation of isosafrol into piperonal. *Process Biochem.* **2004**, *39*, 2269–2275.

264. Tisserand, R.; Rodney, Y. *Essential Oil Safety - E-Book: A Guide for Health Care Professionals*; 2nd ed.; Elsevier Health Sciences, 2013; ISBN 9780702054341.
265. Merck KGaA Isosafrol solution Available online: https://www.sigmaaldrich.com/catalog/product/supelco/crm40157?lang=de&region=DE&cm_sp=Insite-_-caSrpResults_srpRecs_srpModel_120-58-1-_-srpRecs3-1 (accessed on May 5, 2021).
266. Krahe, N.-K.; Berger, R.G.; Kahlert, L.; Ersoy, F. Co-Oxidative Transformation of Piperine to Piperonal and 3,4-Methylenedioxycinnamaldehyde by a Lipoxygenase from *Pleurotus sapidus*. *ChemBioChem* **2021**, cbic.202100183.
267. Krahe, N.; Berger, R.G.; Kahlert, L.; Ersoy, F. Co-Oxidative Transformation of Piperine to Piperonal and 3,4-Methylenedioxycinnamaldehyde by a Lipoxygenase from *Pleurotus sapidus*. *ChemBioChem* **2021**, cbic.202100282. Copyright Wiley-VCH GmbH. Reproduced with permission.
268. Kollmannsberger, H.; Nitz, S.; Drawert, F. Über die Aromastoffzusammensetzung von Hochdruckextrakten. *Z. Lebensm. Unters. Forsch.* **1992**, *194*, 545–551.
269. Zhu, C.; Xu, Z.; Song, R. The endoglucanase from *Bacillus subtilis* BEC-1 bears halo-tolerant, acidophilic and dithiothreitol-stimulated enzyme activity. *World J. Microbiol. Biotechnol.* **2011**, *27*, 2863–2871.
270. Burgess, R.R. Chapter 20 Protein Precipitation Techniques. In *Methods in Enzymology - Guide to Protein Purification Volume 463*; Richard, R.B., Deutscher, M.P., Eds.; Academic Press, 2009; pp. 331–342 ISBN 9780123745361.
271. Buettner, G.R. The Pecking Order of Free Radicals and Antioxidants: Lipid Peroxidation, α-Tocopherol, and Ascorbate. *Arch. Biochem. Biophys.* **1993**, *300*, 535–543.
272. Krings, U.; Vollmer, H.; Latza, E.; Treffenfeldt, W.; Berger, R.G.; Preuss, A. Method for the selective concentration and separation of aroma molecules by adsorption. 2000, 1–15.
273. Gallagher, R.; Shimmon, R.; McDonagh, A.M. Synthesis and impurity profiling of MDMA prepared from commonly available starting materials. *Forensic Sci. Int.* **2012**, *223*, 306–313.
274. Berry, H.; Debat, H.; Larreta-Garde, V. Excess substrate inhibition of soybean lipoxygenase-1 is mainly oxygen-dependent. *FEBS Lett.* **1997**, *408*, 324–326.

Lebenslauf

PERSÖNLICHE DATEN

Name	Nina-Katharina Krahe
	09.11.1991 in Minden

SCHULBILDUNG

1998 – 2002	Grundschule Eidinghausen, Bad Oeynhausen
2002 – 2011	Immanuel-Kant-Gymnasium, Bad Oeynhausen
06/2011	Abitur; Prüfungsfächer: Mathematik, Chemie, Deutsch, Religion

WEITERER WERDEGANG

10/2011 – 09/2014	B. Sc. Life Science, Leibniz Universität Hannover Abschluss: Bachelor of Science Abschlussarbeit: „Screening auf Calcium- und Chlorid-insensitive Laccasen aus Basidiomyceten für den Einsatz in fermentierten Milchprodukten“
10/2014 – 10/2016	M. Sc. Life Science, Leibniz Universität Hannover Abschluss: Master of Science Abschlussarbeit: „Identifizierung und biochemische Charakterisierung von neuartigen Anthocyan-abbauenden Enzymen aus Basidiomycota“
01/2017-03/2021	Wissenschaftliche Mitarbeiterin Institut für Lebensmittelchemie, Leibniz Universität Hannover
Seit 01/2017	Promotionsvorhaben Institut für Lebensmittelchemie, Leibniz Universität Hannover

Liste der wissenschaftlichen Veröffentlichungen

Diese Dissertationsschrift basiert auf Arbeiten, die in den folgenden *peer reviewed* Publikationen veröffentlicht wurden:

- **Krahe, N.-K.**; Berger, R.G.; Ersoy, F. A DyP-Type Peroxidase of *Pleurotus sapidus* with Alkene Cleaving Activity. *Molecules* 2020, 25, 1536. https://doi.org/10.3390/molecules25071536
- **Krahe, N.-K.**; Berger, R.G.; Witt, M.; Zorn, H.; Omarini, A.B.; Ersoy, F. Monokaryotic *Pleurotus sapidus* Strains with Intraspecific Variability of an Alkene Cleaving DyP-Type Peroxidase Activity as a Result of Gene Mutation and Differential Gene Expression. *Int. J. Mol. Sci.* 2021, 22, 1363. https://doi.org/10.3390/ijms22031363
- **Krahe, N.-K.**; Berger, R.G.; Kahlert, L.; Ersoy, F. Co-Oxidative Transformation of Piperine to Piperonal and 3,4-Methylenedioxycinnamaldehyde by a Lipoxygenase from *Pleurotus sapidus*. *ChemBioChem* 2021, cbic.202100183. https://doi.org/10.1002/cbic.202100183

Zur letztgenannten Publikation wurde zudem ein Titelbild in *ChemBioChem* veröffentlicht:

- **Krahe, N.-K.**; Berger, R.G.; Kahlert, L.; Ersoy, F. Co-Oxidative Transformation of Piperine to Piperonal and 3,4-Methylenedioxycinnamaldehyde by a Lipoxygenase from *Pleurotus sapidus*. *ChemBioChem* 2021, cbic.202100182. https://doi.org/10.1002/cbic.202100282

Nachfolgend gelistete Veröffentlichungen, Vorträge, Poster und Patente sind im Rahmen dieser Doktorarbeit entstanden, sind jedoch nicht Gegenstand dieser Dissertationsschrift.

Veröffentlichte Artikel:

- Behrens, C.J.; **Krahe, N.K.**; Linke, D.; Berger, R.G. BadGluc, a *β*-glucosidase from *Bjerkandera adusta* with anthocyanase properties. *Bioprocess. Biosyst. Eng.* 2018, 41, 1391–1401. https://doi.org/10.1007/s00449-018-1966-4

Veröffentlichte Abstracts:

- **Krahe, N.-K.**; Nieter; A.; Berger, R.G. Alkenspaltende Aktivität von *Pleurotus sapidus* zur Gewinnung von natürlichen Aromastoffen. *Lebensmittelchemie* 2019, 73. https://doi.org/10.1002/lemi.201951126
- **Krahe, N.-K.**; Omarini, A.B.; Zorn, H.; Berger, R.G. Alkene cleavage activity of *Pleurotus sapidus* to obtain natural flavors. *Chem. Ing. Tech.* 2020, 92, 1338-1339. https://doi.org/10.1002/cite.202055129
- Bürger, F.; Omarini, A.; **Krahe, N.K.**; Fraatz, M.A.; Berger, R.G.; Zorn, H. Herstellung natürlicher Aromastoffe durch monokaryotische Stämme von *Pleurotus sapidus* unter Nutzung von Nebenströmen der *Citrus*-verarbeitenden Industrie. *Lebensmittelchemie* 2019, 73. https://doi.org/10.1002/lemi.201951121

Vorträge auf Konferenzen:

- **Krahe, N.-K.**; Berger, R.G. Monokaryotic strains of *Pleurotus sapidus* to obtain bioactive compounds. Young Scientist Conference „Food Biotechnology“, 23. – 25. September 2019, Stuttgart, Deutschland.

Posterpräsentationen:

- **Krahe, N.-K.**; Nieter; A.; Berger, R.G. Alkenspaltende Aktivität von *Pleurotus sapidus* zur Gewinnung von natürlichen Aromastoffen. 48. Deutscher Lebensmittelchemikertag, 16.− 18. September 2019, Dresden, Deutschland.
- **Krahe, N.-K.**; Omarini, A. B.; Zorn, H.; Berger, R.G. Alkene cleavage activity of *Pleurotus sapidus* to obtain natural flavors. 10. ProcessNet-Jahrestagung und 34. DECHEMA-Jahrestagung der Biotechnologen 2020: Processes for Future, 21.−23. September 2020, Online-Konferenz.
- Große, M.; **Krahe, N.-K.**; Rottmann, E.; Berger, R. G. Cultivation of Enzyme Secreting Higher Fungi on Side Streams of the Food Processing Industries. 9th International Congress on Biocatalysis, Biocat, 26.−30. August 2018, Hamburg, Deutschland.
- Bürger, F.; Omarini, A.; **Krahe, N.K.**; Fraatz, M.A.; Berger, R.G.; Zorn, H. Herstellung natürlicher Aromastoffe durch monokaryotische Stämme von *Pleurotus sapidus* unter Nutzung von Nebenströmen der *Citrus*-verarbeitenden Industrie. 48. Deutscher Lebensmittelchemikertag, 16.−18. September 2019, Dresden, Deutschland.

Patente:

- Mussmann, N.; Wieland, S.; Degering, C.; Berger, R.G.; Behrens, C.; Linke, D.; **Krahe, N.-K.** Glucosidase und eine solche enthaltende Wasch- und Reinigungsmittel. DE102017220670 (A1), 2019.

Nachfolgend gelistete Veröffentlichung ist vor Beginn der Doktorarbeit entstanden und nicht Teil dieser Dissertationsschrift:

- Struch, M.; **Krahe, N.-K.**; Linke, D., Mokoonlall, A.; Hinrichs, J.; Berger, R.G. Dose dependent effects of a milk ion tolerant laccase on yoghurt gel structure, LWT - Food Sci. Technol. 2016, 65, 1144-1152, htttps://doi: 10.1016/j.lwt.2015.10.004.